
High Temperature Series Expansions
for Spin- and Spin-Phonon-Systems

Inaugural-Dissertation
zur
Erlangung des Doktorgrades
der Mathematisch-Naturwissenschaftlichen Fakultät
der Universität zu Köln

vorgelegt von
Alexander Bühler
aus Karlsruhe

Köln 2003

Berichterstatter

Priv.-Doz. Dr. G. S. Uhrig
Prof. Dr. M. Braden

Vorsitzender der Prüfungskommission

Prof. Dr. A. Freimuth

Tag der mündlichen Prüfung

5.12.2003

Contents

Motivation	1
Outline of this work	2
1. Spin Systems	3
1.1. Introduction	5
1.2. Fundamentals	6
1.3. Series Extrapolation	9
1.3.1. Dlog-Padé Approximants	10
1.3.2. Extrapolation in Internal Variable	12
1.4. Dimerized, Frustrated Chain	15
1.4.1. Introduction	15
1.4.2. Model	15
1.4.3. Computation	17
1.4.4. Extrapolation	20
1.4.5. Results	25
1.4.6. Conclusions	38
1.5. Ladder with Cyclic Exchange	41
1.5.1. Introduction	41
1.5.2. Model	42
1.5.3. Computation	43
1.5.4. Extrapolations	50
1.5.5. Results	58
1.5.6. Estimation of the Ground State Energy	62
1.5.7. SrCu_2O_3	66
1.5.8. Conclusions	70
1.6. Shastry-Sutherland Model	71
1.6.1. Introduction	71
1.6.2. Model	71
1.6.3. Computation	74
1.6.4. Results	76
1.6.5. $\text{SrCu}_2(\text{BO}_3)_2$	80
1.6.6. Conclusions	91
2. Spin-Phonon System	93
2.1. Introduction	95

2.2. Model	96
2.3. Method and Computation	98
2.3.1. Cluster Expansion	100
2.3.2. Free Energy	102
2.3.3. Susceptibility	104
2.4. Results	108
2.4.1. Susceptibility	108
2.4.2. Specific Heat	115
2.5. Conclusions	119
Summary	121
Outlook	124
A. Coefficients	125
A.1. Dimerized, Frustrated Chain	126
A.2. Dimerized Chain	129
A.3. Ladder with Cyclic Exchange	131
A.3.1. Pure 4-Spin Operator	131
A.3.2. Permutation Operator	136
A.4. Shastry-Sutherland Model	139
A.5. Spin-Phonon System	140
B. Perturbation Theory for Spin-Phonon System	148
Bibliography	153
Abstract	167
Deutsche Zusammenfassung	169

Motivation

The theoretical description of condensed matter is a complex task since even a small sample of material contains 10^{23} atoms. Strongly correlated electron systems in particular which are addressed in this thesis pose a difficult problem. The interaction between neighboring or next-neighboring electrons is so strong that the electrons cannot be considered independently. If they could be viewed as independent particles the simple picture of free electrons could be used. However, the strong correlations of the electrons lead to quite a different picture. The strong interactions on the microscopic level scale up to a macroscopic strongly interacting ensemble.

The orbital of an electron represents the shape of the electron cloud in the solid. In transition-metal oxides with anisotropic-shaped d-orbital electrons, the Coulomb interaction between the electrons lead to strong correlation effects. Their interactions are of importance to understand the metal-insulator transitions and properties such as high temperature superconductivity and colossal magnetoresistance [1].

The generic model describing the dynamics of correlated electrons is the Hubbard model where the electrons are allowed to move on the crystal lattice underlying the solid with a hopping amplitude t . The free motion of the electrons is restricted by an on-site Coulomb repulsion U which prohibits double occupancies energetically. In the limit of small t/U the Hubbard model at half filling can be mapped in leading order t/U to an antiferromagnetic Heisenberg model.

The Heisenberg operator models the spin-spin interactions of the electrons and can be understood as an effective model describing the magnetic properties of the system. Thus, the Heisenberg model serves as a realistic description of insulating magnetic materials. The Heisenberg model and extensions of it will be used in this thesis to investigate the magnetic properties of various systems.

The first part of this thesis investigates pure spin- $\frac{1}{2}$ models in (quasi) one dimension and in two dimensions. The second part investigates a one-dimensional spin- $\frac{1}{2}$ system extended by the coupling to the lattice vibrations, the phonons. Low dimensional (spin-) systems in general provide a fascinating and challenging area of activity from a theoretical point of view. Due to their strong quantum fluctuations the systems show interesting phenomena and rich phase diagrams. Many compounds can be described in a first approach by such low-dimensional systems. Whenever possible the theoretical findings of the appropriate model are compared to experimental data. The models and their significance in the framework of condensed matter physics will be highlighted in separate introductions.

The models under consideration are solvable analytically only in a few special cases, like the isotropic Heisenberg model [2, 3] or the system of isolated dimers for instance. However,

there are a number of powerful approaches which yield the desired physical quantities of interest in the non-analytic cases, which can be considered as the generic cases.

This thesis is dedicated to the method of series expansions, 'the most venerable approach to the study of quantum systems' [4]. Series expansions have been performed at all times to obtain a first impression of the behavior of a physical quantity about a known limit. Due to the rapid increase in computation power it was possible to significantly increase the orders of expansion one can practically carry out 'by hand'. The series expansions performed in this thesis will be used to derive thermodynamical quantities like the magnetic susceptibility or the specific heat, quantities which are in most cases easily accessible experimentally.

The general approach in this thesis to evaluate the quantities of interest is the method of high temperature series expansions. High temperature series expansions have been used for a long time to compute thermodynamical quantities. So far, numerous methods exist to perform a high temperature series expansion for a given system, see for instance Refs. [5, 6]. In this thesis various approaches are presented to derive the results for the system under consideration. The implementation of the explicit calculations in a computer program yields results up to very high orders in the expansion parameter. Thus, the results can serve for reliable and quantitative predictions of the thermodynamical quantities in almost the whole temperature regime. Compared to other numerical methods like exact complete diagonalization [7] or quantum Monte-Carlo [8] the results still contain full dependence on all external parameters. Hence, fitting procedures of the theoretical findings to experimental data can be performed fast and easily.

Outline of this work

The work is organized as follows. The thesis is divided into two main parts: one for the pure spin-models and another addressing a spin-system coupled to phononic degrees of freedom. In Chapter 1.4 a spin-1/2 chain with nearest and next-nearest neighbor interaction is investigated. Chapter 1.5 analyzes a spin ladder with an additional four-spin (cyclic) exchange and the last Chapter 1.6 in the first part is dedicated to the analysis of a two-dimensional system, the Shastry-Sutherland model. The second part investigates a spin-1/2 system locally coupled to Einstein phonons. A comprehensive summary is given at the end rounded off by an outlook for future investigations.

In the Appendix the series coefficients computed in this thesis are tabulated. These coefficients form the basis information of this work. Hence, the coefficients are provided in the most natural way, i.e. printed, to put for use for the interested reader.

The work closes with an abstract of the thesis both in English and in German.

1. Spin Systems

1.1. Introduction

Quantum spin systems are amongst the most interesting and challenging problems of many-body theory in solid state physics. Due to their intrinsic many-body quantum character it is not possible to compute even simple quantities like magnetic susceptibilities or specific heats in a straightforward fashion. But there are by now a number of powerful approaches like exact diagonalization [7], quantum Monte-Carlo [8], temperature density-matrix renormalization [9, 10] or high temperature series expansion [5, 6] which yield the desired quantities. The aim of the first part of this thesis is to provide high temperature series data which can serve as an input for quick data analysis. High order series expansions constitute an efficient, frequently used technique [4]. Exact diagonalization and temperature density-matrix renormalization will serve as benchmarks to assess the reliability of the method proposed. Similar analyses are carried out in Refs. [11, 12] for unfrustrated dimerized spin chains and ordinary spin ladders.

The systems under consideration are interesting because they constitute disordered antiferromagnets with low coordination number. This means that their ground state is not given by a Néel-type state (i.e. with finite sublattice magnetization) but by a Resonating-Valence Bond (RVB) state made of superposed singlet-product states [13]. If the systems are indeed gapped the average range of the singlet pairs present in the ground state is finite. In other words, the correlation length is finite. Generally, an RVB state is favored over a Néel state by low coordination numbers, by low values of the spin and by frustration (which simply weakens the classical ordered Néel-state) [14].

Throughout this thesis, where $S = 1/2$ systems are investigated, an elementary excitation, or quasi-particle, from a singlet ground state to one of the three triplet states will be denoted as triplon. This terminology was introduced recently by K. P. Schmidt and G. S. Uhrig in Ref. [15].

If it is possible to dope the insulating magnetic systems unusual electronic properties emerge due to the strong interplay between charge and spin degrees of freedom. Some spin ladders like $\text{Sr}_{0.4}\text{Ca}_{13.6}\text{Cu}_{24}\text{O}_{41.84}$ become even superconducting under pressure [16]. Of course, the appearance of a true phase transition at finite temperatures requires a dimensionality higher than one [17–19]. But the driving mechanisms can be present already in the low-dimensional systems. Therefore, a deeper understanding of unusual electronic behavior in doped antiferromagnets requires a thorough understanding of the magnetic subsystem. It is in this context that the present investigation is performed which is designed to determine the relevant magnetic couplings easily and reliably.

The models under consideration can often be used to investigate and interpret experimental results. In a first approach the models are well suited to characterize the appropriate substance. Higher-dimensional interactions like interchain, interladder, or interplane interactions are often negligible. Thus, the theoretical models yield a precise description for the substance at hand. However, as will be seen in Chapter 1.6, the theoretical findings can also account for the three-dimensionality of the substances in so far as the one-dimensional building blocks can be treated by mean-field theory.

1.2. Fundamentals

This part of the thesis addresses Heisenberg models with antiferromagnetically coupled spins of size $S = 1/2$. The generic Hamilton operator for such systems is given by

$$H = \sum_{i,j} J_{ij} \mathbf{S}_i \mathbf{S}_j, \quad (1.1)$$

with $J_{ij} > 0$ modeling the exchange coupling between site i and j . The results presented in the following are not restricted to the antiferromagnetic case, but can also be used in the ferromagnetic case. In this thesis, however, only the antiferromagnetic case is addressed. In Eq. 1.1 only two-spin interactions are assumed. Chapter 1.5 investigates a model which includes also four-spin interactions. The general considerations presented in this section are not affected by this additional interaction.

The series expansions carried out in this thesis for the pure spin-models are high temperature series expansions (HTSE). Conventional HTSE considers a thermodynamical density like the free energy per site $f(\beta = 1/k_B T)$ expanded about $\beta = 0$ (in the following k_B will be set to unity). Hence, a perturbation expansion about the small parameter β is performed. The explicit calculations lead to the identification and evaluation of cumulants or connected clusters contributing in every order of the expansion. For an overview of the methods applied so far for high temperature series expansions, esp. to the Heisenberg model, the reader is referred to Refs. [5, 6]. For the pure spin systems addressed in the first part of this thesis a novel approach is used. The basic ideas are given below, for a detailed explanation see Refs. [20, 21].

The numerical approach explained in the following makes use of the result of the linked cluster theorem [22, 23]. The physical quantities are evaluated in the thermodynamical limit by means of finite systems. For concreteness, the magnetic susceptibility per site at vanishing magnetic field given by

$$\chi(T) = \frac{\beta}{N} \frac{\text{Tr} \{ M^2 e^{-\beta H} \}}{\text{Tr} \{ e^{-\beta H} \}} \quad (1.2)$$

with the uniform magnetization

$$M = \sum_{i=1}^N S_i^z \quad (1.3)$$

is computed. N denotes the (finite) system size. Denominator and numerator are computed separately by expanding the corresponding exponential functions. The resulting rational function is again expanded around $\beta = 0$ to obtain a truncated series (polynomial) in the inverse temperature β

$$\left. \begin{array}{l} \langle S | M^2 e^{-\beta H} | S \rangle \\ \langle S | e^{-\beta H} | S \rangle \end{array} \right\} \begin{array}{l} \xrightarrow{\beta=0} \\ \xrightarrow{\beta=0} \end{array} \text{truncated series.} \quad (1.4)$$

Hence, the physical quantity is expanded in powers of the Hamiltonian H , i.e. in powers of $\beta J = J/T$ when assuming a isotropic exchange coupling $J = J_{ij}$. Performing the expansion

of the rational function in the last step in Eq. 1.4 cancels the different dependences from the system size term by term such that the resulting truncated series does not depend on the system size any more. This is an obvious fact since the considered quantities are independent of the system size. The results are not evaluated for each set of parameters entering the specific model. Once the physical quantity has been computed, it has the full dependence of all model parameters, i.e. the result is an algebraic polynomial in the parameters entering the given model. In contrast to other numerical methods like exact diagonalization or temperature density-matrix renormalization, where for each set of parameters a new program run is required, the advantage of the HTSE is obvious. Especially fits of the HTSE results to experimental data can be done in a fast and easy way.

The advantage of the approach 1.4 compared for instance to the linked cluster expansion method [23] is that it is not necessary to determine and classify all contributing clusters explicitly. The linked cluster expansion method uses explicitly the linked cluster theorem such that only the connected clusters are taken into account in the calculations. This task should not be underestimated in view of the lack of efficient algorithms comparing graphs. This point matters in particular for complicated lattices with various types of bonds. In this respect, the approach used in this thesis for the pure spin models is simpler than the linked cluster method approach. The disadvantage may be that the finite systems which have to be dealt with are fairly large, in particular for elevated orders in β and higher dimensions, see for instance Chapter 1.6 where a two-dimensional system is investigated.

The system sizes which have to be considered to obtain results in the thermodynamical limit depend strongly on the distance between spins which interact with each other. Suppose the Hamilton operator in Eq. 1.1 depends only on interactions between neighboring sites, i.e. $J = J_{i,i+1}$, in a one-dimensional system. Then the resulting Hamilton operator can be written as a sum of local terms consisting of spin-products between neighboring sites. The result from the linked cluster theorem states that the largest connected cluster in n th order has to be embedded in the finite system to obtain valid results in the thermodynamical limit. Thereby a cluster is identified by the bonds where a local term of the Hamilton operator has been applied. Thus, in n th order the largest connected cluster contains $n + 1$ sites for nearest neighbor interaction. Allowing also for next-nearest neighbor interaction the largest connected cluster already contains $2n + 1$ sites for a one-dimensional system. To compute the traces for the numerator and denominator a finite system size N is used, where N is assumed to be large enough to obtain the results in the maximum order n of expansion in the thermodynamical limit. As long as the system size N is not too large the complete Hilbert space $|N\rangle$ of the finite system with dimension 2^N can be constructed using the Ising basis. An obvious by-product are then the relations

$$\begin{aligned} \langle N|H^{2m}|N\rangle &= \langle N|H^m H^m|N\rangle \\ &= |H^m|N\rangle|^2 \end{aligned} \quad (1.5a)$$

$$\langle N|H^{2m+1}|N\rangle = \langle N|H^m H^{m+1}|N\rangle, \quad (1.5b)$$

which imply that for a given order n in β one needs to calculate only about $n/2$ applications of H to the Ising basis $|N\rangle$ of the finite system. This statement remains true for the numerator of the susceptibility as in Eq. 1.2 if the observable commutes with H . This is

the case for the uniform magnetization 1.3. Replacing $|N\rangle$ by $M|N\rangle$ makes the relations 1.5 also applicable to the numerator of Eq. 1.2.

For the two-dimensional system considered in Chapter 1.6 the complete Hilbert space of the finite system under consideration could not be constructed. Instead, the moment-algorithm was applied, which basically reduces the computation of the trace to a computation of an expectation value with respect to an appropriately chosen state, for details see Chapter 1.6.

Another important quantity of interest in this thesis is the magnetic specific heat $C(T)$. The specific heat is derived from the denominator of Eq. 1.2 which is the partition function of the system by

$$C(T) = \frac{1}{N} \frac{\partial}{\partial T} \frac{\text{Tr}\{He^{-\beta H}\}}{\text{Tr}\{e^{-\beta H}\}} \quad (1.6a)$$

$$= \frac{1}{N} \frac{\partial}{\partial T} \left(\frac{-\frac{\partial}{\partial \beta} \text{Tr}\{e^{-\beta H}\}}{\text{Tr}\{e^{-\beta H}\}} \right). \quad (1.6b)$$

It is worth mentioning that due to the derivation in Eq. 1.6b one order in β is lost. It is regained, however, by the subsequent derivation with respect to T .

The obtained truncated series for the susceptibility and the specific heat are well suited to give a precise description for temperatures $\beta J = J/T < 1$. But it is intended to obtain results which are also valid in the low temperature regime, i.e. $J/T > 1$. For this purpose an efficient extrapolation technique is necessary to obtain valid results outside the radius of convergence of the computed series. The following section will explain the techniques applied in this thesis in detail.

The low temperature behavior of the considered quantities is often known, especially for gapped spin system. Having this information at hand the extrapolations of the truncated series can be biased in the low temperature regime to the known behavior, yielding a stable continuation from the computed high temperature limit to the known low temperature behavior. In the following, the basic formulas describing the low temperature behavior of the specific heat and of the susceptibility for the spin-systems under consideration in this thesis are given.

For gapped spin-systems the susceptibility at zero temperature vanishes and at finite but small temperatures the deviation is exponentially small due to the spin gap Δ ,

$$\chi(T) \approx e^{-\Delta/T} \quad \text{for } T \ll \Delta. \quad (1.7)$$

Furthermore, the leading power in T can be determined on the basis of the dimensionality of the problem and of the behavior of the dispersion close to its minima. For (quasi-) one-dimensional systems as considered in Chapters 1.4 and 1.5 with quadratic minima, which is generic for gapped systems, one obtains [24]

$$\chi(T) \approx \frac{1}{\sqrt{T}} e^{-\Delta/T} \quad \text{for } T \ll \Delta. \quad (1.8)$$

A similar analysis can be carried out for the specific heat yielding the low temperature behavior for the (quasi-) one-dimensional system with [24]

$$C(T) \approx T^{-\frac{3}{2}} e^{-\Delta/T} \quad \text{for } T \ll \Delta. \quad (1.9)$$

For the two-dimensional model investigated in Chapter 1.6 a similar analysis as in Ref. [24] is performed to obtain the low temperature behavior of the susceptibility and the specific heat.

1.3. Series Extrapolation

The physical quantities under study are computed as truncated series in the appropriate expansion parameter. Suppose $f_n(x)$ to be the truncated series, i.e. a polynomial, of some quantity in the variable x expanded about $x = x_0$ up to order $(x - x_0)^n$. The obtained polynomial $f_n(x)$ represents an approximation of the true function $f(x)$. The approximation is valid in the vicinity of x_0 . It is intended to gain valid results for values of x far away from x_0 . For example, a high temperature series expansion in the inverse temperature β about $\beta = 1/T = 0$ yields precise results for high temperatures but fails for low temperatures which in turn means high values of β . Examination of the radius of convergence R of the series $f_n(x)$ using the formula of Cauchy-Hadamard [25] for the infinite series with

$$R = \liminf_{n \rightarrow \infty} |a_n|^{-1/n}, \quad (1.10)$$

where a_n is the coefficient in n th order, gives a rough estimate where the series will always diverge even for arbitrary high orders in $(x - x_0)$. For instance, the radius of convergence for the high temperature series expansion of the susceptibility $\chi(T)$ is estimated for the frustrated chain in the ungapped phase. It is found that the radius of convergence presented in the inverse temperature is given by $\beta_R \approx 2/J$ which in turn means that the series representation will always fail for temperatures below $T \approx J/2$. Physically interesting properties like the maximum of the susceptibility, which can be used best to determine the model parameters from experimental results, are often outside the radius of convergence. Thus, they are not accessible by the bare truncated series $f_n(x)$. Therefore, an effective extrapolation scheme is necessary to obtain quantitative results outside the radius of convergence. Basically, the extrapolations yield results which are valid also outside the radius of convergence of the truncated series. The basic extrapolation scheme used is the method of Padé approximants furnishing an effective analytic continuation beyond the radius of convergence of the series $f_n(x)$ [26]. The $f[l, m](x)$ Padé approximant to the function $f_n(x) = \sum_{k=0}^n a_k x^k$ is the fraction of the polynomials $P_l(x)$ and $Q_m(x)$ of degree l and m respectively with

$$f[l, m](x) = \frac{P_l(x)}{Q_m(x)} = \frac{p_0 + p_1 x + \dots + p_l x^l}{q_0 + q_1 x + \dots + q_m x^m}, \quad (1.11)$$

where the coefficients of the polynomials are uniquely chosen such that the Taylor expansion of $f[l, m](x)$ agrees with the first $l + m + 1$ series coefficients of $f_n(x)$. Without loss of generality q_0 can be set to unity. For the determination of the coefficients of the polynomials P and Q in floating point arithmetic it is important to ensure that rounding errors do not erode the results. Baker [26] proposed a rule of thumb that one should retain as many significant digits as there are series coefficients. Here, we do not have to consider rounding

errors since fractions of integers are used in the computation of the series coefficients. Thus, the results used in this thesis are exact up to the given expansion order.

It has to be noted that Padé approximants are a powerful tool to extrapolate meromorphic functions, i.e. functions which can be represented as a ratio of analytic functions. Logarithmic singularities which emerge in the calculations for the isotropic Heisenberg chain [3] are not accessible by Padé approximants. This problem can often be circumvented approximately by incorporating the known asymptotics of the computed series. In general, it is possible to bias the extrapolations in the limit for x far away from x_0 , as long as the behavior is known in that limit.

In the following, details of the extrapolation schemes and its extensions used in this thesis are explained. To adapt the explanations to the problems and to the quantities considered in this work it is always assumed that the series expansions are performed in the limit $x = 0$, i.e. $x_0 = 0$. The results are then biased by incorporating additional information in the limit $x \rightarrow \infty$, where x can always be assumed to be positive. For a general investigation of biasing Padé approximant the reader is referred to the literature, see e.g. Ref. [26].

1.3.1. Dlog-Padé Approximants

Even though bare Padé approximants already yield good extrapolations of the truncated series $f_n(x)$ one might also be interested in incorporating additional information. In the limit of infinite x the bare Padé approximant 1.11 can be biased either to a constant value p_l/q_l by using a diagonal representation $l = k$ or to diverge by taking $l > m$ or to vanish for $l < m$. The constraint to use diagonal approximants $[l, l]$ to bias the approximants in the limit $x \rightarrow \infty$ to a constant value p_l/q_l reduces the possible orders of approximants significantly. A first step to circumvent this constraint is using an Euler transformation

$$x = \frac{u}{c - u} \leftrightarrow u = c \frac{x}{1 + x} \quad (1.12)$$

where $c \geq 0$ is an arbitrary but fixed constant. Thereby the complete interval $x \in [0, \infty]$ is mapped to the interval $u \in [0, c]$. This mapping is justified by the continuity of the considered functions in the limit $x \rightarrow \infty$. The extrapolations can now be biased in the limit $u \rightarrow c$ ($x \rightarrow \infty$) to a constant value for arbitrary order $[l, m]$ of the Padé approximant and not only for diagonal approximants $[l, l]$, as mentioned above. Disturbing poles for $u = c$ are unlikely to occur. Singularities inside the physical disc in the complex plane can also be transformed outside the (transformed) disc by the use of Eq. 1.12. The constant c can be chosen such that the approximations are not disturbed by poles inside the physical disc. It turns out that using values of order 1 for c yields stable approximations most of the time. Thus $c = 1$ is used in the following. To complete the analysis of the Euler transformation it has to be remarked that the 1 in the denominator of the term on the right hand side of Eq. 1.12 is arbitrarily chosen. One could also use a constant different from 1. But, this fact does not influence the extrapolations in this thesis and thus is not investigated in more detail.

So far, only bare Padé approximants are considered which are biased to a specific value in the limit $u \rightarrow 1$ ($x \rightarrow \infty$). Suppose we wish to bias the series expansion $f_n(u)$ in the limit

$u \rightarrow 1$ ($x \rightarrow \infty$) to obey a power law of the form

$$f_n(u) \approx (1-u)^\lambda \text{ for } u \rightarrow 1. \quad (1.13)$$

In the general case where λ is not an integer such a power law cannot be expressed by a meromorphic function. Thus, with a bare Padé approximant it is not possible to bias this behavior. However, functions of the form Eq. 1.13 can be transformed into a meromorphic function by taking the logarithmic derivative

$$p_n(u) = \partial_u \ln f_n(u) = \frac{\partial_u f_n(u)}{f_n(u)} = \frac{\lambda}{u-1} (1 + \mathcal{O}(u-1)). \quad (1.14)$$

Obviously, λ is the residual of the logarithmic derivative $p_n(u)$ of $f_n(u)$ at the point $u = 1$. The information of the residual can then be built in by extending the series $p_n(u)$ by one order to $p_{n+1}(u) = p_n(u) + Au^{n+1}$ with the free parameter A which has to be determined by Eq. 1.14.

The approximant $P_m^l(u)$ of the logarithmic derivative $p_n(u)$ of $f_n(u)$ is henceforth called Dlog-Padé approximant. Possible orders of $P_m^l(u)$ have to fulfill $l + m \leq n$. The loss of one piece of information due to the derivative of $f_n(u)$ in Eq. 1.14 is compensated by the extension of the truncated series by one order with the additional parameter A . It has to be noted that this extrapolation technique is only applicable for functions which do not change sign in the considered interval. The truncated series expansion $f_n(x)$ is also assumed to start in zeroth order. Otherwise, the reduced series $\tilde{f}_j(x)$ has to be extrapolated according to

$$f_n(x) = x^k (a_0 + a_1 x + \dots + a_j x^j) = x^k \tilde{f}_j(x). \quad (1.15)$$

Using $\tilde{f}_j(x)$ with $j \neq n$ also affects the maximum order possible in the bare (not extended) Dlog-Padé extrapolation P_m^l with $l + m \leq j - 1$.

Besides a power law it may also occur that it is intended to incorporate an exponential decay in the limit $x \rightarrow \infty$, motivated for instance by the low temperature behavior of the magnetic susceptibility of gapped spin-systems. Dlog-Padé approximants are best suited for incorporating such a behavior. We are interested in extrapolating functions which show an asymptotic behavior of the form

$$f(x) \approx x^\lambda e^{-\Delta x} \quad (1.16)$$

in the limit $x \rightarrow \infty$ where $\Delta > 0$ is the spin gap. A Dlog-Padé representation $f_m^l(x)$ of the truncated series $f_n(x)$ is used with

$$f_m^l(x) = a_0 e^{\int_0^x P_m^l(x') dx'} \quad (1.17)$$

where $P_m^l(x')$ is the Dlog-Padé approximant of $f_n(x')/a_0$. Dividing by the leading coefficient a_0 ensures that the lower integration limit vanishes. By taking the logarithmic derivative one piece of information is lost and thus $l + m \leq n - 1$ has to be fulfilled for $P_m^l(x')$. To bias $f_m^l(x)$ following Eq. 1.16 the behavior of the Dlog-Padé approximant translates to

$$P_m^l(x') = -\Delta + \frac{\lambda}{x'} + \mathcal{O}(x'^{-2}) \quad (1.18)$$

in the limit $x \rightarrow \infty$. The above equation constitutes two additional conditions, namely for Δ and for λ , which can be incorporated in the representation by extending $p_n(x)$ by two orders

$$p_{n+2}(x) = p_n(x) + Ax^{n+1} + Bx^{n+2} . \quad (1.19)$$

Equation 1.18 then determines the free parameters A and B . To make use of the advantages of an Euler transformation the variable x is transformed following Eq. 1.12. The asymptotic behavior from Eq. 1.18 transforms under the Euler transformation to

$$P_m^l(u)|_{u=1} = -\Delta \quad (1.20a)$$

$$\partial_u P_m^l(u)|_{u=1} = -\lambda , \quad (1.20b)$$

where $P_m^l(u)$ is now the Dlog-Padé approximant in the variable u .

In this way, reliable interpolations between the limit of infinite x ($u \rightarrow 1$) and the limit $x = 0$ ($u = 0$) of the series expansion $f_n(x)$ can be obtained for arbitrary orders $[l, m]$. This complies with $l + m = n + 1$ due to the two orders gained by the knowledge of the asymptotic behavior.

To assess the range of validity of the Dlog-Padé approximant various orders of $f_m^l(u)$ are investigated and compared to lower orders or to results from other methods.

The series expansion $f_n(x; p_1, p_2, \dots)$ may also depend on additional parameters p_1, p_2, \dots . To obtain a consistent description within each model various orders of approximants are investigated for various sets of parameters. It is attempted to represent the quantities under study with the same order in the approximant for all sets of parameters. The interplay between the convergence of the extrapolations and their corruption by spurious poles has to be considered carefully. This will be illustrated in the appropriate sections.

1.3.2. Extrapolation in Internal Variable

The extrapolation technique presented in this section is specifically customized to improve the representations of the magnetic specific heat $C(T)$. Various sum rules are known for the specific heat. In this context, the specific heat is represented in an internal variable, namely the energy e , to implement the known sum rules.

The results obtained can be used to represent other thermodynamic quantities like the magnetic susceptibility $\chi(T)$ by the same technique. The main idea is based on the method proposed in Refs. [27, 28]. In Ref. [28] B. Bernu and G. Misguich presented a detailed investigation of an improved representation of the magnetic specific heat. Basically, the specific heat is represented as a function of the new variable $e - e_0$, where e_0 is the ground state energy and $e = e(T)$ is the average energy per site, an increasing function of temperature in the canonical ensemble. To obtain the best description possible all known sum rules are implemented.

To express the specific heat $C(T)$ (per site) in the variable e the entropy $S(T)$ (per site) is considered. Applying the elementary thermodynamic relation

$$\frac{dS(T)}{dT} = \frac{C}{T} \quad (1.21)$$

it follows that

$$S'(e) = \frac{C}{T} \frac{dT}{de} . \quad (1.22)$$

The dependence of the temperature in the specific heat can then be eliminated by

$$C(e) = \frac{de}{dT} = \left(\frac{dT}{de} \right)^{-1} = \left(\frac{d}{de} \frac{1}{S'(e)} \right)^{-1} = -\frac{S'(e)^2}{S''(e)} \quad (1.23)$$

using $S'(e) = 1/T$. $S(e)$ is defined inside the interval $[e_0, e_m]$, where e_m is the energy at infinitely high temperature $\beta = 0$. For the spin-1/2 systems described by the Heisenberg type Hamiltonian 1.1 e_m is the free spin average of the energy at infinite temperature with $e_m = 0$ because $\langle \mathbf{S}_i \mathbf{S}_j \rangle = 0$ holds in this limit. In general, the groundstate energy e_0 is not known exactly for antiferromagnetic models. But it may be taken from methods like high order perturbation theory, exact diagonalization or Monte Carlo simulations.

The entropy $S(e)$ is a function starting at 0 for $e = e_0$ with an infinite slope and reaching the value $\ln 2$ at $e = e_m = 0$, where $\ln 2$ is the entropy per site for a spin-1/2 system at $e = e_m$.

To obtain a series expansion of the entropy $S(e)$ in the vicinity of $e = e_m = 0$ in powers of e up to order n , the high temperature series expansion in the inverse temperature $\beta = 1/T$ of the specific heat $C(T)$ up to order β^n is used. The expansion for the entropy can be computed by solving Eq. 1.23 order by order with the ansatz

$$S(e) = \ln 2 + \sum_{i=2}^n a_i e^i . \quad (1.24)$$

So far, two additional pieces of information are incorporated in the representation of the entropy, the ground state energy e_0 and the sum rule $\int_{T=0}^{\infty} C(T)/T = S(T \rightarrow \infty) - S(T = 0) = \ln 2$. In most cases, the low energy physics is also known and the low energy limit of the specific heat is predictable for the model under consideration. Using this piece of information the extrapolations can be biased additionally to the known behavior in the limit $e \rightarrow e_0$. In the appropriate sections the procedure to incorporate this piece of information is explained in detail.

By using the representation in the internal variable $e - e_0$ a high accuracy can be obtained for the high temperature series expansion of the specific heat even down to zero temperature. The specific heat as function of $e - e_0$ is extrapolated using Padé or Dlog-Padé approximants.

Other thermodynamical quantities like the magnetic susceptibility $\chi(T)$ can also be represented in the variable e with the temperature $T(e)$ as a function of e at hand. The low energy (low temperature) asymptotics can be built-in as it is done for the specific heat. But, no sum rules are known for the susceptibility. Compared to the Dlog-Padé extrapolations explained in Sec. 1.3.1, the representations of the susceptibility in the internal variable e yield in fact no real gain. A detailed comparison is carried out in the appropriate sections.

With the above extrapolation techniques at hand it is possible to obtain results not only for values of x close to the limit of the series expansion but also far away from it. Quantitative

information is accessible beyond the radius of convergence of the series. Besides the calculation of the series expansion itself the extrapolations are a main point of investigation in this thesis. Therefore, each section contains a separate paragraph explaining the model specific implementation of the extrapolation techniques used.

1.4. Dimerized, Frustrated Chain

1.4.1. Introduction

In this section we focus on quasi one-dimensional spin systems. These form a large class comprising dimerized spin chains, strongly frustrated spin chains but also spin ladders (see Sec. 1.5), cf. Fig. 1.2. A representative for a moderately dimerized spin chain is $(\text{VO})_2\text{P}_2\text{O}_7$ [29–31]; a strongly dimerized spin chain realized in $\text{Cu}_2(1,4-\text{C}_5\text{H}_{12}\text{N}_2)_2\text{Cl}_4$ [32–35]; an example for a significantly frustrated spin chain is the spin-Peierls substance CuGeO_3 (see e.g. Ref. [36] and the discussion therein) which is undimerized in its high temperature phase ($T > T_C \approx 14\text{K}$), but weakly dimerized in its low temperature phase. An important spin ladder compound is SrCu_2O_3 [37], which is investigated in detail in Sec. 1.5.

The detailed investigation of the obtained results is completed by the demonstration that it is essentially impossible to deduce from one quantity like the magnetic susceptibility $\chi(T)$ at not too small temperatures alone more than two of the three magnetic couplings of dimerized and frustrated spin chains. This should caution anybody who is analyzing such data in great detail. To illustrate the type of problem one can run into the reader is referred to the analysis of $(\text{VO})_2\text{P}_2\text{O}_7$ which was considered at the very beginning as dimerized chain [38]. Then it was thought to be a two-leg spin-ladder with $J_{\parallel} \approx J_{\perp}$ [39]. But lately unambiguous evidence from inelastic neutron scattering has been found [29] that it is a set of weakly coupled dimerized chains [30, 31], see Fig. 1.1. The magnetic susceptibility $\chi(T)$ is compatible with both scenarios [40].

Exact complete diagonalization (ECD), quantum Monte-Carlo (QMC), and temperature density-matrix renormalization (T-DMRG) will serve as benchmarks to assess the reliability of the method proposed. The ECD and QMC data which are published in parts in Ref. [42] is made available by Ute Löw. The T-DMRG results were obtained by a T-DMRG program put for use by Friedhelm Schönfeld and Rainer Raupach. Thus, no explicit citations are made in the following concerning the external data originating from these methods.

The sections are organized as follows. The next section explains the model, Sec. 1.4.3 deals briefly with the computational details, and Sec. 1.4.2 explains the extrapolation techniques specific to the model. The results are discussed in Sec. 1.4.5 and the conclusion is given in Sec. 1.4.6.

1.4.2. Model

Starting point of the theoretical study is the Hamilton operator

$$H = J \sum_{i=1}^N ((1 + (-1)^i \delta) \mathbf{S}_i \mathbf{S}_{i+1} + \alpha \mathbf{S}_i \mathbf{S}_{i+2}) \quad (1.25)$$

with dimerized nearest and uniform next-nearest neighbor interaction. The dimerization is parameterized by δ . The ratio of nearest and next-nearest neighbor interaction is given by α . The dimerization can arise from chemically different bonds as is the case in $(\text{VO})_2\text{P}_2\text{O}_7$. As can be seen in Fig. 1.1 the alternating chain is realized along the b axis via alternating exchange paths along double V-O-P-O-V and V-O-V links.

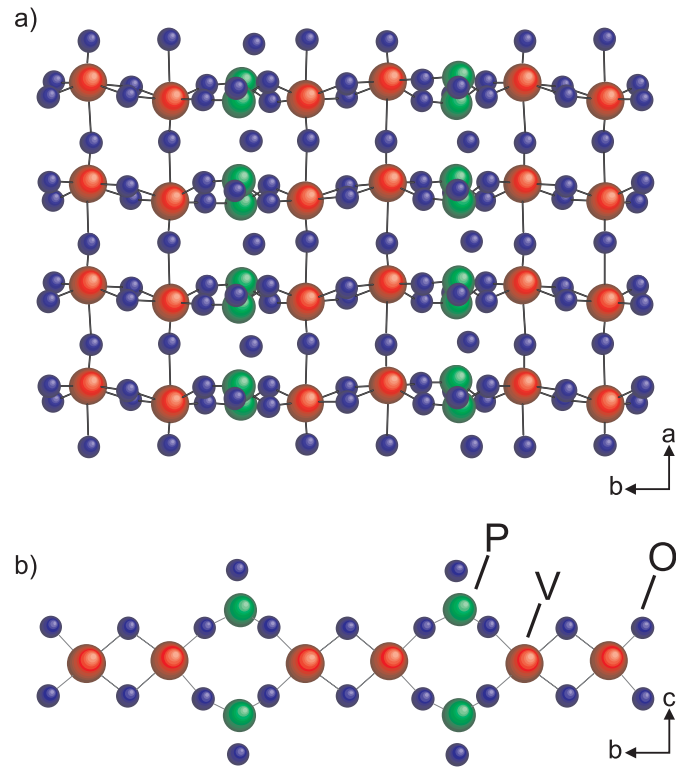


Figure 1.1.: Crystal structure of $(VO)_2P_2O_7$ in the ab and bc plane. In b) the alternating chain along the b axis is shown (picture taken from Ref. [41])

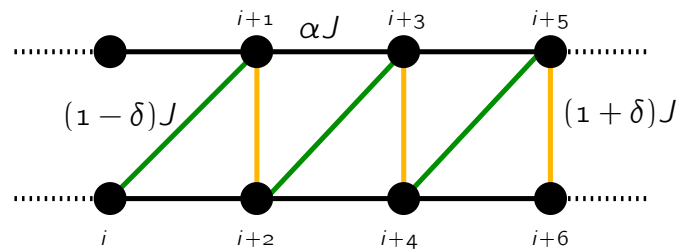


Figure 1.2.: Dimerized and frustrated $S = 1/2$ spin chain. For $\delta = 1$ a two-leg ladder is obtained.

Alternatively, it may be induced by a static lattice distortion via spin-phonon coupling as in $CuGeO_3$. The Hamiltonian can also be viewed as a spin ladder with an extra diagonal coupling $(1 - \delta)J$ (see Fig. 1.2). In the limit $\delta = 1$ it is equivalent to a regular ladder model which is investigated in detail in Sec. 1.5. In the limit $\delta = 1$, $\alpha = 0$ a system of isolated dimers is obtained. The results for the dimerized, frustrated chain can be cross-

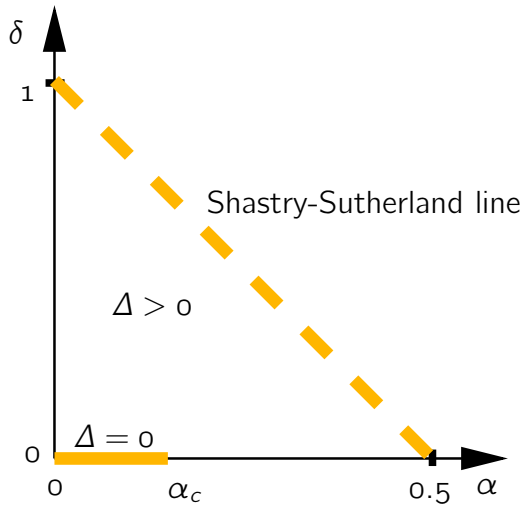


Figure 1.3: Phase diagram of dimerized, frustrated chain characterized by the singlet-triplet gap Δ .

checked in the limit of isolated dimers without frustration, where the system is exactly solvable. Another check is the limit of an isotropic ladder where published results of high temperature series expansions are available [43].

The ground state properties of the model (Eq. 1.25) have been investigated recently in numerous papers, see e.g. [44–51]. Figure 1.3 shows the phase diagram characterized by the singlet-triplet gap Δ . Below the critical value $\alpha_c \approx 0.241$ [52] for the frustration the system is gapless on the $\delta = 0$ line. The Shastry-Sutherland line $2\alpha + \delta = 1$ constitutes the special case, where the ground state is exactly known to be a product of singlets on neighboring spins [53, 54].

1.4.3. Computation

For the computations a system of size $N = 18$ was used. The susceptibility and the specific heat could be expanded up to order 10 in β for the dimerized and frustrated spin chain. The results for the unfrustrated, dimerized spin chain were computed up to order 18 in β using the same system size. For the computation a transformed Hamiltonian (N even) was used with the sum running over all plaquettes (see Fig. 1.2) with

$$H_\lambda = J_0 \sum_{i=0}^{N/2-1} (\mathbf{S}_{2i} \mathbf{S}_{2i+1} + \lambda \mathbf{S}_{2i} \mathbf{S}_{2i-1} + \alpha_0 [\mathbf{S}_{2i-1} \mathbf{S}_{2i+1} + \mathbf{S}_{2i} \mathbf{S}_{2i-2}]) . \quad (1.26)$$

To obtain H_λ the following parameters were substituted in the Hamiltonian from Eq. 1.25

$$J_0 = J(1 + \delta) \quad (1.27a)$$

$$\lambda = \frac{1 - \delta}{1 + \delta} \quad (1.27b)$$

$$\alpha_0 = \frac{\alpha}{1 + \delta} . \quad (1.27c)$$

In earlier calculations for the frustrated Heisenberg chain the moment-algorithm [20, 21] was used. Here, it became evident that the construction of the complete Hilbert space of dimension $2^{18} = 262144$ was more efficient. With each base state containing a polynomial in the two variables λ and α_0 the maximum number of coefficients to be kept in memory could be reduced by employing the condition

$$a_{k,l,n} \lambda^k \alpha_0^l \beta^n \leftrightarrow k + l \leq n. \quad (1.28)$$

The indices denote the exponents of the given parameters. This condition accounts for the allowed processes in each order n of expansion. The sum between nearest-neighbor processes (accounted for by λJ and J) and next-nearest neighbor processes ($\alpha_0 J$) is always n . Hence, the condition 1.28 translates to a reduction from $(n+1)^2$ coefficients in the general case of a n th order polynomial in two variables to $(n+1)(n+2)/2$ coefficients in n th order for the actual problem. The coefficients themselves were stored as integers of type `long long int`. It has to be noted that the program has to be checked dynamically for overflows in the coefficients. Using the integer type `long long int` only numbers up to ± 1073741824 can be accessed correctly. Due to the multiple multiplications which have to be performed the range of this variable type was almost fully exploited. Thus, a careful check has to be implemented whether the results are in the range of this type of variable or not. The system itself is not able to check for such overflows. As will be mentioned in Sec. 1.5 this variable type is no longer sufficient for slightly bigger system sizes. Due to the translational invariance of the system it was sufficient to use the reduced squared magnetization

$$M^2 = \sum_{i=1}^N S_1^z S_i^z \quad (1.29)$$

in the calculations. This reduces the number of calculations which need to be performed when incorporating the magnetization from N^2 to N .

By the use of periodic boundary conditions in the calculations different wrap-around effects occurred as explained in detail for the frustrated chain [20, 21]. Processes are calculated in the finite system which do not contribute in the infinite system. These artificial contributions have to be corrected by hand. Here, the affected terms are explained below for the calculations of a system of size $N = 2n - 2$, where n is the maximal order of expansion for the dimerized, frustrated chain where the wrap around effects can be corrected by hand. For the dimerized system the maximal order which can be obtained is N . The contributions of the given wrap-around effects are listed separately for the numerator and denominator for the calculations of the magnetic susceptibility and specific heat respectively, see Eqs. 1.2, 1.6. To obtain the correct results in the given order these terms have to be subtracted from the computed results. The following terms are affected, where the bold links in the pictures depict the processes yielding a wrap around effect. Open bold links denote the periodic boundary conditions. The pictures should only serve as an illustration. Below the pictures the multiplicity of the wrap-around effect is denoted.

i. $\alpha^{n-1} \beta^{n-1}$

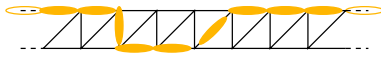


2 chains of length $n - 1$

$$C_{\text{denominator}}^i = 2 \cdot 3 \left(\frac{1}{4}\right)^{n-1} 2^N (n-1)! \quad (1.30a)$$

$$C_{\text{numerator}}^i = - \left(-3 \cdot 2 + 2 + \frac{8}{3!} \right) \left(\frac{1}{4}\right)^n 2^N (n-1)! \quad (1.30b)$$

The contributions to the numerator split into three parts. The first part in Eq. 1.30b accounts for the S^z components of the squared magnetization acting on the same site, where the factor of 2 accounts for the two possibilities to arrange the chains wrapping around. The second addend originates from the terms which contribute in the infinite system but have not been calculated in the finite system. The last addend keeps track of sites which are threefold occupied by a spin operator. The latter contributions need not be multiplied with a factor of two, since the two possibilities of chains wrapping around cannot be seen independently from each other when evaluating these specific contributions. The explicit calculations leading to these terms are explained in detail in Refs. [20, 21]. It has to be mentioned that the result for the given term $\alpha^{n-1}\beta^{n-1}$ is already known from Refs. [20, 21] but here the corrections are given explicitly for a better understanding.

ii. $\lambda \alpha^{n-2} \beta^n$ 
 n^2 chains of length n .

$$C_{\text{denominator}}^{\text{ii.}} = n^2 \cdot 3 \left(\frac{1}{4}\right)^n 2^N n! \quad (1.30c)$$

$$C_{\text{numerator}}^{\text{ii.}} = - \left(-3 \cdot n^2 + \left(\frac{n(n-1)}{2}\right) \left(2 + \frac{8}{3!}\right) \right) \left(\frac{1}{4}\right)^{n+1} 2^N n! \quad (1.30d)$$

For the contributions to the denominator the same arguments as for the above contributions hold. The first addend has a multiplicity of n^2 , whereas the last two addends contribute only with a multiplicity of $(n-1) + (n-2) + \dots + 1 = n(n-1)/2$.

iii. $\alpha^{n-1} \beta^n$ Result known

iv. $\alpha^n \beta^n$ Result known

Thus, in the first two cases the corrections are similar to the results given in Refs. [20, 21] by identifying the connected chains. The last two terms need not be corrected, since the exact results are known from Refs. [20, 21].

For the dimerized system only the following term $\lambda^{N/2} \beta^N$ is affected in order N of the expansion

v. $\lambda^{N/2} \beta^N$ 
 1 chain of length N

$$C_{\text{denominator}}^{\text{v.}} = 3 \left(\frac{1}{4}\right)^N 2^N N! \quad (1.30e)$$

$$C_{\text{numerator}}^{\text{v.}} = - \left(-3 + 2 + \frac{8}{3!}\right) \left(\frac{1}{4}\right)^{N+1} 2^N N! \quad (1.30f)$$

These are exactly the same corrections as explained in Refs. [20, 21], where the occurring wrap around effect is fully described by the picture.

With the use of a minimal system size in the calculations the correct results in the infinite system are given by identifying the occurring wrap-around effects and evaluating their corrections.

1.4.4. Extrapolation

With the truncated series up to order 10 for the dimerized, frustrated chain and up to order 18 in β for the dimerized chain at hand the extrapolation schemes explained in Sec. 1.3 are employed here. In the following paragraphs the extrapolation schemes for the specific heat and the susceptibility adapted to the model under consideration are investigated.

Specific heat In a first step the extrapolation scheme in the internal variable following Sec. 1.3.2 is adapted and compared to the results which can be obtained by Dlog-Padé extrapolations, see Sec. 1.3.1.

In the case that the system is in the gapless phase i.e. $\delta = 0$ and $\alpha \leq \alpha_c$ the low temperature asymptotics is known to be

$$C(T) = \frac{T}{3} + \mathcal{O}(T^2) \quad \text{for } T \ll 1. \quad (1.31)$$

From the linear behavior of the dispersion $\omega(k) \propto k$ in one dimension this follows for the isotropic chain with $\delta = 0$ and $\alpha = 0$ [55]. The linear behavior in T of the specific heat is also valid for values of the frustration $0 \leq \alpha < \alpha_c$, where the elementary excitations can still be described by asymptotically free spinons.

At the isotropic point the ground state energy $e_0 = -\ln 2 + 1/4$ [2] is exactly known whereas for values $\alpha > 0$ results of a high order series expansion about the limit of isolated dimers [51] is used.

Considering the sum rule

$$e - e_0 = \int_0^T C(T') dT' \approx T^2 \quad \rightarrow \quad T(e) \approx \sqrt{e - e_0} \quad (1.32)$$

yields the temperature as a function of energy $T(e)$. Substituting the temperature function into the sum rule for the entropy leads to

$$S(T(e)) = \int_0^T \frac{C(T')}{T'} dT' \approx T(e) \approx \sqrt{e - e_0}. \quad (1.33)$$

To avoid the square-root singularity at $e = e_0$ for $S(e)$ the function

$$G(e) = \frac{S'(e)}{S(e)}(e - e_0) \quad (1.34)$$

is extrapolated requiring $G(e)|_{e=e_0} = 1/2$. The entropy is finally given by

$$S(e) = \ln 2 \exp \left(\int_0^e \frac{\tilde{G}(e')}{e' - e_0} de' \right), \quad (1.35)$$

where \tilde{G} is the Padé extrapolation of G .

For the gapped phase of the system the low temperature information from Eq. 1.9 is incorporated considering the sum rule

$$e - e_0 = \int_0^T C(T') dT' \approx AT^{\frac{1}{2}} e^{-\frac{\Delta}{T}} \quad (1.36)$$

in the limit $T \ll \Delta$ with the excitation gap Δ . Only the leading order contribution in T is taken into account, higher orders in T are neglected; A is a constant factor. Inverting the above equation provides an implicit expression for $T(e - e_0)$ with

$$\ln \left(\frac{e - e_0}{A} \right) = \frac{1}{2} \ln T - \frac{\Delta}{T}. \quad (1.37)$$

Only an approximate solution is possible, because Eq. 1.37 cannot be inverted analytically. In a first iteration step the addend $1/2 \ln T$ in Eq. 1.37 is neglected leading to

$$T_1 = \frac{-\Delta}{\ln \left(\frac{y}{A} \right)} \quad (1.38a)$$

with $y = e - e_0$. Inserting T_1 in a further iteration step yields

$$T_2 = \frac{-\Delta}{\ln \left(\frac{y}{A} \right) - \frac{1}{2} \ln T_1} = \frac{-\Delta}{\ln \left(\frac{y}{A} \right) - \frac{1}{2} \ln \frac{-\Delta}{\ln \left(\frac{y}{A} \right)}}. \quad (1.38b)$$

Obviously, further iteration steps lead to logarithmic functions of logarithmic arguments. Their contributions become less important with increasing number of steps of iteration. Neglecting those emerging multiple-logarithmic functions in Eqs. 1.38 yields the approximate solution for T

$$T(y) \approx -\frac{\Delta}{\ln(y)} \quad \text{for } y \ll 1. \quad (1.39)$$

Combining Eqs. 1.36, 1.9, and the following sum rule

$$S = \int_0^T \frac{C(T')}{T'} dT' \approx AT^{-\frac{1}{2}} e^{-\frac{\Delta}{T}} \quad \text{for } T \ll \Delta \quad (1.40)$$

yields the low temperature behavior of the entropy

$$S(y) \approx -\frac{y}{\Delta} \ln(y) \quad \text{for } y \ll 1. \quad (1.41)$$

The logarithmic singularity at $e = e_0$ ($y = 0$) can be described best by extrapolating the function

$$G(y) = y \partial_y \frac{S(y)}{y}. \quad (1.42)$$

The value of the gap Δ is incorporated by requiring

$$G(y = 0) = -\frac{1}{\Delta}. \quad (1.43)$$

The value of Δ is taken from the explicit $T = 0$ calculation in Ref. [51]. It is used to stabilize the extrapolation procedure. This constitutes an extension of the procedure applied in Ref. [28]. There, Eq. 1.43 is exploited to estimate the gap Δ . Here, the value of the gap is built in explicitly.

Finally, the entropy is given by

$$S(e) = (e - e_0) \left(\int_0^e \frac{\tilde{G}(e')}{e' - e_0} de' - \frac{\ln 2}{e_0} \right), \quad (1.44)$$

where \tilde{G} is the Padé extrapolation of G .

The specific heat can also be extrapolated by biased Dlog-Padé extrapolations in the Euler-transformed variable u as described in Sec. 1.3.1. For the gapped phase Eq. 1.9 translates to

$$P_l^k(u)|_{u=1} = -\Delta \quad (1.45)$$

$$\partial_u P_l^k(u)|_{u=1} = \frac{1}{2}, \quad (1.46)$$

where $P_l^k(u)$ denote the Dlog-Padé approximants in the variable u of order $[k, l]$. These two equations determine the two additional parameters extending the obtained series by two orders. In Fig. 1.4 the different extrapolation schemes are compared.

The biased Dlog extrapolation in u does not fulfill the low temperature behavior properly for temperatures $0.1 \lesssim T/J \lesssim 0.4$ (see upper left panel). Even though the linear behavior for low temperatures is reproduced the specific heat is slightly overestimated in the temperature regime mentioned above. The position and height of the maximum is represented correctly. The information used in this representation is not sufficient for temperatures below the maximum, whereas the extrapolations in the internal variable yield very good results even down to zero temperature. This is shown in the left panel by comparing to the exactly known result. To get an impression of the accuracy in the difficult test case of the isotropic chain the extrapolations are compared to each other for the appropriate extrapolations (see panels on right hand side). Here, the diagonal extrapolations $[n, n]$ yield the best convergence for increasing order n , whereas the other extrapolations e.g. show increasing

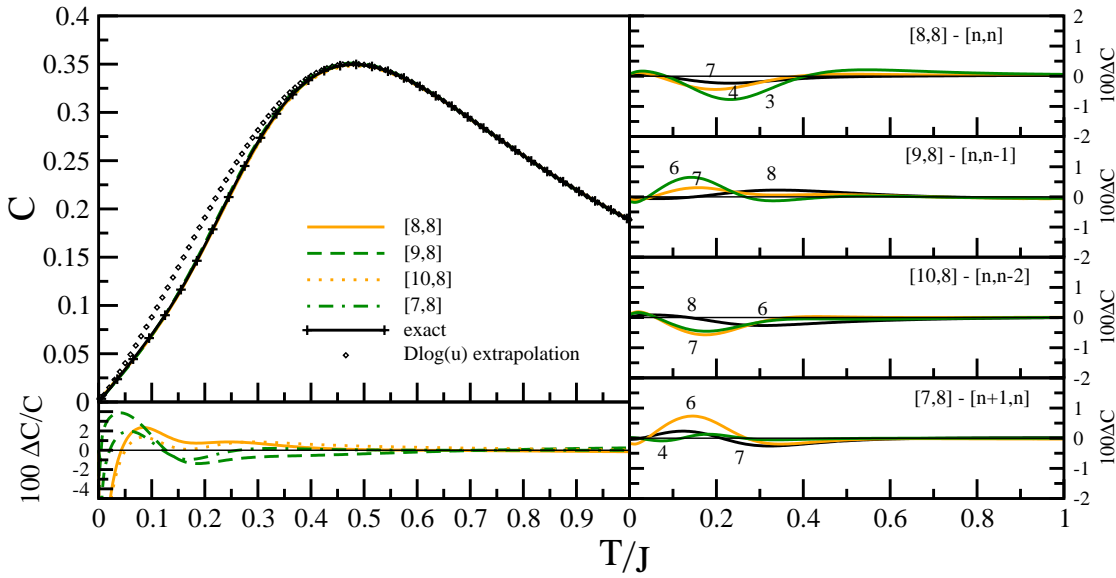


Figure 1.4.: Left side: extrapolations of the specific heat C of the isotropic chain compared to the exact result [3]. The extrapolations in the energy e cannot be discerned in the upper panel. Right side: absolute differences between various extrapolations.

deviations for increasing order n at $T \approx 0.4J$. Thus, the diagonal extrapolations are used in the following.

The lower left panel shows the relative difference of the highest orders available of the various extrapolations to the exactly known result from Ref. [3]. The relative difference between the exact result and the [8, 8] extrapolation is of order 1%-2%. This estimation seems to be more realistic than the one given in Ref. [28] with a relative error of only 0.1%.

Susceptibility With the temperature as function of e at hand it is possible to represent also the susceptibility as function of e . The low temperature behavior from Eq. 1.8 can also be incorporated in the extrapolations. Considering the sum rule from Eq. 1.36 and the low temperature behavior of $4T\chi(T)$ [24] for the gapped system with

$$4T\chi(T) \approx T^{\frac{1}{2}} e^{-\frac{\Delta}{T}} \quad \text{for } T \ll \Delta \quad (1.47)$$

leads to an approximate description of the susceptibility for energies close to the ground state energy e_0

$$y = e - e_0 \approx T^{\frac{1}{2}} e^{-\frac{\Delta}{T}} \approx 4T\chi(T) \quad \text{for } y \ll 1. \quad (1.48)$$

To incorporate the linear behavior of $\chi(e)$ in e for energies close to the ground state energy a Dlog-Padé extrapolation is used, where the residual of 1 is built in explicitly, for details see Sec. 1.3.1.

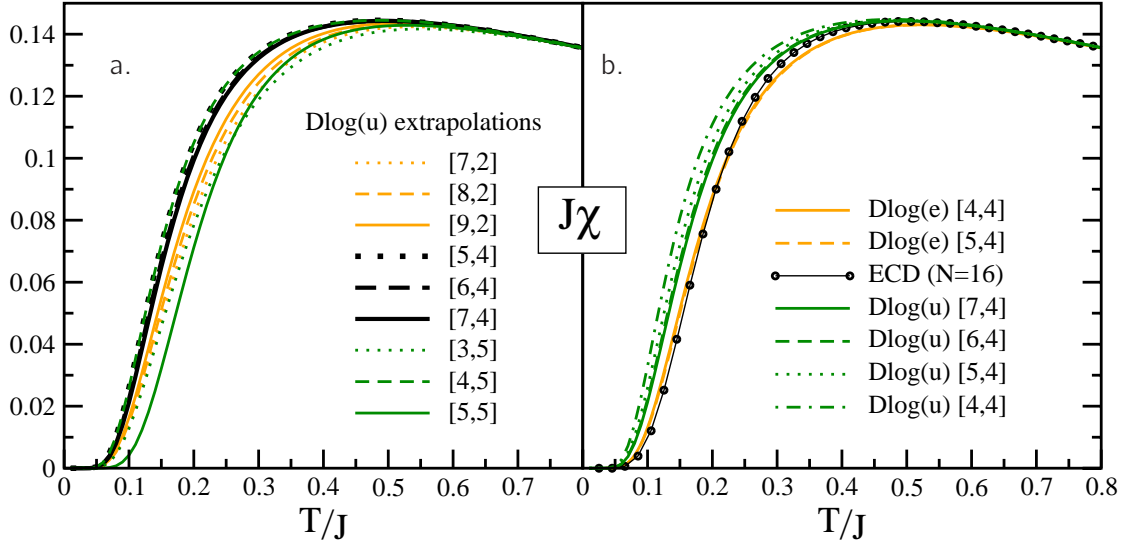


Figure 1.5.: a. Dlog(u) extrapolations of the susceptibility for $\delta = 0.1$ and $\alpha = 0.36$.
 b. Dlog(u) and Dlog(e) extrapolations compared to ECD result for $\delta = 0.1$ and $\alpha = 0.36$.

In Fig. 1.5 various extrapolations are shown. In the left plot (a.) various Dlog-Padé extrapolations in the Euler transformed variable u are presented for $\alpha = 0.36$ and $\delta = 0.1$. The extrapolations follow the procedure explained in Sec. 1.3.1. The low temperature information is built in using the relations

$$P_l^k(u) \Big|_{u=1} = -\Delta \quad (1.49a)$$

$$\partial_u P_l^k(u) \Big|_{u=1} = 1/2, \quad (1.49b)$$

where the value of the gap Δ is taken from Ref. [51].

For fixed order l of P_l^k the Dlog-Padé extrapolation of χ moves for $l = 2$ upwards, for $l = 4$ downwards and for $l = 5$ in both directions (for $l = 3$ no evaluation is possible due to defective extrapolations in all orders). All representations converge for increasing orders meaning that on the one hand for increasing orders the coincidence between successive orders reaches lower temperatures and on the other hand the overall difference between successive orders decreases. The $[5, 4]$ and $[4, 5]$ extrapolations cannot be distinguished. But this is not a general feature. Other reflected extrapolations of the type $[k, l]$ and $[l, k]$ yield substantially differing results. The $[6, 5]$ extrapolation is not possible due to spurious poles. In order to decide for the optimal extrapolation the $[n, 4]$ extrapolations are used because their convergence is the best compared to the convergence of the extrapolations $[n, 2]$ and $[n, 5]$. The convergence does not change significantly for other sets of parameters.

The plot on the right hand side (b.) compares exemplary the chosen Dlog-Padé extrapolations in u (Dlog(u)) and in the energy e (Dlog(e)) with the result obtained by ECD calculations for the same set of parameters, namely $\alpha = 0.36$ and $\delta = 0.1$. The extrapolation in the energy seems to underestimate the susceptibility already at temperatures close to the position of the maximum of χ , whereas the Dlog(u) extrapolations converge nicely with increasing order. The extrapolations in e describe the low energy (low temperature) regime better than the representation in u does. But the sum rules implicitly built-in in the extrapolations in e also affect higher energies (higher temperatures) such that the continuation between the calculated results for high energies and the low energy behavior somehow influences the higher energy regime too much. This leads to representations where already the height and position of the maximum of the susceptibility is not sufficiently described. The following investigations will focus the position and the height of the maximum of the susceptibility which is accessible experimentally in most cases when the magnetic exchange coupling is not too large. Thus, the Dlog(u) representation is used throughout this chapter yielding the best extrapolations in the temperature regime of the maximum and below as described above. In order to present our results in a systematic and unbiased way we choose the P_4^m representation for all curves shown below (if not denoted otherwise). Deduced from Fig. 1.5 one expects quantitatively reliable results down to $T \approx 0.25J$ for the dimerized, frustrated chain. This conclusion is based on considering the highest orders and comparing the range of T/J where successive orders coincide.

It is in order to compare the procedure used here to deal with gapped spin systems with another closely related one proposed by Elstner and Singh [35]. These authors perform a cluster expansion in the weak couplings, i.e. they compute the susceptibility on small clusters exactly. The results obtained are exact up to 8th order in the weak bonds. For large dimerization this approach works very well since the results are reliable without extrapolation. But for smaller dimerization, i.e. smaller gaps, the method proposed here works much better since one is able to include a much better value for the energy gap via Eq. 1.49. This is possible because the value of the gap itself can be obtained by careful extrapolation. Only for very small values of the dimerization ($\delta < 3\%$) the values of the gap become less reliable. In any case, the susceptibility $\chi(T)$ at moderate to higher temperatures is very little affected by small inaccuracies in Δ .

1.4.5. Results

Magnetic Susceptibility

Applicability of the High Temperature Series Expansion In the purely dimerized case ($\alpha = 0$), see Fig. 1.6, almost the whole temperature regime is excellently described. This is due to the high orders reached ($\mathcal{O}(\beta^{18})$). In Fig. 1.6, the HTSE results are depicted in comparison to results from numerical methods (ECD, QMC) and the exact result of the uniform chain [3]. In particular, the agreement between the HTSE result and the exact one for the uniform chain is impressive. We think that this is the optimum which can be obtained by high temperature expansion since it is certainly not possible to assess the logarithmic low temperature corrections coming from the high temperature end. Technically, the obvious

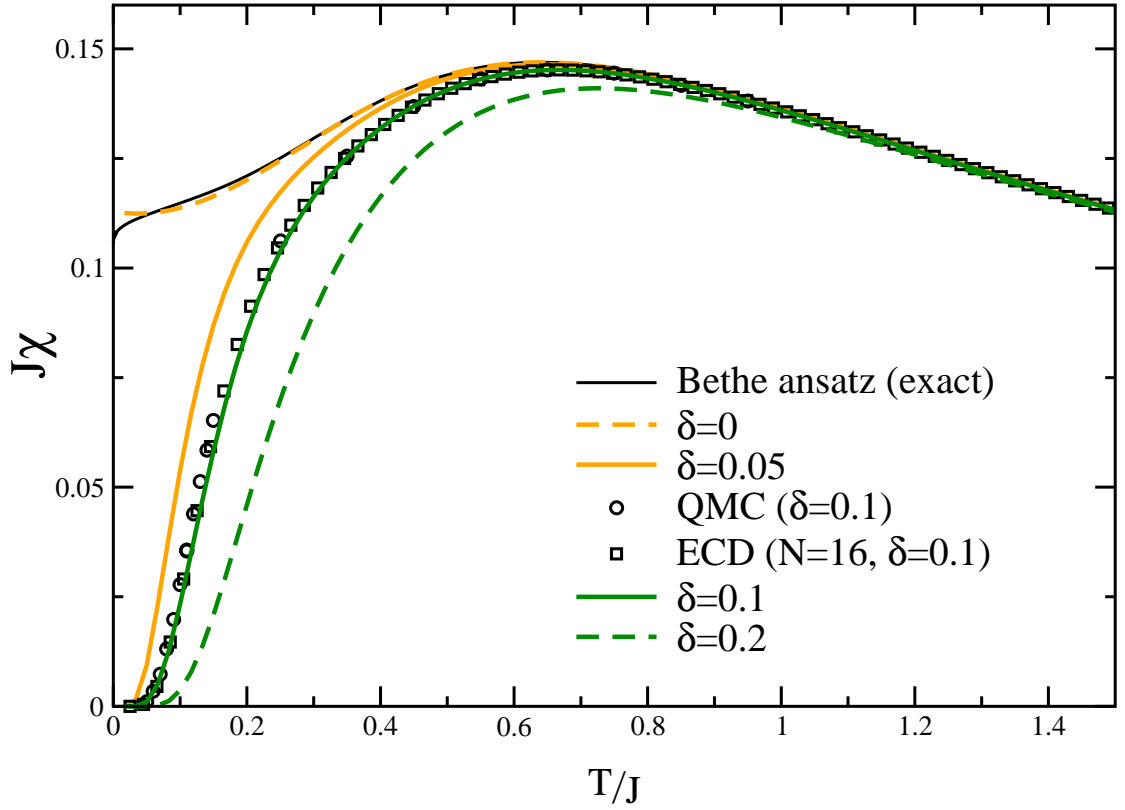


Figure 1.6.: Susceptibility of the dimerized chain for various values of δ . The Dlog-Padé extrapolations are of order $[15, 4]$

relations

$$P_f^k(u) \Big|_{u=1} = 0 \quad (1.50a)$$

$$\partial_u P_f^k(u) \Big|_{u=1} = 1 \quad (1.50b)$$

were used for the uniform chain instead of (1.49). The second relation (1.50b) reflects the fact that $\chi(T=0)$ is finite.

In Fig. 1.7 the $[7, 4]$ HTSE representation chosen is compared to exact complete diagonalization and temperature density-matrix renormalization data [56]. The results are in very good accordance with one another. Only in the regime $T/J < 0.2$ is there a slight difference between the HTSE representation and the numerical results.

In Fig. 1.9 the susceptibilities for various sets of parameters are shown. The behavior of the maximum of the susceptibility depends upon the parameters under study. For fixed next-nearest neighbor interaction α the position of the maximum moves to higher values of T/J for increasing δ while the maximum value decreases. These effects are induced by the increasing gap [7].

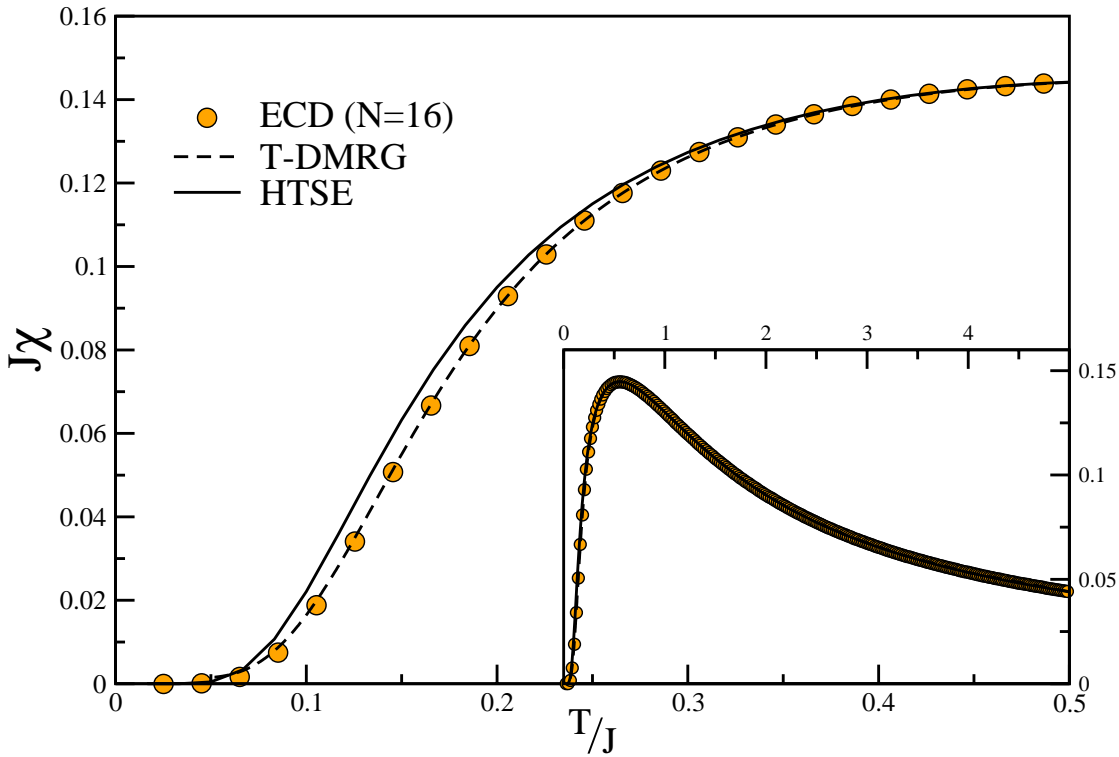


Figure 1.7.: Comparison of high temperature series expansion, exact complete diagonalization and temperature density-matrix renormalization data for $\alpha = 0.24$ and $\delta = 0.1$.

Fixing δ , the position of the maximum moves to lower temperatures for increasing α . This can be understood from the reduction of the dispersion on increasing frustration, as depicted in Fig. 1.8. The mobility of the excitations is more and more restricted [45, 46, 51]. The maximum value of $\chi(T)$ remains almost constant. This can be seen as the result of a compensation of two contrary effects. On the one hand, the susceptibility rises due to the shift of the maximum position to lower temperatures where the global $1/T$ factor (cf. (1.2)) enhances its value. But on the other hand, the frustration provides an additional antiferromagnetic coupling in the system which works against an alignment of the spins. For instance, the antiferromagnetic next-nearest neighbor coupling induces a strong repulsion between aligned adjacent triplets on the dimers [45, 46, 51].

Information Content In this paragraph the question is addressed to which extent the parameters of the model in Eq. 1.25 can be extracted from measurements of the susceptibility. In other words, the experimentalist's point of view is adopted who wants to determine the coupling parameters from experimental data. Obviously, the main feature in the susceptibility curve is the maximum. So it is natural to use in the first place the

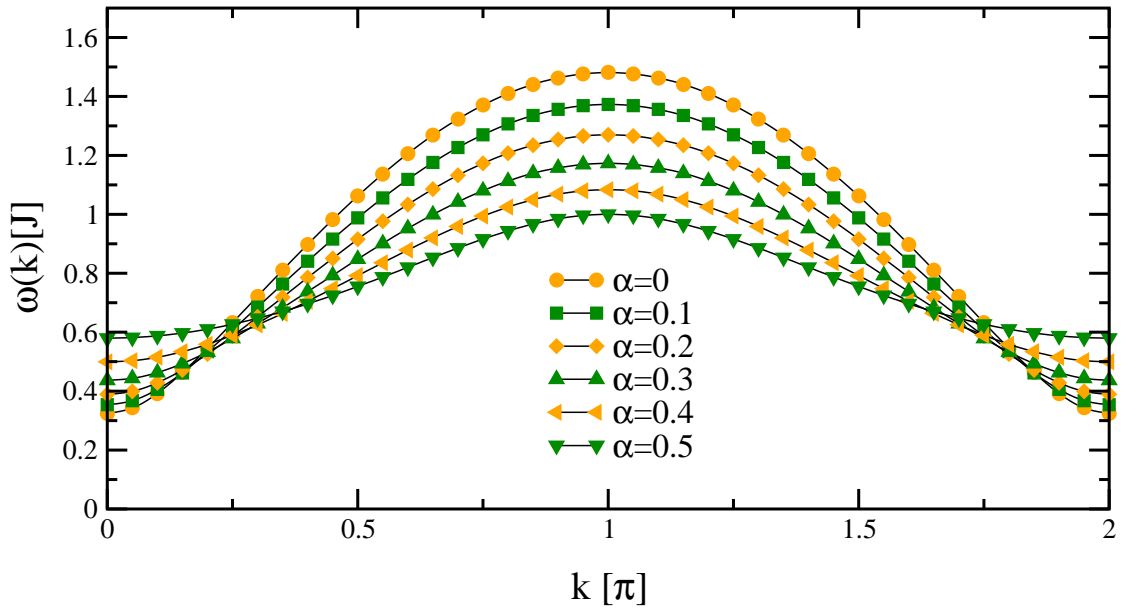


Figure 1.8.: Triplet dispersion of the dimerized, frustrated spin chain for fixed dimerization $\delta = 0.1$ and increasing frustration $\alpha = 0, 0.1, 0.2, 0.3, 0.4, 0.5$: the results are obtained by a high order series expansion about the limit of isolated dimers [57, 58].

maximum value χ_{\max} and its position $T = T_{\max}$. The product $\chi_{\max} T_{\max}$ is considered since it is experimentally easily accessible and does not depend on the exchange coupling J .

The HTSE data (lines) shown in Fig. 1.10 are compared to ECD results (circles) performed on a 16 site system. Due to spurious poles occurring within the $[7, 4]$ Dlog-Padé extrapolations $[9, 2]$ extrapolations were used instead highlighted through dark grey lines in the figure. The accuracy compared to the $[7, 4]$ extrapolation is conserved because the $[9, 2]$ extrapolations are used only for high values of the dimerization $\delta \gtrsim 0.4$, where the system is sufficiently gapped and thus well described by the used HTSE extrapolation even down to zero temperature for not too high values of α .

For high values of the frustration $\alpha \gtrsim 0.5$ and low values of the dimerization $\delta \lesssim 0.1$ small differences between the ECD and HTSE results occur. These effects result from finite size effects of several percent specific to the ECD calculations in this parameter regime and also from inaccuracies in the HTSE extrapolations due to the position of the maximum at low temperatures (see discussion above). The exactly known points (filled circles) for $\alpha = 0$ and $\delta = 0, 1$ are reproduced perfectly by both methods.

Note that for $\delta = 0$ the quantity $\chi_{\max} T_{\max}$ reaches its minimum at $\alpha \approx 0.36$ and then starts to increase again. The general behavior that the quantity $\chi_{\max} T_{\max}$ at $\delta = 0$ decreases and then starts to increase again is due to the fact, that on growing α the system approaches two independent chains of half the size of the original chain with $\alpha = 0$. Figure 1.10 can

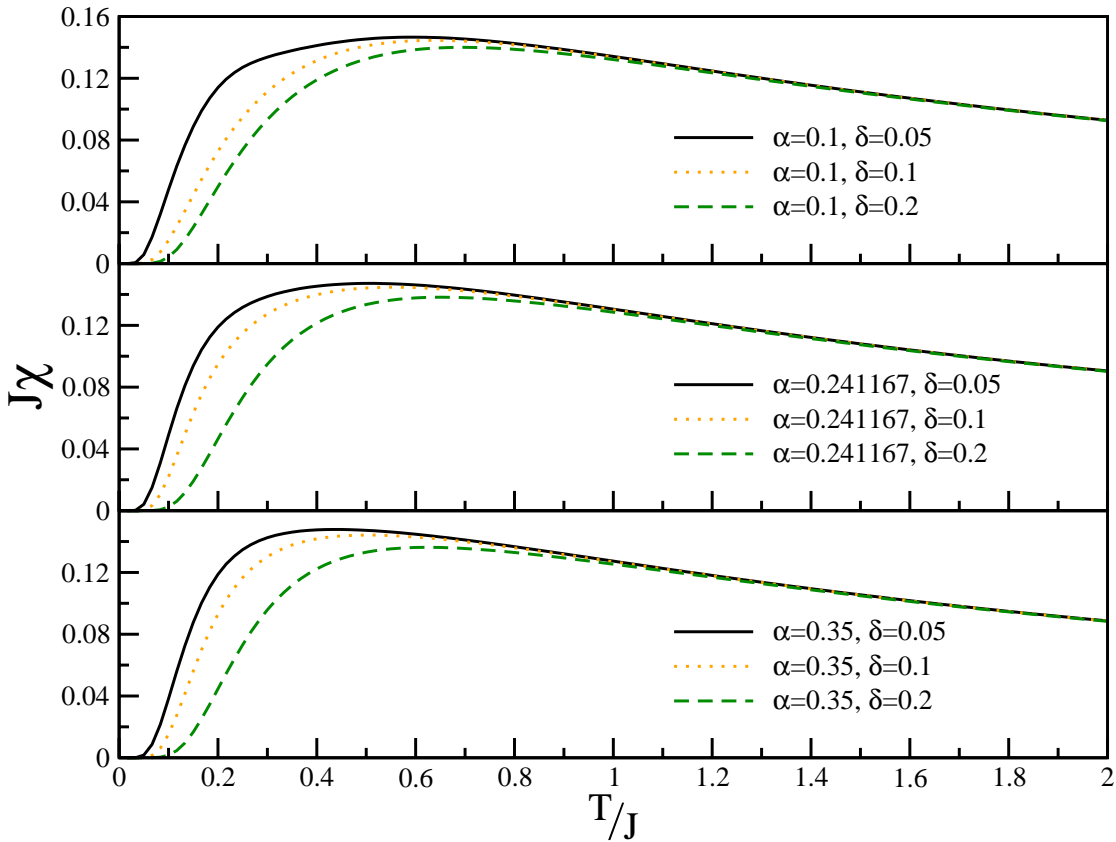


Figure 1.9.: Susceptibility for various values of δ and α : The susceptibility is represented using $[7, 4]$ extrapolation except for the solid line in the uppermost panel where the $[7, 4]$ extrapolation is defective and the $[8, 3]$ extrapolation is used.

be used easily: given the experimental input for $\chi_{\max} T_{\max}$ one can read off the value for δ for a chosen α .

To complete the analysis the variable J/T_{\max} is plotted in Fig. 1.11 as a function of δ for various values of α . So, once the value of δ (for given α) is determined from Fig. 1.10, Fig. 1.11 helps to determine the exchange coupling J by reading off J/T_{\max} and multiplying by T_{\max} . The HTSE results (lines) are compared also to the ECD results (circles). The discrepancy between the two methods for $\alpha \geq 0.5$ and $\delta \leq 0.1$ is of same origin as discussed above for the quantity $\chi_{\max} T_{\max}$. The low lying maximum of the susceptibility in this parameter regime leads to inaccuracies in the HTSE extrapolations and the ECD results suffer from finite size effects.

It has to be pointed out that it is almost impossible to determine the values of J , α and δ from the temperature dependence of the susceptibility alone (cf. also Ref. [59]). This phenomenon is well known from the investigations of $(\text{VO})_2\text{P}_2\text{O}_7$. In the case of this substance the susceptibility of the isotropic ladder i.e. a ladder with $J_{\parallel} = J_{\perp}$ and

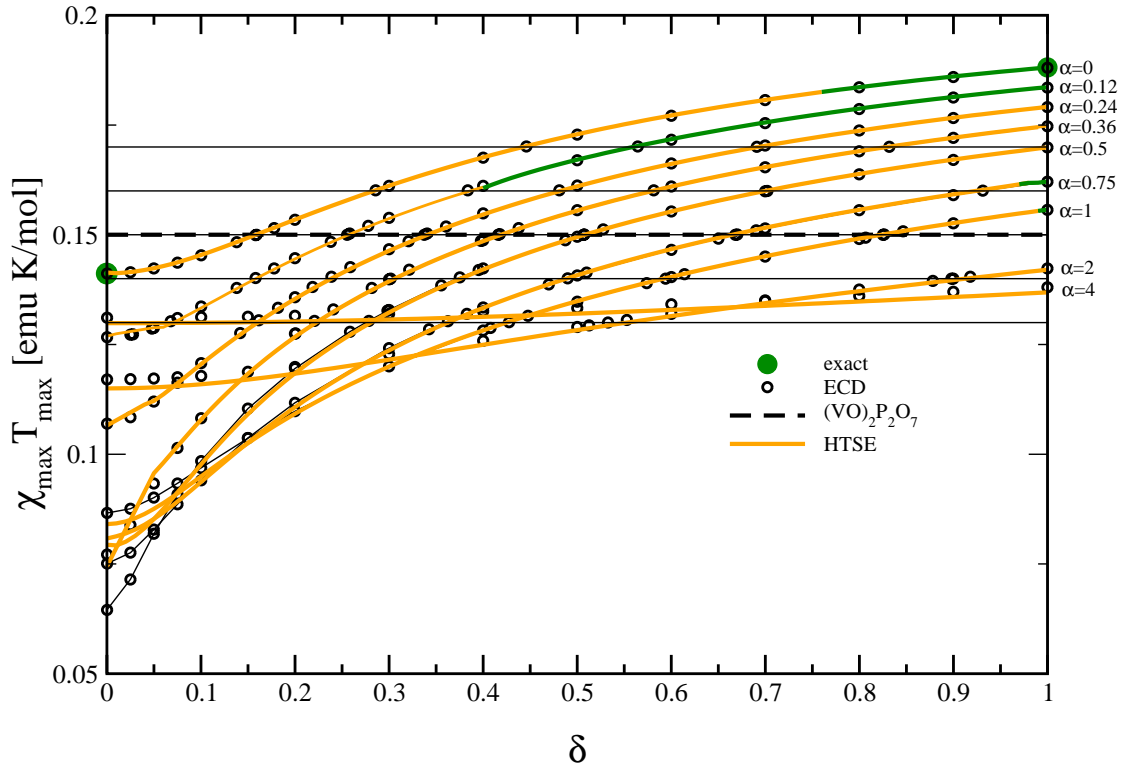


Figure 1.10.: $\chi_{\max} T_{\max}$ versus δ for $\alpha = 0.0, 0.12, 0.24, 0.36, 0.50, 0.75, 1.0, 2.0$ and 4.0 (in descending order at the right side of the graph, i.e. $\delta = 1.0$). The symbols are obtained by ECD calculations. For illustration, the dashed line refers to the experimental value of $(VO)_2P_2O_7$ [30].

the susceptibility of a dimerized spin chain with $\delta = 0.2$ fit both the experimental data equally well. For illustration the possible results for $(VO)_2P_2O_7$, where $\chi_{\max} = 2.07 \cdot 10^{-3}$ emu/mol V and $T_{\max} = 74K$ correspond to the horizontal dashed line at 0.15 emu K/mol V in Fig. 1.10. The difficulty to distinguish different sets of (J, δ, α) yielding the same value of $\chi_{\max} T_{\max}$ is visualized strikingly in Fig. 1.12. The re-scaled susceptibilities belonging to various values of $\chi_{\max} T_{\max}$ are depicted. In the temperature region around the maxima and for larger temperatures the differences within each set are minute. This fact leads to the conclusion that it is impossible to determine all three coupling parameters from $\chi(T)$ at moderate and at large values of temperature alone. With the precise knowledge of low temperature quantities like the spin gap Δ the problem of determining a unique parameter set for a given substance can be solved. But it has to be mentioned that also in the low temperature regime disturbing effects exist hampering the determination of the model parameters. For a detailed discussion see below. In Fig. 1.13 the values of α and δ are shown which belong to the various sets displayed in Fig. 1.12 (connected filled circles). It should be added that the precise value of the gyromagnetic ratio g is assumed to be

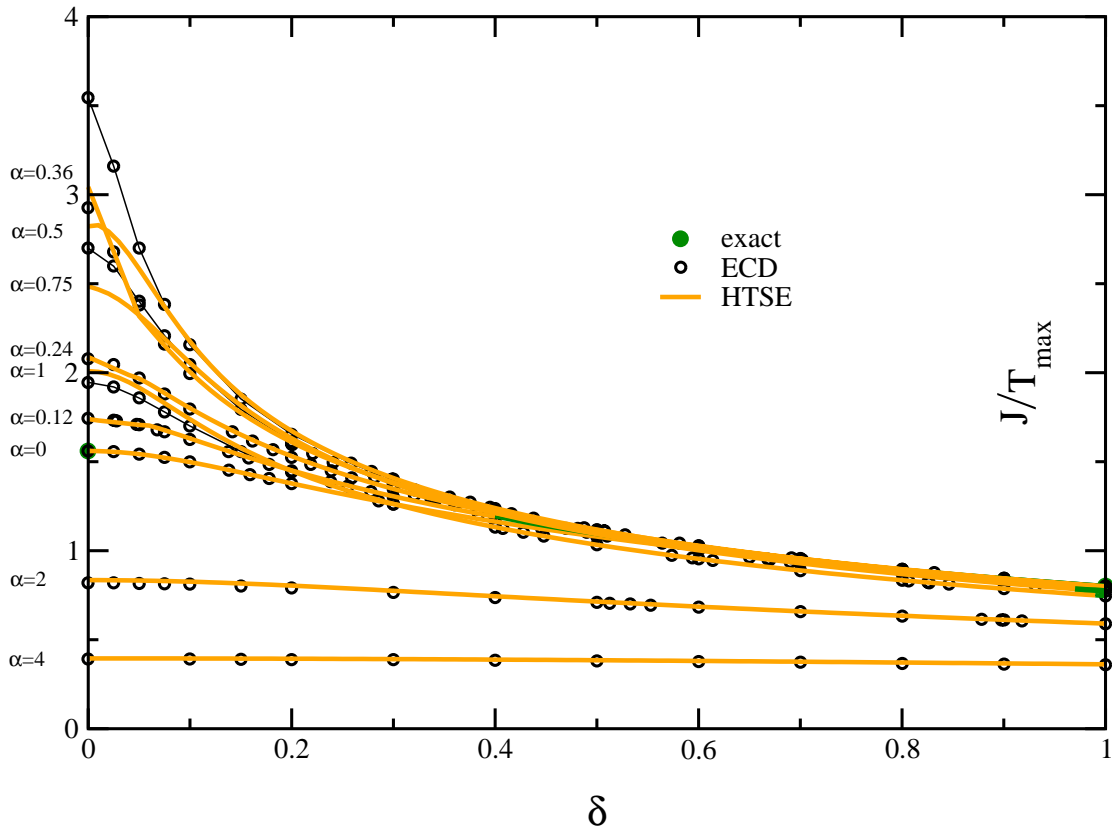


Figure 1.11.: $\frac{J}{T_{\max}}$ versus δ for $\alpha = 0.36, 0.5, 0.75, 0.24, 1.0, 0.12, 0.0, 2.0$ and 4.0 (in descending order at the left side i.e. $\delta = 0.0$): The thin lines are a guide to the eyes to distinguish the ECD results for different sets of parameters.

known from independent experiments, for instance ESR. Thus no fitting is assumed for this material dependent property.

Next the high temperature expansion results (see Appendix A.1) are used to analyze such a scaling behavior as deduced from the values for $\chi_{\max} T_{\max}$ in the lowest orders of β . It is obvious that the zeroth order $4T\chi \approx 1$ does not allow the determination of any parameters. The first order of the susceptibility of a model with given frustration α and exchange coupling J is identical to the first order of another model with frustration α_1 and coupling J_1 if

$$J_1(1 + \alpha_1) = J(1 + \alpha) \quad (1.51)$$

holds. In other words, if one had only first order results for the susceptibility it would be impossible to determine J and α independently.

The second order of the HTSE depends on δ . But again one can choose a particular value δ_1 such that the sets (J, α, δ) and $(J_1, \alpha_1, \delta_1)$ lead to identical zeroth, first and second order terms in β . This choice is

$$\delta_1^2 = 2\alpha_1 - (2\alpha - \delta^2) \left(\frac{1 + \alpha_1}{1 + \alpha} \right)^2. \quad (1.52)$$

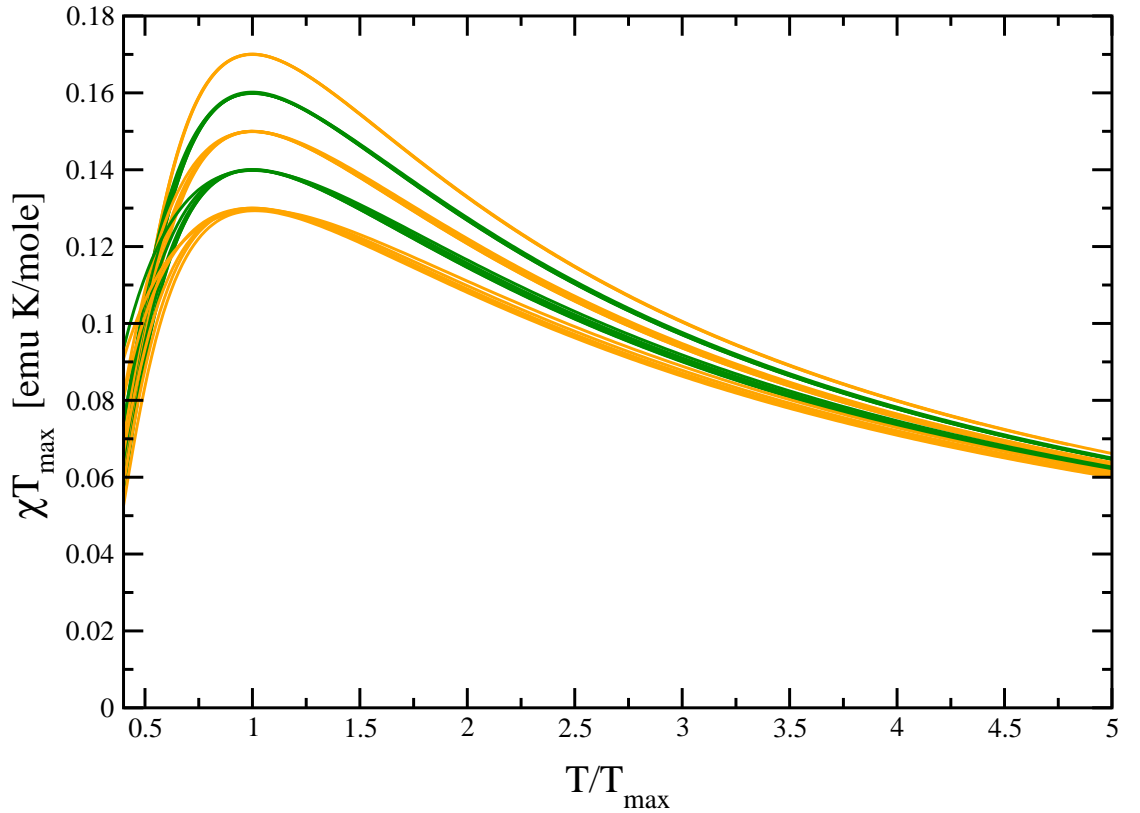


Figure 1.12.: Re-scaled susceptibilities for $\chi_{\max} T_{\max} = 0.17, 0.16, 0.15, 0.14, 0.13$ emu K/mol for the α and δ values shown in Fig. 1.13 (g -factor set to 2).

If the susceptibility is determined mainly by the first three orders, the relations (1.51,1.52) provide the recipe to re-scale the susceptibility such that different parameter sets yield similar temperature dependences. Indeed, if one focuses on the high temperature range this is true. The precise position and value of the maxima, however, cannot be deduced from the first three orders alone. This implies that Eq. 1.52 provides only very rough estimates for the curves as displayed in Fig. 1.13.

We like to stress that we are not claiming that it is impossible to determine all three coupling J, α, δ if sufficient low temperature data is available to obtain the value of the gap. The gap Δ depends in a different way on the couplings than $\chi(T)$ does [51]. Very often, however, the dependence at low values of the temperature is either not accessible or it no longer corresponds to a pure 1D system. In particular, interchain couplings J_{\perp} lead to significantly altered gaps (for examples see refs. [36, 60]) although the behavior at higher temperatures $T > J_{\perp}$ is still well described by a 1D model. Another source of disturbing effects may be impurities in the substance leading to effects which are not described by the given theoretical model.

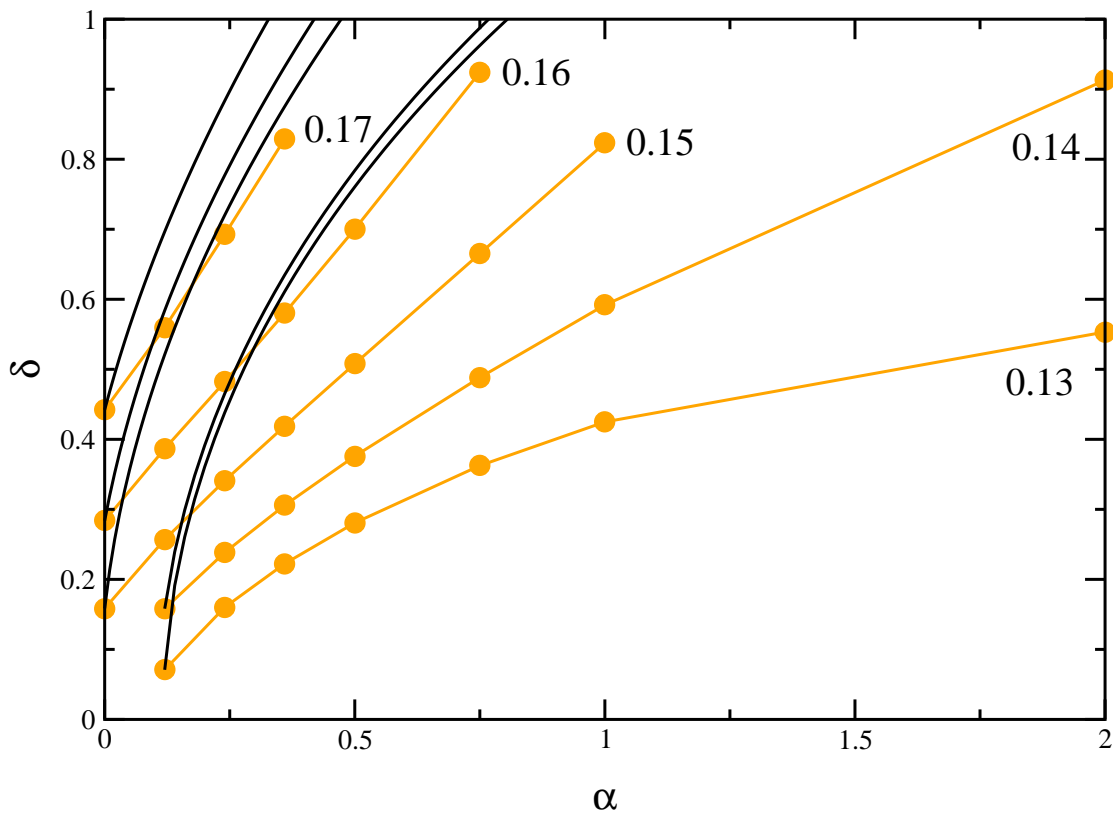


Figure 1.13.: Lines of constant height $\chi_{\max} T_{\max} = 0.17, 0.16, 0.15, 0.14, 0.13$ emu K/mole in the α - δ plane: The black solid lines depict the results using the parameter sets with the lowest value of α and evaluating the δ - α regime where the first two orders of the high temperature series expansion yield the same result, following Eq. 1.52.

Specific Heat

It is a straightforward idea to extract further information about the magnetic properties of certain materials by considering also the specific heat C . Only in very rare cases, however, the *magnetic* part of C can be extracted in a reliable way from the measured data because the phononic contributions dominate C whenever the energy scale of the lattice vibrations is of the order of the magnetic coupling J .

At low temperatures where the phononic contributions vanish following the usual T^3 law a reliable extraction of the magnetic part of the specific heat C is possible, because $T^3 \ll T$ for $T \ll 1$ holds. For high temperatures such a procedure will fail in general as can be seen, for instance, in a simple model of Einstein (dispersionless) phonons coupled to Heisenberg chains [61]. So the full temperature dependence of the magnetic part of C can be measured only in substances with a small exchange coupling J as it occurs, for instance, in organic magnetic materials, see e.g. Ref. [62].

Furthermore, it is in order to mention that there are indirect techniques to obtain the magnetic part of $C(T)$ where the energy fluctuations are linked to dissipation. The latter is measured by the intensity of elastic scattering in spectroscopic investigations, see e.g. [41, 63]. The indirect approaches, however, may provide information on T_{\max} of $C(T)$ but not on C_{\max} itself since overall factors are not known. The obtained data may also be inaccurate. (In this section T_{\max} always refers to $C(T)$. The position of the maximum of $\chi(T)$ is denoted T_{\max}^{χ} .)

In the Appendices A.2 and A.1 the coefficients for the specific heat are provided. In order to compute $C(T)$ additional information on the low temperature behavior is included as was done for $\chi(T)$. For $C(T)$ the extrapolations were performed in the variable energy e as described in Sec. 1.4.4.

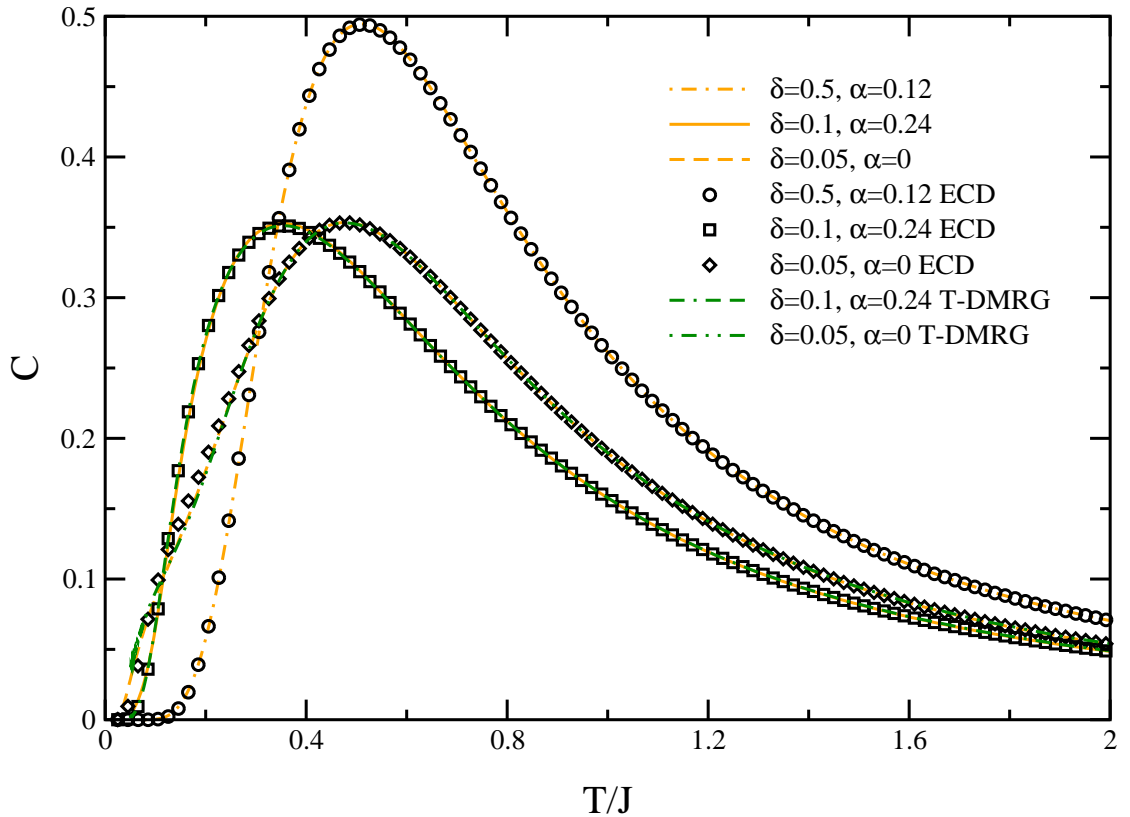


Figure 1.14.: Specific heat C for various values of δ and α . The HTSE data are compared to ECD and T-DMRG results.

In Fig. 1.14 the specific heat for various sets of parameters α and δ is compared to numerical ECD and T-DMRG results. The results of all methods coincide in almost the complete temperature regime. Only for $\alpha = 0$ and $\delta = 0.05$ the ECD result differs slightly from the HTSE and T-DMRG results for temperatures $T \leq 0.2J$. Such an excellent consistency between the different methods supports the accuracy of the extrapolation scheme used for the HTSE data.

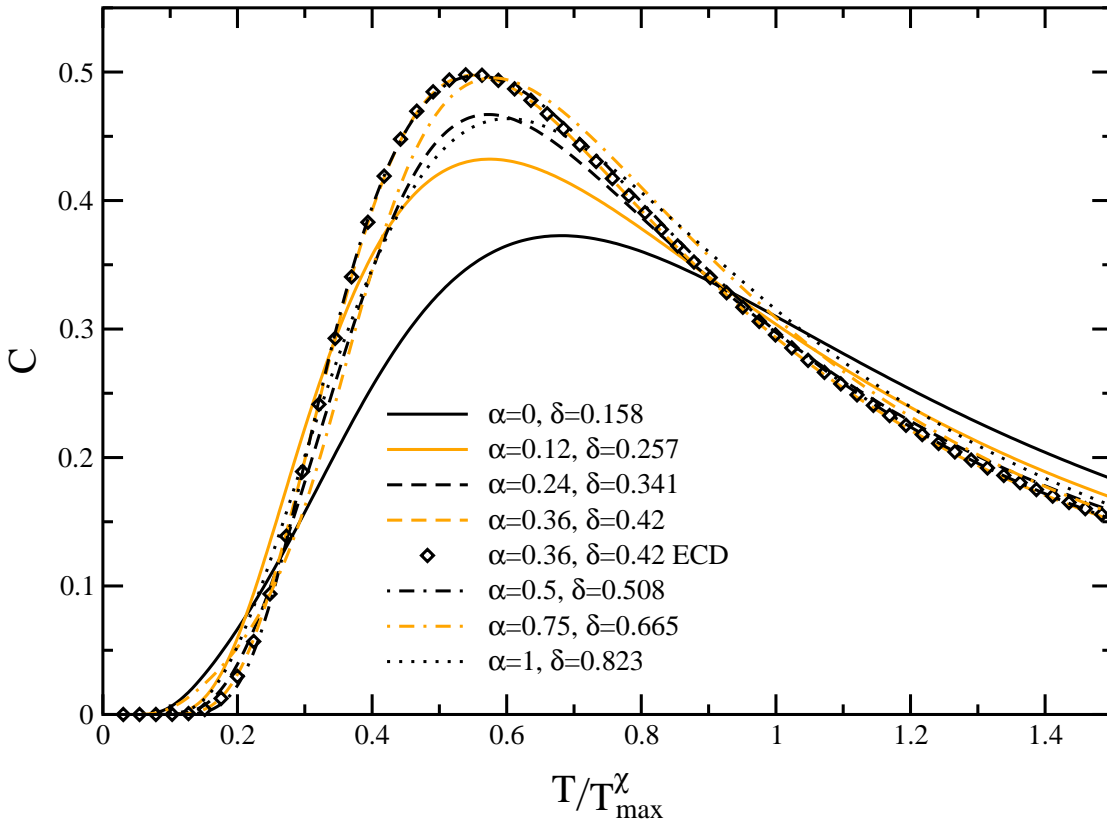


Figure 1.15.: Re-scaled specific heat C for various values of δ and α all yielding the same value $\chi_{\max} T_{\max}^{\chi} = 0.15$ emu K/mol.

Figure 1.15 displays $C(T)$ for the points in Fig. 1.13 belonging to $\chi_{\max} T_{\max}^{\chi} = 0.15$ emu K/mol V. Therefore, the temperature dependence is given in units of the maximum temperature T_{\max}^{χ} of the susceptibility. Clearly, the curves differ from one another. Hence the knowledge of $C(T)$, in addition to the knowledge of $\chi(T)$, renders a complete determination of all three couplings possible. This is the main point in the present section. In other words, the knowledge of $\chi(T)$ allows to fix δ and J for given α . But α cannot be determined easily since there are sets of parameters leading to very similar $\chi(T)$ curves, see Fig. 1.12. The corresponding $C(T)$ curves, however, differ significantly as illustrated in Fig. 1.15 and thus provide a proper distinction of different parameter sets.

To complete the analysis for the specific heat the analogs of Figs. 1.10 and 1.11 for $\chi(T)$ are provided for $C(T)$ in the Figs. 1.16 and 1.17. Figure 1.16 displays the dimensionless (if k_B is set to unity) maximum value of the specific heat which is independent of the value of the exchange coupling J . For given dimerization δ the frustration parameter α can be read off. Once α is known the curves in Fig. 1.17 allow the energy scale to be determined. To give an example, the HTSE results are compared for two sets of parameters

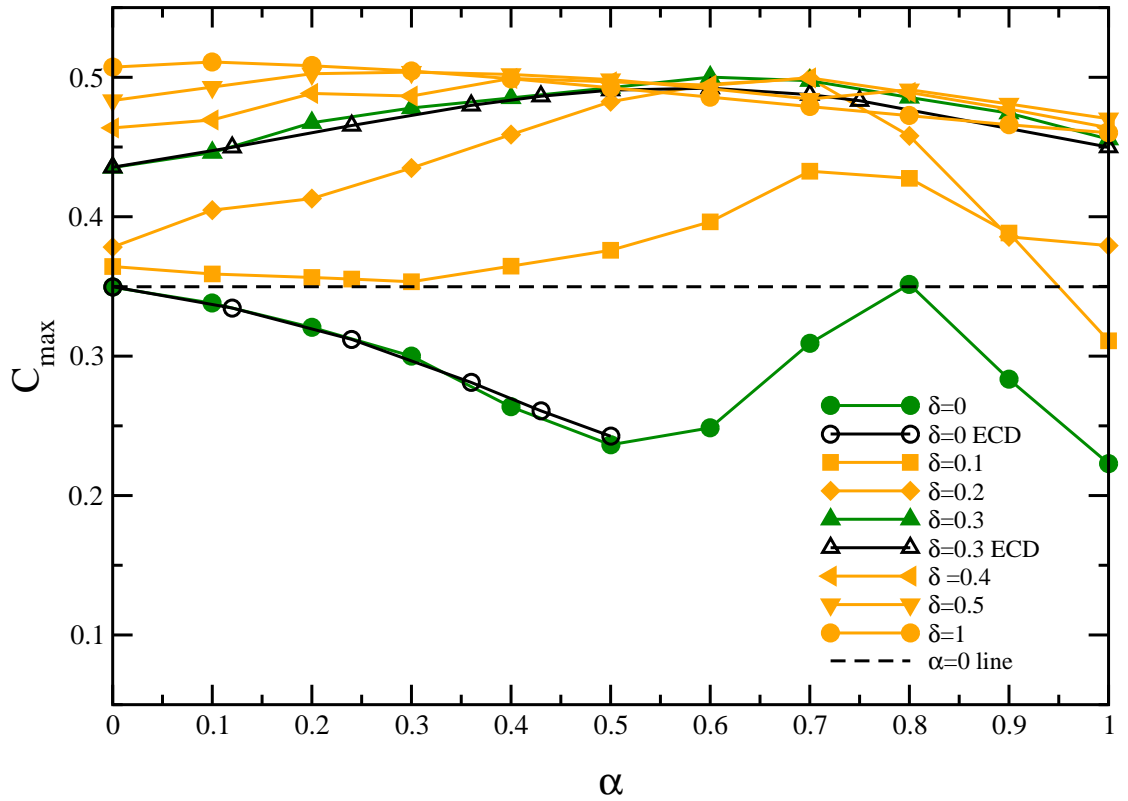


Figure 1.16.: Maximum value C_{\max} of the specific heat as function of the frustration α for various values of the dimerization δ . For $\delta = 0$ the HTSE results shown beyond $\alpha = 0.5$ are affected by an increasing error (see text for details).

to the results obtained by ECD in Figs. 1.16 and 1.17. The HTSE extrapolations and the ECD data slightly differ from each other for values $\alpha \gtrsim 0.5$ (where available). Here, the HTSE extrapolations seem to be more reliable due to the incorporated sum rules and low temperature information on $C(T)$. But, especially the case $\delta = 0$ is a difficult test case also for the HTSE extrapolations. The inaccuracy in the knowledge of the ground state energy influences the position and the height of the maximum of $C(T)$ strongly. For values $\alpha \geq 0.5$ the relative error of the results for C_{\max} in Fig. 1.16 and T_{\max}^C in Fig. 1.17 are of one order above the error of the ground state energy. The error of the ground state energy is estimated to increase roughly from 0.1% at $\alpha \approx 0.5$ to 1% at $\alpha \approx 1$.

In the following the principal behavior of $C(T)$ is briefly described as a function of δ and α . Some of the features of the curves can be understood by simple arguments. In Fig. 1.16 all curves converge to the dashed line for increasing values of α . The value of the dashed line is C_{\max} of a uniform chain without dimerization and frustration. This is implied by the simple fact that the system approaches the limit of two independent chains for $\alpha \rightarrow \infty$. Then the couplings $J(1 + \delta)$ and $J(1 - \delta)$ between the two legs (cf. Fig. 1.2) become less

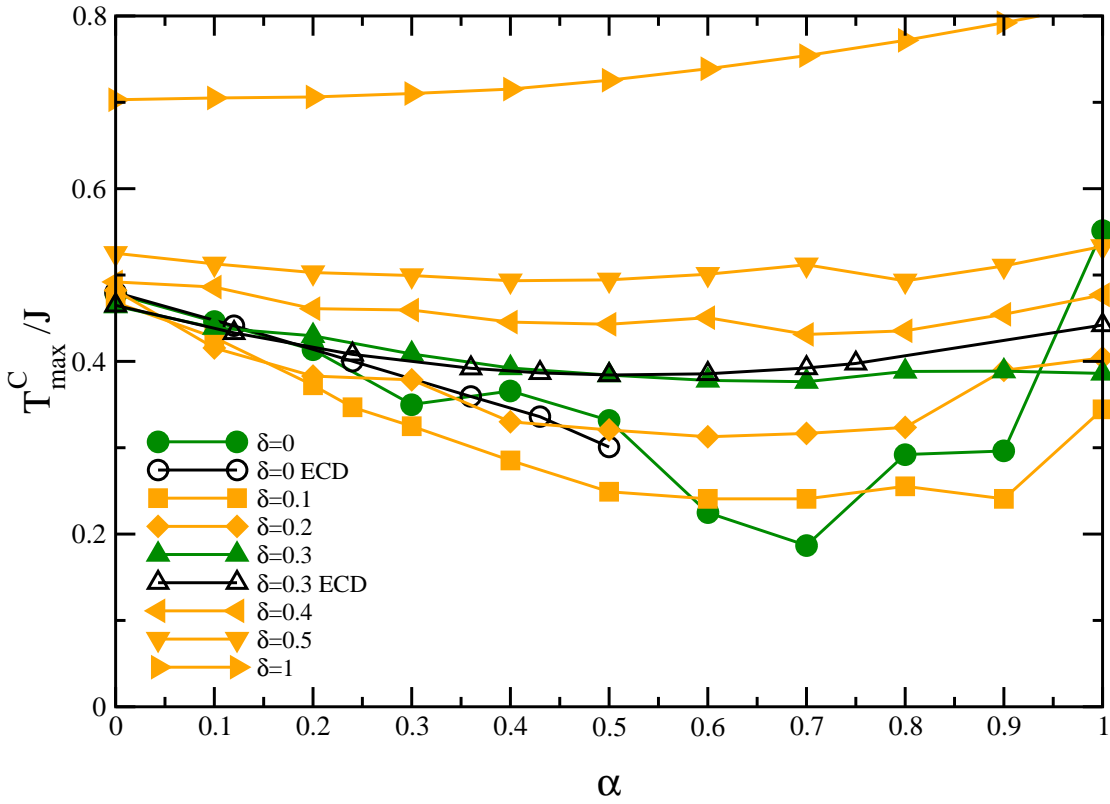


Figure 1.17.: Position T_{\max}^C of the maximum of $C(T)$ as function of the frustration α for various values of the dimerization δ . For $\delta = 0$ the HTSE results shown beyond $\alpha = 0.5$ are affected by an increasing error (see text for details).

and less important, hence we have

$$\lim_{\alpha \rightarrow \infty} C_{\max}(\alpha, \delta) = C_{\max}(\alpha = 0, \delta = 0) . \quad (1.53)$$

For fixed value of the dimerization δ the position T_{\max}^C of the maximum of C is shifted to lower values on increasing α . This can be understood by the suppression of the dispersion of the elementary excitations due to the frustration [45, 46, 51], see also Fig. 1.8. Thereby the overall energy scale on which excitations exist is reduced. The same was observed for the susceptibility as discussed in the preceding paragraph. A minimum is reached for a certain value of $\alpha \approx 0.6$ because T_{\max}^C has to rise again since the system approaches the limit of two independent chains. Quantitatively, the large α limit fulfills

$$\lim_{\alpha \rightarrow \infty} \frac{T_{\max}^C(\alpha, \delta)}{J\alpha} = \frac{T_{\max}^C(\alpha = 0, \delta = 0)}{J} . \quad (1.54)$$

independent of δ .

It should be noted that for large δ (cf. Fig. 1.16) the value of C_{\max} does not substantially change which makes it difficult to discriminate the curves experimentally. The ECD data shown are obtained for a $N = 16$ cluster. A finite size analysis shows that the finite cluster results agree with the infinite chain result except for points with $\delta = 0$ and $\alpha > 0.5$ where finite size effects dominate [64].

1.4.6. Conclusions

The aim of the present section was two-fold. In the first place, results and tools were provided to facilitate and to expedite the analysis of experimental data in terms of a one-dimensional $S = 1/2$ model, namely the dimerized and frustrated spin chain. This model can also be seen as zig-zag chain and comprises in particular the usual spin ladder which is investigated in detail in Sec. 1.5. Secondly, it was demonstrated to which extent it is possible to determine the model parameters quantitatively from the temperature dependences of the magnetic susceptibility χ and of the specific heat C .

It was shown in detail how analytic high temperature series in high orders can be used to obtain reliable extrapolations, namely Dlog-Padé extrapolations and extrapolations in the internal variable energy. The key point is to use additional well-known information on the $T = 0$ and on the low-temperature behavior to stabilize the extrapolations in the low-temperature region. The size of the gap, the form (linear or quadratic) of the dispersion in the vicinity of its minimum, the dimensionality of the system, and the ground state energy were used as additional input. Thereby very good results were achieved in a straightforward fashion. The validity of the results is comparable to the one achieved by the extrapolation procedure introduced previously [21] for the susceptibility. There the susceptibility was extrapolated biased with the knowledge of the zero temperature dispersion of the elementary excitations. The extrapolations for the magnetic specific heat were improved considerably by incorporating additional information and by representing C as a function of energy. The approach used in the present work is simpler since it requires less additional input. In Ref. [21] information on the whole dispersion was used.

With the help of computer algebra programs the extrapolations can be computed very quickly and easily. Thereby efficient data analysis becomes possible.

The extrapolated series expansion results were gauged carefully by investigating their convergence and by comparing them to numerical data. The methods to which we compared are exact complete diagonalization, quantum Monte-Carlo and temperature density-matrix renormalization.

To ease data analysis further results for many sets of parameters were included in the present section. Figures 1.10, 1.11, 1.16 and 1.17 make it possible to read off the coupling parameters J, α and δ if as little as the maximum values of the magnetic susceptibility and of the specific heat as well as their corresponding positions T_{\max}^{χ} and T_{\max}^C are known.

It turned out that the knowledge of $\chi(T)$ at moderate and high temperatures alone is not sufficient to determine the three model parameters (the gyromagnetic ratio g is assumed to be known from independent experiments, e.g. ESR). Any additional knowledge, for instance on $C(T)$ or on the singlet-triplet gap Δ , solves the problem. But such additional information

is difficult to obtain. The specific heat is mostly dominated by the phonon contribution making it difficult to be extracted. The gap Δ is in principle well defined. Frequently, however, the real systems lose their one-dimensionality at low energies, for instance due to small interchain couplings. Then the gap is influenced decisively by these additional residual couplings although the behavior at moderate and higher temperatures is perfectly described by a one-dimensional model. In the analysis of experimental data it is certainly helpful to consider these facts carefully.

1.5. Ladder with Cyclic Exchange

1.5.1. Introduction

In the limit of small ratio t/U the Hubbard model at half filling with hopping amplitude t and on-site Coulomb repulsion U can be mapped in leading order t/U to an antiferromagnetic nearest-neighbor Heisenberg spin model. Terms of higher order in t/U yield besides bilinear exchange terms between further neighbors also biquadratic exchange terms containing a product of four or more spin operators [65–67]. Often, these higher order terms have been neglected. But recently, it has been pointed out that both for spin ladder systems and the parent compounds of high- T_c superconductors [68] in addition to the bilinear exchange terms also biquadratic exchange terms, so-called cyclic exchange terms are important. It became evident that the minimal model describing the magnetic part of the cuprate systems has to contain such four-spin exchange terms [67, 69–71]. Similar multiple spin exchange interactions are known to be relevant in other parts of condensed matter physics like the nuclear magnetism of ^3He [72] or the spin structure of a Wigner crystal [73].

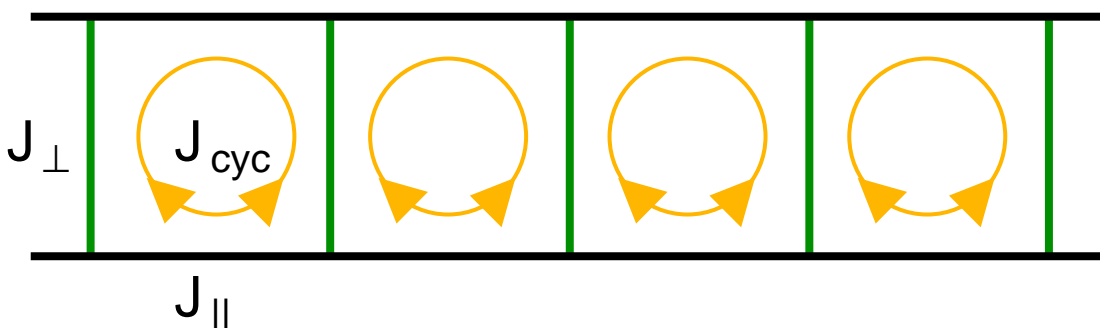


Figure 1.18.: Two-leg ladder with cyclic (4-spin) exchange

The modification of the low temperature behavior of spin systems due to this new exchange interaction has been discussed in detail in Refs. [74–77]. The results have been applied in various experimental works e.g. on the spin ladder compounds $\text{Sr}_{14}\text{Cu}_{24}\text{O}_{41}$, $\text{La}_6\text{Ca}_8\text{Cu}_{24}\text{O}_{41}$ and $(\text{La,Ca})_{14}\text{Cu}_{24}\text{O}_{41}$ [78–81] or on the layered cuprate La_2CuO_4 [80, 82–84]. In the two-leg ladder compound SrCu_2O_3 a ring exchange term also seems to be relevant [85]. A detailed comparison of the experimental results with the results obtained in the present work is carried out in Sec. 1.5.7. Without the inclusion of a ring exchange term, especially in the ladder compounds, the ratio between the leg and the rung exchange coupling was fitted to an unexpected high value of $x = J_{\parallel}/J_{\perp} \approx 2$ (see e.g. [86]) which is neither expected from the geometrical nor from the electronic structure of the ladders [87]. It was shown that only a four-spin exchange term does remove this discrepancy [88]. The possibility of other effects removing this discrepancy cannot be excluded, but up to now the inclusion of a four-spin exchange yields promising results.

However, only few investigations [11] of the impact of this new type of interaction on the finite temperature properties are available up to now. Therefore, the question how

the thermodynamic properties of two-leg spin-1/2 ladders are modified by cyclic exchange interactions is addressed here. In particular, the present part of the work provides the high temperature series (HTSE) data for the magnetic susceptibility and the specific heat and compares to results from exact complete diagonalization (ECD) [7]. It is expected that such an analysis constitutes an important supplement to the study of spin-ladders at finite temperatures, furnishing additional information about couplings and interactions.

1.5.2. Model

The model under study is given by the Hamiltonian

$$H = \sum_i \left(J_{\perp} \mathbf{S}_{1,i} \mathbf{S}_{2,i} + J_{\parallel} [\mathbf{S}_{1,i} \mathbf{S}_{1,i+1} + \mathbf{S}_{2,i} \mathbf{S}_{2,i+1}] \right. \\ \left. + 2J_{\text{cyc}} [(\mathbf{S}_{1,i} \mathbf{S}_{1,i+1})(\mathbf{S}_{2,i} \mathbf{S}_{2,i+1}) + (\mathbf{S}_{1,i} \mathbf{S}_{2,i})(\mathbf{S}_{1,i+1} \mathbf{S}_{2,i+1}) \right. \\ \left. - (\mathbf{S}_{1,i} \mathbf{S}_{2,i+1})(\mathbf{S}_{2,i} \mathbf{S}_{1,i+1})] \right) \quad (1.55)$$

where $J_{\perp} > 0$ and $J_{\parallel} > 0$ are the rung and leg couplings, respectively; the subscript i denotes the rungs and 1,2 the two legs. $J_{\text{cyc}} > 0$ parameterizes the cyclic (4-spin) exchange. The above Hamiltonian 1.55 is closely related to a Hamiltonian where the leading four-spin exchange is included by cyclic permutations P_{ijkl} on a plaquette [69, 75, 89]

$$H^{\text{P}} = \sum_i \left(J_{\perp}^{\text{P}} \mathbf{S}_{1,i} \mathbf{S}_{2,i} + J_{\parallel}^{\text{P}} [\mathbf{S}_{1,i} \mathbf{S}_{1,i+1} + \mathbf{S}_{2,i} \mathbf{S}_{2,i+1}] \right) \\ + \frac{J_{\text{cyc}}^{\text{P}}}{2} \sum_{\langle ijkl \rangle} (P_{ijkl} + P_{ijkl}^{-1}) \quad (1.56)$$

with an analogous description of the exchange constants and the last sum running over all plaquettes $\langle ijkl \rangle$ on the ladder. The permutation operator P_{ijkl} describes a permutation of the spins on a plaquette consisting of four spins. Thereby the spins are rotated clockwise by one site and the inverse operator denote a rotation counterclockwise, respectively. The permutation operator is the abbreviated form of a sum of two-spin and four-spin interactions (and a constant which only shifts the overall energy scale and is thus neglected in the considerations). Therefore the ring exchange part of the Hamiltonian in Eq. 1.56 can be represented by the Hamiltonian from Eq. 1.55 by effective couplings identified through

$$J_{\perp} = J_{\perp}^{\text{P}} + J_{\text{cyc}}^{\text{P}}, \quad J_{\parallel} = J_{\parallel}^{\text{P}} + \frac{1}{2} J_{\text{cyc}}^{\text{P}} \quad \text{and} \quad J_{\text{cyc}} = J_{\text{cyc}}^{\text{P}}. \quad (1.57)$$

Thereby 'diagonal' two-spin products $\mathbf{S}_{1,i} \mathbf{S}_{2,i+1}$ and $\mathbf{S}_{2,i} \mathbf{S}_{1,i+1}$ contained in the cyclic part of H^{P} are omitted. The form 1.55 is used here, because the derivation of the cyclic exchange terms from the underlying multiband Hubbard model for planar cuprates indicate that the four-spin terms are indeed the most significant ones [90]. In Fig. 1.19 the truncated series expansions for $\chi(T)$ and $C(T)$ illustrate the relation between H^{P} and H . As expected, there is still a difference between the representation of H^{P} and the re-parameterized H originating from the neglected two-spin products, but the main effects are indeed the same.

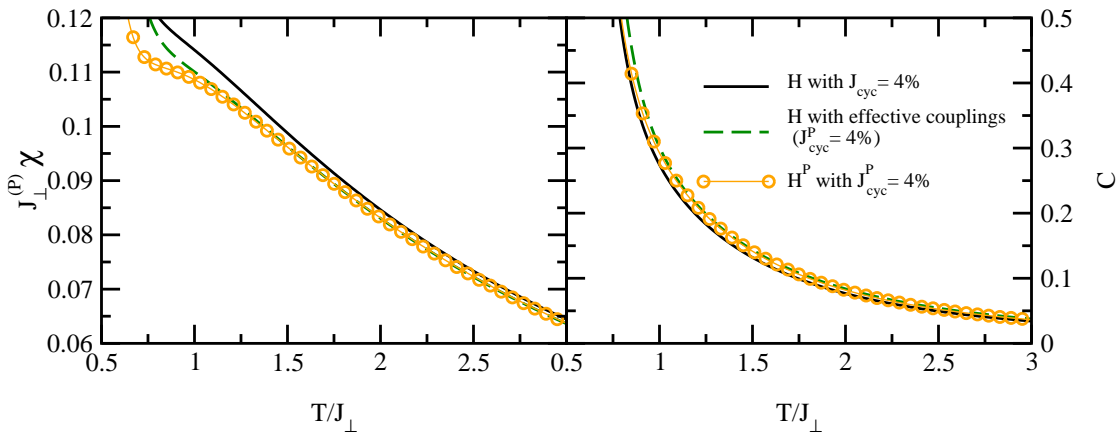


Figure 1.19.: Truncated series (up to β^8 only for consistency between the results) for the magnetic susceptibility $\chi(T)$ (left panel) and the specific heat $C(T)$ (right panel) for $J_{\text{cyc}}^{(p)}=4\%$ compared to H from Eq.1.55 with effective couplings derived from Eq. 1.57 .

In this thesis, the Hamiltonian with a cyclic exchange consisting only of four-spin products (Eq. 1.55) is investigated in detail. In Appendix A.3 the series coefficients of a high temperature series expansion are tabulated for the magnetic susceptibility $\chi(T)$ and the specific heat $C(T)$ up to order 10 in the inverse temperature $\beta = J_{\perp}/T$. Series coefficients for the same quantities are also tabulated for the Hamiltonian in Eq. 1.56 up to order 8 in $\beta = J_{\perp}^p/T$.

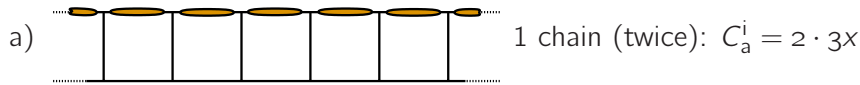
1.5.3. Computation

In contrast to the previous calculations for the dimerized, frustrated spin chain, here, it was necessary to consider bigger systems to obtain the results in the thermodynamic limit. Still, finite size effects had to be corrected when using periodic boundary conditions in the calculations. The corrections will be explained below in detail.

To compute the 10th order in β a system of size $N = 20$ was used corresponding to 10 rungs. Here, the construction of the complete Hilbert space of dimension $2^{20} = 1\,048\,576$ was possible with each base state containing a polynomial in the two variables $x = J_{\parallel}/J_{\perp}$ and $x_{\text{cyc}} = J_{\text{cyc}}/J_{\perp}$. Using an efficient memory algorithm the program needed about 1.5Gb of memory and about 250 cpu days. The high dimension of the Hilbert space and the high order in the expansion made it necessary to use integers of arbitrary length to store the intermediate and final results. The variable type `long long int` ($\approx 10^{19}$) provided by the system was not sufficient. With the help of the GNU Multiple Precision Arithmetic Library [91] this problem was resolved, providing integers of arbitrary length. The use of periodic boundary conditions yields wrap-around effects as was the case for the frustrated, dimerized system. Thus, for contributions $J_{\text{cyc}}^n \beta^n$ ($n \leq 10$) an independent program was written,

Denominator The following terms in the denominator are affected in order β^n yielding a contribution in the finite size system but no contribution in an infinite system (not all possibilities/permutations are listed).

i. $(J_{\parallel})^n, x = n!2^{2n}(\frac{1}{4})^n$



ii. $(J_{cyc})^n, x = n!2^{2n}(\frac{1}{8})^n$



The latter contributions of the type (iib-iiid) to $(J_{cyc})^n$ can be written in a closed form. Therefor one has to identify only contributions where either none, or $0 < m \leq n$ terms of type \square (henceforth identified by the index j in the sum of the equations below) occur in the products. The other addends in the J_{cyc} term are identified by the index i (\square) and by the index k (\boxtimes) in the sums. For $m > 0$ the wrap-around effects then consist of m chains yielding a prefactor of 3^m . The remaining addends of type k (\boxtimes) and i (\square) are distributed arbitrarily. The addends i contribute with a factor of 1 and the addends k with a factor of $(-1)^{\text{number of occurrence}}$. Summing up all possibilities putting in the different types of addends and accounting for the number of possible permutations by a binomial factor leads to the contribution

$$C_{b,d}^{ii} = \sum_{m>0}^n \sum_{i+k=n-m} 3^m 1^i (-1)^k \binom{n-m}{k} x = \sum_{m>0}^n 3^m (1 + (-1))^{n-m} x = 3^n x. \tag{1.59a}$$

For $m = 0$, i.e. no addend of type \square , the multiplicity of terms of kind k (\boxtimes) leads to even-odd effects in the number of closed chains wrapping around. For an odd number the wrap-around effects consist of one chain and for an even number they consist of two chains. Considering for instance only the contributions which lead to an even number of chains, namely 2, the contribution is evaluated by summing up all terms of type $m = 0$ and adding the same term where the prefactor of the addend k is multiplied by -1 . This leads then to twice the contribution with an even number

of terms of type k in the product, because odd numbers in k do cancel. A similar consideration for the terms with an odd number of addends of type k lead to the contributions

$$C_{c,\text{even}}^{\text{ii}} = \frac{1}{2}3^2 \left(\sum_{i+k=n} 1^i (-1)^k \binom{n}{k} + \sum_{i+k=n} 1^i 1^k \binom{n}{k} \right) x = 3^2 2^{n-1} x \quad (1.59b)$$

$$C_{c,\text{odd}}^{\text{ii}} = \frac{1}{2}3 \left(\sum_{i+k=n} 1^i (-1)^k \binom{n}{k} - \sum_{i+k=n} 1^i 1^k \binom{n}{k} \right) x = -3 \cdot 2^{n-1} x \quad (1.59c)$$

Equations 1.59 add up to the simple formula

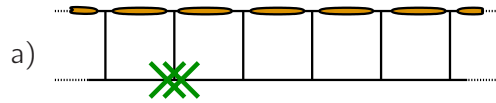
$$C^{\text{ii}} = \left(2^n 3 + 3^n \right) x \quad (1.60)$$

The overall wrap-around contributions for the denominator in order β^n are thus given by

$$C_{\text{denominator}}^{\text{ladder}} = \left(6 \cdot \left(\frac{1}{4} \right)^n J_{\parallel}^n + \left(2^n 3 + 3^n \right) \cdot \left(\frac{1}{8} \right)^n J_{\text{cyc}}^n \right) n! 2^{2n} (-\beta)^n \quad (1.61)$$

Numerator The numerator contains the following products affected in order β^n (not all possibilities/permutations are listed) where the crosses visualize the S^z arising from the squared magnetization M . First, there is a contribution $\propto (J_{\parallel})^n$ as depicted in contribution i for the denominator. This wrap-around effect yields a slightly modified contribution as given in Eq. 1.58b with

$$\text{vi. } J_{\parallel}^n, x = n! 2^{2n} \left(\frac{1}{4} \right)^{n+1}$$



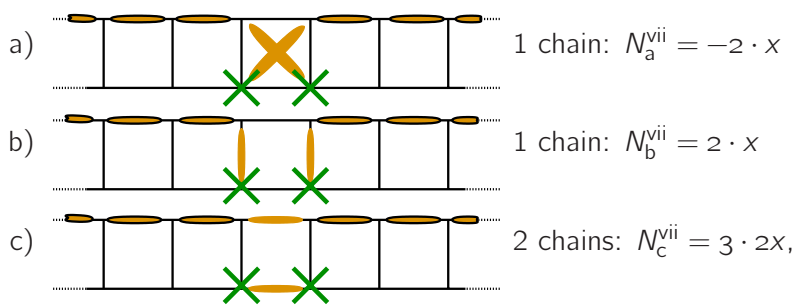
$$N^{\text{vi}} = \left(3 \cdot 2 - 2 - \frac{8}{3!} \right) x = \frac{8}{3} x, \quad (1.62)$$

where the factor of 2 in the first addend originates from the two possibilities for generating a chain $\propto J_{\parallel}^n$ and the S^z components of the magnetization acting on the same site. The factor of 2 is missing in the latter two addends because the two possibilities of chains wrapping around cannot be seen independently from each other when evaluating these specific contributions.

The following wrap-arounds are illustrative examples for contributions which can be expressed in a closed form, but they are depicted for a better understanding. In contrast to the considerations concerning the contributions from wrap-around effects of the numerator in the linear chain as given in Eq. 1.58b, the terms which have to be taken into account

in the following are simpler. Due to the combination of at least one four-spin term and two-spin terms the wrap-around effects consist of open chains meaning that at least two sites are occupied by a single spin operator. The S^z components of the magnetization have to act on these two sites to yield a contribution in the finite system which is not present in the infinite system. Considering the missing contributions in the infinite system the wrap-around has to be broken up leading to four sites which are occupied by a single spin operator. Thus, despite putting in the magnetization, these terms will always lead to a vanishing contribution for the infinite system. Identifying these contributions and evaluating their weight lead to the results valid in the infinite system. The contributions are sorted by the number of four-spin terms contributing to the wrap-around effects.

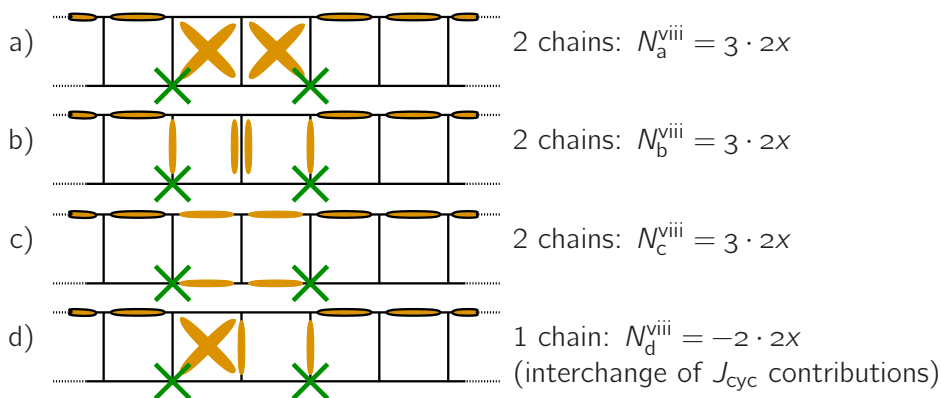
vii. $(J_{\parallel})^{n-1} J_{\text{cyc}}, x = n! 2^{2n} \left(\frac{1}{4}\right)^n \left(\frac{1}{8}\right)^1$

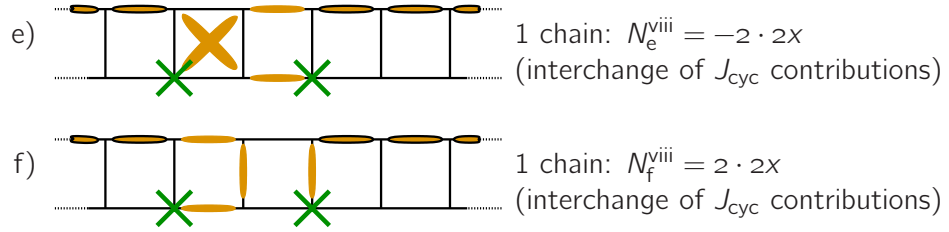


where the factor of 2 originates from the interchange of the S^z components. The contributions a) and b) are restricted to the S^z component. The S^z components of the magnetization fix the contribution to the z-component alone. In the case c) the contribution is restricted to the S^z component only for the short chain on the lower leg (see picture). The chain on the upper leg leads to independent contributions for all components of the spin \mathbf{S} yielding the factor of three, because its contribution can be evaluated independently from the lower chain.

These contributions add up to $N^{\text{vii}} = 6 \cdot x$

viii. $(J_{\parallel})^{n-2} J_{\text{cyc}}^2, x = n! 2^{2n} \left(\frac{1}{4}\right)^{n-1} \left(\frac{1}{8}\right)^2$





A factor of three in the cases a), b) and c) accounts for the independent evaluation of the contributions for the different chains as mentioned for the term c) in vii.

Summing up yields $N^{viii} = 14 \cdot x$.

∴ etc.

Contributions $\propto J_{cyc}^m$ with $2 < m < n$ which are not listed explicitly.

The contributions vii, viii, ... can be put in a closed form for the orders $J_{||}^{n-1} J_{cyc}^1, \dots, J_{||}^{n-m} J_{cyc}^m, \dots, J_{||} J_{cyc}^{n-1}$. Therefore, the corrections for an arbitrary value of $1 < m < n$ are considered, where the particular factor $x = J_{||}^{n-m} J_{cyc}^m n! (\frac{1}{8})^m (\frac{1}{4})^{n-m+1} 2^{2n}$ is omitted for a better reading.

Firstly, only contributions are considered which do not contain a term of type j (\square). Here, products with even and odd orders in k (\boxtimes) have to be distinguished. Even orders in k yield a factor of 3 because the system consists of two chains, whereas an odd order in k yields a prefactor of -1 because the system can be considered as one chain. The contributions even and odd in the number of terms of type \boxtimes are identified as was done for the denominator, see Eqs. 1.59b, 1.59c. Calculating the even order contributions in k yields

$$N_{j=0, \text{even}}^{vii, \dots} = \frac{1}{2} 3 \left(\sum_{i+k=n} 1^i (-1)^k \binom{m}{k} + \sum_{i+k=m} 1^i 1^k \binom{m}{k} \right) = \frac{3}{2} ((1-1)^m + 2^m) = 3 \cdot 2^{m-1}. \quad (1.63a)$$

An analogous calculation for the odd orders in k produces a correction

$$N_{j=0, \text{odd}}^{vii, \dots} = \frac{1}{2} \left(\sum_{i+k=m} 1^i (-1)^k \binom{m}{k} - \sum_{i+k=m} 1^i 1^k \binom{m}{k} \right) = \frac{1}{2} ((1-1)^m - 2^m) = -2^{m-1}. \quad (1.63b)$$

Therefore, the contributions for $j = 0$ sum up to

$$\underline{N_{j=0}^{vii, \dots} = 3 \cdot 2^{m-1} - 2^{m-1} = 2^m}. \quad (1.63c)$$

Lastly, the contributions with at least one term of kind (\square), i.e. $j > 0$ have to be considered. For $j > 0$ the system under consideration consists of j chains independent of k (\boxtimes) requiring a prefactor of $(-1)^k 3^{j-1}$. Summing up these contributions (where $j = 0$ is allowed in the evaluation and subtracted in the end) leads to

$$N_{j \geq 0}^{vii, \dots} = \frac{1}{3} \sum_{j+i+k=m} 3^j 1^i (-1)^k \binom{m}{j \ k} = 3^{m-1}, \quad (1.63d)$$

where the abbreviation ($m = j + i + k$)

$$\binom{m}{j \ k} = \binom{m}{j} \binom{m-j}{k} = \frac{m!}{j!k!(m-j-k)!} \quad (1.63e)$$

was used. In a final step the $j = 0$ contribution of Eq. 1.63d with

$$\frac{1}{3} \sum_{i+k=m} 3^0 1^{m-k} (-1)^k \binom{m}{k} = (1-1)^m = 0 \quad (1.63f)$$

has to be subtracted from the latter results yielding the value to be corrected for $j > 0$ to be

$$\underline{N_{j>0}^{vii,\dots}} = 3^{m-1} . \quad (1.63g)$$

Altogether, in order $J_{\parallel}^{n-m} J_{\text{cyc}}^m$ the underlined wrap-around values from Eqs. 1.63c and 1.63g add up to

$$N^{vii,\dots} = 2 \cdot 3^{m-1} + 2^{m+1} , \quad (1.64)$$

where the additional factor of 2 originates from the interchange of the S^z components of the magnetization.

In summary, the wrap-around effects for the numerator (without the $(J_{\text{cyc}})^n$ -terms) from Eqs. 1.63 sum up to

$$\begin{aligned} N_{\text{numerator}}^{\text{ladder}} &= \frac{8}{3} 2^{2n} \left(\frac{1}{4}\right)^{n+1} (-\beta)^n J_{\parallel}^n \quad (1.65) \\ &+ \sum_{1 < m < n} [2 \cdot 3^{m-1} + 2^{m+1}] 2^{2n} \left(\frac{1}{4}\right)^{n+1-m} \left(\frac{1}{8}\right)^m J_{\parallel}^{n-m} J_{\text{cyc}}^m (-\beta)^n \end{aligned}$$

There are also wrap-around effects in the numerator of order $J_{\text{cyc}}^n \beta^n$. The explicit calculation of these contributions is a tedious task. Many configurations and alignments of the S^z -components of the magnetization have to be considered and their wrap-around value to be calculated. The direct calculation of a Hamiltonian with only 4-spin interaction for a slightly bigger system size ($2n + 2$) can easily be done without finite-size errors in n -th order. The degree of complexity and computation time is comparable to the calculations for the isotropic Heisenberg chain with only nearest neighbor interaction. Therefore, the orders J_{cyc}^n were not corrected by hand.

To get an impression of the results the first orders for the susceptibility $\chi(T)$ and the specific heat $C(T)$ are listed below.

$$4T\chi = 1 + \left(-\frac{1}{4} - \frac{1}{2}x\right)\beta \quad (1.66a)$$

$$+ \left(\left(\frac{1}{4} + \frac{3}{16}x_{\text{cyc}}\right)x - \frac{7}{32}x_{\text{cyc}}^2 - \frac{1}{16} + \frac{3}{16}x_{\text{cyc}}\right)\beta^2 + \mathcal{O}(\beta^3)$$

$$16C = \left(\frac{3}{2} + 3x^2 + \frac{21}{8}x_{\text{cyc}}^2\right)\beta^2 \quad (1.66b)$$

$$+ \left(\frac{3}{4} + \frac{3}{2}x^3 - \frac{27}{8}x_{\text{cyc}} - \frac{27}{8}x_{\text{cyc}}x^2 + \frac{45}{8}x_{\text{cyc}}^2 + \frac{45}{8}x_{\text{cyc}}^2x - \frac{9}{8}x_{\text{cyc}}^3\right)\beta^3$$

$$+ \mathcal{O}(\beta^4)$$

The complete set of coefficients up to order ten in the inverse temperature β is listed in Appendix A.3

1.5.4. Extrapolations

The basic ideas for the extrapolation schemes used are explained in Sec. 1.3. Here, the details of the extrapolations specific to the model are described in various paragraphs: one for the susceptibility, another for the specific heat and a last one for the gapless point of the model. Whenever possible, the extrapolations are compared to results of other methods, mainly ECD. Otherwise, the extrapolations are compared to lower and higher orders of extrapolations to show the convergence of the representations, used as a measure of the accuracy of the extrapolation.

Specific Heat The specific heat is extrapolated using the method presented in Sec. 1.3.2. Basically, the entropy $S(T)$, obtained from the HTSE data of the specific heat, is expressed in the new variable $e - e_0$, where e_0 is the ground state energy and $e = e(T)$ is the average internal energy per site. The temperature and the specific heat are then derived from the entropy as functions of e . The ground state energy $e_0(x, x_{\text{cyc}})$ is obtained from Ref. [92]. It is calculated up to order 11 in x and x_{cyc} in a high order series expansion about the limit of isolated rungs. One sets $r = x_{\text{cyc}}/x = \text{const}$ and uses standard Dlog-Padé extrapolations on $de_0(x, rx)/dx$ which yield highly accurate results [92].

To incorporate the low temperature information from Eq. 1.9 the sum rule

$$e - e_0 = \int_0^T C(T')dT' \approx AT^{\frac{1}{2}}e^{-\frac{\Delta}{T}} \quad (1.67)$$

is considered in the limit $T \ll \Delta$. Only the leading order contribution in T is taken into account, higher orders in T are neglected; A is a constant factor. Inverting the above equation provides an expression $T(e - e_0)$ with

$$\ln\left(\frac{e - e_0}{A}\right) = \frac{1}{2}\ln T - \frac{\Delta}{T}. \quad (1.68)$$

Only an approximate solution is possible, because Eq. 1.68 cannot be inverted analytically. In a first iteration step the addend $\frac{1}{2}\ln T$ in Eq. 1.68 is neglected leading to

$$T_1 = \frac{-\Delta}{\ln\left(\frac{y}{\Delta}\right)} \quad (1.69a)$$

with $y = e - e_0$. Inserting T_1 in a further iteration step yields

$$T_2 = \frac{-\Delta}{\ln\left(\frac{y}{\Delta}\right) - \frac{1}{2}\ln T_1} = \frac{-\Delta}{\ln\left(\frac{y}{\Delta}\right) - \frac{1}{2}\ln\frac{-\Delta}{\ln\left(\frac{y}{\Delta}\right)}}. \quad (1.69b)$$

Obviously, further iteration steps lead to logarithmic functions of logarithmic arguments. Their contributions become less important with increasing number of steps of iteration. Neglecting those emerging multiple-logarithmic functions in Eqs. 1.69 yields the approximate solution for T with

$$T(y) \approx -\frac{\Delta}{\ln(y)} \quad \text{for } y \ll 1. \quad (1.70)$$

Combining Eqs. 1.67, 1.9 and the following sum rule

$$S = \int_0^T \frac{C(T')}{T'} dT' \approx AT^{-\frac{1}{2}} e^{-\frac{\Delta}{T}} \quad \text{for } T \ll \Delta \quad (1.71)$$

provides the low temperature behavior of the entropy

$$S(y) \approx -\frac{y}{\Delta} \ln(y) \quad \text{for } y \ll 1. \quad (1.72)$$

The logarithmic singularity at $e = e_0$ ($y = 0$) can be described best by extrapolating the function

$$G(y) = y \partial_y \frac{S(y)}{y}. \quad (1.73)$$

The value of the gap Δ is incorporated by requiring

$$G(y = 0) = -1/\Delta. \quad (1.74)$$

The value of the gap is taken from the explicit $T = 0$ calculation in Ref. [92] and used to stabilize the extrapolation procedure. This constitutes an extension of the procedure applied in Ref. [28]. There, Eq. 1.74 is exploited to estimate the gap Δ . Here, the value of the gap is built in explicitly.

The entropy is finally given by

$$S(e) = (e - e_0) \left(\int_0^e \frac{\tilde{G}(e')}{e' - e_0} de' - \frac{\ln 2}{e_0} \right) \quad (1.75)$$

where \tilde{G} is the Padé extrapolation of G . Whenever possible diagonal Padé representations, i.e. the same order in numerator and denominator are used since it is found that they converge generically best. This fact was investigated in detail in the previous chapter for the

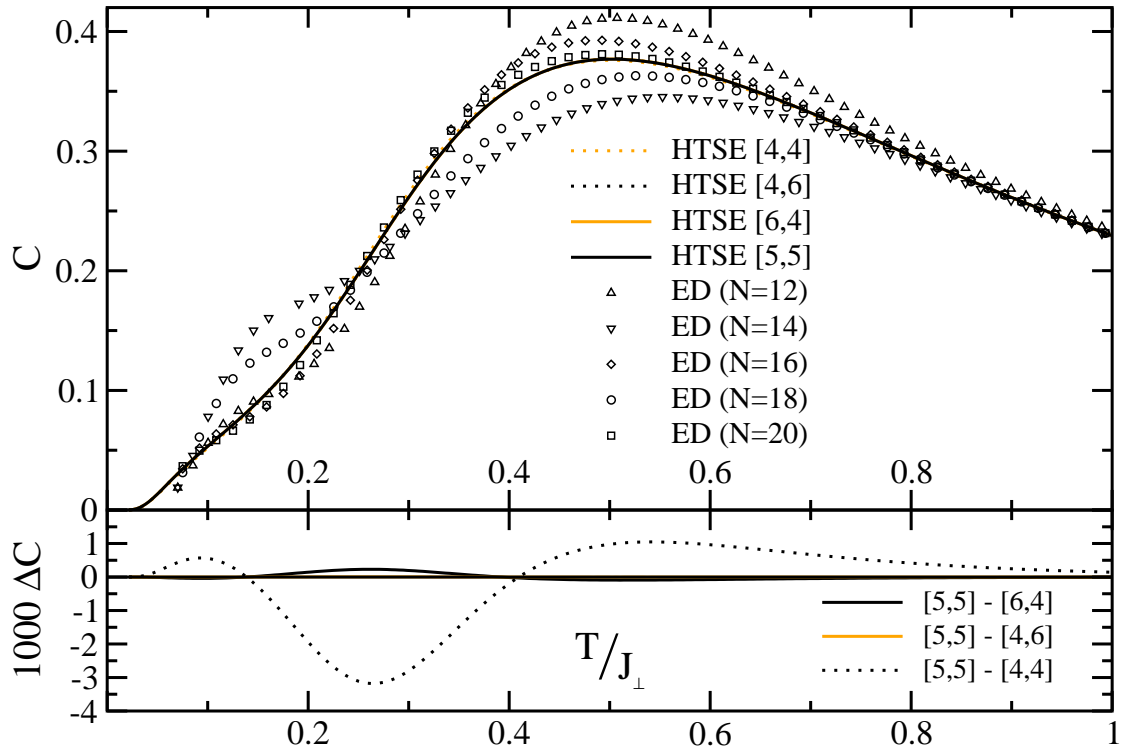


Figure 1.20.: Specific heat for $x = J_{\parallel}/J_{\perp} = 1$ and $x_{\text{cyc}} = J_{\text{cyc}}/J_{\perp} = 0.1$, upper plot: $C(T)$ for various orders of Padé extrapolations and ECD results [64] from $N = 12$ to $N = 20$. Lower plot: differences between various HTSE representations. The difference [5,5] - [4,6] cannot be discerned in the figure.

frustrated, dimerized spin chain, see for instance Fig. 1.4. For the considered model such a detailed investigation was performed also but no explicit figure will be shown. Basically, the result that diagonal Padé representations converge best is obtained by considering the differences between successive orders of extrapolations without spurious poles. The smaller the differences are for increasing orders the better the convergence is. The convergence of the extrapolations is also checked by comparing to the ECD data. Exceptions to the use of the diagonal Padé extrapolations will be stated explicitly; they are necessary where spurious poles occur in the diagonal representations.

Comparison to ECD results [64] shows that diagonal representations yield the best results, see Fig. 1.20. The convergence shown in the lower plot is very convincing. The HTSE extrapolations are compared to ECD data for system sizes up to $N = 20$. It is systematic to the ECD calculations that for increasing system sizes the results alternately yield an upper ($N = 12, 16, 20$) or a lower ($N = 14, 18$) bound on the specific heat for not too low temperatures. Therefore, the result for $N = \infty$ should be in between the results with $N = 18$ and $N = 20$ [93], which is fulfilled by the HTSE extrapolations.

It is assumed that the pronounced shoulders below $T = 0.2J_{\perp}$ seen in the ECD data for $N = 14$ and $N = 18$ in Fig. 1.20 are due to finite size effects. This view is corroborated by the fact that the shoulders occur in ladders made from chains of odd number of sites whereas they are absent in the ladders made from chains with even number of sites. Additionally, the shoulder diminishes quickly on passing from $N = 14$ to $N = 18$. Furthermore, the extrapolated HTSE does not display a comparable feature. Only a weak tendency towards a small bump at about $T = 0.1J_{\perp}$ is found. The size of this bump is sensitive to the precise values for the ground state energy and for the gap used in the extrapolation.

It has to be noted that the precise knowledge of the ground state energy e_0 is of particular importance for the extrapolation of the HTSE data for the specific heat. Even a small uncertainty of half a percent in e_0 leads to significant differences in the specific heat at and below its maximum. The high temperature part is unaffected thereby.

Susceptibility With the temperature as function of e at hand it is possible to represent also the susceptibility as function of e . The low temperature behavior from Eq. 1.8 can also be incorporated in the extrapolations.

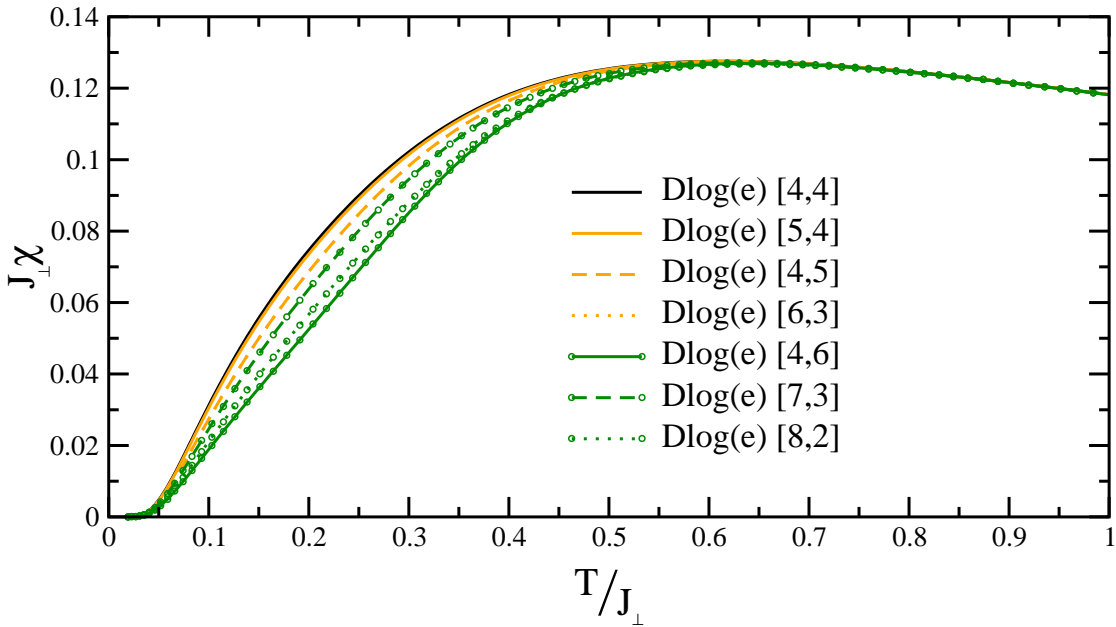


Figure 1.21.: Overview of various orders of Dlog-Padé representations in e for $x = 1$ and $x_c = 0.1$. The low temperature behavior from Eq. 1.77 is built in.

Considering the sum rule from Eq. 1.67 and the low temperature behavior of $4T\chi(T)$ [24] with

$$4T\chi(T) \approx T^{\frac{1}{2}} e^{-\frac{\Delta}{T}} \quad \text{for } T \ll \Delta \quad (1.76)$$

leads to an approximate description of the susceptibility for energies close to the ground

state energy e_0

$$y = e - e_0 \approx T^{\frac{1}{2}} e^{-\frac{A}{T}} \approx 4T\chi(T) \text{ for } y \ll 1. \quad (1.77)$$

To incorporate the linear behavior of $\chi(e)$ for energies close to the ground state energy a Dlog-Padé representation is used where the residual of 1 is explicitly built in, for details see Sec. 1.3.1. Unfortunately, the convergence of the extrapolations investigated is not as satisfying as for the specific heat. Fig. 1.21 shows a representative overview of various orders of Dlog-Padé representations in e . Most diagonal Padé extrapolations are not possible due to spurious poles. Even for the same overall order of extrapolation the possible Padé extrapolations differ much from each other. The position and height of the maximum is not described quantitatively. The low temperature regime seems to be underestimated and the extrapolations are very sensitive to the order of numerator and denominator in the Padé representations. A possible explanation could be that the sum rules built in implicitly in the extrapolations of the susceptibility influence also higher energies, i.e. higher temperatures where simple Padé extrapolations in the inverse temperature β already yield stable results. Hence we refrain from using a $\chi(e)$ representation.

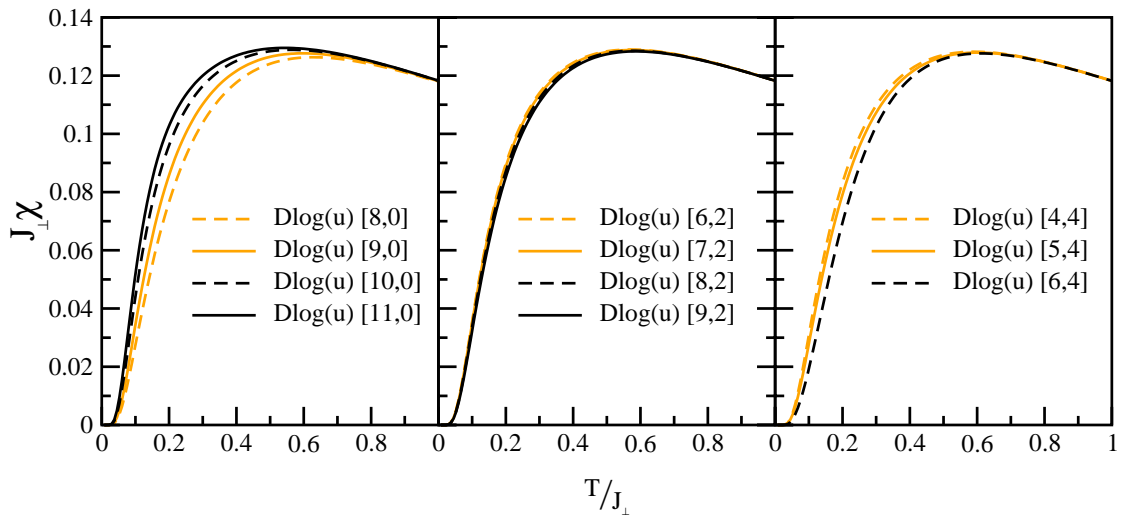


Figure 1.22.: Various Padé extrapolations of Dlog-Padé representations in u for $x = 1$ and $x_{\text{cyc}} = 0.1$ extended by the low temperature information given in Eq. 1.76

The extrapolation of the susceptibility $\chi(T)$ follows the procedure described in Sec. 1.3.1. Basically, the low temperature behavior of Eq. 1.8 (see also Eq. 1.76) is used to improve the representation. To incorporate the low temperature information it is advantageous to map the temperature regime $T \in [0, \infty]$ to the interval $[0, 1]$ via the substitution $u = \beta/(1 + \beta)$. All extrapolations are finite for $u \rightarrow 1$ and the stabilized representations are no longer restricted to diagonal Dlog-Padé extrapolations. All representations for $\chi(T)$ are extrapolated with the same order of Dlog-Padé extrapolations to retain a consistent description of the HTSE results. Here, the $[n, 2]$ representations are used. Spurious poles

are unlikely to occur in these representations due to the low order in the denominator of the approximants. This allows for generating representations for almost arbitrary sets of parameters and extract specific information as it is done e.g. in Fig. 1.27 for the value of $T_{\max}\chi_{\max}$.

In Fig. 1.22 various orders in the denominator of the Padé extrapolation for the susceptibility with $x = 1$ and $x_{\text{cyc}} = 0.1$ are shown in three panels. The left panel shows the truncated series of the Dlog-Padé extrapolation for orders 8 to 11 in β . The middle panel displays extrapolations with order two and the right panel with order four in the denominator of the approximant. Odd orders and orders higher than four in the denominator are very likely to produce spurious poles. Therefore they are not considered in detail here. The $[7, 4]$ extrapolation has a spurious pole and is consequently not plotted. The convergence of the $[n, 2]$ approximants is very convincing in comparison to the other approximants and thus supporting their use for the representation of the susceptibility χ . In the following the quality of the $[n, 2]$ approximants are checked by comparing to ECD data.

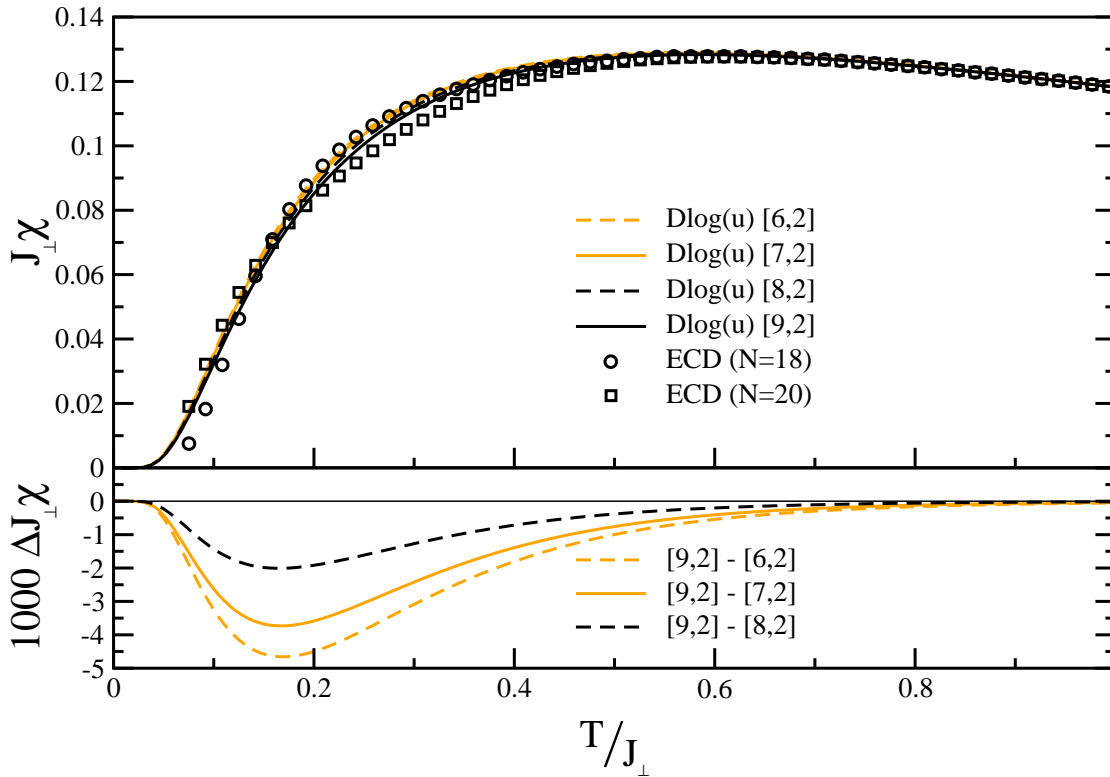


Figure 1.23.: Convergence of the $[n, 2]$ approximants for the susceptibility χ with $x = 1$ and $x_{\text{cyc}} = 0.1$

In Fig. 1.23 the $[n, 2]$ approximants are compared to the highest order available ($n+2 = 11$). The orders 8 to 10 differ only by $10^{-3}T/J_{\perp}$ from the 11th order for χ . This observation does not change significantly for other sets of parameters considered in this thesis. The

representation is also checked with ECD data [64]. Here, as described for the specific heat in the previous paragraph the susceptibility for an infinite system lies in-between the results for $N = 18$ and $N = 20$. The extrapolations of the HTSE data fulfills this observation down to very low temperatures. It has to be mentioned that for temperatures below $T \approx 0.2J_{\perp}$ where the ECD results intersect the ECD data is no more valid for quantitative predictions [64]. In general, the representation chosen for the HTSE data is also checked in the limit of the (isotropic) ladder and the Heisenberg chain, where precise [43, 94, 95] or exact [3] results are available. The comparison to the isotropic ladder is not shown explicitly and the comparison to the Heisenberg chain was already performed in the previous Chapter 1.4.

Gapless Point This paragraph is dedicated to the investigation of the parameter choice where the system is gapless, see below. In doing so, it is pointed out, that the described extrapolation schemes do not require a gapped behavior in the considered quantities. Here, an analogous extrapolation scheme is used to represent trustworthy results from the HTSE data in the ungapped phase.

Fig. 1.24 shows data for the susceptibility and the specific heat for the gapless point $x = 0.2$ and $x_{\text{cyc}} = 0.2$ [92]. The triplet dispersion and the gap can be computed exactly for the parameter regime $x = x_{\text{cyc}}$ leading to the exactly known gapless point $x = x_{\text{cyc}} = 0.2$. The inset sketches the phase line where the gap vanishes. The results are obtained by a high order series expansion about the limit of isolated rungs. The solid line about the exact point shows the highly convergent results. The dotted lines give a sketch of the phase line for parameters far away from the exact point. The phase diagram is investigated in detail in Ref. [92]. To the left of the phase line the system is in a gapped rung singlet phase. To the right of the phase line the system is in a staggered dimer phase [96–98].

To derive the low temperature behavior of C and χ at the gapless point the exactly known triplet dispersion

$$\omega(q) = \frac{2}{5} (1 - \cos q) \approx q^2 \quad \text{for } q \approx \pi \quad (1.78)$$

at the antiferromagnetic wave vector [92] is used. A similar analysis as in Ref. [24] yields the approximate low temperature behavior for the internal energy

$$e(\beta) - e_0 \approx \int_{-\pi}^{\pi} \omega(q) n(q) dq \approx \int_{-\infty}^{\infty} \omega(q) e^{-\beta\omega(q)} dq \propto \beta^{-3/2} \quad \text{for } T \ll 1, \quad (1.79)$$

where the elementary excitations are triplons. Therefore a (hard-core) boson-like description is valid and the occupation number $n(q)$ for bosons in the limit of low temperatures is used with

$$n(q) = \frac{1}{e^{\beta\omega(q)} - 1} \approx e^{-\beta\omega(q)} \quad \text{for } T \ll 1, \quad (1.80)$$

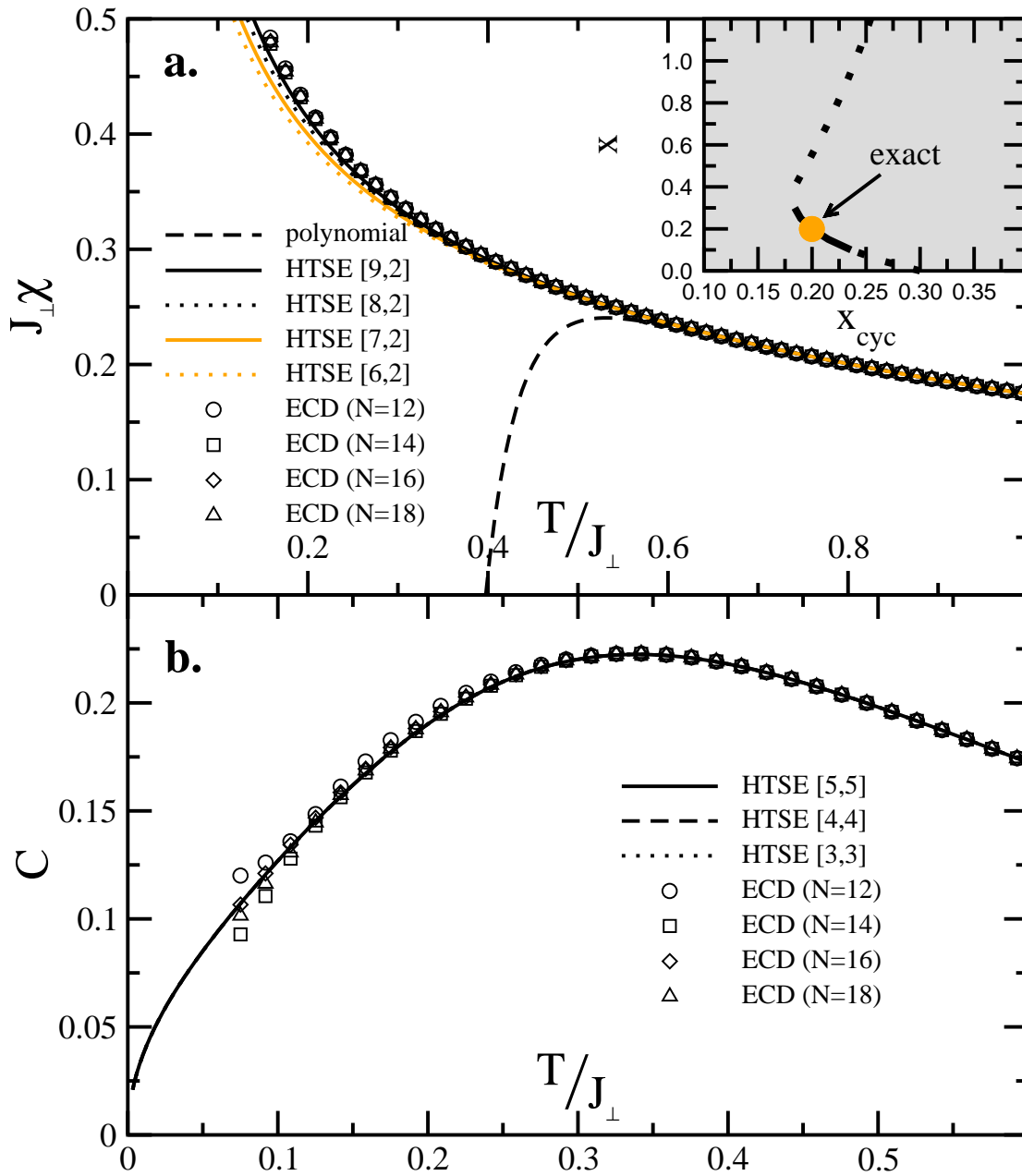


Figure 1.24.: Susceptibility (a.) and specific heat (b.) for $x = 0.2$ and $x_{cyc} = 0.2$ for various orders of Dlog-Padé representations and ECD results for $N = 12, 14, 16, 18$. The HTSE representations in b. cannot be resolved in the plot because they almost coincide. Inset: Phase line with $\Delta = 0$, for details see Ref. [92].

where the hard-core constraint need not to be built in explicitly since it is not relevant at low temperatures. Combining the relation from Eq. 1.79 and the low temperature behavior of the susceptibility and the specific heat following Ref. [24]

$$\chi(T) \approx \frac{1}{\sqrt{T}} \text{ for } T \ll 1 \quad (1.81a)$$

$$C(T) \approx \sqrt{T} \text{ for } T \ll 1. \quad (1.81b)$$

leads to an entropy

$$S(e) \approx (e - e_0)^{1/3} \text{ for } e - e_0 \text{ small}, \quad (1.82)$$

where the sum rule

$$S(T) = \int_0^T \frac{C(T')}{T'} dT' \approx \sqrt{T} \text{ for } T \ll 1 \quad (1.83)$$

was used.

The entropy is extrapolated using Dlog-Padé extrapolations biased to contain the extra information from Eq. 1.82, following the description in Sec. 1.3.1. As seen in Fig. 1.24 the obtained representations of the HTSE data are in excellent agreement with the results of the ECD calculations. The extrapolations of the HTSE data of the specific heat lie in-between the results of the ECD calculations for $N = 16$ and $N = 18$. The ECD results for the susceptibility and the extrapolations of the HTSE data are also in convincing agreement.

Summarizing the extrapolation section, the chosen representations of the HTSE results yield stable and trustworthy results for the calculated thermodynamical properties. Especially the experimentally interesting position and height of the maximum of both the susceptibility and the specific heat are sufficiently well described for quantitative predictions. For parameters where the system is sufficiently gapped the HTSE extrapolations of the susceptibility and the specific heat yield representations which are valid in almost the whole temperature regime. As soon as the gap becomes smaller the position of the maximum of the susceptibility moves to lower temperatures. This also affects the extrapolations in these parameter regimes. There, quantitative predictions can be made down to $T \approx 0.3J_{\perp}$ deduced from Fig. 1.24 for the susceptibility. The same arguments hold for the specific heat. Due to the incorporation of the known sum rules and the incorporation of the low temperature behavior quantitative predictions are possible at slightly lower temperatures than it is possible for the susceptibility. Considering the lower plot in Fig. 1.24 quantitative predictions are possible for temperatures $T \gtrsim 0.15J_{\perp}$. Therefore the gapless point serves as a reference for the estimation of the range of validity for parameter sets, where the gap of the system is significantly smaller than for the isotropic ladder, where $\Delta \approx 0.5J_{\perp}$ [58], see also Fig. 1.26.

1.5.5. Results

The aim is to provide results which show the quantitative behavior of the considered thermodynamic properties and in particular the effects of a cyclic spin exchange. With the help

of computer algebra programs the HTSE results can be used easily to determine the model parameters of a substance. Only data of standard quantities like the magnetic susceptibility are necessary. The occurring ambiguity in determining the model parameters (see also Chapter 1.4 and below) by only one quantity like $\chi(T)$ can be resolved by the knowledge of other quantities, e.g. the spin gap Δ or the magnetic specific heat $C(T)$ as far as they are accessible experimentally.

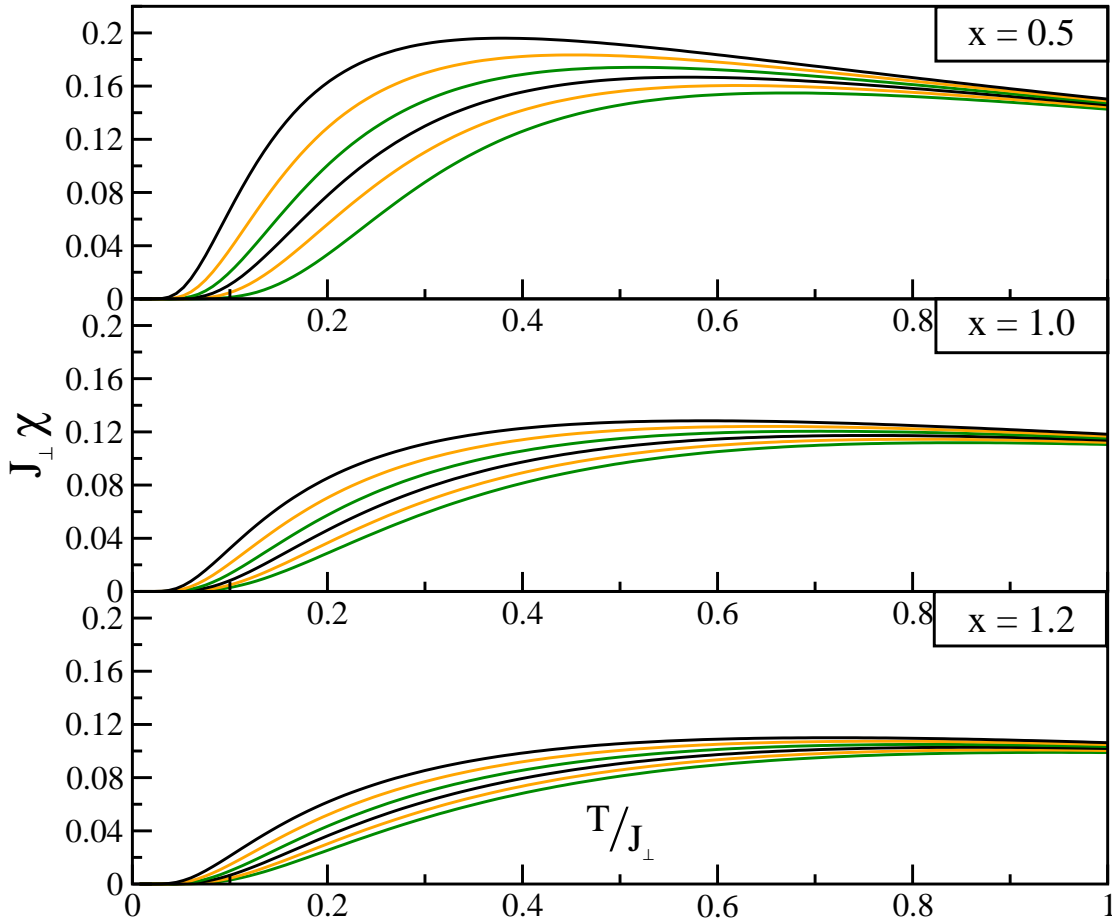


Figure 1.25.: $\chi(T)$ for various values of x for $x_{\text{cyc}} = 0, 0.02, 0.04, 0.06, 0.08$ and 0.1 in ascending order from bottom to top in each panel.

Susceptibility Fig. 1.25 shows an overview of the magnetic susceptibility for various values of the cyclic exchange x_{cyc} and the leg coupling x . The choice of the parameter regime shown is taken from published values for substances presently investigated [78, 80, 81]. The substance $\text{La}_6\text{Ca}_8\text{Cu}_{24}\text{O}_{41}$ was analyzed in a Raman response experiment [99] and in a measurement of the optical conductivity [81]. So far, it is assumed that only the

inclusion of a cyclic exchange with $x \approx 1.2$ and $x_{\text{cyc}} \approx 0.1$ can explain the experimental data. Examining the neutron scattering data by fitting theoretical results yields a slightly lower value of $x \approx 1$ [78]. Other substances like the two dimensional system La_2CuO_4 are also under investigation. Analyzing the spin wave excitation spectrum in La_2CuO_4 leads to a consistent description when a cyclic exchange of $x_{\text{cyc}} \approx 0.12$ is assumed [84].

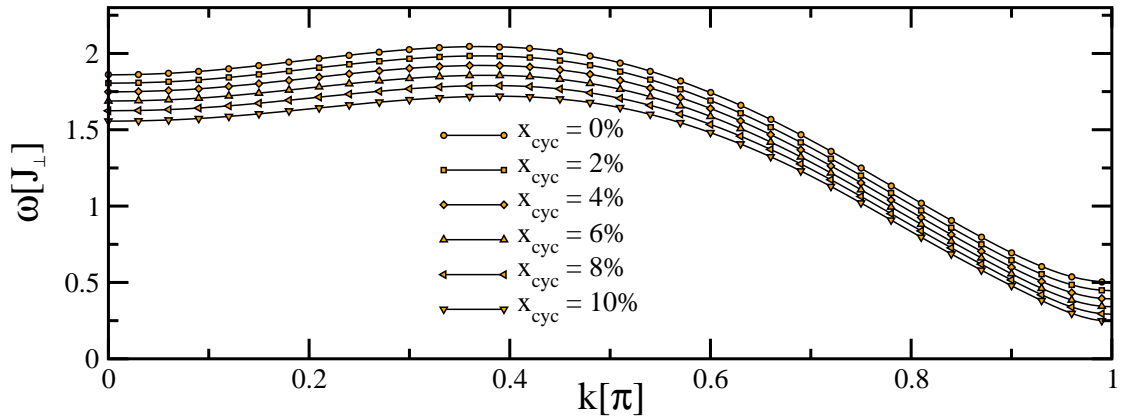


Figure 1.26.: Triplet dispersion for $x = 1$ with $x_{\text{cyc}} = 0, \dots, 10\%$ [58]

A general behavior for increasing J_{cyc} at fixed J_{\parallel} is the shift of the position of χ_{max} to lower temperatures in combination with an increase of χ_{max} . This effect is induced by the decrease of the whole dispersion, i.e. all energies are lowered [58, 69] as depicted in Fig. 1.26. The global $1/T$ factor enhances the value of χ_{max} when its position is moved to lower temperatures. For increasing x this effect is weakened. The increasing leg coupling provides an additional antiferromagnetic coupling stabilizing the system against magnetic perturbations. Thus, an increasing x stabilizes the system and counteracts an increasing x_{cyc} which destabilizes it.

In Figs. 1.27 and 1.28 the information content of a measurement of $\chi(T)$ is addressed (cf. Chapter 1.4). Fig. 1.27 shows the energy-scale independent quantity $\chi_{\text{max}}T_{\text{max}}$ which is a characteristic in experimental measurements. Note that for increasing x the differences between the curves for various values of x_{cyc} become smaller, because J_{\parallel} and J_{\perp} set the changing energy scale, whereas J_{cyc} stays constant. In the limit of large x the system approaches two independent chains with a decreasing relative interchain coupling induced by J_{\perp} and J_{cyc} . The arrow indicates the exactly known value of $\chi_{\text{max}}T_{\text{max}}$ for the isotropic Heisenberg chain [3].

Once the value of $\chi_{\text{max}}T_{\text{max}}$ is measured the parameter set (x, x_{cyc}) can be read off from the figure. But there is still an ambiguity which cannot be resolved by a measurement of $\chi(T)$ alone as illustrated in Fig. 1.28. There the rescaled susceptibilities are shown for the indicated values of $\chi_{\text{max}}T_{\text{max}}$ in Fig. 1.27 (solid horizontal lines). The main feature in the susceptibility curves is the maximum. For different sets of parameters for a specific value of $\chi_{\text{max}}T_{\text{max}}$ the qualitative and quantitative behavior cannot be distinguished unless precise measurements in the low temperature regime are possible.

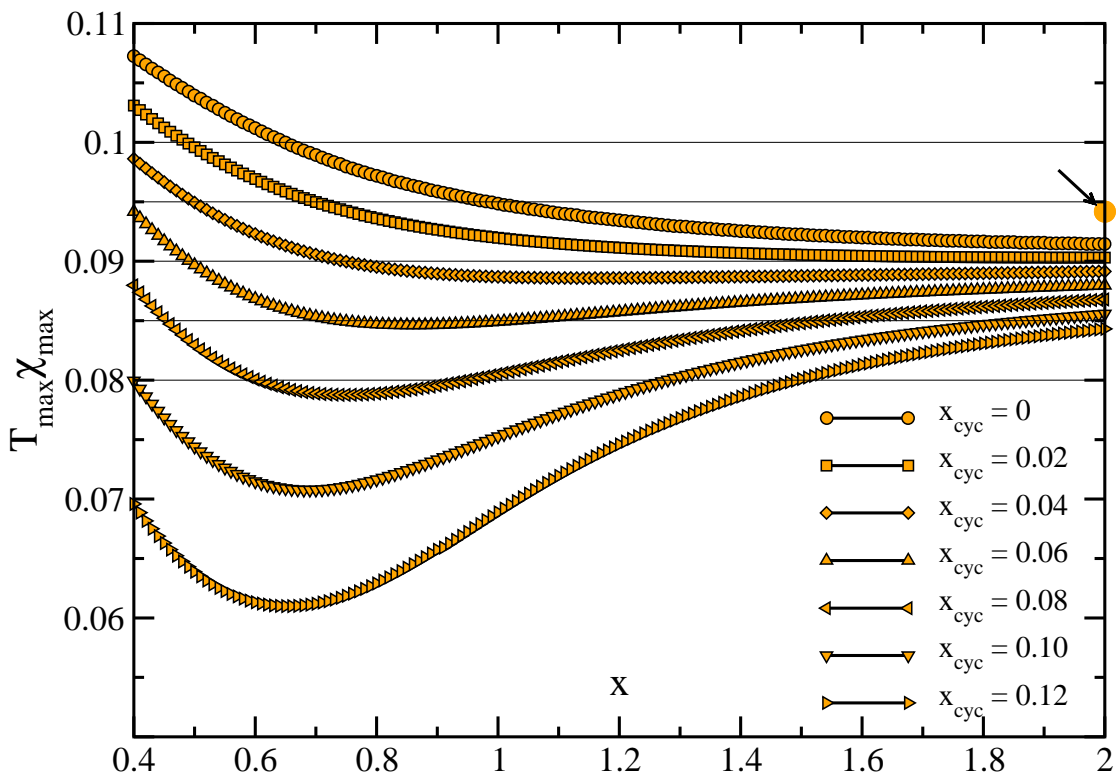


Figure 1.27.: $\chi_{\max} T_{\max}$ versus x for $x_{\text{cyc}} = 0, 0.02, 0.04, 0.06, 0.08$ and 0.1 in descending order. The symbols are the calculated data points from the HTSE. The solid circle on the right side indicates the $\chi_{\max} T_{\max}$ value for an isotropic chain which is known exactly [3]. Horizontal lines show the constant values used to rescale $\chi(T)$ in Fig. 1.28.

To summarize the latter results it is stated that with the present results of ECD and HTSE it is difficult to ascertain all model parameters from the temperature dependence of the susceptibility alone, see also discussion in the previous Chapter 1.4. It has to be pointed out that it might well be possible to determine all three coupling parameters J , x , and x_{cyc} if sufficient low temperature data is available. The magnetic specific heat can also give further insight when determining the model parameters, see the following paragraph. Considering low temperature quantities like the gap Δ can also help fix the parameters for a given substance. But, in the low temperature regime disturbing effects like impurities or longer range interactions may also hamper the determination of the model parameters.

Specific Heat Further information on the magnetic properties of a certain substance can be obtained by measuring also the magnetic specific heat $C(T)$. It is, however, difficult to extract the magnetic contribution from the measured specific heat if the energy scale of the lattice vibrations is of the same order as the magnetic couplings. In this case the

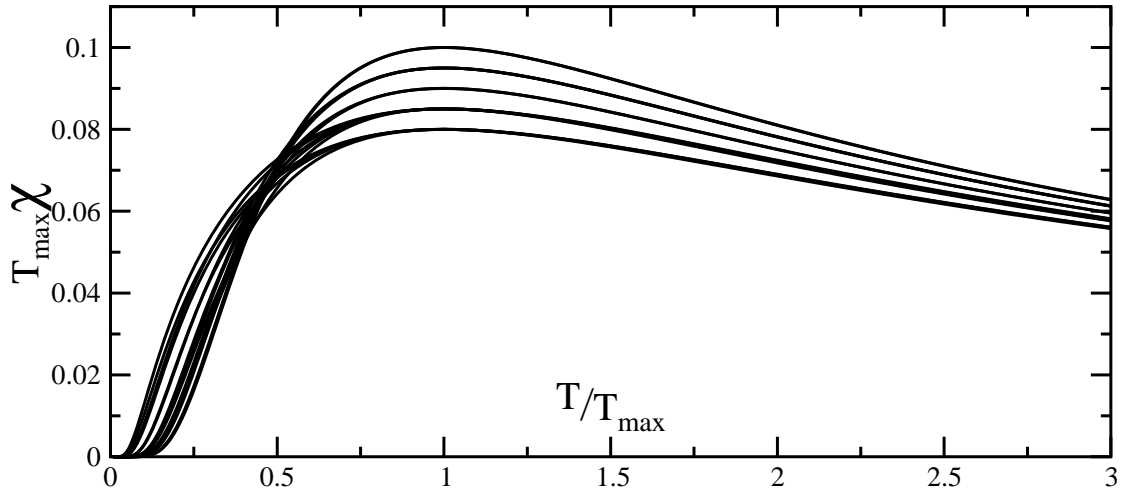


Figure 1.28.: Rescaled susceptibilities for $\chi_{\max} T_{\max} = 0.1, 0.095, 0.09, 0.085, 0.08$ for the x and x_{cyc} values shown in Fig. 1.27

specific heat is dominated by the phononic contributions and the magnetic part cannot be extracted thereof reliably. If the energy scale of the lattice vibrations is much larger than the magnetic couplings the specific heat of the magnetic subsystem can be distinguished from the contributions of the lattice vibrations following the usual T^3 law for $T \ll 1$ in contrast to the magnetic contribution vanishing linear in T .

Once the magnetic specific heat is known the ambiguity in determining the parameters can be resolved. Fig. 1.29 shows an overview of the magnetic specific heat for $x = 0.5, 1, 1.2$ and $x_{\text{cyc}} = 0, \dots, 0.1$. For increasing leg coupling x and fixed x_{cyc} the position of C_{\max} shifts to higher temperatures and the height lowers slightly for $x_{\text{cyc}} = 0, 0.02$, stays almost constant for $x_{\text{cyc}} = 0.04, 0.06$, and increases slightly for $x_{\text{cyc}} = 0.08, 0.1$. For increasing cyclic exchange x_{cyc} and fixed leg coupling C_{\max} moves to lower temperatures and decreases. This behavior is induced by the decreasing overall dispersion, see also the above discussion for $\chi(T)$ and Fig. 1.26.

1.5.6. Estimation of the Ground State Energy

This section is dedicated to a slightly different topic compared to the previous investigations. So far, thermodynamical properties have been derived from a series expansion about the limit of infinite temperature $\beta = 0$. For a high temperature series expansion these are the natural quantities to extract. Here, the investigation of a $T = 0$ quantity is addressed, namely the ground state energy e_0 . The results obtained by the method described in the following are rather qualitative than quantitative in nature. For sufficiently gapped systems though the results are very promising compared to results obtained by other methods developed for $T = 0$ properties.

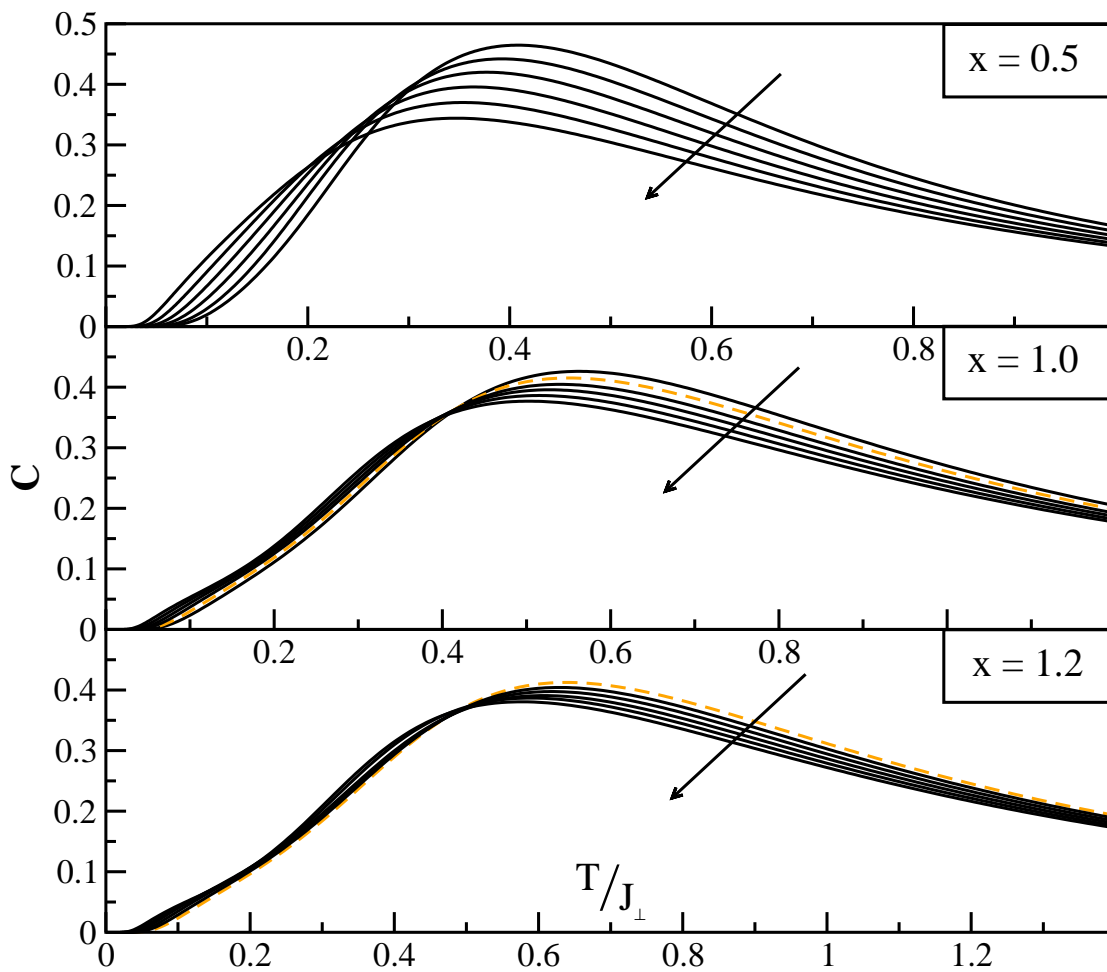


Figure 1.29.: $C(T)$ for three values for x with $x_{\text{cyc}} = 0, 0.02, 0.04, 0.06, 0.08$ and 0.1 in ascending order in direction of arrows. Dashed lines show $[6,4]$ Padé representations.

At first sight it is not obvious how to extract a ground state property out of a HTSE. When extrapolating the specific heat it became evident that the extrapolations are very sensitive to the precise knowledge of the ground state energy e_0 . Even a small uncertainty of 0.5% could lead to representations where for instance the height and position of the maximum of the specific heat deviate by one order of magnitude more, i.e. 5%. This behavior leads to the conclusion that it should be possible to extract information about the ground state energy out of the high temperature series expansion. Following an idea proposed in Ref. [27] one considers a quantity which displays a singularity on the real axis at e_0 .

Considering the internal energy $e - e_0$, a monotonic function of β , it is possible to invert

this relation in order to obtain a function $\beta(e - e_0)$ as was done in Eq. 1.70 with

$$\beta(e - e_0) \propto -\ln(e - e_0) , \quad (1.84)$$

where the low temperature information of the specific heat is incorporated. The inversion of the function $e(\beta)$ onto a function $\beta(e)$ is done by comparing the coefficients in each

Table 1.1.: Estimation of the ground state energy e_0^{HTSE} derived from HTSE compared to results e_0^{D} of a high order series about the limit of isolated rungs. The number in brackets denotes the error of the last significant digit(s).

x	x_{cyc}	e_0^{D}	e_0^{HTSE}
0.5	0%	-0.4297(1)	-0.428(18)
	2%	-0.4060(1)	-0.409(8)
	4%	-0.3825(1)	-0.389(6)
	6%	-0.3591(1)	-0.369(8)
	8%	-0.3359(1)	-0.350(10)
	10%	-0.3130(2)	-0.332(14)
1	0%	-0.5777(1)	-0.587(80)
	2%	-0.5569(1)	-0.580(80)
	4%	-0.5366(1)	-0.568(60)
	6%	-0.5169(3)	-0.556(40)
	8%	-0.4975(4)	-0.540(50)
	10%	-0.4785(4)	-0.530(50)
1.2	0%	-0.6490(1)	-0.671(120)
	2%	-0.6291(1)	-0.659(110)
	4%	-0.6097(1)	-0.648(110)
	6%	-0.5908(1)	-0.637(110)
	8%	-0.573(1)	-0.626(100)
	10%	-0.555(1)	-0.615(120)

order of expansion. With the function

$$G(e - e_0) = e^{\beta(e-e_0)} \propto \frac{1}{e - e_0} \quad (1.85)$$

the ground state energy e_0 should show up in $G(e - e_0)$ as the position of a pole on the real axis. Thus, the ground state energy can be estimated by investigating the poles of the Padé approximants of $G(e - e_0)$. The estimated ground state energies are listed in Table 1.1.

The estimated ground state energy e_0^{HTSE} from the analysis of the HTSE data is compared to the values e_0^{D} obtained by a high order series expansion about the limit of isolated rungs [58]. There, explicit $T = 0$ calculations were performed leading to precise values for the ground state energy. The obtained series expansion is extrapolated using Dlog-Padé approximants. Investigating different orders of extrapolations the error bars as given in Tab. 1.1 were determined. Considering low values of x_{CYC} a good agreement between e_0^{HTSE} and e_0^{D} is achieved when the error bars of both methods are taken into account. The relative deviation $(e_0^{\text{HTSE}} - e_0^{\text{D}})/e_0^{\text{D}}$ is of order 1%. For increasing x and x_{CYC} the estimated values deviate up to 10% from the very precise values e_0^{D} . In Ref. [27] the ground state energy of the Heisenberg model was estimated using a high temperature series expansion results for the internal energy up to order 22 in β . The authors estimated the relative error to be of order 1%. Here, the relative error bars should already be slightly higher due to the lower orders reached in the expansion of the specific heat. Thus, a realistic estimation of the error bars of the obtained values e_0^{HTSE} should also account for the uncertainty of the estimation itself. The error bars deduced from the investigation of the different orders of extrapolation were doubled to account for this fact. This should yield a rough upper bound of the real error bars of the estimations. The $[5, 4]$, $[4, 5]$, $[4, 4]$, $[3, 3]$, $[7, 2]$, $[6, 2]$ and $[5, 2]$ Padé extrapolations were used to obtain the values given in Tab. 1.1 with the approximated errors. Here, not only the diagonal approximants are considered but also the ones with a low order in the denominator. In low orders the pole appearing should be the pole originating from the ground state energy. Approximants with more than one real pole on the energy axis are neglected, because in general further poles strongly influence the shape of the function. They have no physical origin. The error bars deduced from the investigation of the different orders of extrapolation were estimated by computing the average value of the above listed extrapolations and considering the maximum deviations from it. A more sophisticated error estimation is not considered to be necessary here.

Further investigations can be made by inserting the estimated ground state energy into the representation of the specific heat $C(T)$. The sensitivity of the extrapolations to the precise knowledge of the ground state energy can yield a better approximation of e_0 . We refrain here from pursuing this route further since the direct computation of the $T = 0$ properties remains more reliable. Hence, the idea proposed above should rather serve as an illustration of what can be extracted out of the information already contained in the HTSE data for a $T = 0$ quantity than an actual algorithm. For models, however, in which the ground state energy cannot be determined the approach via the HTSE can indeed be useful.

1.5.7. SrCu_2O_3

This section is dedicated to the comparison of the theoretical findings with experimental results of the two-leg ladder compound SrCu_2O_3 . The substance SrCu_2O_3 is part of a homologous series of oxides, $\text{Sr}_{n-1}\text{Cu}_{n+1}\text{O}_{2n}$. These oxides consist of $\text{Cu}_{n+1}\text{O}_{2n}$ planes separated by Sr atoms along the crystallographic c -axis. The $\text{Cu}_{n+1}\text{O}_{2n}$ planes are cut into $(n+1)/2$ -leg ladders [100]. The systems with $n = 3, 7, 11, \dots$ can be characterized as frustrated quantum antiferromagnets with spin-liquid groundstates whereas the systems with $n = 5, 9, 13, \dots$ should have a gapless ground state [101] since the systems consist of ladders with an odd number of legs. For $n = 3$ ($\text{Sr}_2\text{Cu}_4\text{O}_6$ or SrCu_2O_3) a system of two-leg ladders is obtained as depicted in Fig. 1.30. Fig. 1.30 shows a schematic view on the plane containing the ladders. In a first approach the interladder coupling is negligible since the superexchange via a Cu-O-Cu path with a 90° bond angle has a smaller orbital overlap than with a bond angle of 180° along the ladders [102]. Furthermore, the interaction between the ladders is highly frustrated.

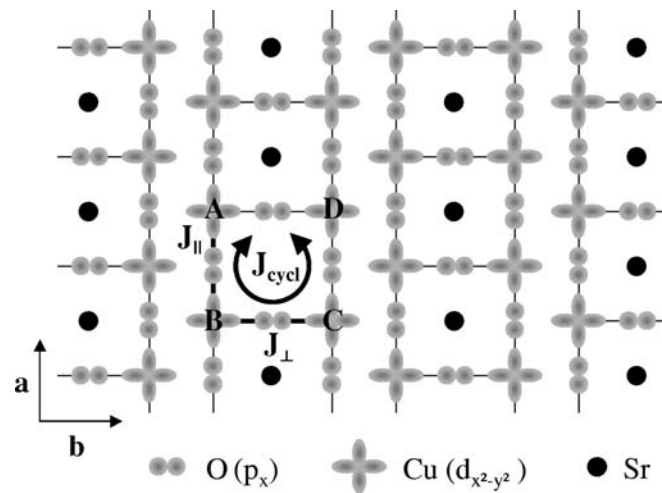


Figure 1.30.: Schematic view on the a - b plane of SrCu_2O_3 : The Sr atoms are located in-between the planes containing the Cu_2O_3 atoms. The coupling between two Cu d -orbitals is caused by superexchange interaction via an O p -orbital (reprinted from Ref. [85]).

The electronic properties of SrCu_2O_3 were studied experimentally by means of SQUID magnetometry [37], NMR [103], μSR [104], ESR [105], INS [106], and recently by Raman scattering [85]. The aim of the present section is to fit the theoretical findings to the experimental data of the magnetic susceptibility [37]. As preparation the most relevant information about the system is summarized. Using Cu-NMR [37, 103] the authors claimed a spin gap of $\Delta = 680\text{K}$. This value was questioned in Ref. [107]. The authors of Ref. [107] proposed the value extracted from a susceptibility fit to be more accurate with $\Delta = 420\text{K}$ [37]. Later on, this value was supported by INS results with $\Delta \approx 400\text{K}$ [106]. Performing an ESR experiment the Landé g -factor was determined as $g = 2.14$ [105].

Various theoretical methods have been applied to determine the relevant parameter sets for SrCu₂O₃. From the theoretical point of view it was remarked that a system of isolated ladders is not sufficient to describe the experimental results. An interladder coupling J' should also be included to describe the real conditions in SrCu₂O₃. The resulting two-dimensional model is known as trellis-lattice [108]. Using a mean-field type ansatz it could be shown that the interladder interaction is ferromagnetic with $J'/J \approx 10\% \dots 20\%$ [108]. In this analysis, the authors assumed isotropic ladders with $J = J_{\perp} = J_{\parallel}$. In Refs. [109, 110] QMC results for the trellis-lattice were fitted to the susceptibility data. The authors used a much higher fraction $J_{\parallel}/J_{\perp} = 2$ to fit their results and showed that the interladder coupling hardly influences the results compared to the isolated ladder. The findings from the analysis of the chemical structure (see above) support a fraction J_{\parallel}/J_{\perp} close to the isotropic case. Thus, a theoretical description with the Hamilton operator as given in Eq. 1.55 is a justified approach to fit the experimental results of the magnetic susceptibility, i.e. assuming a system of isolated ladders.

So far, the results for the fraction J_{\parallel}/J_{\perp} are ambiguous, ranging from $J_{\parallel}/J_{\perp} = 1 \dots 2$. The overall energy scale J_{\perp} is also not well defined. At a first guess, J_{\perp} was estimated to be about 1300K, judged from the resemblance of the ladder to the usual CuO₂ plane [37]. Using QMC results the best fit to the experimental results of the susceptibility was obtained using $J_{\perp} \approx 900\text{K}$, $J_{\parallel}/J_{\perp} \approx 1.2$, and an anomalously low g-factor of $g \approx 1.4$. Using the known g-factor with $g = 2.14$ and $J_{\parallel}/J_{\perp} = 2$ the experiment could be described best with $J_{\perp} \approx 1000\text{K}$ [110]. More recent results using a quantum chemical density functional technique proposed the value $J_{\perp} \approx 1670\text{K}$ with $J_{\parallel}/J_{\perp} \approx 1.1$ [102]. Recently, a Raman scattering study was performed with the result that a significant ring exchange must be included in the theoretical descriptions to explain their data [85]. The authors obtained the values $J_{\perp} \approx 1750\text{K}$, $J_{\parallel}/J_{\perp} = 1.1$, and $J_{\text{cyc}}/J_{\perp} \approx 0.04, \dots, 0.12$.

In the following, the results from the HTSE will be used to explain the experimental results of the susceptibility. The latest data was provided by M. Azuma. The data were collected up to 750K. Above this temperature the sample decomposed. Due to the high energy scale of J_{\perp} a clear maximum in the susceptibility is not visible in the temperature regime where the susceptibility could be measured, see Fig. 1.31. It is not intended to derive parameter sets completely independent from published values. The experimental data for the susceptibility at hand does not allow a sophisticated fitting procedure. At least the maximum of the susceptibility should be available to fit the HTSE data more reliably and in greater detail than will be done here. But with the HTSE results at hand it is possible to support or to discard parameter sets published so far.

In a first step the raw susceptibility data is corrected for the Curie-like contributions χ_{Curie} originating from magnetic impurities. A constant contribution from van-Vleck parts and from non-magnetic parts is extracted usually from the high temperature regime above the position of the maximum. Here, these contributions could only be estimated by adding a constant χ_0 to the Curie-like contribution χ_{Curie} because no data for temperatures above the maximum is available. Fig. 1.31 depicts the raw data and the data corrected by $\chi_{\text{imp}} = \chi_{\text{Curie}} + \chi_0$. A fit in the temperature regime $T < 75\text{K}$ yields $\chi_{\text{imp}} \approx (6.24/T + 0.075) \cdot 10^{-4} \text{emu/mol Cu}$.

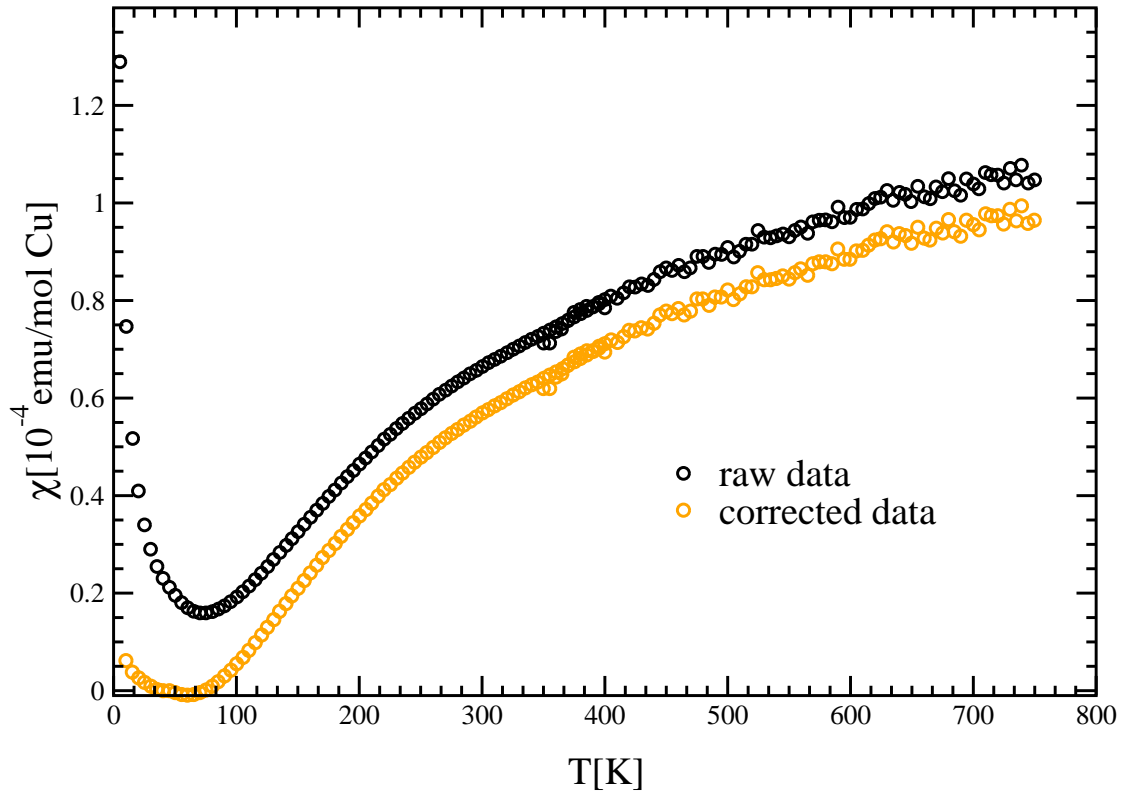


Figure 1.31.: Susceptibility of SrCu_2O_3 : the raw data and the corrected data are depicted (see main text).

In Ref. [37] the authors corrected the susceptibility only for a Curie-Weiss-like term neglecting constant contributions. They obtained a larger value for the Curie-like contributions with $\chi_{\text{Curie-Weiss}} \approx 9.86/(T + 2.03) \cdot 10^{-4} \text{emu/mol Cu}$. A more detailed discussion of the corrections is not possible because only little is known about the sample used in the experiment. The correction as performed here seems to be reliable since the corrected susceptibility goes down to zero for low temperatures as expected for a gapped system. The slight upturn for $T \lesssim 30\text{K}$ is due to slight inaccuracies in the corrections. But it does not affect the following considerations.

The aim of the fitting procedure of the HTSE data cannot be to determine all parameters entering the model 1.55, as discussed in the previous sections. In this thesis, the effects of an inclusion of a cyclic exchange term in contrast to ladder systems without this type of exchange is addressed. In Fig. 1.32 various parameter sets are used to fit the corrected experimental data.

For all representations of the susceptibility the known g -factor with $g = 2.14$ was used. The extrapolations were biased in the low temperature regime as described in Sec. 1.5.4 with the known gap $\Delta = 400\text{K}$. Firstly, the parameter sets $J_{\perp} = 1670\text{K}$, $x = 1.1$, $x_{\text{cyc}} = 0$ [102]

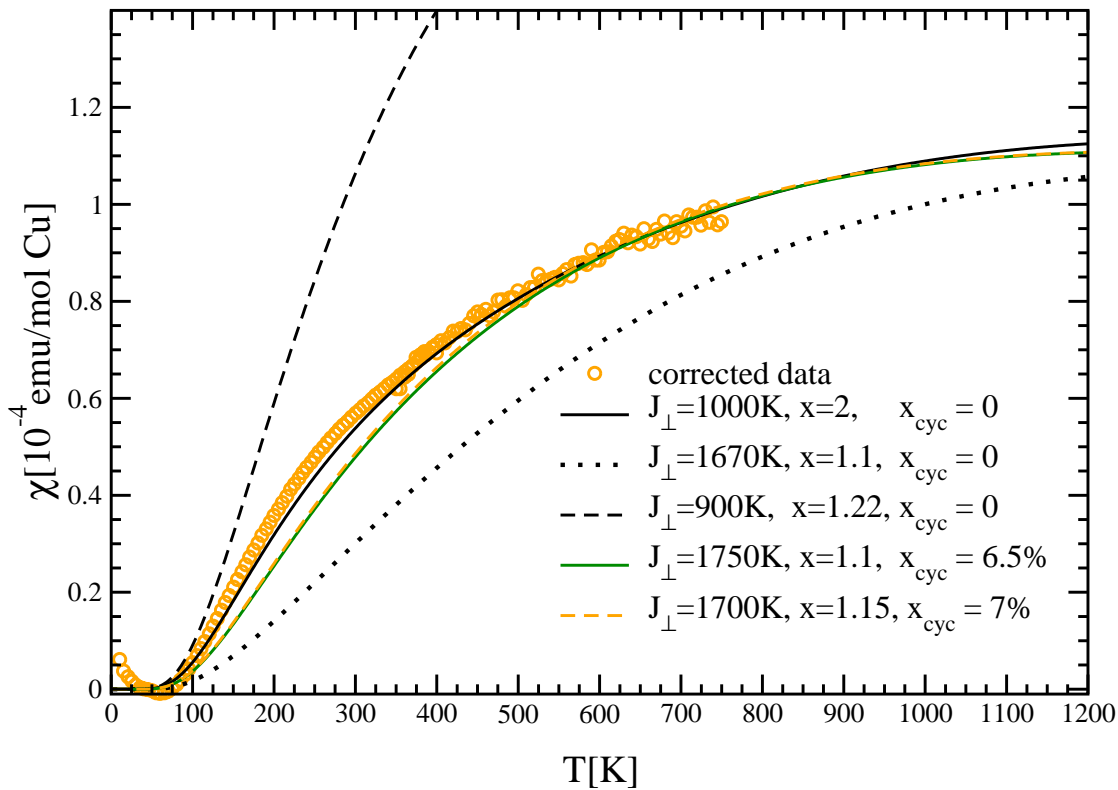


Figure 1.32.: Various susceptibility fits: The susceptibility is fitted to the corrected experimental data (see main text). The known g -factor with $g = 2.14$ and the gap with 400K was used for all curves.

and $J_{\perp} = 900\text{K}$, $x = 1.22$, $x_{\text{cyc}} = 0$ [107] are addressed. These parameter sets do not provide a quantitative description of SrCu₂O₃ when using the correct g -factor. The values proposed in Ref. [110] with $J_{\perp} = 1000\text{K}$, $x = 2$, $x_{\text{cyc}} = 0$ yield a good description of the experimental data, although the high value of the fraction $J_{\parallel}/J_{\perp} = 2$ is unexpectedly large, in view of the chemical structure of SrCu₂O₃, see discussion above. The last two parameter sets are examples that the inclusion of a small cyclic exchange can remove this discrepancy. The values $J_{\perp} = 1750\text{K}$, $x = 1.1$, $x_{\text{cyc}} = 6.5\%$ are taken from Ref. [85] where the amount of cyclic exchange x_{cyc} lies in the range proposed by the authors with $x_{\text{cyc}} = 4\%, \dots, 12\%$. This amount of cyclic exchange was also proposed by the authors of Ref. [81] for the structurally related compound La₆Ca₈Cu₂₄O₄₁. The last parameter set $J_{\perp} = 1700\text{K}$, $x = 1.15$, $x_{\text{cyc}} = 7\%$ depicts a fit with slightly different values compared to the latter values. The differences in the representations are not discernible in the figure. For temperatures $120\text{K} < T < 400\text{K}$ the curves differ slightly from the experimental data. As mentioned in the extrapolation section 1.5.4 the extrapolations are valid for $T \gtrsim 0.3J_{\perp}$, due to the low gap of $\Delta \approx 0.24J_{\perp}$. This in turn means that for temperatures below 450K

the extrapolations suffer from small inaccuracies. The exponential decay for $T < 120\text{K}$ is well described. Compared to the values used in Refs. [109, 110] with $J_{\perp} = 1000\text{K}$, $x = 2$, $x_{\text{cyc}} = 0$ the latter representations provide a similar agreement as the data for $J_{\perp} = 1000\text{K}$, $x = 2$. Furthermore, it is assumed that a significant amount of phases not contributing to the ladder system are contained in the sample of SrCu_2O_3 [111].

To summarize the fitting procedure of the HTSE data to the experimental results it can be assessed that the inclusion of a small amount of cyclic exchange can explain the more realistic values of x close to the isotropic ladder and the latest results of the overall energy scale J_{\perp} . The parameter set with $x = 2$ uses an overall energy scale which seems to be too low, thus not suitable for SrCu_2O_3 . Clearly, not all parameters could be obtained by the fits to the experimental data. We have rather attempted to explain that with a finite contribution of cyclic exchange the experimental results could be fitted with values closer to the supposed values for J_{\perp} and x in SrCu_2O_3 . The accuracy in determining the parameter sets for SrCu_2O_3 could be enhanced significantly if experimental data for the susceptibility was available for higher temperatures i.e. at least describing the maximum of χ better.

1.5.8. Conclusions

Summarizing, the thermodynamic properties of the two-leg spin-1/2 ladder with cyclic exchange were investigated. The representation of the HTSE results were optimized by using Dlog-Padé and Padé extrapolations including the behavior of the considered quantities, $\chi(T)$ and $C(T)$, at low temperatures. Comparison to ECD results showed the excellent accuracy of the HTSE results with the extrapolation scheme used down to very low temperatures. The aim was to present the effects of a cyclic spin-exchange on the ladder model.

The results can serve as input for quick and easy data analysis to determine the model parameters. In particular, the experimentally interesting position and height of the maxima of $\chi(T)$ and $C(T)$ can be described quantitatively. In Sec. 1.5.7 a direct comparison to experimental results is performed for the two-leg ladder compound SrCu_2O_3 . A set of the specific parameters is extracted from experimental $\chi(T)$ data [37]. In doing so, the knowledge of the singlet-triplet gap Δ obtained from INS measurements [106] and the known g -factor [105] are incorporated.

It was shown that with the measurement of one quantity alone, e.g. the magnetic susceptibility, it is difficult to determine all model parameters unless precise low temperature information is available. Additional information like the spin gap or the specific heat from other experiments is needed to fix the parameters reliably.

1.6. Shastry-Sutherland Model

1.6.1. Introduction

The previous investigations had their main focus on quantum antiferromagnets in (quasi-) one dimension with spin $S=1/2$: the dimerized, frustrated chain and the spin-ladder with cyclic exchange. Here, a two dimensional system is addressed which shows a rich zero temperature phase diagram. The model displays phases with long range ferromagnetic, antiferromagnetic and helical order as well as an interesting short range spin liquid order phase. The results presented here will emphasize the spin gapped phase where a direct comparison between experiment and theory is possible.

In 1981 the model was introduced by Shastry and Sutherland [112] as a two-dimensional generalization of the one-dimensional Majumdar-Ghosh model [54]. Some exact results for the ground state of the Shastry-Sutherland model were derived. The rich phase diagram is still of great theoretical interest since it is not completely understood.

The system attracted attention with the experimental realization of the Shastry-Sutherland model in the orthoborate $\text{SrCu}_2(\text{BO}_3)_2$ synthesized by Smith and Kezler in 1991 [113]. Now, it is possible to compare directly the theoretical findings to experimental data.

In the literature the main focus is on the low temperature properties of the system such as the ground state, elementary excitations and magnetization plateaus, but the thermodynamical properties of the system also attracted attention. By means of high temperature series expansion results the thermodynamical properties are presented in this chapter. A separate section addresses the theoretical results compared to thermodynamical data of $\text{SrCu}_2(\text{BO}_3)_2$.

This chapter is organized as follows. The following section presents the model and the results obtained so far. Sec. 1.6.3 is dedicated to the computational details. The results are introduced in Sec. 1.6.4 and applied to $\text{SrCu}_2(\text{BO}_3)_2$ in Sec. 1.6.5. Sec. 1.6.6 concludes the chapter.

1.6.2. Model

The Hamilton operator describing the Shastry-Sutherland model, see Fig. 1.33, with spins of size $S = 1/2$ on the vertices is given by

$$H = J_1 \sum_{\substack{\text{intra dimers} \\ i,j}} \mathbf{s}_i \mathbf{s}_j + J_2 \sum_{\substack{\text{inter dimers} \\ k,l}} \mathbf{s}_k \mathbf{s}_l . \quad (1.86)$$

The sums are running over all couplings between the sites connecting diagonal bonds (J_1), henceforth denoted as dimers, and between sites on different dimers (J_2), respectively. In the limit $J_1 = 0$ a simple square lattice is obtained. Thus, the model can be seen as a square lattice with additional (frustrating) diagonal bonds. The ratio $x = J_2/J_1$ is introduced as the inverse frustration. The two dimensional Heisenberg model with $J_1 = 0$ is of special interest since it is used as the minimal magnetic model describing the undoped copper-oxide planes in high T_c superconductors.

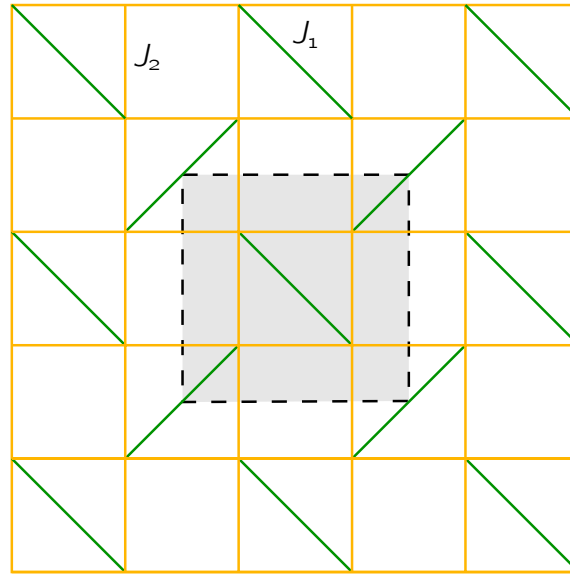


Figure 1.33.: Shastry-Sutherland model with spins on the vertices. The couplings on the square lattice are parameterized by J_2 and the diagonal couplings (dimers) are parameterized by J_1 . The grey shaded region depicts the unit cell of the system.

Since the discovery of an experimental realization of the Shastry-Sutherland model numerous publications are dedicated to the investigation of that specific model. The main focus was put on the low temperature properties.

Shastry and Sutherland showed in their early work [112] that the dimer-singlet state is always an eigen state of the Hamiltonian in Eq. 1.86. The dimer-singlet state is a product of singlets on every dimer. For values of the inverse frustration $x = J_2/J_1 < 1/2$ ($S = 1/2$) and for $x < 1/(2S + 2)$ ($S \geq 1$) this is also the ground state. The ground state energy is then given by $e_0 = E_0/N = -J_1/2 \cdot S(S + 1)$ where N is the number of sites.

In Fig. 1.34 the $T = 0$ phase diagram is shown, taken from Ref. [114]. In the regime $|J_2| > J_1$ the ground state orders antiferromagnetically for $J_2 > J_1$ and ferromagnetically for $J_2 < J_1$. For $J_2 = 0 > J_1$ a phase of independent spin- $2S$ dimers is obtained. In the regime $0 < |J_2| < J_1$ a finite region of the phase diagram is occupied by a dimer phase which exists for all finite values of the spin S . The nature of the two adjacent phases is not completely understood. In Ref. [114] improved upper and lower bounds on the phase boundaries of the dimer phase were derived using a variational ansatz. In the ferromagnetic case $J_2 < 0$ the intermediate phase between the dimer and ferromagnetic exists for values of the spin $S > 1/2$ and vanishes for $S = 1/2$. For $S = 1/2$ there is a first order phase transition directly from the dimer to the ferromagnetic (FM) phase. The phase line is exactly known to be at $J_2 = -J_1 \rightarrow x = -1$. On the antiferromagnetic side ($J_2 > 0$) for all values of the spin S an intermediate phase between the dimer and antiferromagnetic phase exists.

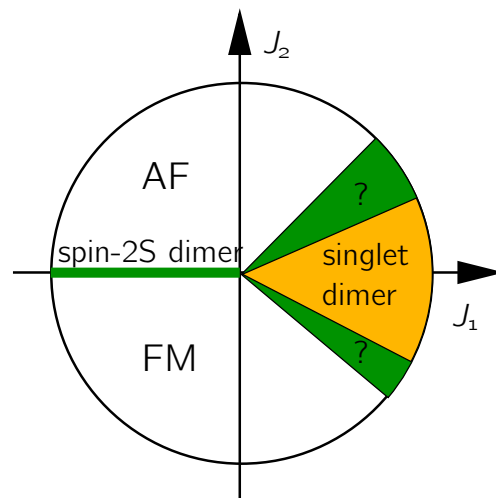


Figure 1.34.: Phase diagram for the Shastry-Sutherland model with $S < \infty$. For $S = 1/2$ there is a first order phase transition directly from the dimer to the ferromagnetic (FM) phase. The phase line is exactly known to be at $J_2 = -J_1$ [114].

The nature of the phases adjacent to the dimer phase are under intense investigation at the moment. A first approach is considering the classical phase diagram ($S \rightarrow \infty$) where for $0 < |J_2| < J_1$ a long range helical phase exists [114]. Using Schwinger boson mean field theory such a phase was indeed verified for finite values of the spin S , vanishing in a second order phase transition in favor of the Néel phase [115]. But, using field theoretical arguments the intermediate phase is characterized by a weakly incommensurate spin density wave [116] or as Bose condensates where the adjacent regime exhibit collinear and helical phases [117].

Numerous articles focus on the $S = 1/2$ case and especially on the phase boundary where the dimer phase vanishes on the antiferromagnetic side ($J_2 > 0$) [118–124]. In Ref. [118] exact diagonalization and fourth order perturbation theory were used finding a direct dimer to Néel transition of first order at $x \approx 0.7$. Large scale exact diagonalizations [122] yield an upper critical value of $x_c = 0.67$ for the dimer phase. For $0.67 < x < 0.7$ the authors support an intermediate plaquette phase and exclude an intermediate columnar phase. In Ref. [123] a helical intermediate phase is claimed again using a novel operator variational method. Perturbational approaches could not resolve the problem of determining a precise critical value of x where the dimer phase vanishes. In Ref. [125] a plaquette phase in the interval $0.677 < x < 0.861$ is claimed whereas Refs. [119, 121] exclude such an intermediate plaquette phase. The authors propose a columnar phase for $0.67 < x < 0.83$. A detailed investigation of the behavior of the gap as a function of the inverse frustration yields $x = 0.697$ signaling the breakdown of the dimer phase [120, 124]. The results can be summarized in an upper critical value of the inverse frustration $J_2/J_1 = x$ slightly below

$x_c = 0.7$ where the dimer phase vanishes in favor of an intermediate phase. The nature of the intermediate phase is so far not completely understood. The interested reader is referred to current publications.

The Shastry-Sutherland model can be generalized to three and more dimensions in such a way that these models have still an exact dimer-singlet ground state [126, 127]. Such investigations are also helpful for a better understanding of $\text{SrCu}_2(\text{BO}_3)_2$, for details see Sec. 1.6.5, which represents indeed a three dimensional system.

1.6.3. Computation

The computation of the thermodynamical quantities by means of a high temperature series expansion cannot be done as explained in the previous chapters for the one-dimensional systems. To obtain results correct in the thermodynamical limit in every order of expansion the system size has to be adjusted properly. The extension from one to two dimension poses no more problems, theoretically and methodically. But, numerically the minimal system size to be considered in every order of expansion increases quadratically with the system size and not linear as is the case for the one-dimensional models. Thus, the orders of expansion reached are lower than the ones for the one dimensional systems. To obtain results e.g. up to order 6 in the inverse temperature β a system of size 4×4 dimers has to be considered, see Fig. 1.35 a. In the following the representation of the Shastry-Sutherland model as depicted in Fig. 1.35 is used. The equality between the representation from Fig. 1.33 and from Fig. 1.35 becomes obvious when rotating the system by $\pi/4$ and slightly distorting the J_2 bonds. The dimension of the complete Hilbert space of the system with 4×4 dimers and 32 sites respectively is 2^{32} . This in turn means that 4GB memory is needed to store all the necessary information for the whole system when assuming only one byte of information per base state. Hence, a complete enumeration of the Hilbert space is not feasible.

A more useful ansatz for the computation of the results is the one presented and explained in detail in Refs. [20, 21], the so-called moment-algorithm. Basically, the computation of the trace is reduced to the computation of an expectation value. To this end, the system is virtually doubled and a product state of singlets $|S\rangle$ with

$$|S\rangle = \prod_{i=1}^N \frac{1}{\sqrt{2}} (|\uparrow_r \downarrow_v\rangle - |\downarrow_r \uparrow_v\rangle) |i\rangle \quad (1.87)$$

between every real site and its virtual partner (denoted with index r and v , respectively) is introduced, also depicted in Fig. 1.36. In every order of expansion traces of powers of the Hamiltonian have to be computed, e.g. $\text{Tr} H^n$ in n th order. By using the singlet product state $|S\rangle$ from Eq. 1.87 the trace of an operator operator A is reduced to the computation of the expectation value with respect to this state, leading to $\text{Tr}\{A\} = \langle S|A|S\rangle$. A simple calculation for a two site system should serve as an illustration that the equality between

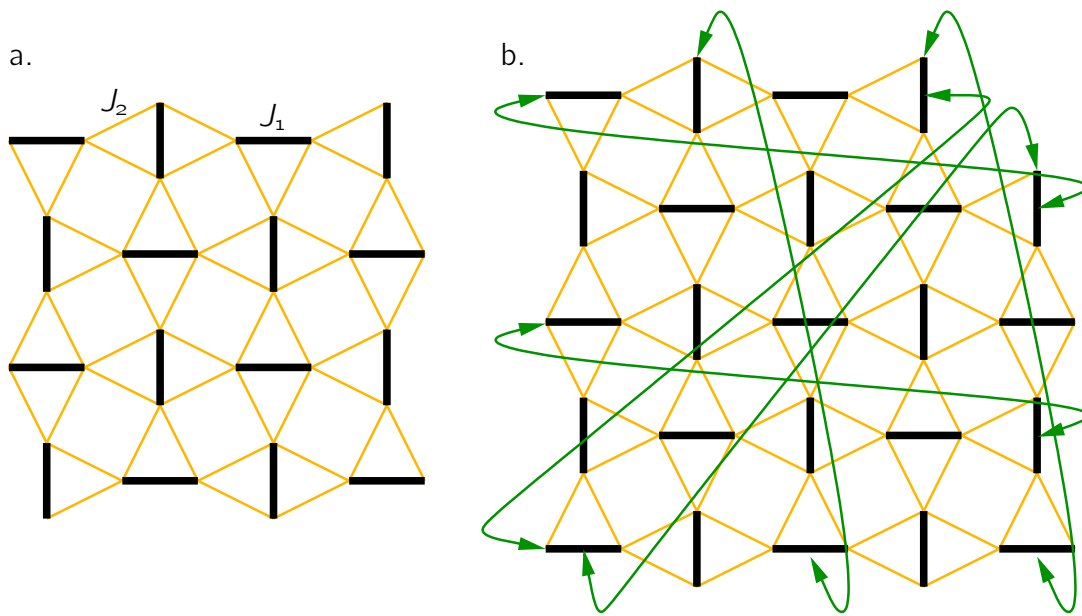


Figure 1.35.: a. 4×4 Dimers system with periodic boundary conditions (not shown). b. System of 24 dimers computed with indicated periodic boundary conditions. Thick lines present the dimers, thin ones the interactions between the dimers. The arrows indicate the (shifted) periodic boundary conditions.

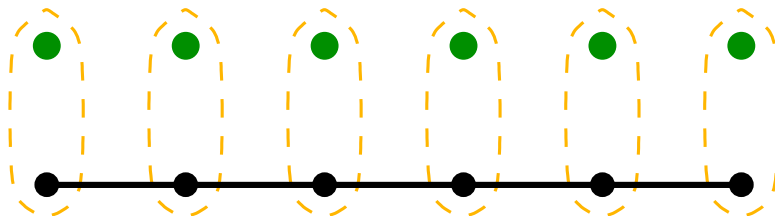


Figure 1.36.: Virtually doubled system, where the linear chain serves as an example. The solid line represents the real system and the dashed objects together with the virtually doubled sites depict the singlet states introduced for every pair of real and virtual site, see Eq. 1.87.

the trace and the expectation value holds.

$$\begin{aligned}
 \text{Tr}A &= \langle \uparrow | A | \uparrow \rangle + \langle \downarrow | A | \downarrow \rangle \\
 &= \langle \uparrow_r \downarrow_v | A_{\text{ext.}} | \uparrow_r \downarrow_v \rangle + \langle \downarrow_r \uparrow_v | A_{\text{ext.}} | \downarrow_r \uparrow_v \rangle \\
 &= \langle S | A_{\text{ext.}} | S \rangle ,
 \end{aligned}
 \tag{1.88}$$

where $A_{\text{ext.}}$ acts on the tensor product of the real and doubled Hilbert space in the canonical

way. That is A becomes $A_{\text{ext.}} = A \otimes 1$ acting as the identity on the doubled Hilbert space. A detailed description is given in Refs. [20, 21].

In every order of expansion only the base states with nonvanishing matrix elements $\langle S|H^n|S\rangle$ are generated. By applying the Hamiltonian H multiply to $|S\rangle$ the so-called Krylov space $\{|S\rangle, H|S\rangle, H^2|S\rangle, \dots\}$ is constructed.

The model presented in Fig.1.35 b. can be treated up to order 8 in the inverse temperature β . The occurring wrap-around effects can be corrected as explained in the previous sections by identifying the wrap-around paths, which only are possible because of the finite system size.

Fig. 1.35 b. shows a system of 24 dimers and 48 sites, respectively, with shifted periodic boundary conditions. Due to the doubling of the system each site together with its partner can be in one of the four possible states: singlet or one of the three triplets. To represent a basis state in the virtually doubled system a combination of two integers is required: one of the type `long int` and one of type `long long int`. The combination leads to an integer of size $2^{32} \cdot 2^{64} = 2^{96}$. Thus, each basis state of the complete Hilbert space of this system can unambiguously be identified by the combination of these two integers.

Using the system depicted in Fig. 1.35 b. it was possible to compute the 8th order result in β for the specific heat and the 7th order result for the susceptibility. The amount of memory needed was about 30GB with a total running time of about three days.

1.6.4. Results

The magnetic susceptibility and the magnetic specific heat are provided as series expansion in the inverse temperature up to order β^8 for the specific heat and up to order β^7 for the susceptibility, respectively, with the full dependency on the model parameters, i.e. $\beta = J_1/T$ and the inverse frustration x . The coefficients are obtained as fractions of integers such that no accuracy is lost. Weihong et al. published a high temperature series expansion for the same quantities up to order seven [119]. The coefficients were not listed in their publication. All series coefficients obtained in this thesis are listed in App. A.4.

Different approximation schemes are used to extrapolate the quantities compared to Ref. [119]. Especially for the specific heat the extrapolation in this thesis poses a significant improvement. The known sum rules of the energy and entropy are built in explicitly to bias the extrapolations. The susceptibility is extrapolated by using additional information about the zero temperature behavior, which improves the convergence of the extrapolations.

The following two paragraphs are dedicated to the results and to their extrapolations for the specific heat and the magnetic susceptibility, respectively. The results presented are restricted to the gapped phase on the antiferromagnetic side, i.e. values of $0 \leq x < 0.7$ and $J_1 > 0$ are considered. But it has to be pointed out that the series expansion results are also valid outside the dimer phase.

To obtain the best representations possible of the quantities under study the highest orders available are used, i.e. 7th order in β for $\chi(T)$ and 8th order in β for the specific heat.

Specific Heat The specific heat is extrapolated using the representation in the internal variable as described in Sec. 1.3.2. For the actual model no comparison between the extrapolation in the internal variable and the extrapolations using Dlog-Padé representations are done. With the orders available at hand, the extrapolations used in the following yield much better representations than the extrapolations using Dlog-Padé approximants could achieve. In this thesis the focus is laid on the gapped spin liquid phase for $0 \leq x \lesssim 0.7$, the so-called dimer phase, see Fig. 1.34. In this parameter regime the ground state is exactly known with $e_0 = E_0/N = -3/8J_1$ [112]. The precise knowledge of the ground state is a basic requirement for the extrapolation in the internal variable. Further low temperature information can be built in by using the knowledge of the specific heat $C(T)$ for low temperatures, for a detailed explanation see Chapter 1.3.

The behavior of $C(T)$ for $T \ll 1$ is derived by an analysis similar to the one done in Ref. [24] for a ladder system. The calculations are also valid for the two dimensional Shastry-Sutherland model. In Ref. [24] the authors obtained an expression for the free energy taking into account that the elementary excitations i.e. singlet-triplet excitations on a dimer, obey a hard-core statistics: no more than one triplet can be excited on a dimer at the same time. At low enough temperatures $T \ll \Delta_{01}$, where Δ_{01} is the singlet-triplet gap, the residual interactions between these excitations and their kinematical interactions are negligible. Then, the free energy f is given by

$$f = -\frac{3}{2\beta}z(\beta) \quad \text{with} \quad z(\beta) = \frac{1}{(2\pi)^2} \iint_{-\pi}^{\pi} dk_x dk_y e^{-\beta\omega(\mathbf{k})} \quad (1.89)$$

Due to the localized nature of the triplet excitations the singlet-triplet dispersion $\omega(\mathbf{k})$ is almost flat [120]. Thus, in a first approach the dispersion can be estimated to be constant for the current purpose with $\omega(\mathbf{k}) = \Delta_{01}$ leading to

$$f = -\frac{3}{2\beta} e^{-\Delta_{01}\beta} . \quad (1.90)$$

The behavior of the specific heat is then derived using standard thermodynamic relations with

$$C(T) = \beta^2 \partial_\beta^2 \ln Z = \beta^2 \partial_\beta^2 (-\beta f) \propto \beta^2 e^{-\Delta_{01}\beta} \quad \text{for} \quad T \ll \Delta_{01} . \quad (1.91)$$

For the explicit extrapolations the value of the gap Δ_{01} is built-in. It is taken from explicit $T = 0$ calculations using a high order series expansion about the limit of isolated dimers [57], see also Fig. 1.38. To obtain the low energy (low temperature) behavior of the entropy the reader is referred to Sec. 1.4.4 where an analogous calculation was carried out. Basically, the function

$$G(y) = y \partial_y \frac{S(y)}{y} \quad \text{with} \quad y = e - e_0 \quad (1.92)$$

is extrapolated using the gap information via

$$G(y = 0) = -\frac{1}{\Delta_{01}} . \quad (1.93)$$

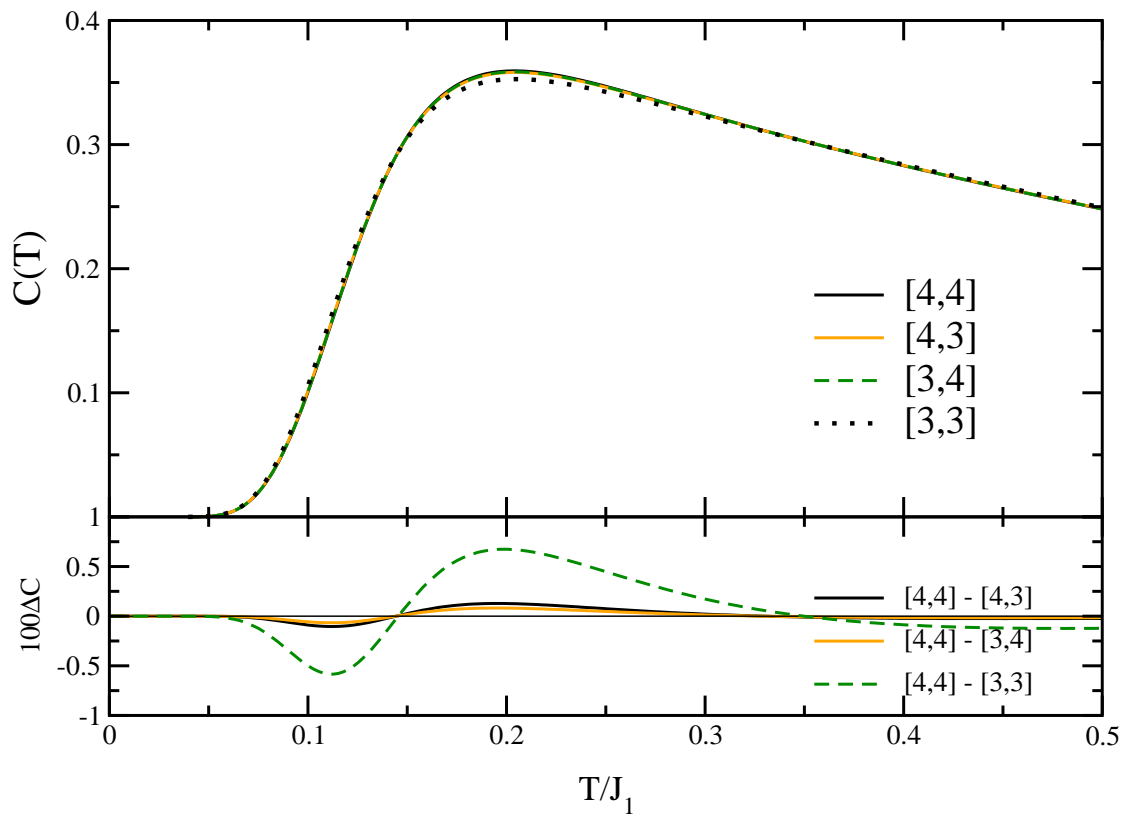


Figure 1.37.: Specific heat for the Shastry-Sutherland model with $x = 0.5$. Different extrapolations in the internal variable are shown (upper plot) and compared to the best representation found (lower plot)

In Fig. 1.37 various orders of extrapolations of the specific heat are shown. Due to spurious poles lower orders are not accessible. The [4, 4] representation is compared to the lower orders available. The convergence of the representations are even in low orders very satisfying though unfortunately no data sets are available for the [2, 2] extrapolations due to spurious poles.

Concluding the extrapolation and representation of the specific heat it has to be noted that even with lower orders in the series expansion than for the one-dimensional systems very good representations of the results are possible. For increasing values of x , where the gap Δ_{01} becomes small the representations suffer from inaccuracies in the low temperature regime. This is mainly due to the fact that for a decreasing gap the maximum of the specific heat shifts to lower values of the temperature and thus is harder to access by means of a HTSE and its extrapolations.

Susceptibility Making use of the experience from the previous chapters for the one dimensional systems the susceptibility is extrapolated using Dlog-Padé representations in the

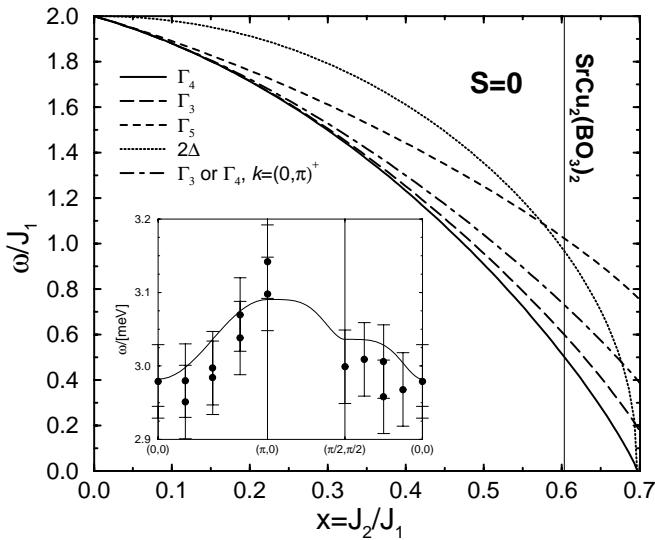


Figure 1.38: Reprint of Fig. 3 in Ref. [120], showing the energies per dimer of the lowest lying $S = 0$ states: the curves refer to $\mathbf{k} = 0$ except the dash-dotted one. The dotted curve displays the continuum at $2\Delta_{01}$. The inset shows the one triplet dispersion of $\text{SrCu}_2(\text{BO}_3)_2$ and the theory with $x = 0.603$ and $J_1 = 72\text{K}$.

Euler transformed variable $u = \beta/(1 + \beta)$. Here also, the low temperature behavior is built in as explained in Sec. 1.3.1. Sum rules as existing for the extrapolations of the specific heat are not available for the susceptibility. But the behavior of the susceptibility at low temperatures is known and hence built in to bias the extrapolations in this temperature regime.

The behavior of the susceptibility at low temperatures in the gapped phase is derived similarly to the low temperature behavior of the specific heat. The calculations from Ref. [24] are adapted to the Shastry-Sutherland model. Using $z(\beta)$ from Eq. 1.89 which is the Laplace transform of the density of the excited states the susceptibility is given by

$$\chi(T) = \beta z(\beta) \propto \beta e^{-\Delta_{01}\beta} \text{ for } T \ll \Delta_{01}, \quad (1.94)$$

with the singlet-triplet gap Δ_{01} obtained from Ref. [57]. In Fig. 1.38 the behavior of the gap $\Delta_{01} = \omega(k = 0)$ as function of the inverse frustration x is shown. The picture is a reprint of Fig. 3 in Ref. [120].

Fig. 1.39 shows an overview of the possible Dlog-Padé extrapolations for $x = 0.5$. Extrapolations with higher orders in the denominator e.g. $[n, 3]$ or $[n, 4]$ are not possible due to spurious poles. In the following, the $[n, 2]$ extrapolations will be used leading to the best extrapolations possible of the results. Higher orders in the denominator with $n > 2$ are not recommendable because of the lower orders reached in the series expansions compared to the one-dimensional systems. With increasing order of the extrapolations reliable predictions of the susceptibility are possible for $T \gtrsim 0.6J_1$. For lower temperatures the error bars of the representations are significant, not allowing for quantitative predictions.

Summarizing the extrapolations for the susceptibility, it is possible to obtain results quantitatively valid down to $T \approx 0.6J_1$ for the highest order possible. In contrast to the one-dimensional systems the convergence is less satisfying due to the lower orders reached. It has to be mentioned that the accuracy of the extrapolations is sensitive to the value of the inverse frustration x . For values $x \lesssim 0.6$ the extrapolations yield very good results but

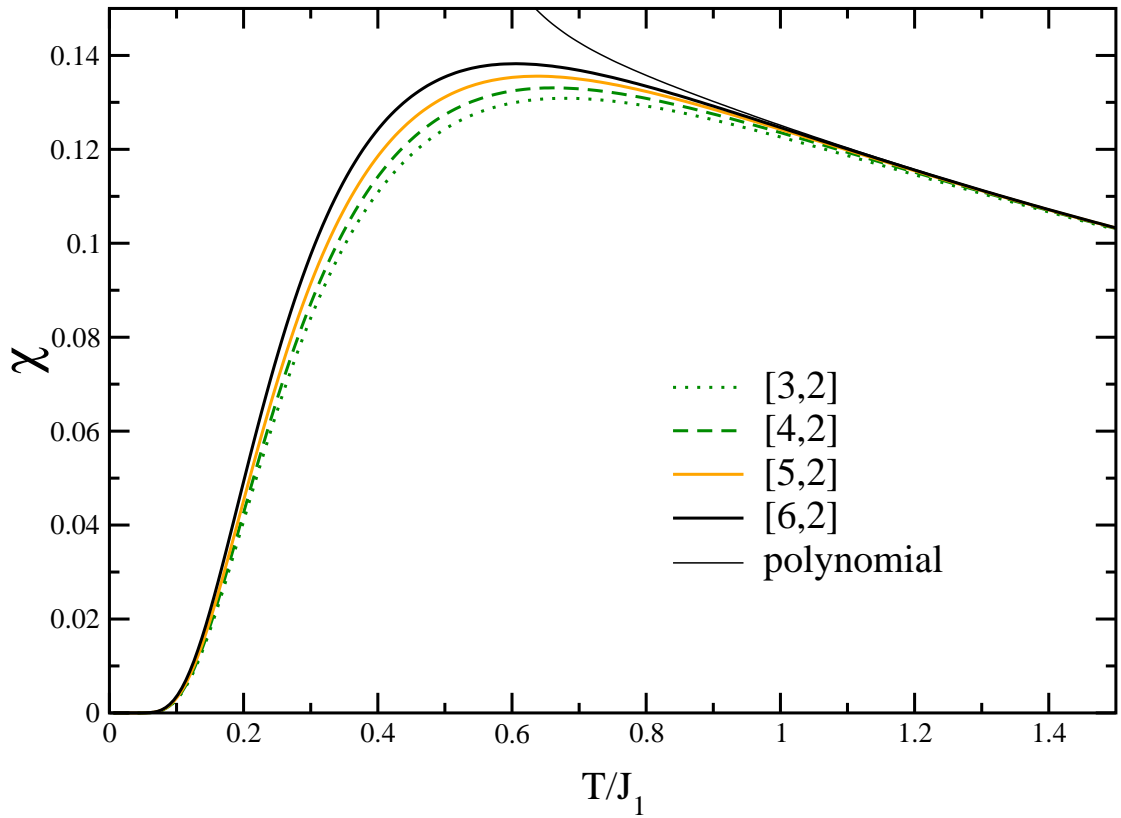


Figure 1.39.: Susceptibility for $x = 0.5$. Various orders of Dlog-Padé extrapolations and the polynomial are shown.

in the regime $0.6 \lesssim x \lesssim 0.7$ the extrapolations of the HTSE data become less reliable in the low temperature regime. The position of the maximum of the susceptibility moves to lower temperatures with increasing x , mainly due to the decrease of the gap. Hence, the maximum of the susceptibility can hardly be described by means of extrapolations of the HTSE data. But even the 7th order results can be used for a quantitative analysis as it will be done in the following.

1.6.5. $\text{SrCu}_2(\text{BO}_3)_2$

With the synthesis of the orthoborate $\text{SrCu}_2(\text{BO}_3)_2$ by Smith and Kezler in 1991 [113] the Shastry-Sutherland model experienced new vital interest. The schematic crystal structure is shown in Fig. 1.40. The compound $\text{SrCu}_2(\text{BO}_3)_2$ has a layered structure with $\text{Cu}(\text{BO}_3)$ planes separated by Sr atoms. For temperatures below $T_S = 395\text{K}$ these planes are slightly buckled as depicted in the left figure. At T_S a second order structural phase transition occurs where the planes become completely flat [128]. The vertical direction corresponds to the crystallographic c -axis. The right figure in Fig. 1.40 depicts the ab -plane constructed

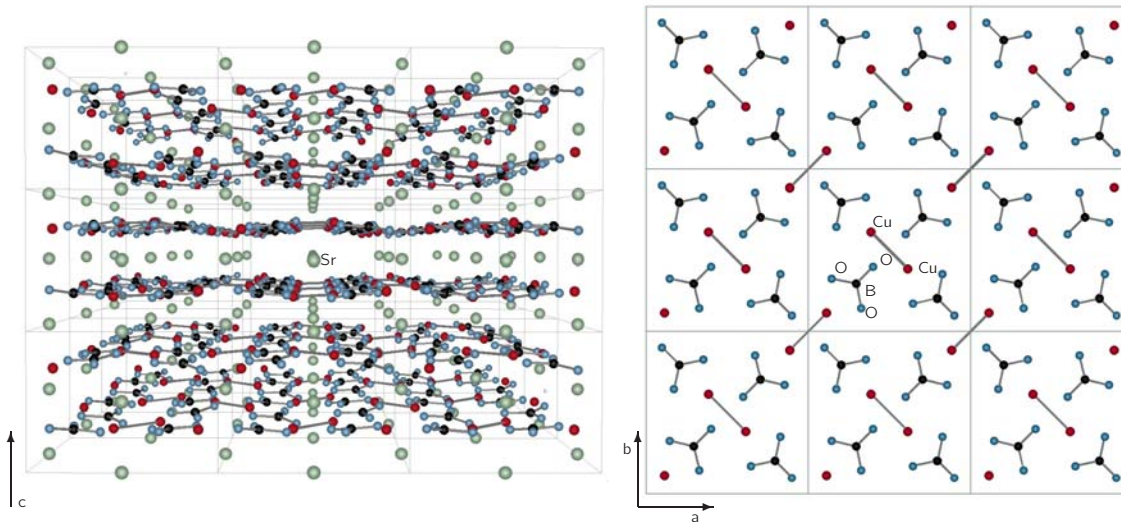


Figure 1.40.: Crystal structure of SrCu₂(BO₃)₂: it is a layered compound with slightly buckled Cu(BO₃)₃-planes for temperatures below T_S (see main text) separated by Sr-atoms as depicted in the left figure. The right figure displays a top view of a single Cu(BO₃)₃-plane (nine unit cells).

by the Cu(BO₃)₃-units. The magnetism is governed by $S = 1/2$ spins located on the Cu²⁺ ions, where two adjacent Cu²⁺ ions are connected by a line in the figure. They form the dimers with interaction strength J_1 . The exchange path between second nearest Cu²⁺ ions is mediated by the borate groups. These couplings are modeled by the interaction J_2 . The depicted Cu(BO₃)₃-plane can be mapped onto the $S = 1/2$ Shastry-Sutherland model (see for comparison Fig. 1.33) which was first observed in Ref. [129].

The first measurements on SrCu₂(BO₃)₂ were performed by Kageyama et al. [131] in 1999. They published data on the magnetic response of the system. The theoretical findings will be used to fit their data of the magnetic susceptibility, see below. By a simple exponential fit to the magnetic susceptibility they derived a rather low value for the singlet-triplet gap of $\Delta_{01} = 19\text{K}$. One year later Kageyama et al. published inelastic neutron scattering (INS) data confirming a small gap, but at higher energies with $\Delta_{01} \approx 34\text{K}$ [130]. The data is shown in Fig. 1.41. The experimental findings on the singlet-triplet excitation spectrum confirms the theoretical predictions of a rather flat band [118, 120]. The solid line shown for the band above, the two-triplon excitation spectrum is somewhat misleading. Latest results show a less pronounced structure in the dispersion relation [124].

The value of the one-triplet gap was confirmed by other experiments like electron spin resonance [132], far infrared studies [133], nuclear magnetic resonance [134] or Raman experiments [135] with $\Delta_{01} = 34\text{K}$. These experiments also support the singlet nature of

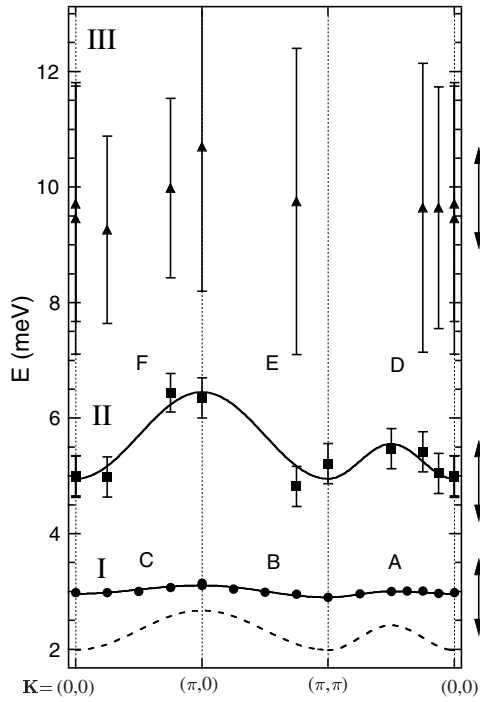


Figure 1.41: Inelastic neutron scattering results for $\text{SrCu}_2(\text{BO}_3)_2$ (reprint of Figure 3 from Ref. [130]): The rather flat band at energies close to 3meV corresponds to the one triplet excitations from the singlet ground state. The band above shows the two triplet sector. The solid curves are only guides to the eye. The two-triplet dispersion is indeed flatter than suggested by the solid line [124]

the ground state, except for the ESR-experiments where a residual interaction, for instance a Dzyaloshinsky-Moriya interaction, has to be taken into account to explain the excitation of a triplet out of a singlet ground state [132, 136].

Concluding the experimental side of $\text{SrCu}_2(\text{BO}_3)_2$ the exchange couplings must be considered to be positive. The crystal is an antiferromagnet. The ratio $x = J_2/J_1$ is sufficiently small such that the system is in the dimer phase.

x	$J_1[\text{K}]$	g	Ref. , fitted quantity
0.68	100	2.14	Miyahara et al. (1999) [118], χ
0.664(0.678)	83.2(82)	2.108	Weihong et al. (1999) [119], χ
0.603(0.59)	72(77)	—	Knetter et al. (2000) [137], $\omega_{01}(\mathbf{k})$
0.635	85	?	Miyahara et al. (2000) [129], χ
0.65	87	—	Munehisha et al. (2003) [123], $\omega_{01}(\mathbf{k})$

Table 1.2.: Fitted model parameters to $\text{SrCu}_2(\text{BO}_3)_2$, sorted chronologically. Values in brackets denote alternative fits.

Various publications are dedicated to fit the model parameters x and J_1 to the experimental

data. In Tab. 1.2 the values for the model parameters are listed chronologically. The range of the given x -values is close to the critical value $x_c \approx 0.7$ where a phase transition to an intermediate phase occurs, see above. An unambiguous parameter set obtained from a fit to the triplet dispersion $\omega_{01}(\mathbf{k})$ alone is not possible [137]. An instructive review of the theoretical results of the Shastry-Sutherland model applied to SrCu₂(BO₃)₂ is given in Ref. [138].

The following two paragraphs are dedicated to the investigation of the magnetic susceptibility and the magnetic specific heat. The results from the HTSE are fitted to the experimental data and the model parameters are determined.

Susceptibility The extrapolations of the HTSE susceptibility data are fitted using experimental data of the magnetic susceptibility obtained from a powder sample of SrCu₂(BO₃)₂ [131, 139]. Obtaining accurate estimates of the model parameters out of experimental data can be a tedious task. The experiment not only measures the pure spin susceptibility but also a Curie-like contribution from (non interacting) magnetic impurities and/or defects of Cu²⁺ ions, van-Vleck contributions and temperature independent diamagnetic contributions. Thus, an essential part of the fitting procedure should be to use all information available of the sample.

Besides the model parameters under consideration the g -factor mainly governs the overall height of the susceptibility. Nojiri et al. [132] performed an electron spin resonance (ESR) experiment to determine the g -factors in the Shastry-Sutherland plane and perpendicular to the plane. The obtained values are $g_{ab} = 2.28$ for the in-plane g -factor and $g_c = 2.05$ along the c -axis. In the following a geometrically averaged g -factor of $g_{\text{eff}} = \sqrt{(2g_{ab}^2 + g_c^2)}/3 = 2.2$ is used to fit the experimental data of the powder sample. A geometrically averaged g -factor is used in favor of an arithmetically averaged one due to the fact that the susceptibility depends quadratically on g . The aim of the fitting procedure of the theoretical results should be to fit the whole temperature regime in a way that the theoretical findings and the experimental data coincide best. Using the extrapolations of the HTSE data the low temperature regime $T/J_1 \lesssim 0.6$ can not be described reliably. The low lying position of the maximum of the susceptibility of SrCu₂(BO₃)₂ at around $T_{\text{max}} = 17\text{K}$ is almost inaccessible by means of a HTSE up to order β^7 . The range of applicability of the HTSE data should be precise down to $T/J_1 \approx 0.6$ as mentioned above. Using realistic parameters for the exchange constant J_1 with $J_1 = 70\text{K} \dots 100\text{K}$ the position of the maximum is in the range $T_{\text{max}} = 0.2J_1 \dots 0.3J_1$ and thus almost impossible to describe by extrapolations of the HTSE data. Here, the best possible fit should be the one which coincides with the experimental data down to $T \approx 0.6J_1$.

In a first step the parameter sets J_1 and $x = J_2/J_1$ obtained in the literature (see Tab. 1.2) are used to represent the extrapolations of the HTSE data. The extrapolations are then compared to the already corrected spin susceptibility from Ref. [131]. There, the authors corrected the raw susceptibility for a constant van-Vleck contribution and for Curie-Weiss-like contributions originating from magnetic impurities. In this thesis the experimentally known effective g -factor is built in, whereas the parameter sets used in previous publications were determined by fitting also the g -factor when comparing to the magnetic susceptibility.

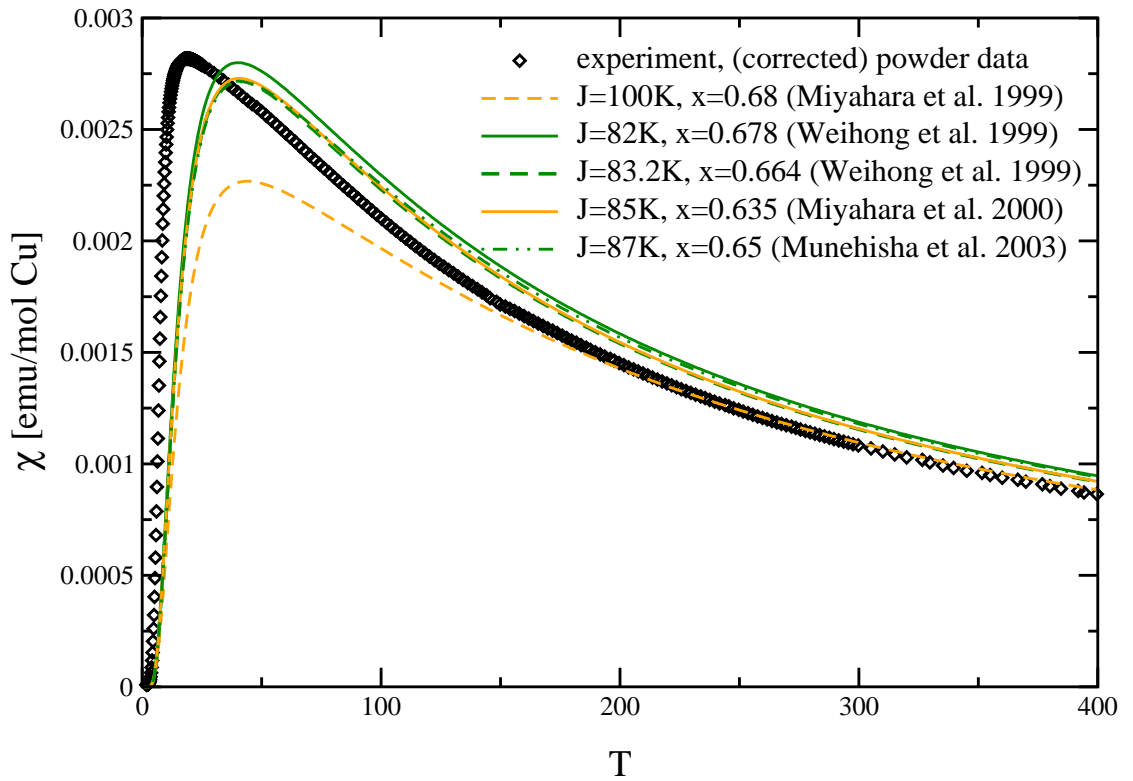


Figure 1.42.: Susceptibility fits from literature as given in Tab. 1.2 using the correct g -factor $g_{\text{eff}} = 2.2$ compared to the corrected experimental data [131]

Either the g -factor was not known at the time of publication or the parameter sets were obtained fitting the singlet-triplet dispersion to experimental data [130].

Fig. 1.42 shows an overview of the HTSE extrapolations with various parameter sets compared to the experimentally corrected data. The extrapolations are biased in the low temperature regime as described above. The value of the singlet-triplet gap Δ_{01} is taken from INS-measurements with $\Delta_{01} = 34\text{K}$ [130]. In the publications of Weihong et al. [119] and Miyahara et al. [118, 129] the used g -factor was substantially smaller than the experimentally determined one. Thus the representations fail to reproduce the high temperature regime properly. Rescaling of the g -factor as given in Tab. 1.2 yields representations which coincide with experimental data in the high temperature regime.

The following approaches will use the raw data from the susceptibility measurements [131]. Building in the known effective g -factor the truncated series is fitted to the raw data assuming a temperature independent χ_0 consisting of diamagnetic and van-Vleck parts. The fit function is given by

$$\chi_{\text{fit}}(T, J_1, x, \chi_0) = \chi_{\text{theo}}^{\text{tr. series}}(T, J_1, x) + \chi_0. \quad (1.95)$$

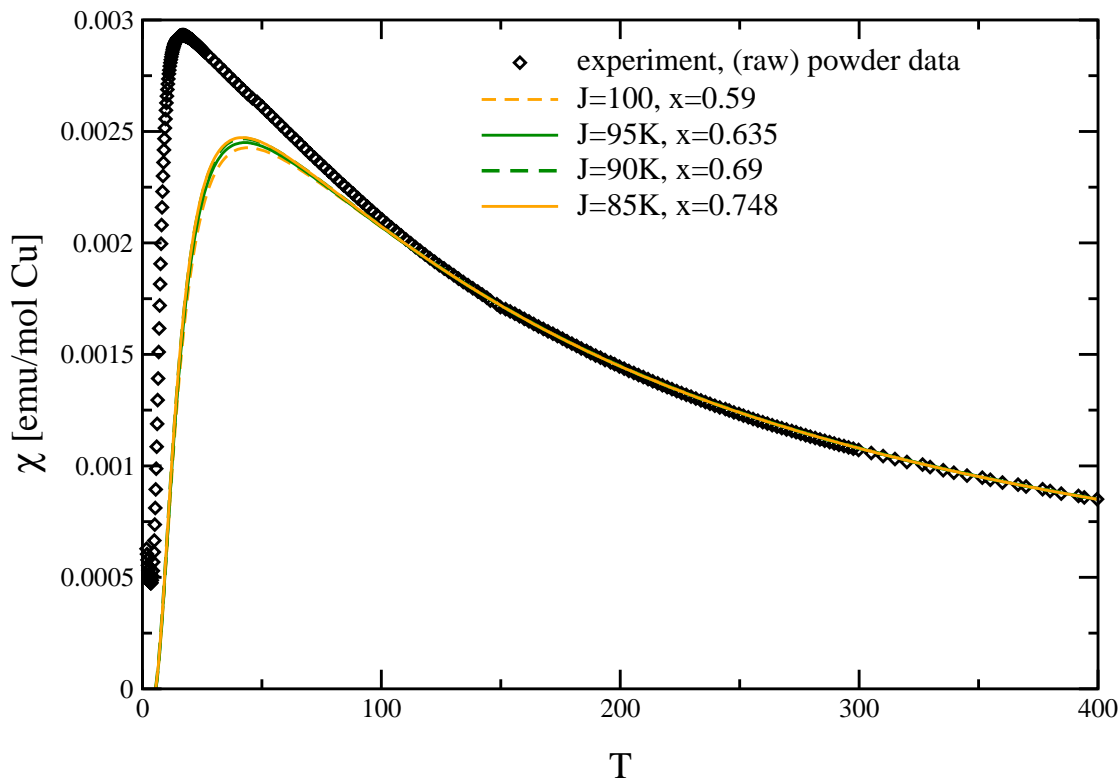


Figure 1.43.: Fitted susceptibility from HTSE, where $\chi_{\text{exp}} = \chi_{\text{theo}} + \chi_0$ with fitted $\chi_0 = -7.7 \cdot 10^{-5} \text{emu/mol Cu}$ in the temperature range $T = 200\text{K} \dots 400\text{K}$.

It is used in the temperature regime $T = 200\text{K} \dots 400\text{K}$. A Curie-like term as described above is neglected. The $1/T$ behavior of the $S = 1/2$ impurities leads to negligible contributions in that temperature regime.

Fig. 1.43 shows an overview of the obtained parameter sets in the high temperature regime. The determined parameters are used in the extrapolations of the truncated series and compared to the raw experimental data. For all parameter sets (J_1, x) a constant susceptibility $\chi_0 \approx -7.7 \cdot 10^{-5} \frac{\text{emu}}{\text{mmol Cu}}$ was fitted. Kageyama et al. [131] found a slightly lower value of $\chi_0 \approx -2 \cdot 10^{-5} \frac{\text{emu}}{\text{mmol Cu}}$ using a lower g -factor of $g = 2.14$.

The extrapolations reproduce nicely the high temperature regime but fail for temperatures below $T = 100\text{K}$. The parameters obtained also differ significantly from published values. Using $J = 85\text{K}$ the fitted frustration $x = 0.748$ is already beyond the phase transition point at around $x = 0.7$, where the system should be already in a long range order Néel phase, away from the dimer phase. Thus, this parameter set is definitely not appropriate for SrCu₂(BO₃)₂.

A more detailed investigation of the system properties is necessary to obtain more significant estimates of the relevant parameter sets. In the remaining part of this chapter the three-dimensionality of the system is explicitly taken into account. An investigation of the

chemical structure of $\text{SrCu}_2(\text{BO}_3)_2$ shows that every second $\text{Cu}(\text{BO}_3)$ -plane (see Fig. 1.40) is rotated by an angle of $\pi/2$ about one of the dimer centers such that each dimer has a rotated dimer above and below. In Fig. 1.44 a schematic picture of the three-dimensional arrangement of the dimers in $\text{SrCu}_2(\text{BO}_3)_2$ is shown. The resulting tetrahedral inter-plane

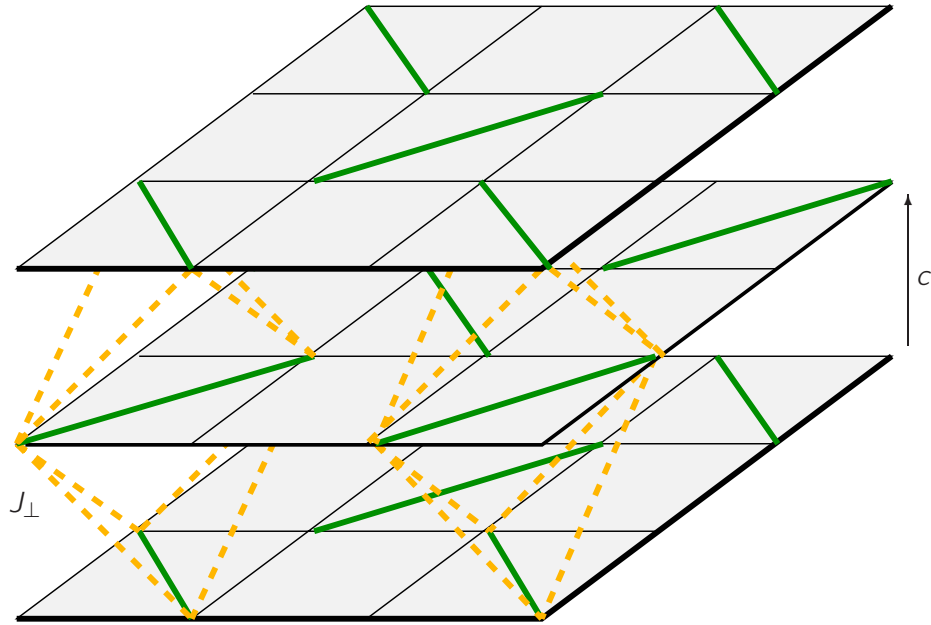


Figure 1.44.: The three-dimensional model of $\text{SrCu}_2(\text{BO}_3)_2$: the dashed lines indicate the interplane interaction J_{\perp} . For reasons of clarity only the interaction paths for the two dimers on the front side of the middle plane are shown. The thick lines depict the dimers and the thin lines the interaction paths between them. The dimers above and below a given dimer are rotated by an angle of $\pi/2$.

interaction geometry is fully frustrated: the dimers above and below must be excited out of the singlet ground state for this interaction to be relevant. It is obvious that a triplon cannot move along the c -axis [129]. Thus, the spin gap Δ_{01} and the dispersion of the triplon excitations in the three dimensional model is not changed compared to the results of the two dimensional model.

On the other hand at high temperatures a weak inter-layer coupling has to be taken into account since there is a finite concentration of triplons excited. They lead to an interaction between dimers on neighboring planes. A mean field type scaling ansatz should be sufficient to include a weak inter-layer coupling. To estimate the magnitude of the inter-layer coupling J_{\perp} in $\text{SrCu}_2(\text{BO}_3)_2$ the following ansatz is used (see for instance Ref. [110])

$$\chi^{3\text{D}}(J_1, x, J_{\perp}) = \frac{\chi^{2\text{D}}(J_1, x)}{1 + 4J_{\perp}\chi^{2\text{D}}(J_1, x)}. \quad (1.96)$$

The factor of 4 corresponds to the coordination number of a site having two interaction neighbors in the plane above and two in the plane below.

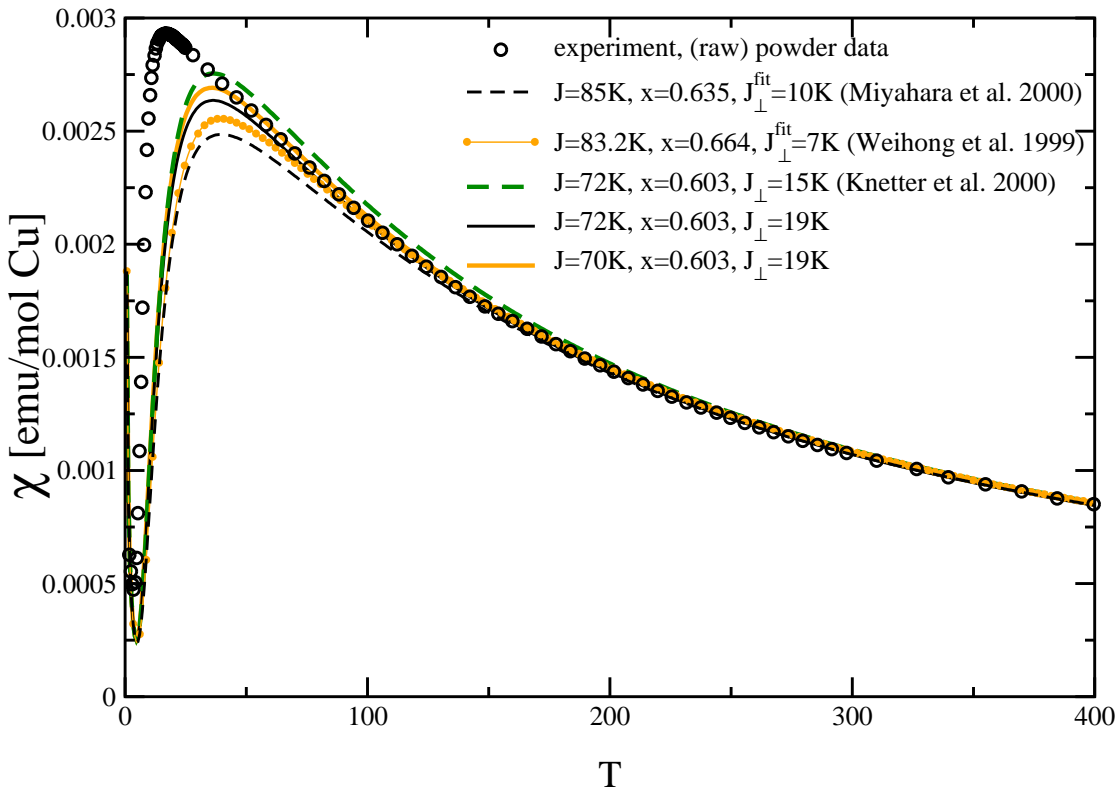


Figure 1.45.: Fitted susceptibility including interlayer coupling J_{\perp} , where $\chi_{\text{exp}} = \chi_{\text{theo}}^{3\text{d}} + \chi_0 + C/T$ with fitted $\chi_0 = 7 \cdot 10^{-5} \text{emu/mol Cu}$ in the temperature range $T = 200\text{K} \dots 400\text{K}$ and $C = 1.3 \cdot 10^{-3} \text{emu K/mol Cu}$ in the temperature range $T = 0\text{K} \dots 3\text{K}$.

In Fig. 1.45 the three dimensional susceptibility is fitted to the raw powder data. In a first step the temperature independent contribution χ_0 was estimated to be $\chi_0 = -7 \cdot 10^{-5} \text{emu/mol Cu}$ almost independent of the applied parameter sets. The truncated series of $\chi^{2\text{D}}$ was used for the representation of $\chi^{3\text{D}}$ and then fitted in the temperature regime $T = 200\text{K} \dots 400\text{K}$. In this temperature regime the description of the truncated series is sufficient to characterize the experiment quantitatively. As can be seen from Fig. 1.39 the difference between the extrapolations and the bare polynomial for $T/J_1 > 1$ is not discernible.

The Curie-like upturn at low temperatures originating from non interacting $S = 1/2$ impurities was fitted in the temperature regime $T = 0\text{K} \dots 3\text{K}$ with

$$\chi_{\text{imp}} = \frac{C}{T} \text{ leading to } C \approx 0.0013 \frac{\text{emu K}}{\text{mol Cu}}. \quad (1.97)$$

Kageyama et al. [131] fitted a slightly larger value with $C \approx 2.7 \cdot 10^{-3} \frac{\text{emu K}}{\text{mol Cu}}$. But, they also fitted a Curie-Weiss behavior, which is neglected in this thesis. Using the obtained

values for χ_{imp} and χ_o the three-dimensional susceptibility

$$\chi^{3\text{D}}(J_{\perp}, x, J_{\perp}) = \frac{\chi^{2\text{D}}}{1 + 4J_{\perp}\chi^{2\text{D}}} + \chi_{\text{imp.}} + \chi_o \quad (1.98)$$

was fitted to the raw powder data using the best extrapolations for $\chi^{2\text{D}}$.

Fig. 1.45 depicts the fitted susceptibilities for various parameter sets compared to the experimental data. Taking the values $J_{\perp} = 85\text{K}$ and $x = 0.635$ as proposed by Miyahara et al. [129] the perpendicular interaction J_{\perp} has to be fitted to be $J_{\perp} = 10\text{K}$ to obtain an agreement at least in the high temperature regime. In their publication the authors used a lower value for J_{\perp} with $J_{\perp} = 8\text{K}$ and a presumably lower g-factor (not given explicitly in the publication).

The parameter set $J_{\perp} = 83.2\text{K}$ and $x = 0.664$ taken from Weihong et al. [119] yields a nice fit down to $T \approx 80\text{K}$ using $J_{\perp} = 7\text{K}$. The remaining parameter sets are close to the ones published by Knetter et al. [137]. Accepting a small error in $J_{\perp} = 71(1)\text{K}$ and $J_{\perp} = 17(2)\text{K}$ with $x = 0.603$ the theoretical susceptibility represents the experimental data best. The coincidence is very good down to $T \approx 40\text{K}$ which in turn means $T/J_{\perp} \approx 0.56$. Thus, the range of applicability of the extrapolations of the HTSE data is completely exploited for the given parameter sets. Using the values proposed by Miyahara et al. and by Weihong et al. lead to an inter-plane frustration $J_{\perp}/J_{\parallel} \approx 10\%$. In this thesis the estimated fraction is significantly higher with $J_{\perp}/J_{\parallel} \approx 24\%$ due to the different values for J_{\perp} and x , which is the best parameter set obtained by a fit of the HTSE results.

The small value for x used in the best representation is much smaller than other published values, see Tab. 1.2. Concluding the fitting procedure for the susceptibility, the parameter set $J_{\perp} = 71(1)\text{K}$, $J_{\perp} = 17(2)\text{K}$ and $x = 0.603$ is suggested to characterize the susceptibility of $\text{SrCu}_2(\text{BO}_3)_2$ best.

The following paragraph is dedicated to the investigation of the specific heat, where the values for the model parameters obtained from the susceptibility fits are used to describe the specific heat.

Specific Heat The specific heat of $\text{SrCu}_2(\text{BO}_3)_2$ was measured for low temperatures ($T = 1.3\text{K} \dots 25\text{K}$) under various magnetic fields by Kageyama et al. [140]. In this thesis the interest is focused on the specific heat for vanishing magnetic field. The aim is to fit the extrapolations (as described above) of the HTSE data to the experimental results. A measurement of the specific heat is always sensitive not only to the magnetic degrees of freedom but also to the phononic degrees of freedom. Identifying and subtracting the phononic contributions at low temperatures is only possible if the energy scales of the magnetic and phononic subsystem differ significantly from each other. This is the case for $\text{SrCu}_2(\text{BO}_3)_2$ where in Ref. [140] a low temperature behavior of the phononic contributions to the specific heat C_{phonon} was fitted assuming the well known T^3 scaling with $C_{\text{phonon}} \approx 0.46 \cdot T^3 \text{mJ/K}^4 \text{ mol Cu-dimers}$.

The maximum of the specific heat was measured to be situated at $T_{\text{max}} = 7.5\text{K}$. Assuming the above given values for the exchange constant J_{\perp} yields $T_{\text{max}} \approx 0.1J_{\perp}$. Concerning fits using HTSE data this is a very low value where quantitative predictions for the parameter

sets are hard to determine if possible at all. A side effect of the low-lying maximum concerns also the convergence of the extrapolations. Even the small increase from $x = 0.5$ as depicted in Fig. 1.37 to the values used in the following changes the convergence behavior. For $x = 0.5$ a good convergence of the extrapolations was found. The convergence for higher x -values is less satisfying as depicted in Fig. 1.46. For the parameter sets used in

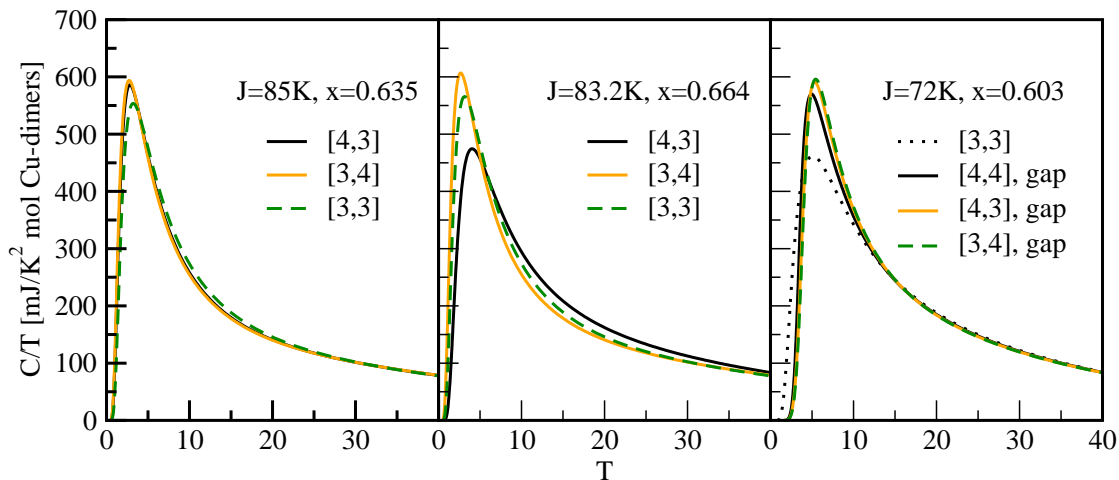


Figure 1.46.: Extrapolations of the specific heat divided by temperature in experimental units: various parameter sets are shown. Only for $J = 72\text{K}$ and $x = 0.603$ the value of the gap Δ_{01} could be included. All other sets showed spurious poles leading to defective extrapolations.

the middle and left plot the extrapolations could not be biased by the value of the gap Δ_{01} . Spurious poles yield defective extrapolations. Therefore, the parameters J_1 and x obtained from the fitting procedure of the susceptibility are used for the extrapolations of the specific heat and compared to the experiment. No attempt is made to fit the parameters independently from the values obtained by fitting to the susceptibility data. Due to the low temperatures $T < \Delta_{01}$ where the pronounced structure of the specific heat is visible the two dimensional model is sufficient to describe the experiment. In first order in β there is also no contribution from J_{\perp} to the specific heat.

Fig. 1.47 depicts the specific heat divided by temperature versus temperature. The open circles represent the experimental data and the dashed line the fitted phononic contribution. The increase of the total specific heat with temperature up to T_{max} and the rapid decrease for temperatures $T > T_{\text{max}}$ is a generic feature of spin-singlet systems with a finite spin gap, also known as Schottky anomaly. The solid lines are various extrapolations. All parameter sets chosen are not able to reproduce the position of the maximum properly. For the values $J = 72\text{K}$ and $x = 0.603$ the maximum is closest to the experimentally measured maximum. A short remark concerns the extrapolations of the parameter sets ($J_1 = 85\text{K}$, $x = 0.635$) and ($J_1 = 83.2\text{K}$, $x = 0.664$). Here, it was not possible to include the value of the spin gap into the extrapolations. All extrapolations were defective. One could assume a physical

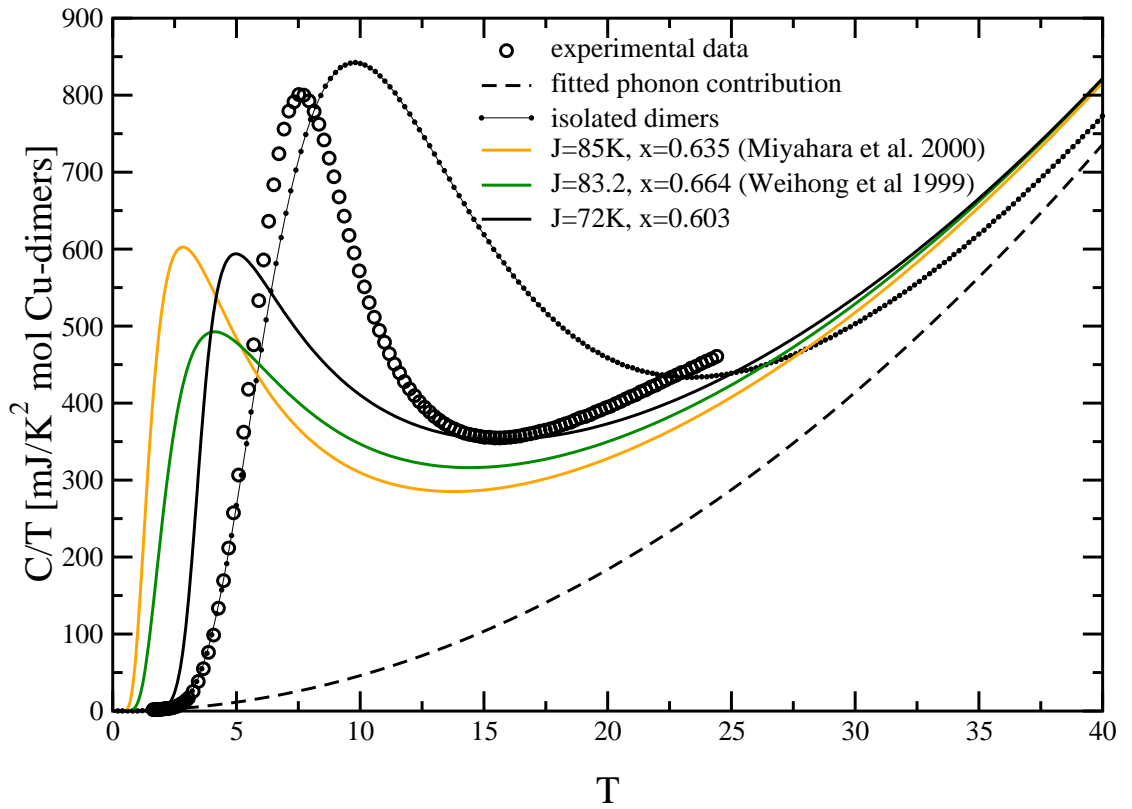


Figure 1.47.: Extrapolations of the specific heat compared to experimental results. The model of isolated dimers with $\Delta_{01} = 34\text{K}$ is also plotted. The phonon contribution was estimated to be $C_{\text{phonon}} \approx 0.46T^3\text{mJ/K}^4 \text{ mol Cu-dimers}$ [140].

background of the occurring poles but these poles are rather artifacts of the extrapolations. The connected closed circles depict the results of a simple model of isolated dimers

$$C_{\text{dimer}} = 3\left(\frac{\Delta_{01}}{T}\right)^2 \frac{e^{-\Delta_{01}/T}}{(1 + 3e^{-\Delta_{01}/T})^2} \quad (1.99)$$

with the singlet-triplet gap Δ_{01} . The height of the maximum is nicely reproduced but the position is at too high temperatures.

As expected, the position of the maximum of the specific heat cannot be reproduced correctly by extrapolations of the HTSE data. The values $J = 72\text{K}$ and $x = 0.603$ lead to a fit which shows the best representation of the theoretical results compared to the other sets used. Taking the latter values the low temperature behavior including the gap reproduces the experimental data for $T < 3\text{K}$. With increasing temperature the theory deviates significantly from experiment. More information by means of higher orders in the series expansion are necessary to obtain a better coincidence.

Besides the problem of the low lying maximum other sources can be relevant for the discrepancy between theory and experiment. In particular, effects of spin-phonon coupling may be important. Small distortions of the dimer bonds may break their orthogonal order leading to a strong coupling between the triplet excitations and the phonons [129, 138, 141]. Thus, effects of the spin-phonon coupling may play an important role to understand the behavior of the specific heat. The following chapter addresses this particular problem. A one-dimensional system was chosen as the starting point for such investigations.

1.6.6. Conclusions

This chapter was dedicated to the investigation of the Shastry-Sutherland model and its applicability for the description of the experimental results of $\text{SrCu}_2(\text{BO}_3)_2$. The computation of the series expansion could be done up to order 8 in the inverse temperature for the specific heat and up to order 7 for the susceptibility. The complete enumeration of the Hilbert space was not possible for the system sizes under consideration. It was more efficient to use the moment-algorithm. Thus, the results could be computed in a straightforward fashion exploiting the capacities of current computers. Other methods like the linked cluster expansion method [23] need more precise knowledge of the system and its geometry. The orders achieved using the linked cluster algorithm are of the same size as or below the orders achieved in this thesis.

Advanced extrapolations are necessary to represent the truncated series for quantitative predictions. With the realization of the Shastry-Sutherland model in $\text{SrCu}_2(\text{BO}_3)_2$ a detailed comparison between theory and experiment was possible. The theoretical results for the magnetic specific heat and for the susceptibility were compared to experiment. To satisfy the three-dimensionality of $\text{SrCu}_2(\text{BO}_3)_2$ a mean-field scaling ansatz was taken into account to describe the susceptibility. Including an inter-layer coupling J_\perp the best fits to the susceptibility were obtained using $J_1 = 71(1)\text{K}$, $J_\perp = 17(2)\text{K}$ and $x = 0.603$. The theory can reproduce the experiment down to very low temperatures. The Shastry-Sutherland model and its extension to three dimensions yield a consistent description of $\text{SrCu}_2(\text{BO}_3)_2$. Investigation of the data of the specific heat was more difficult due to the low-lying maximum. The above parameter set showed the best tendency to be the relevant one for $\text{SrCu}_2(\text{BO}_3)_2$. Further investigations have to be done. The most promising ansatz should be to include a spin-phonon coupling. Inclusion of this additional coupling could improve the consistency between theory and experiment.

2. Spin-Phonon System

2.1. Introduction

This chapter is concerned with the problem of a spin-system coupled to phonons. The previous chapters considered pure isolated spin-systems. Here such a spin-system is extended by the coupling to phononic degrees of freedom. This extension is motivated by the fact that an alteration of the local ordering in the lattice due to phononic degrees of freedom also influences the electronic transition matrix elements and thus the magnetic exchange couplings. The Holstein model [142] is widely used as a first ansatz to couple electronic degrees of freedom to dispersionless quantum phonons. The electrons are modeled by spinless fermions. Applying a Jordan-Wigner transformation the Holstein model can be mapped to a pure spin model. In the resulting spin model the spin-phonon coupling is restricted to the z-components of the spins. Especially in one dimension the quantum fluctuations are of great importance. Thus, an appropriate model should also include the coupling of the phonons to the spin fluctuations and not only to their z-component.

The phenomenological interest in the model of quantum phonons coupled to quantum spins has been intensified since the fundamental work of Pytte [143]. He showed that a spin-1/2 Heisenberg chain coupled to three-dimensional phonons undergoes a transition from an ungapped phase to a massive phase showing dimerization, generally referred to as spin-Peierls transition [144]. The spin-Peierls instability of quasi one-dimensional spin systems is the analogue of the Peierls instability of quasi one-dimensional metals towards lattice modulations with a wave vector $2k_F$. Due to the coupling of the lattice degrees of freedom to the one-dimensional magnetic degrees of freedom the system can lower its energy by undergoing a phase transition into a dimerized state. The loss in elastic energy is overcompensated by the gain in magnetic energy [145].

With the synthesis of the first inorganic spin-Peierls substance CuGeO_3 [146] the interest in such systems has rekindled. Single crystals of high quality made investigations possible that were not possible for the long known organic spin-Peierls substances. The organic compounds of the TTF and TCNQ family are the most prominent examples [144].

As mentioned in the previous chapters the spin-phonon coupling is of great importance in general. Besides CuGeO_3 there are other substances like $\text{SrCu}_2(\text{BO}_3)_2$ [131] or $(\text{VO})_2\text{P}_2\text{O}_7$ [29], to mention just a few, which show strong experimental evidence for non-negligible spin-phonon coupling [41, 129]. The experimental results show a discrepancy between the parameters fitted at $T = 0$ and those fitted at finite temperatures. Thus, it is of general interest to investigate and to analyze these systems in detail.

The spin-phonon model as introduced in the following section cannot be solved analytically. There are practically no analytic method to handle extended coupled systems of spins and phonons when all energy scales and coupling strengths are considered. Many numerical methods have been applied to obtain a deeper understanding. In this thesis, the spin-phonon model is investigated using a cluster algorithm to derive thermodynamical properties like the specific heat and the susceptibility by means of a high temperature series expansion.

This chapter is organized as follows. Sec. 2.2 presents the model and its known properties. In Sec. 2.3 the computational details are highlighted. The computational ansatz is different from the one used in the previous chapters. The results will be presented in Sec. 2.4 and summarized in Sec. 2.5.

2.2. Model

The isotropic spin-1/2 Heisenberg chain is extended by the coupling to phononic degrees of freedom, the quantized lattice vibrations. The phonons are treated in harmonic approximation which is valid in the low-energy limit corresponding to small displacements. The Hamilton operator for harmonically approximated phonons is given by noninteracting bosons in second quantization. For small phononic displacements the coupling of the phonons to the magnetic subsystem is sufficiently described in linear order in the displacements. Then, the Hamilton operator reads

$$H = J \sum_i (1 + g(b_i^\dagger + b_i)) \mathbf{S}_i \mathbf{S}_{i+1} + \omega \sum_i b_i^\dagger b_i \quad (2.1a)$$

$$= J \sum_i \mathbf{S}_i \mathbf{S}_{i+1} + \omega \sum_i b_i^\dagger b_i + J \sum_i g(b_i^\dagger + b_i) \mathbf{S}_i \mathbf{S}_{i+1} \quad (2.1b)$$

$$= H_S + H_B + H_{SB} . \quad (2.1c)$$

The magnetic exchange coupling is parameterized by J , the coupling between the phononic subsystem and the magnetic subsystem is given by gJ , and the energy of the dispersionless phonons is ω . The abbreviations H_S , H_B and H_{SB} , respectively, are used in the following. The Hamiltonian in Eq. 2.1 represents the so called bond-coupling model in contrast to the difference-coupling model. The difference coupling model is given by the Hamilton operator

$$H_{\text{diff}} = J \sum_i (1 + g(b_{i+1}^\dagger + b_{i+1} - b_i^\dagger - b_i)) \mathbf{S}_i \mathbf{S}_{i+1} + \omega \sum_i b_i^\dagger b_i . \quad (2.2)$$

In the difference-coupling model the spin-spin interaction depends on the distance between neighboring spins. The bond-coupling model used in this thesis describes the case where the interaction between neighboring sites depends for instance on the variation of bond angles. The phonons can be seen as vibrations of the ions mediating the super-exchange between the spin carrying ions. For instance, this corresponds to the sidegroup effects mediated through the Ge-atoms in CuGeO_3 [147–149]. In Fig. 2.1 the bond-coupling model is depicted schematically.

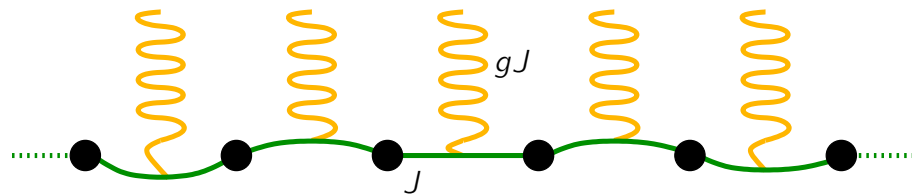


Figure 2.1.: Schematic picture of the bond-coupling model as it is used in the present chapter

Neither the difference-coupling model nor the bond-coupling model are exactly solvable. The pure phonon part H_B is diagonal and thus easy to solve. But the spin part H_S

alone already poses a problem which is hard to tackle. Therefore, numerous numerical methods have been applied to understand the spin-phonon model in detail: DMRG [150], continuous unitary transformations [151–153], exact diagonalization [154], linked cluster expansion [155], renormalization group [156] and quantum Monte Carlo [61, 153, 157–160]. Due to their one-dimensionality these models show no phase transition at finite temperatures. For $T = 0$ there is a phase transition from an ungapped spin fluid phase to a gapped phase showing dimerization. This transition is referred to as spin-Peierls transition as analogue to the above mentioned three-dimensional counterpart. Roughly speaking, a large spin-phonon coupling in units of the phonon energy induces dimerization whereas for small spin-phonon coupling the ungapped phase is present. Fig. 2.2 displays the zero tempera-

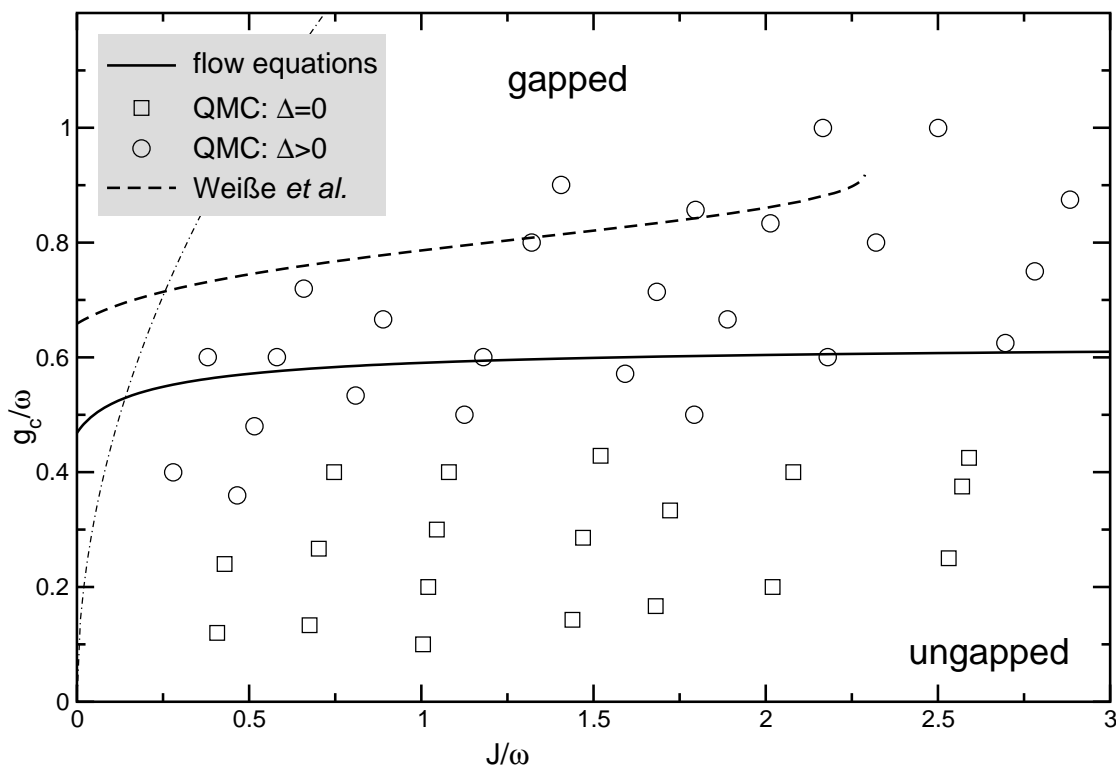


Figure 2.2.: Zero temperature phase diagram of the spin-Peierls antiferromagnetic chain of spins interacting with phonons, taken from Ref. [153]. Approximate results are shown for the bond-coupling model. The solid line depicts results from a flow equation approach and the open symbols have been obtained using QMC [153]. QMC data can only be computed to the right of the dot-dashed line. ED results from Ref. [154] are given as dashed line to identify the phase transition line between the ungapped and gapped phase.

ture phase diagram. The critical spin-phonon coupling g_c is plotted versus the exchange coupling J in units of the phonon frequency ω . In their calculations the authors used a

slightly different parameterization of the spin-phonon coupling: the spin-phonon coupling g used in Ref. [153] corresponds to the spin-phonon coupling gJ used in this thesis.

So far, the previous investigations are mainly restricted to two limits. In the adiabatic limit $\omega \ll J$ the spin system is assumed to be ‘fast’ compared to the ‘slow’ phonon system.

Using approaches analogue to the ones applied by Pytte [143] and the more detailed one by Cross and Fisher [145] the model in Eq. 2.1 can be mapped to a statically dimerized model as it was discussed in Chapter 1.4. The dimerization parameter δ depends on the coupling constants of the starting Hamiltonian as given in Eq. 2.1.

The antiadiabatic limit $\omega \gg J$ can be handled by an appropriate mapping of the starting Hamiltonian to a frustrated spin model as discussed in Chapter 1.4. Thereby, also interactions of a wider range are induced and the phonon frequency is renormalized [20, 150–154]. Above a critical frustration, i.e. a next-nearest neighbor interaction, the system becomes gapped. In the limit $J/\omega \rightarrow 0$, the critical spin-phonon coupling for a phase transition from an ungapped to gapped phase is given by $g_c/\omega \approx 0.4682$ for the bond-coupling model as depicted in Fig. 2.2 using the flow equation approach [153]. In the following, only the bond-coupling model as given in Eq. 2.1 is addressed for simplicity.

Investigations of the regime between the adiabatic and antiadiabatic limit with $\omega \approx J$ are difficult. So far, only a renormalization group analysis [156] and Monte-Carlo calculations [61, 153] have been done.

Besides the $T = 0$ properties also the thermodynamic behavior of the system is affected by the spin-phonon coupling. In the antiadiabatic limit it could be shown that the magnetic susceptibility can be fitted by a frustrated spin model with temperature independent couplings. But this approach fails for increasing values J/ω [61, 153].

Further investigations are necessary to understand the model under consideration in more detail. In this thesis, the thermodynamical aspects of the model are emphasized. A series expansion about the limit of vanishing J/T is performed. The phononic subspace is treated exactly at each temperature. No cutoff in the phonon subspace is necessary. The resulting quantities are given as truncated series with the full dependence of the model parameters.

2.3. Method and Computation

The aim of this section is to calculate the partition function Z of the spin-phonon system as given in Eq. 2.1. Once the partition function is obtained, quantities like the free energy, the specific heat or the susceptibility can easily be derived from Z . An ordinary high temperature series expansion, as was done in the previous chapters for the isolated spin models, is not possible. The expansion in the inverse temperature would lead to a divergence in the phonon subspace. In the limit of infinite temperature the phonon occupation number diverges. For this reason, we chose to perform a formal expansion in the exchange coupling J , where the phonon subspace is treated exactly. Compared to other methods like QMC or ED no cutoff of the phonon subspace is necessary. The full phonon dynamics are taken into account. To our knowledge, this is the first approach of a cluster expansion about the limit $J = 0$ at finite temperatures, where no approximation in the phonon subspace is necessary.

The Hamilton operator 2.1 is split into its diagonal part H_0 and a perturbation V with

$$H = H_0 + JV = H_B + (H_S + H_{SB}) \quad (2.3a)$$

$$= \underbrace{\omega \sum_i b_i^\dagger b_i}_{H_0} + J \underbrace{\sum_i (1 + g(b_i^\dagger + b_i)) \mathbf{S}_i \mathbf{S}_{i+1}}_V \quad (2.3b)$$

The diagonal part H_0 is exactly solvable describing free dispersionless (Einstein) phonons. The perturbation V includes the isolated magnetic part and the spin-phonon interaction. The standard way to treat such a problem is to change to the interaction representation where the off-diagonal perturbation governs the non-trivial dynamics of the system. In this framework the partition function is given as an infinite series in the expansion parameter J with

$$Z = \text{tr} \{ e^{-\beta H} \} = Z_0 \left\{ 1 + \sum_{n=1}^{\infty} (-J)^n \int_0^\beta d\tau_1 \cdots \int_0^{\tau_{n-1}} d\tau_n \langle \tilde{V}(\tau_1) \cdots \tilde{V}(\tau_n) \rangle \right\}, \quad (2.4)$$

where the following abbreviations have been used: the unperturbed part H_0 of the Hamiltonian 2.3 leads to the exactly solvable contribution Z_0 to the partition function

$$Z_0 = \text{tr} \{ e^{-\beta H_0} \} = 2^N \left\{ \prod_i \left(\sum_{n_i} e^{-\beta \omega n_i} \right) \right\} = 2^N z_0^N \quad (2.5)$$

with $z_0 = 1/(1 - e^{-\beta \omega})$ and the phonon occupation number $n_i = b_i^\dagger b_i$. The system size is denoted by N . The perturbation V given in the interaction representation as \tilde{V} reads

$$\tilde{V}(\tau) = e^{\tau H_0} V e^{-\tau H_0} \quad (2.6a)$$

$$= \sum_i \mathbf{S}_i \mathbf{S}_{i+1} \left(1 + g e^{\tau H_0} (b_i^\dagger + b_i) e^{-\tau H_0} \right) \quad (2.6b)$$

$$= \sum_i \mathbf{S}_i \mathbf{S}_{i+1} \left(1 + g (b_i^\dagger e^{\omega \tau} + b_i e^{-\omega \tau}) \right). \quad (2.6c)$$

The angular brackets in Eq. 2.4 are an abbreviated notation for

$$\langle \tilde{V}(\tau_1) \cdots \tilde{V}(\tau_n) \rangle = \frac{1}{Z_0} \text{tr} \left\{ e^{-\beta H_0} \tilde{V}(\tau_1) \cdots \tilde{V}(\tau_n) \right\}. \quad (2.7)$$

As can be seen from the above equations the calculations for the partition function Z of the magnetic system and of the phononic system factorize. In each order of expansion in J the contribution from the spin system can be evaluated separately from the phononic contributions.

Calculating the partition function in Eq. 2.4 requires repeated integrations over functions of the type

$$I(k, l; x_n) = x_n^k e^{l x_n} \quad \text{with } k \in \mathbf{N}_0, l \in \mathbf{Z}, x_n \in \mathbf{R}. \quad (2.8)$$

The resulting integrals can be solved exactly with

$$l \neq 0 : \int_0^{x_{n-1}} dx_n x_n^k e^{lx_n} = k! \left(-\frac{1}{l}\right)^{k+1} + \sum_{i=0}^k (-1)^i \frac{1}{l^{i+1}} \frac{k!}{(k-i)!} x_{n-1}^{k-i} e^{lx_{n-1}} \quad (2.9a)$$

$$l = 0 : \int_0^{x_{n-1}} dx_n x_n^k = \frac{1}{k+1} x_{n-1}^{k+1} . \quad (2.9b)$$

These equations allow an iterative evaluation of the multiple integrals entering the partition function Z .

A useful check of the calculations is the limit $g = 0$. This special case yields

$$Z_{g=0} = Z_{\text{isol. phonons}} Z_{\text{isol. spins}} = z_0^N Z_{\text{isol. spins}} . \quad (2.10)$$

As check, the results of the isolated spin model can be compared to results obtained previously, see Chapter 1.4.

2.3.1. Cluster Expansion

So far, the equations for calculating the partition function are given. To calculate the quantities under consideration an efficient method to implement the calculations in a computer program is necessary. A first ansatz would be to use the methods presented in the previous chapters. They make use of the fact that once an observable O has been applied n times to an appropriate starting state $|S\rangle$ one can obtain the physically relevant results up to order $2n$. A simple scalar product of the resulting state is performed, e.g. $(\langle S|O^n)(O^n|S) = \langle S|O^{2n}|S\rangle$ leading to the $(2n)$ th order result. For the actual system using the interaction representation this method is not applicable, mainly due to the infinite Hilbert space of the phonons. Furthermore, the multiple integrals entering the calculations forbid such an approach.

The next idea coming into mind is the linked cluster expansion algorithm [23]. The key idea is to restrict calculations to finite connected clusters. To obtain the contribution of the calculations made for a finite cluster to an observable in the infinite system, all results previously obtained for the connected subclusters of the cluster at hand have to be subtracted. The identification of the clusters and their subclusters is a very sophisticated problem.

Due to the one-dimensionality of the system under consideration a simple cluster algorithm will be used (for an instructive review see Ref. [161]). Therein not only the connected clusters are taken into account but also the disconnected clusters. The problem of subtracting subclusters occurring in the linked cluster expansion algorithm is replaced by the evaluation of the lattice constants for a given cluster, for details see below.

The cluster expansion technique is a systematic method to perform high order perturbation expansions. It can be applied best to systems that are described by a Hamilton operator

which can be expressed as a sum of local operators

$$H = \sum_k h_k . \quad (2.11)$$

The index k runs over all pairs of sites that are connected by the given interaction expressed by the local operator h_k . Such a local interaction stands for a bond of a cluster. In the present problem only bonds between nearest-neighbor sites are involved. Multiple applications of such local operators lead to clusters whose contributions have to be calculated. A multiple application of the same local operator is denoted in the cluster representation as the multiplicity of the associated link.

The first step in the calculations is to identify all contributing clusters in each order of the expansion. The next step involves the evaluation of their weights, i.e. calculating the trace and the integrals as given in Eq. 2.4 for the cluster studied. In a last step, the number of embeddings of the given cluster in the system has to be determined, commonly referred to as the lattice constant.

To this end, the system size is set to N , where N is assumed to be infinitely large. Finally, only contributions proportional to N have to be taken into account because the physical quantities are extensive.

For connected clusters where all involved sites are connected by at least one link the lattice constant l_c is simply N . Disconnected clusters consist of isolated connected clusters and their lattice constant in one dimension is given by

$$l_c = \frac{N}{S} \prod_{i=1}^{c-1} (N - (b + i)) = (-1)^{c+1} \frac{N}{S} \prod_{i=1}^{c-1} (b + i) + \mathcal{O}(N^2) , \quad (2.12)$$

where c is the number of connected clusters, b the number of links involved and S accounts for a symmetry factor, which is the number of permutations which leave the cluster unchanged. Fig. 2.3 depicts a disconnected cluster occurring in the 10th order calculations.

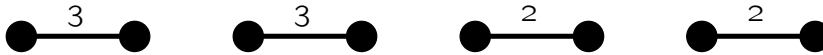


Figure 2.3.: Example of a disconnected cluster in 10th order: the numbers above the links denote their multiplicity.

With $c = 4$, $b = 4$ and $S = 2 \cdot 2$ the lattice constant is $l_c = -\frac{N}{4} 5 \cdot 6 \cdot 7 + \mathcal{O}(N^2) = -\frac{105}{2} N + \mathcal{O}(N^2)$. A step by step consideration putting in each connected cluster one after another into the system of size N leads to a lattice constant of N for the first cluster, the lattice constant for the second cluster evaluates to $N - 3 - 2$, where the factor of 3 accounts for the three links which are prohibited by the first cluster and the factor of 2 for the remaining two clusters. The third cluster then multiplies with $N - 6$ and the last with $N - 7$. Multiplying all lattice constants and dividing by a symmetry factor of 4, originating from the interchange of the clusters with same multiplicities, lead to the above

result. In the following, only the contribution of the lattice constant proportional to N is given. Higher orders in N are irrelevant for extensive results.

The following two sections are dedicated to the description of the calculational details for the free energy and for the susceptibility.

2.3.2. Free Energy

The free energy per site f is derived from the partition function using standard relations from statistical physics

$$f = F/N = -\frac{1}{\beta} \frac{1}{N} \ln Z . \quad (2.13)$$

To obtain the expansion for the free energy the expansion of the partition function 2.4 is considered exemplarily up to 4th order in J

$$Z = Z_0 \left(1 - \frac{Z_1}{Z_0} J + \frac{Z_2}{Z_0} J^2 - \frac{Z_3}{Z_0} J^3 + \mathcal{O}(J^4) \right) , \quad (2.14)$$

where Z_i are the contributions in i th order to Z . An expansion of the logarithm of the partition function about the limit $J = 0$ yields

$$\begin{aligned} \frac{1}{N} \ln Z = \frac{1}{N} \left\{ \ln Z_0 - \frac{Z_1}{Z_0} J + \left(\frac{Z_2}{Z_0} - \frac{1}{2} \frac{Z_1^2}{Z_0^2} \right) J^2 \right. \\ \left. - \left(\frac{Z_3}{Z_0} + \frac{1}{3} \frac{Z_1 Z_2}{Z_0^2} + \frac{1}{3} \frac{(2Z_2 Z_0 - Z_1^2) Z_1}{Z_0^3} \right) J^3 + \mathcal{O}(J^4) \right\} . \quad (2.15) \end{aligned}$$

So, once the contributions Z_i to the partition function are evaluated the free energy series expansion can be derived from Eq. 2.15.

In each order of expansion, the clusters with nonvanishing weight have to be identified. In the first order of expansion these are the clusters consisting of one link with multiplicity one. Considering the relevant operator \tilde{V} describing the clusters as given in Eq. 2.6 only clusters with links with multiplicity two or more yield nonvanishing contributions. For the pure spin part H_S a cluster with a link with multiplicity one vanishes under the trace. The phonon part in \tilde{V} also needs at least a multiplicity of two per link to have a phonon excited and de-excited on a given link resulting in a nonvanishing matrix element in the trace. Thus, the pure phonon part contributes only for even multiplicities, but for the full problem the coupling to the spin system leads also to contributions for odd multiplicities greater equal two. Thus, the first order contribution Z_1 to the partition function Z is zero.

The connected clusters of length p are given by the clusters depicted in Fig. 2.4 with multiplicities $m_i \geq 2$. The order of expansion to which such a cluster contributes is the sum of its multiplicities m_i . Up to order 16 in J there are 858 connected clusters. The disconnected clusters are obtained by combining the connected clusters. Up to order 16 in J 2579 disconnected clusters have to be evaluated.

In Tab. 2.1 all clusters contributing to the 6th order of expansion of Z are listed. In the left column the clusters are depicted and in the right column the appropriate lattice constants

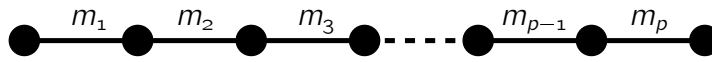


Figure 2.4.: Connected cluster

are given. The connected cluster in the second row has a lattice constant of $l_c = 2N$ because the ‘mirrored’ cluster with multiplicities $(2, 4)$ instead of $(4, 2)$ yields the same contribution to Z_6 and thus is not needed to be distinguished explicitly in the listing. As can be seen from Eq. 2.12 negative lattice constants can also be obtained in order N .

Cluster	p_c	$l_c [N]$
	1	1
	15	2 (symmetry)
	20	1
	90	1
	15	-3
	20	$-\frac{3}{2}$
	90	-4
	90	$\frac{10}{3}$

Table 2.1.: Contributing clusters in the 6th order expansion of the free energy: the lattice constant l_c and the number of permutations p_c are listed.

The middle column represents the most time consuming part in the calculations: the number of permutations p_c . The clusters are a shorthand notation for the local operators which have to be taken into account. But the cluster notation does not account for the various possibilities to arrange the local operators. The number of permutations p_c is given by

$$p_c = \frac{(\sum_{i=1}^p m_i)!}{\prod_{i=1}^p (m_i!)} . \tag{2.16}$$

The more links are involved the larger is the number of permutations. For each permutation the weight of the cluster has to be calculated. The number of permutations for a given cluster can reach numbers of order 10^7 in the calculations of the 13th order of the free energy. Connected and disconnected clusters need not to be considered separately because only the links and their multiplicities are required to evaluate the number of permutations. The invariance of the trace under cyclic permutations can be exploited to evaluate the spin trace using the result from calculations of cyclic equivalent permutations. For the phonon part it is not obvious how to simplify the explicit evaluation. The arrangement of

the operators is important due to the multiple integrals entering the calculations for the partition function Z in Eq. 2.4.

The identification of the contributing clusters and the evaluation of their weights were implemented in a computer program. Using fraction of integers to represent the results, the free energy was calculated up to order 11 in J . Jaan Oitmaa was able to obtain results up to order 13 in J [162]. He used floating point arithmetics in his program to store the results. Using floats instead of fractions of integers accelerates the program significantly leading to higher orders. The results up to order J^{11} are listed in App. A.5. Up to order J^{11} the results are given as fractions of integers. To illustrate the result the first orders of the free energy series are given by

$$\begin{aligned}
-\beta f &= \frac{1}{N} \ln(Z) = \ln z_0 + J^2 \left(\frac{3}{32} \beta^2 + \frac{3}{16} \frac{g^2 \beta}{\omega} \right) \\
&+ J^3 \left(\frac{1}{64} \beta^3 + \frac{3}{32} \frac{g^2 \beta^2}{\omega} \right) + J^4 \frac{1}{256} \left(-\frac{5}{4} \beta^4 + 6 \frac{g^2 \beta^3}{\omega} \right) \\
&+ \left((24z_0^2 - 24z_0 + 6) \frac{g^4}{\omega^2} + (-48z_0 + 24) \frac{g^2}{\omega^2} \right) \beta^2 \\
&+ \left((12 - 24z_0) \frac{g^4}{\omega^3} + 48 \frac{g^2}{\omega^3} \right) \beta + \mathcal{O}(J^5). \tag{2.17}
\end{aligned}$$

2.3.3. Susceptibility

The series expansion of the susceptibility is obtained from the previous considerations by incorporating slight changes. In a first step, the unperturbed Hamilton operator H_0 is modified leading to a modified free energy series expansion. In a second step, the susceptibility can be derived from the free energy series in a simple way which will be explained in detail. At the end of this section, a separate paragraph is dedicated to the explicit calculation for a given cluster to illustrate the details of the calculation and their computational complexity.

The unperturbed part H_0 of the Hamilton operator 2.3 is extended by a magnetic field term leading to

$$H_0 = \omega \sum_i b_i^\dagger b_i - h \sum_i S_i^z = H_B - hM \tag{2.18}$$

with the magnetic field h given in units of $g\mu_B$. The additional term proportional to the magnetization M commutes not only with the free phonon part H_B but also with the perturbation V as given in Eq. 2.3. Thus, the expression for $\tilde{V}(\tau)$ in Eq. 2.6 is unchanged compared to the previous investigations. Only H_0 has a slightly different meaning.

The partition function in Eq. 2.4 is still the same except the zeroth order contribution Z_0 . Following Eq. 2.18 Z_0 can be calculated exactly

$$Z_0 = \text{tr} (e^{-\beta H_0}) = \text{tr} (e^{-\beta H_B} e^{\beta h M}) = z_0^N \left(2 \cosh \left(\frac{\beta h}{2} \right) \right)^N. \tag{2.19}$$

Taking the logarithm of the partition function Z yields

$$\frac{1}{N} \ln Z = \ln z_0 + \ln \left(z \cosh \left(\frac{\beta h}{2} \right) \right) + \sum_{n=1}^{\infty} (-J)^n \left\{ \int_0^{\beta} d\tau_1 \cdots \int_0^{\tau_{n-1}} d\tau_n \langle \tilde{V}(\tau_1) \cdots \tilde{V}(\tau_n) \rangle \right\} \quad (2.20)$$

with z_0 as given in Eq. 2.5. The angular brackets $\langle \cdots \rangle$ denote the coefficients proportional to N in the trace, see Eq. 2.7. To derive the susceptibility the above equation has to be differentiated two times with respect to the magnetic field h . Finally h is set to zero.

$$T\chi = \frac{1}{\beta^2} \frac{\partial^2}{\partial h^2} \left(\frac{1}{N} \ln Z \right) \Big|_{h=0} \quad (2.21)$$

The last term in Eq. 2.20 can formally be expanded in powers of βh

$$\sum_{n=1}^{\infty} (-J)^n \left\{ \int_0^{\beta} d\tau_1 \cdots \int_0^{\tau_{n-1}} d\tau_n \langle \tilde{V}(\tau_1) \cdots \tilde{V}(\tau_n) \rangle \right\} = a_0 + a_2 (\beta h)^2 + \mathcal{O}((\beta h)^4) \quad (2.22)$$

leading to the susceptibility

$$T\chi = \frac{1}{4} + 2a_2. \quad (2.23)$$

Thus, the coefficient of $(\beta h)^2$ in Eq. 2.22 has to be evaluated in order to obtain the susceptibility series.

The equations to obtain the susceptibility are derived. Now, the clusters contributing in each order of expansion have to be identified. In contrast to the free energy series, for the susceptibility also clusters contribute which have links with multiplicity one. Thus, the connected clusters are determined in the same way as for the free energy except that multiplicities m_i of one are allowed. This is due to the fact that the incorporation of the magnetization M lead to nonvanishing contributions in the pure spin sector even for clusters which contain links with multiplicity one. Up to order 14 in J there are 8328 connected clusters which have to be evaluated.

Disconnected clusters are generated using the connected and disconnected clusters of the free energy series and combining them with the connected clusters of the susceptibility series. Only for one connected cluster in a given disconnected cluster array links with multiplicity one are allowed. Up to order 14 in J 11437 disconnected clusters exist with nonvanishing contributions to the susceptibility.

Tab. 2.2 depicts all contributing clusters in 4th order of expansion of the susceptibility. In contrast to the free energy series more clusters contribute in each order. Already in 4th order more clusters have to be taken into account than in 6th order for the free energy.

With the use of fractions of integers the susceptibility could be expanded up to order 10 in J . Jaan Oitmaa was able to reach the 12th order of expansion using floating point

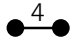
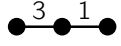
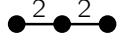

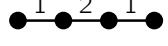
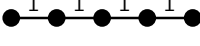


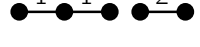
Cluster	p_c	$l_c[N]$
	1	1
	4	2 (symmetry)
	6	1
	12	2 (symmetry)
	12	1
	24	1
	4	-3
	6	$-\frac{3}{2}$
	12	-4

Table 2.2.: Contributing clusters in the 4th order expansion of the susceptibility. The lattice constant l_c and the number of permutations p_c are listed.

numbers [162]. The first orders of expansion are given by

$$\begin{aligned}
T\chi = & \frac{1}{4} - \frac{1}{8}J\beta - \frac{1}{16}J^2\beta\frac{g^2}{\omega} + \frac{1}{96}J^3\beta^3 \\
& + J^4\frac{1}{1536}\left(5\beta^4 + 24\frac{g^2\beta^3}{\omega} + \left((-72z_0^2 + 72z_0)\frac{g^4}{\omega^2}\right.\right. \\
& \left.\left.+ (-96 + 192z_0)\frac{g^2}{\omega^2}\right)\beta^2 + \left((72z_0 - 36)\frac{g^4}{\omega^3} - 192\frac{g^2}{\omega^3}\right)\beta\right) \\
& + \mathcal{O}(J^5) .
\end{aligned} \tag{2.24}$$

A first conclusion can already be drawn from the above equation. The modulus of the Curie-Weiss temperature for antiferromagnetic systems increases by the coupling of the spins to the phonons. The Curie-Weiss temperature is extracted from Eq. 2.24, yielding

$$\Theta_{\text{CW}} = -\left(\frac{1}{2}J + \frac{1}{4}J^2\frac{g^2}{\omega}\right) . \tag{2.25}$$

This was already observed in Ref. [60].

Example In this paragraph the contribution of a given cluster is calculated as an example. The chosen cluster contributes to second order in the expansion of the free energy and of the susceptibility, respectively. The main equations and the main results are given to illustrate the way the calculations are performed. The implementation in a computer

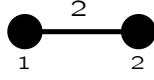


Figure 2.5.: Example of a cluster in second order of the expansion. The numbers below enumerate the sites involved, the number above denotes the multiplicity of the link.

program is straightforward, but still a complex task due to the fact that the calculations involve symbolic operations, in particular the evaluation of multiple integrals.

The connected cluster depicted in Fig. 2.5 has a lattice constant N and one permutation of the local operators has to be evaluated, following Eq. 2.16. To calculate its weight the cluster translates to the following term

$$\bullet \overset{2}{\text{---}} \bullet \triangleq J^2 \int_0^\beta d\tau_1 \int_0^{\tau_1} d\tau_2 \langle \tilde{V}(\tau_1) \tilde{V}(\tau_2) \rangle \quad \text{with} \quad (2.26a)$$

$$\tilde{V}(\tau_1) \tilde{V}(\tau_2) = (\mathbf{S}_1 \mathbf{S}_2)^2 \left(1 + g^2 \left(b_1^\dagger b_1 e^{\omega(\tau_1 - \tau_2)} + b_1 b_1^\dagger e^{-\omega(\tau_1 - \tau_2)} \right) \right). \quad (2.26b)$$

As can be seen from the above term the computation of the trace factorizes, i.e. the trace in the spin subspace can be calculated separately from the trace in the phonon subspace. The angular brackets $\langle \dots \rangle$ serving as an abbreviated notation for the trace can thus be written as

$$\begin{aligned} \langle \tilde{V}(\tau_1) \tilde{V}(\tau_2) \rangle &= \frac{1}{Z_0} \text{tr}_{\text{spin}} \left\{ e^{\beta h M} (\mathbf{S}_1 \mathbf{S}_2)^2 \right\} \cdot \\ &\quad \cdot \text{tr}_{\text{phonon}} \left\{ e^{-\beta H_B} \left(1 + g^2 \left(b_1^\dagger b_1 e^{\omega(\tau_1 - \tau_2)} + b_1 b_1^\dagger e^{-\omega(\tau_1 - \tau_2)} \right) \right) \right\}. \end{aligned} \quad (2.26c)$$

The phonon trace and the multiple integrals yield

$$\iint \text{tr}_{\text{phonon}} \{ \dots \} = \int_0^\beta d\tau_1 \int_0^{\tau_1} d\tau_2 z_0^N \left(1 + g^2 z_0 \left(e^{-\beta \omega} e^{\omega(\tau_1 - \tau_2)} + e^{-\omega(\tau_1 - \tau_2)} \right) \right) \quad (2.26d)$$

$$= z_0^N \left(\frac{1}{2} \beta^2 + g^2 \frac{\beta}{\omega} \right). \quad (2.26e)$$

The spin trace contributes with the following term

$$\text{tr}_{\text{spin}} \left\{ e^{\beta h M} (\mathbf{S}_1 \mathbf{S}_2)^2 \right\} = \left(2 \cosh \left(\frac{\beta h}{2} \right) \right)^{N-2} \text{tr}_{12} \left\{ e^{\beta h (S_1^z + S_2^z)} (\mathbf{S}_1 \mathbf{S}_2)^2 \right\} \quad (2.26f)$$

$$= \left(2 \cosh \left(\frac{\beta h}{2} \right) \right)^N \frac{1}{\left(2 \cosh \left(\frac{\beta h}{2} \right) \right)^2} \left(\frac{9}{16} + \frac{1}{16} e^{\beta h} + \frac{1}{16} + \frac{1}{16} e^{-\beta h} \right) \quad (2.26g)$$

$$= \left(2 \cosh \left(\frac{\beta h}{2} \right) \right)^N \left(\frac{3}{16} - \frac{1}{32} (\beta h)^2 + \mathcal{O}((\beta h)^4) \right). \quad (2.26h)$$

Thereby, the trace tr_{12} is restricted to the subspace with two sites only. In the last equation the cosh was expanded yielding the result up to order $(\beta h)^2$. Putting all results together and using only the coefficient of $(\beta h)^2$ the contribution to the susceptibility for the cluster in Fig. 2.5 is given by Eq. 2.23 and leads to

$$T\chi \Big|_{\bullet\text{---}\bullet} = -\frac{1}{16}J^2 \left(\beta^2 + \frac{\beta}{\omega} \right). \quad (2.26i)$$

The calculation steps performed in this paragraph are always of the same type for different clusters. Implemented in a computer program a cluster is chosen and an outer loop accounts for the permutations whose weights are evaluated. For increasing cluster length the number of permutations also increases resulting in time consuming evaluations, especially in higher orders. Up to 8th order the weights are evaluated in minutes. The necessary cpu time for the calculation of the weights of clusters in higher orders can be as high as a week, depending on the number of permutations which have to be evaluated.

2.4. Results

In this section the results for the susceptibility and the specific heat are presented in separate paragraphs. The bare truncated series will render a first impression of the behavior of the quantities under consideration for various sets of parameters. For quantitative predictions the truncated series are not sufficient as it will be seen in the following. Extrapolation techniques are necessary to improve the representation of the results away from the limit of expansion. Setting the overall energy scale to the magnetic exchange coupling J the expansion about the limit $J = 0$ can also be seen as a formal expansion about $\beta J = 0$, by considering the expansion of the partition function $Z = \text{tr}\{e^{-\beta J \tilde{H}}\}$ where \tilde{H} is the Hamilton operator 2.1 in units of J . Thus, high temperatures $T > J$ will be well described by the truncated series, but especially in the low temperature regime the truncated series will not be able to provide quantitative predictions. There is not as much information available to bias the spin-phonon system as there was for the pure spin systems.

The results presented in this thesis will be benchmarked relative to QMC data for selected sets of parameters. The QMC data is made available by C. Aits [159]. No explicit citations are made in the following for the comparison to QMC data.

The main focus in the representation of the results is laid on the influence of the spin-phonon coupling compared to the pure spin system. As a reference the exact result of the isotropic Heisenberg model [3, 163, 164] is depicted in the figures for the susceptibility. The specific heat is compared to the specific heat of free phonons, obeying the Dulong-Petit law for high temperatures superposed with the exactly known result for $C(T)$ of the Heisenberg model.

2.4.1. Susceptibility

The magnetic susceptibility is of special interest since this quantity is in most cases easily accessible experimentally. Prominent examples are the spin-Peierls substance CuGeO_3

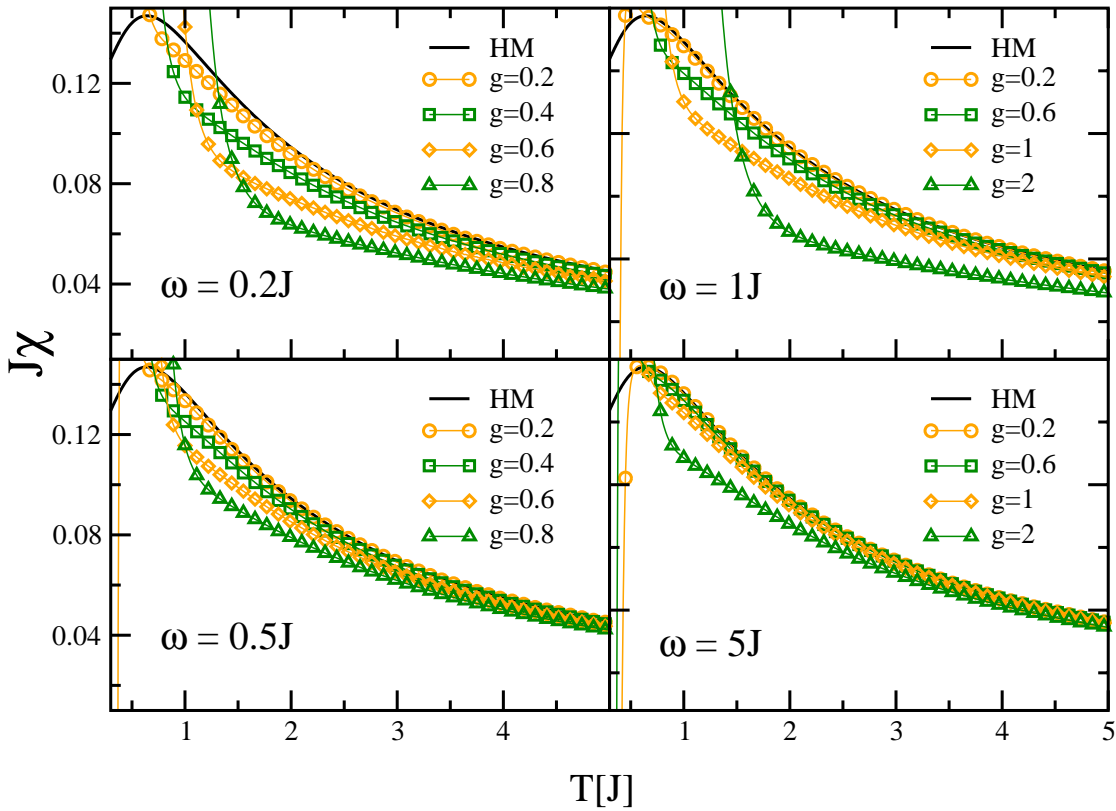


Figure 2.6.: Truncated series of the susceptibility: various sets of parameters are shown. The exactly known results for the Heisenberg model serves as a reference. The left panels illustrate the adiabatic limit whereas the right panels show the results in the antiadiabatic limit.

or $(\text{VO})_2\text{P}_2\text{O}_7$ which shows strong experimental evidence for non-negligible spin-phonon coupling [41]. Concerning $(\text{VO})_2\text{P}_2\text{O}_7$ investigations [60] showed that the thermodynamic magnetic quantities are affected only little by the inclusion of a spin-phonon coupling. Thus, static models like the dimerized and/or frustrated spin chain can yield already a good description of such quantities. But these static models can also be seen as effective models which implicitly contain the effects of a spin-phonon coupling. Thus, further investigations where the spin-phonon coupling is explicitly taken into account are necessary. Especially the magnetic susceptibility of CuGeO_3 has been studied extensively with the result that above the spin-Peierls transition at $T = 14\text{K}$ [146] the experiment can be fitted well by a frustrated Heisenberg model [7, 165, 166]. It is often objected, however, that the agreement might be accidental as no interchain interaction and no spin-phonon couplings are taken into account. The model under consideration in this thesis is certainly too simple to be a realistic model for CuGeO_3 . But it constitutes a valid testing ground to assess the effect of the coupling to dynamic phonons.

In the antiadiabatic limit $\omega \gtrsim J$ detailed investigations were done on the susceptibility. Using the flow equation approach [167] the authors could map the spin-phonon chain onto a frustrated spin chain with temperature dependent spin-spin couplings [153]. Having obtained the temperature dependent couplings they served as input for the HTSE data discussed in Chapter 1.4. It was shown that the susceptibility is only little affected by the temperature dependence of the coupling constants. Thus it can be neglected and a static model is well justified. This finding is in agreement with previous results [60]. In the adiabatic limit $\omega \lesssim J$ the authors expect the temperature dependence to be important, i.e. an effective static model is expected not to be valid to describe the spin-phonon model. In Fig. 2.6 the truncated susceptibility series is depicted for various parameter sets. The energy scales are given in units of the magnetic exchange coupling J . The general feature of diverging results for temperatures below $T \lesssim 1.5J$ is expected for the truncated series. But the qualitative behavior of the susceptibility is already discernible. The exact result of the Heisenberg model serves as a reference to illustrate the effects of the additional coupling to the phonons.

The left panels depict the adiabatic regime and the right panels illustrate the antiadiabatic limit. The following conclusions can already be drawn in the temperature regime $T \gtrsim 1.5J$ from the truncated series alone: fixing the phonon frequency ω the overall height of the susceptibility is lowered for increasing spin-phonon coupling g . Such a behavior can be understood from an increasing effective coupling $J_{\text{eff}} = J(1 + g(\langle b^\dagger + b \rangle))$ which shifts the whole susceptibility to lower temperatures compared to the result of the Heisenberg model. For fixed spin-phonon coupling and increasing phonon frequency ω this effect becomes less pronounced. For increasing phonon frequency the magnetic and phononic degrees of freedom decouple more and more, due to the different energy scales. Thus, for $\omega \rightarrow \infty$ and fixed g the magnetic properties are again dominated by the antiferromagnetic Heisenberg model.

So far, one of the most interesting features of the susceptibility e.g. concerning fitting procedures is not reproduced by the truncated series: the maximum. Especially the height and the position of the maximum are of great interest. The truncated series alone does not describe the maximum as depicted in Fig. 2.6. Extrapolations are necessary to extend the representation of the results beyond the radius of convergence of the truncated series. For the susceptibility the same extrapolation techniques are applied as for the pure spin models in the preceding chapters and as described in Sec. 1.3. Basically, the truncated series is extrapolated using Dlog-Padé approximants in an Euler-transformed variable. In contrast to the pure spin models the extrapolations of the results of the spin-phonon model cannot be performed in the inverse temperature β , but in the magnetic exchange coupling J . This in turn means, that for each temperature point a separate extrapolation in J has to be done. Using standard routines from computer algebra programs this poses no more problems than the previous extrapolations in β .

Another restriction concerns the information about the behavior of the magnetic susceptibility in the low temperature regime. Following the phase diagram depicted in Fig. 2.2 only a decision can be made whether for a given set of parameters the system is gapped or not. The size of the gap or a power law behavior as it is known for the pure spin models is so far

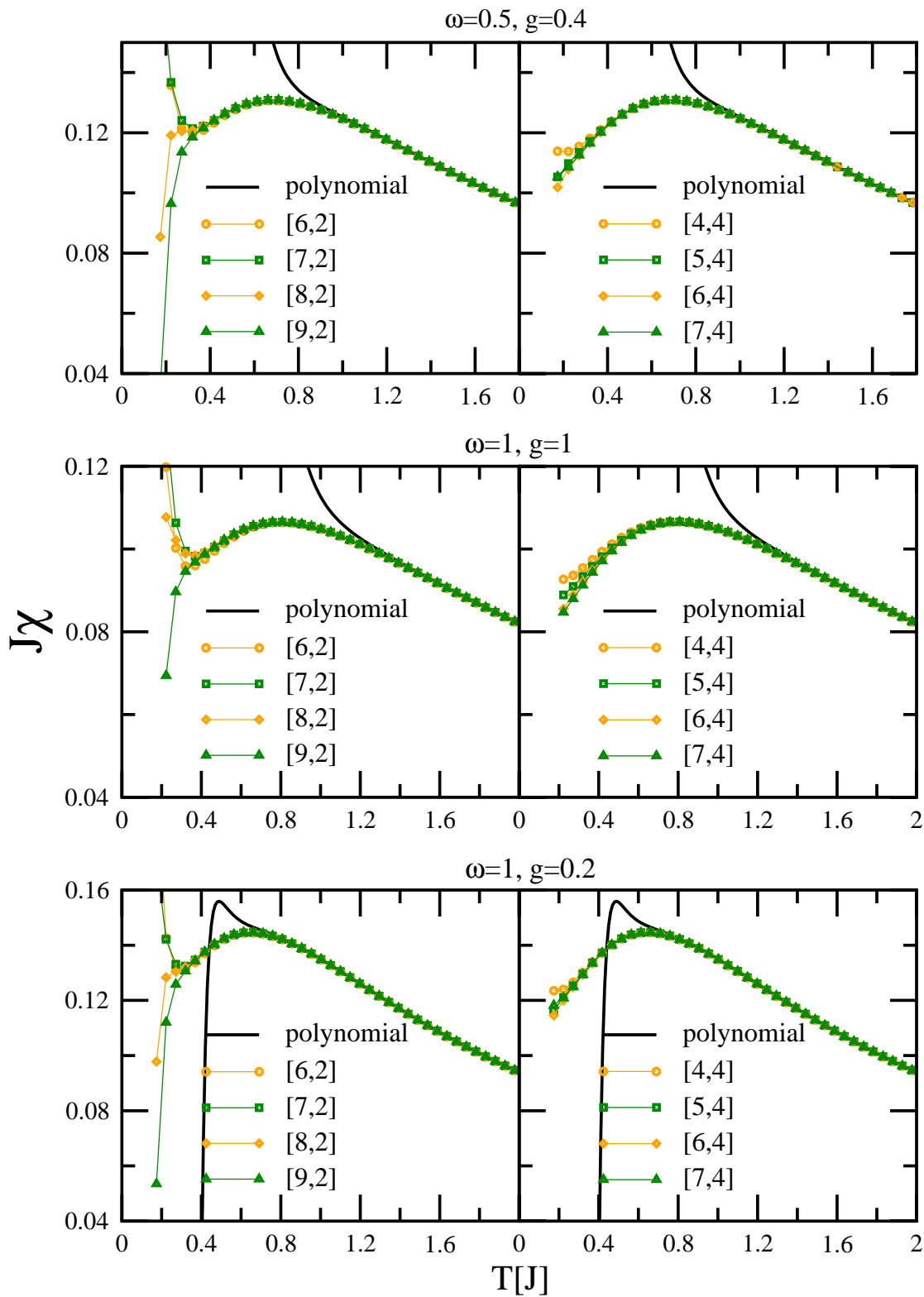


Figure 2.7.: Dlog-Padé extrapolations of the susceptibility: various orders are compared for three different sets of parameters. In the upper two panels the chosen parameters correspond to the gapped regime whereas the lower panels depict results in the ungapped regime.

not known. In the antiadiabatic regime, where the spin-phonon model can be mapped to a frustrated Heisenberg model, the gap could be extracted using the results from a high order series expansion about the limit of isolated dimers as it was done in Chapter 1.4. Here, we refrain from performing such an analysis, because no comparison with static models will be done. Such investigations are published in Ref. [153].

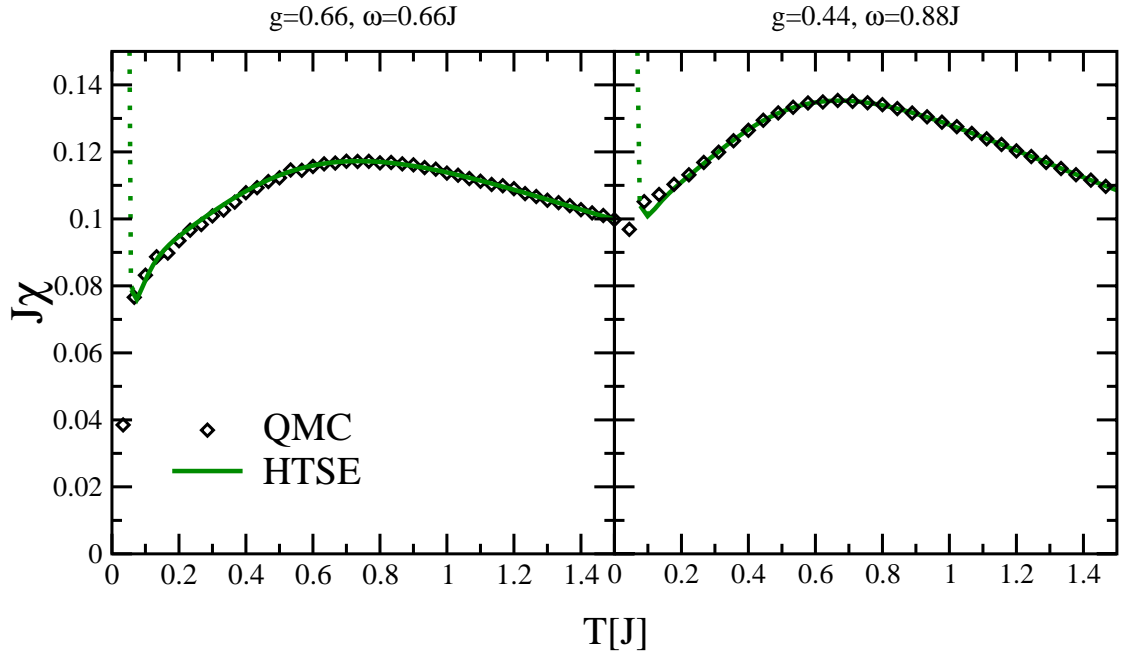


Figure 2.8.: Dlog-Padé extrapolations of the susceptibility compared to QMC data: the left plot shows data for the values $g = 0.66$, $\omega = 0.66J$ (gapped phase), and the right plot depicts the parameters $g = 0.44$, $\omega = 0.88J$ (ungapped phase).

As a first approach to the extrapolations the unbiased Dlog-Padé extrapolations are investigated. Fig. 2.7 shows an overview of the susceptibilities obtained for three different sets of parameters. For $\omega = 0.5$, $g = 0.4$ (upper panel), $\omega = 1$, $g = 1$ (middle panel), and $\omega = 1$, $g = 0.2$ (lower panel), respectively, the results of the Dlog-Padé extrapolations are shown. The upper two panels correspond to results in the gapped regime, whereas in the lower panel the parameters correspond to the ungapped regime, see the phase diagram in Fig. 2.2. The left panels depicts the extrapolations of order $[n, 2]$ and the right panels the extrapolations of order $[n, 4]$. A general feature is the reliably described position and height of the maximum for both orders of extrapolations, justified by the self-consistency of the results for various orders of the extrapolations. As can be directly seen from the figure, the $[n, 4]$ extrapolations converge better than the $[n, 2]$ extrapolations for increasing order. Higher orders or odd orders in the denominator are likely to produce spurious poles. Thus, the $[n, 4]$ extrapolations are used in the following to represent the susceptibility for all para-

meter sets used in this thesis. For temperatures $T < 0.2J$ no results are depicted due to spurious poles in the extrapolations in J . The range of validity of the $[n, 4]$ extrapolations can be estimated to $T \gtrsim 0.25J$ independent of the parameter sets used in this thesis. The results are compared to data obtained by QMC. For two different sets of parameters Fig. 2.8 compares the $[7, 4]$ extrapolations of the HTSE results with the QMC data. The values $g = 0.66$, $\omega = 0.66J$ in the left panel are results for the gapped phase, and the values $g = 0.44$, $\omega = 0.88J$ in the right panel correspond to the ungapped regime. The consistency between both methods is very good. For temperatures above $T/J \gtrsim 0.2$ the results coincide. Below $T \lesssim 0.2J$ the QMC data deviate from the HTSE results. For low temperatures reliable QMC data is difficult to obtain since an infinitely large number of updates need to be performed to obtain precise results. The calculations also suffer from finite size effects. Thus, significant error bars have to be taken into account in that temperature regime. The extrapolations of the HTSE results also suffer from inaccuracies in the low temperature regime. This is mainly due to spurious poles in the extrapolations. In the Dlog-Padé extrapolations the approximants have to be integrated with respect to J for each temperature point, see Sec. 1.3.1. For $T \lesssim 0.1J$ spurious poles occur in the integration interval leading to defective extrapolations. For clarity these defective extrapolations are shown as dotted lines. The conclusion which can be drawn from the comparison between HTSE and QMC is that the consistency between these two methods is very good for temperatures above $T \gtrsim 0.2J$. The position and the height of the maximum of the susceptibility can be described reliably.

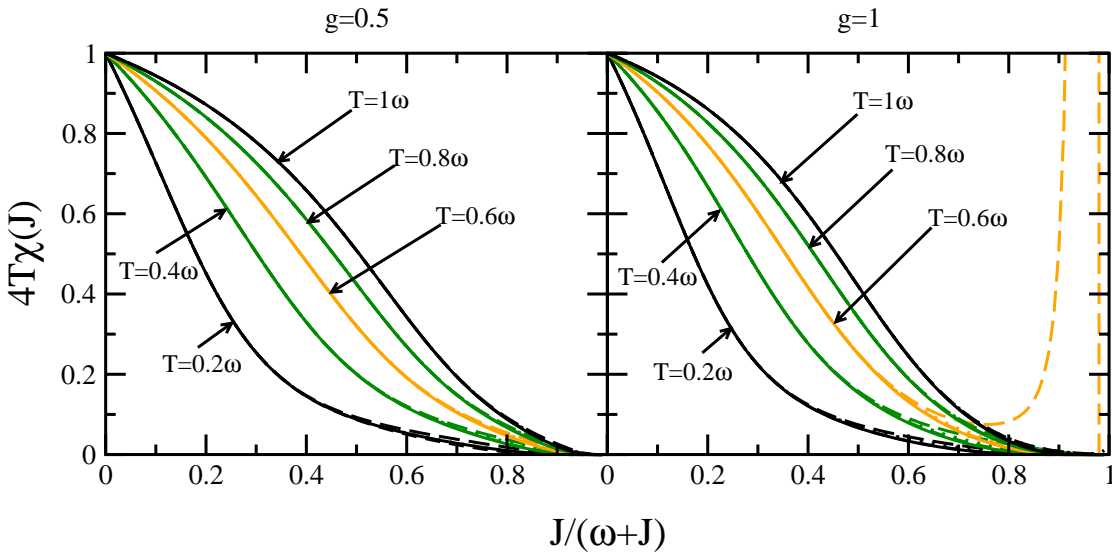


Figure 2.9.: Dlog-Padé extrapolations of the susceptibility: the extrapolations are performed in the magnetic exchange coupling J at fixed temperature. Results for the values $g = 0.5$ (left panel) and $g = 1$ (right panel) are depicted for temperatures $T = 0.2\omega, \dots, 1\omega$.

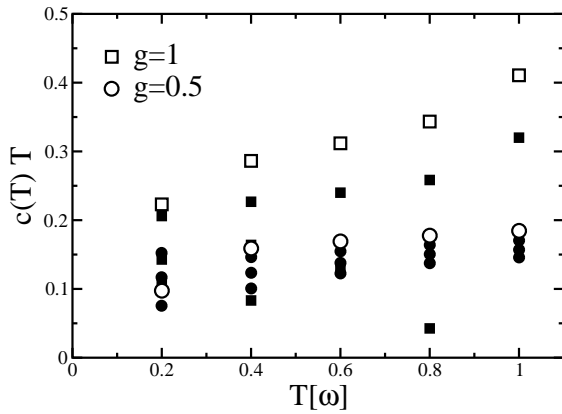


Figure 2.10: The temperature dependent coefficients $c(T)$ derived from the extrapolations of the susceptibility in the limit $J \rightarrow \infty$ following Eq. 2.27. The open symbols correspond to the values extracted from the $[7, 4]$ extrapolations whereas the solid symbols are the results from lower orders in the extrapolations.

Without the explicit knowledge of the behavior of $\chi(J \rightarrow \infty)$ the Dlog-Padé extrapolations for given temperature, spin-phonon coupling, and phonon frequency are investigated further in the following. Fig. 2.9 shows various extrapolations for $4T\chi(J)$ for fixed temperatures $T = 0.2\omega, 0.4\omega, \dots, 1\omega$. The extrapolations are all of the type $[n, 4]$ but no explicit distinction is made. The solid lines always refer to the extrapolations of order $[7, 4]$. To obtain the temperature dependent susceptibility, the appropriate values for J and ω are used to extract $\chi(T)$ for a given temperature T . For instance, fixing J and $\omega = J$ the results derived from the extrapolations in the left panel corresponds to the ungapped phase whereas in the right panel the result in the gapped regime is obtained. In doing so, the temperature dependent susceptibility is obtained by reading off the values $4T\chi(J)$ at the position $J/(\omega + J) = 1/2$ for a given temperature.

So far, no information about the behavior of the susceptibility is built in due to the lack of such information. Already the unbiased Dlog-Padé extrapolations yield convincing results down to fairly low temperatures. But it is expected that the inclusion of information about the limit $J \rightarrow \infty$ would improve the extrapolations. Building in such information may extend the range of validity of the extrapolations of the susceptibility down to lower temperatures. Especially in the gapped regime one should be able to describe the susceptibility in almost the whole temperature range. The relevant correlation length remains finite restricted by the inverse of $\max(k_B T/\hbar\nu, \Delta/\hbar\nu)$, where ν is a typical velocity of the excitations.

In Appendix B a perturbation expansion about the limit of isolated dimers perturbed by the finite temperature fluctuations of the phonons is performed. The aim is to obtain an approximate description of the susceptibility as function of J for fixed temperature, fixed spin-phonon coupling g , and fixed phonon frequency ω in the limit $J \rightarrow \infty$. The results, however, cannot be interpreted in the way we had hoped. This may be due to the ansatz which possibly does not incorporate the most relevant processes in the limit $J \rightarrow \infty$. Further investigations concerning the behavior of the susceptibility in that limit are called for.

Here, the Dlog-Padé extrapolations are used to discuss the behavior of the susceptibility in the limit $J \rightarrow \infty$. Fixing the temperature T and the phonon frequency ω the limit $J \rightarrow \infty$ corresponds to the adiabatic limit. In that limit it was shown that even a marginal spin-phonon interaction leads to a dimerization of the spin system [143, 145]. An analysis of the ground state energy in the adiabatic limit yields that it is energetically most favorable for

the spin system to be fully dimerized. This argument motivated the calculation in Appendix B. The gain in magnetic energy due to the dimerization δ (notation as in Chapter 1.4, see Eq. 1.25) is proportional to $J\delta^{4/3}$ which overcompensates the loss in elastic energy proportional to $\omega\delta^2$ [145]. This leads to a full dimerization of the spin system in the limit $J \rightarrow \infty$ where the phonons are completely softened. The strength of the magnetic exchange coupling alternates between 0 and $2J$ on every second bond. This would lead to a spin gap of $\Delta_{01} = 2J$.

In this context, the susceptibility as function of the magnetic exchange coupling and fixed temperature should show the behavior of a gapped system, namely

$$\chi(J \rightarrow \infty) \propto e^{-c(T)J}. \quad (2.27)$$

The temperature dependent coefficient $c(T) \geq 0$ defines the parameter governing the exponential decay. Using the unbiased Dlog-Padé extrapolations as depicted in Fig. 2.9 for various temperatures the coefficient $c(T)$ can be extracted from the approximants. This is done by setting the Euler-transformed variable $u = J/(1+J)$ in the Dlog-Padé approximant $P_m^l(u)$ to 1 (see Eq. 1.20 in Chapter 1.3.1). The value $u = 1$ corresponds to $J = \infty$. For each temperature point the coefficient $c(T)$ was calculated and the obtained values are shown in Fig. 2.10.

As a first ansatz we assume a temperature dependent behavior of the susceptibility of type $\chi(T) \propto e^{-\Delta/T}$ for low temperatures. The gap is defined by Δ and $\Delta = 0$ is allowed to incorporate also the ungapped case. Hence, the approximate equality $c(T)T \approx \Delta/J$ holds. For temperatures below $T = 0.2\omega$ no estimates for $c(T)$ can be obtained due to spurious poles in the extrapolations. The estimates of $c(T)$ also depend strongly on the order of extrapolation. The results from lower orders are depicted by solid symbols. Open symbols correspond to the highest order available, namely $[7, 4]$. For $g = 1$ the values extracted from lower orders deviate significantly from the value obtained in order $[7, 4]$. To present consistent results the values of the $[7, 4]$ extrapolations are considered in the following for all temperatures. Significant error bars have to be taken into account in particular for lower temperatures and higher values of the spin-phonon coupling g . With the ideas proposed above, one should normally expect a constant value for $c(T)T$, which is not the case for the extracted values as shown in Fig. 2.10. Assuming a temperature dependence of the gap Δ , one could imagine that a continuation of the results for $c(T)T$ down to zero temperature would yield a zero gap for $g = 0.5$ and a finite gap for $g = 1$. These results would support the presented approximate approach in the limit $J \rightarrow \infty$. A more detailed investigation of the limit $J \rightarrow \infty$ is necessary to understand the behavior of the susceptibility. The approach presented should serve as a first approach to the limit $J \rightarrow \infty$.

2.4.2. Specific Heat

A detailed study of the magnetic properties of the system under consideration also includes the investigation of the specific heat. Besides the magnetic susceptibility the specific heat is an observable which can be experimentally easily measured and theoretically easily calculated. However, a direct comparison between theory and experiment is often hindered

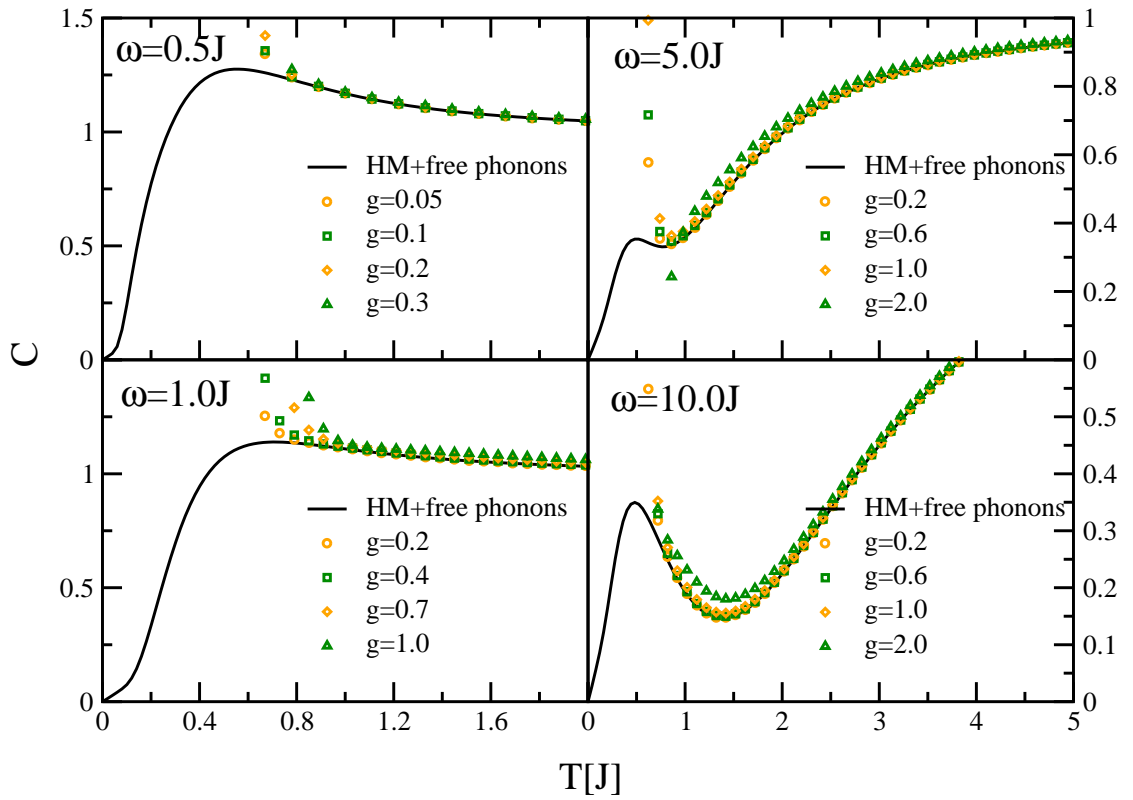


Figure 2.11.: Truncated series of the specific heat: various sets of parameters are shown. The exactly known results for the Heisenberg model superposed with the result for free phonons serves as a reference.

by the fact that the phononic degrees of freedom dominate the specific heat, when the energy scales of the phononic subsystem and the magnetic subsystem are of same order, as mentioned in the previous chapters. The spin-phonon model allows to study the interplay of magnetic and phononic degrees of freedom in a simple transparent toy model. The effects of an explicit spin-phonon interaction is taken into account and its influence on the specific heat is investigated.

Fig. 2.11 depicts the truncated series results of the specific heat compared to a superposition of the free phonon part of the specific heat given by

$$C_B = (\beta\omega)^2 \frac{e^{-\beta\omega}}{(1 - e^{-\beta\omega})^2} \quad (2.28)$$

and the exactly known result C_S for the isotropic Heisenberg model. Various parameter sets are shown. The free dispersionless phonons are dominant at high temperatures. The constancy of the specific heat at high temperatures is visible in the left panels as expected according to the Dulong-Petit rule. In the right panels this constancy would also be visible

if the results were depicted to higher temperatures. As can be seen also in the right panels, the separation of phononic and magnetic degrees of freedom is due to their significantly different energy scales.

From the truncated series alone the following conclusion can be drawn. For small spin-phonon coupling g the specific heat is largely described by the superposition of C_B and C_S . Increasing the coupling of the spin system to the phonons slightly shifts the specific heat to larger values in the temperature regime $T > J$ where the truncated series are expected to yield trustworthy results. Fixing the spin-phonon coupling g and going to larger frequencies ω this effect weakens as expected.

To obtain more detailed insight into the behavior of the specific heat Dlog-Padé extrapolations are used. The extrapolation technique used in the previous chapters for the pure spin models cannot be applied here. The sum rules incorporated previously are still valid for the problem at hand. But they yield infinite values which cannot be incorporated in the extrapolations. Hence, simple Dlog-Padé extrapolations in J are used for each temperature point. To this end, the exactly known result of the free phonons is subtracted and the remaining truncated series is extrapolated.

The series expansion of the specific heat starts with the exactly known result for the free phonons. Hence, the extrapolations are performed for the specific heat subtracted by its free phonon part. The remaining series starts in second order in J . Having obtained the result up to order 13 in J , the maximum order of extrapolation of the remaining specific heat is 10. Ordinary Padé extrapolations would allow a maximum order of 11, but due to the differentiation in the Dlog-Padé extrapolations one more order is lost, leading to the maximum order of 10, as explained in Chapter 1.3.

In Fig. 2.12 three different sets of parameters $\omega = 1J$, $g = 0.7$ (upper panels), $\omega = 1J$, $g = 1.5$ (middle panels) and $\omega = 5J$, $g = 1$ (lower panels) are extrapolated. The left plots depict the $[n, 2]$ and the right plots the $[n, 4]$ extrapolations. A general feature is that both orders of extrapolations converge very well, whereas the $[n, 4]$ extrapolations are more stable in the low temperature regime for both parameter sets. Hence, the $[n, 4]$ extrapolations are used in the following. The range of validity can be specified to $T \gtrsim 0.15J$ as long as the spin-phonon coupling is smaller or of the same order as ω . For values of $gJ/\omega > 1$ the extrapolations suffer very likely from spurious poles. In the middle panels the defective extrapolations are visible. The orders $[5, 2]$, $[6, 2]$, and $[3, 4]$ yield extrapolations which differ significantly from the other orders considered. This is due to spurious poles in the integration interval with respect to J . For $[6, 2]$ even temperatures above $T \approx J$ are not reliably described. In that temperature regime the truncated series alone yields a precise description of the specific heat.

The results obtained from the cluster expansion in J are compared to data obtained by QMC. Fig. 2.13 compares two sets of parameters of the $[6, 4]$ extrapolations of the HTSE results to QMC data. The left panel shows the result for $g = 0.66$, $\omega = 0.66J$, referring to the gapped phase. In the right panel results in the ungapped phase are depicted with $g = 0.44$, $\omega = 0.88J$. The error bars of the QMC data are for both values quite large. The HTSE results are more stable, yielding results which coincide with the QMC data very well. For temperatures below $T/J \approx 0.15$ the dotted lines refer to defective extrapolations

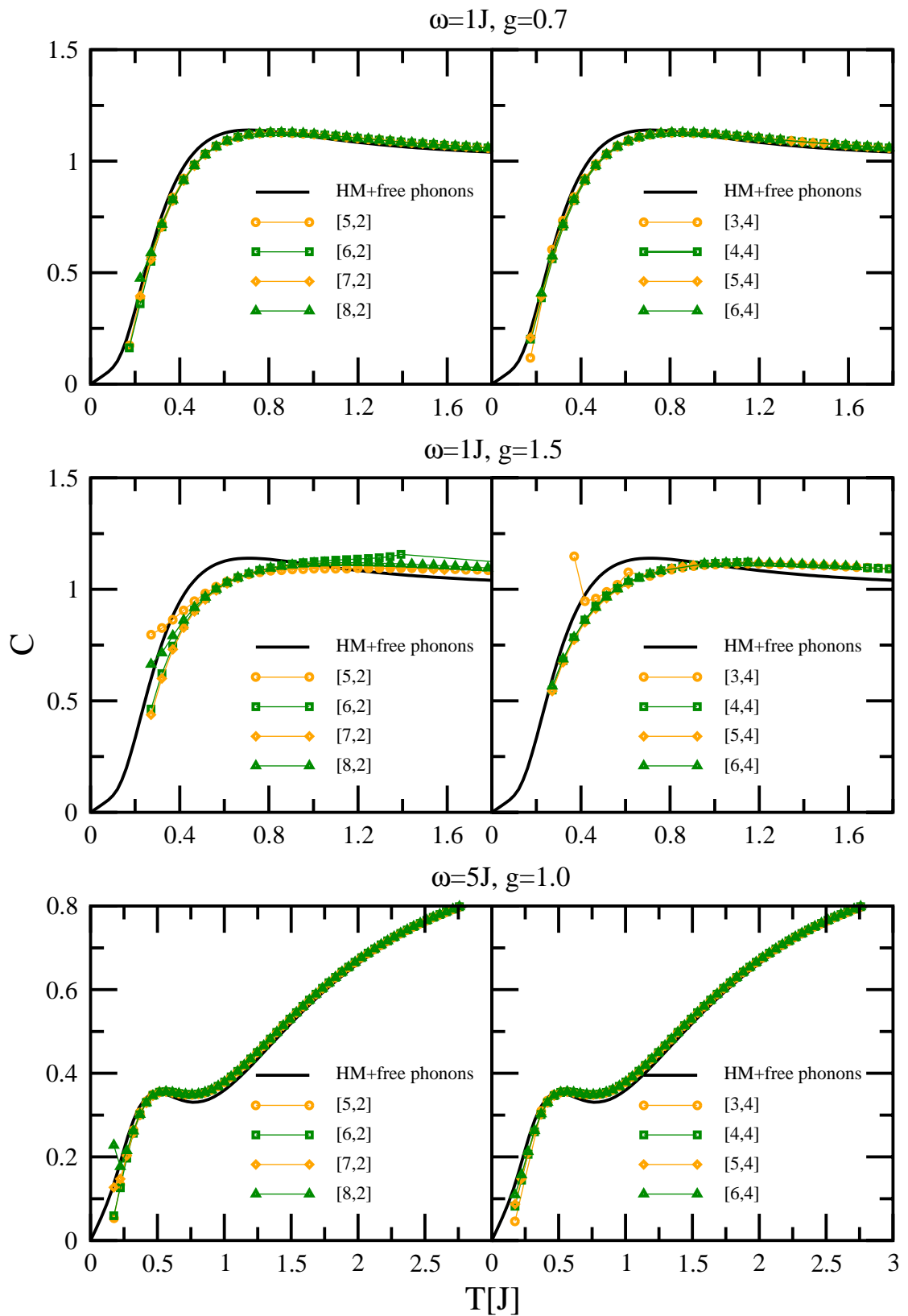


Figure 2.12.: Dlog-Padé extrapolations of the specific heat: various orders are compared to each other for three different sets of parameters.

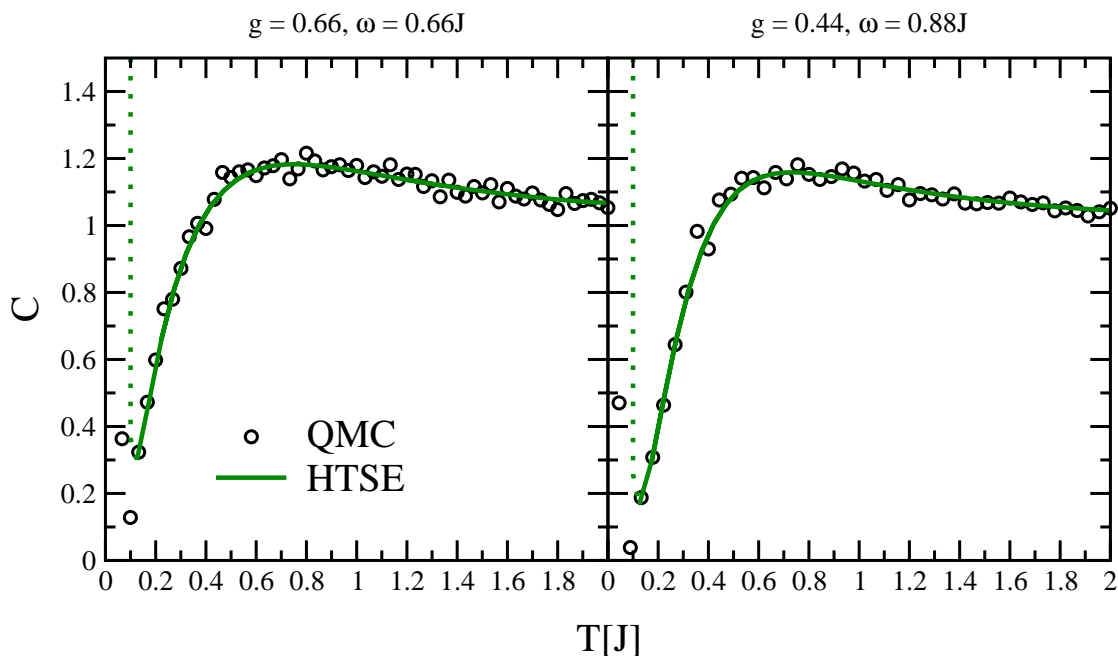


Figure 2.13.: Dlog-Padé extrapolations of the specific heat compared to QMC data: the left plot shows data for the values $g = 0.66$, $\omega = 0.66J$, and the right plot depicts the parameters $g = 0.44$, $\omega = 0.88J$.

which are depicted for illustrative purposes. As it is the case for the extrapolations of the susceptibility spurious poles in the integration interval with respect to J for a given temperature yield defective extrapolations. Thus, the HTSE extrapolations yield reliable results for temperatures $T \gtrsim 0.15J$.

2.5. Conclusions

The problem of a spin-system coupled to phononic degrees of freedom is investigated. The method of a cluster expansion is applied to obtain the high temperature series expansion results for the free energy, specific heat, and magnetic susceptibility. No cutoff in the phononic subspace is necessary since the expansion is performed in the magnetic exchange coupling J about the limit $J = 0$. It is the first approach of a cluster expansion at finite temperatures for the spin-phonon problem. The implementation of the expansion in a computer program yields high orders in the expansion parameter. In an example for a cluster the complexity of the explicit evaluation of the quantities under consideration is illustrated. The comparison of the high temperature series expansion results to a numerical method, namely quantum Monte-Carlo, shows a very good consistency between the two methods. Detailed information in the low temperature limit and in the limit $J \rightarrow \infty$ for fixed temperature is necessary to improve the representations for temperatures below $T \lesssim 0.15J$. The results can serve as input for quantitative data analysis since the main features of the considered quantities at moderate and high temperatures are described reliably.

Summary

The present thesis deals with the thermodynamical properties of low-dimensional spin- and spin-phonon systems. For a thorough study the method of high temperature series expansions is applied. The thesis is divided into two main parts. The first part addresses pure spin- $\frac{1}{2}$ systems in (quasi) one and two dimensions and the second part is dedicated to the study of a one-dimensional spin- $\frac{1}{2}$ system coupled to phononic degrees of freedom, i.e. dispersionless Einstein phonons.

The high temperature series expansions as performed in this thesis provide results that are obtained as truncated series up to the highest orders possible with the full dependence of the parameters entering the model. The series coefficients are given as fractions of integers such that no accuracy is lost. Thus, the results are exact up to the given order. In contrast to other numerical methods like exact complete diagonalization, quantum Monte-Carlo or transfer matrix-renormalization group, where for each set of parameters a new program has to be started, the results obtained by the high temperature series expansion have to be computed only once. Thus, the comparison to experimental data becomes a fast and easy task. Though the computations are done for finite systems, the results are valid in the infinite system, which is the main idea of the linked cluster theorem. The calculations are implemented in computer programs to obtain the highest orders possible.

The truncated series are able to give a precise description of the thermodynamical quantities for temperatures above $T \gtrsim J$, where J denotes the overall energy scale of the appropriate system. However, the experimentally interesting position and height of the maxima of the susceptibility and specific heat, respectively, can only be accessed in very rare cases by the truncated series alone. The maxima normally appear in the temperature regime below the region accessible by the truncated series. Thus, extrapolation techniques are applied to improve the representation of the results down to lower temperatures. The extrapolation techniques used in this thesis are Padé- and Dlog-Padé extrapolations. Basically, the extrapolations yield a valid description also outside the radius of convergence of the computed series. The key point in the extrapolations is to use additional information on the $T = 0$ and on the low-temperature behavior to stabilize the extrapolations in the low-temperature region. As far as available, the size of the spin gap, the form (linear or quadratic) of the dispersion in the vicinity of its minimum, the dimensionality of the system, and the ground state energy are used as additional input. The representations of the specific heat are further stabilized exploiting the sum rules for the energy and the entropy.

The extrapolated series expansion results are gauged carefully by investigating their convergence and by comparing them to numerical data obtained from other methods. For systems with a sufficiently large gap the stabilized extrapolations yield quantitative results in the whole temperature regime.

The dimerized, frustrated spin chain is investigated in Chapter 1.4. This model can also be seen as zig-zag chain and comprises in particular the usual spin-ladder which is investigated in a separate chapter. A first aim is to provide results and tools which facilitate and expedite the analysis of experimental data. The susceptibility and specific heat are calculated up to order 10 in β for the dimerized, frustrated chain and up to order 18 in β for the unfrustrated, dimerized chain. It is shown that the representations of the susceptibility and of the specific heat provide valid descriptions of the thermodynamic quantities for temperatures above $T \approx 0.25J$. In the special case of the isotropic Heisenberg model it is shown that the extrapolation of the specific heat produces results which almost coincide with the exactly known curve. The results for the chains without exact solution are benchmarked to data from exact complete diagonalization and transfer matrix-renormalization group calculations. The analysis of the magnetic susceptibility of $(\text{VO})_2\text{P}_2\text{O}_7$ yielded comparable results for various theoretical models. In this thesis it is demonstrated to what extent it is possible to determine the model parameters quantitatively from the temperature dependence of the magnetic susceptibility and the specific heat for the given model.

Results for many sets of parameters are included to ease data analysis further. For the susceptibility and for the specific heat the maximum values as well as their corresponding positions are provided for a large range of dimerizations $\delta = 0..1$ and of frustrations $\alpha = 0..4$. These results make it possible to read off the coupling parameters J , α , and δ if as little as the maxima and their positions are known. It turns out that the knowledge of the susceptibility at moderate and high temperatures alone is not sufficient to determine the three model parameters J , δ , and α even if the gyromagnetic ratio g is assumed to be known from independent experiments, e.g. ESR. But any additional knowledge, for instance on the specific heat or on the singlet-triplet gap, may solve the problem.

A ladder system is addressed in Chapter 1.5. The influence of an additional four-spin (cyclic) interaction is investigated in detail. The results for the susceptibility and the specific heat are obtained up to order 10 in β . For the calculations a minimal system size of $N = 20$ was chosen, leading to wrap-around effects, which have either to be corrected by hand or to be evaluated in a separate program. The wrap-around effects are presented in detail and their corrections are evaluated. To evaluate the results a cpu-time of about 250 days with a memory usage of 2GB was necessary. The extrapolations provide reliable results down to very low temperatures $T \gtrsim 0.3J_{\perp}$ for the susceptibility and for $T \gtrsim 0.15J_{\perp}$ for the specific heat. The range of validity of the specific heat is slightly larger than for the susceptibility due to the sum rules stabilizing the extrapolations. The results are benchmarked to another numerical method, namely exact complete diagonalization.

Addressing the information content of a susceptibility measurement at moderate and high temperatures, it is found that a unique parameter set from a susceptibility measurement alone can hardly be determined. A detailed comparison of the theoretical findings to the experimental susceptibility data of SrCu_2O_3 is performed.

The experiment can only access the temperature regime below the maximum, which hampers a precise determination of the model parameters using results from a HTSE. Thus, the published values of the model parameters, the known gyromagnetic ratio g , and

the known spin gap Δ are used to represent the susceptibility. Considering carefully the range of validity of the extrapolations, it can be shown that the inclusion of a significant but small amount of cyclic exchange can resolve the unexpected high value of the ratio $x = J_{\parallel}/J_{\perp} \approx 2$ and the low value of the exchange coupling $J_{\perp} \approx 1000\text{K}$ which are published in the literature [110]. Taking the values $J_{\perp} = 1750\text{K}$, $x = 1.1$, and $x_{\text{cyc}} = 6.5\%$, recently determined from a Raman response experiment [85], it can be shown that these values provide a similar agreement as the data for $J_{\perp} = 1000\text{K}$ and $x = 2$.

In Chapter 1.6 a two-dimensional spin-system is investigated, the Shastry-Sutherland model. In contrast to the (quasi) one-dimensional systems a complete enumeration of the Hilbert-space of the finite system is not possible. Instead, the moment-algorithm is used which is more efficient in this case. The results are computed up to order 8 in β for the specific heat and up to order 7 in β for the susceptibility. In doing so, the capacities of the current computers are fully exploited. With a cpu-time of about three days, the program needs 30GB of memory to perform the calculations.

So far, the more sophisticated linked cluster expansion method does not produce higher orders which underlines the efficiency of the moment-algorithm. With the realization of the Shastry-Sutherland model in $\text{SrCu}_2(\text{BO}_3)_2$, a detailed comparison between theory and experiment is possible. The theoretical results for the susceptibility and the specific heat are compared with experimental data. To include the three-dimensionality of the compound in the theoretical model a mean-field like ansatz is used to describe the susceptibility. Extending the two-dimensional model by an inter-layer coupling J_{\perp} the best fits to the susceptibility are obtained using $J_{\parallel} = 71(1)\text{K}$, $J_{\perp} = 17(2)\text{K}$, and $x = 0.603$. The Shastry-Sutherland model and its extension to three dimensions reproduces the experimental susceptibility data of $\text{SrCu}_2(\text{BO}_3)_2$ down to fairly low temperatures. Unfortunately, one of the main features of the susceptibility, namely the maximum, is not accessible by means of the HTSE extrapolations. The extrapolations provide valid results down to $T \approx 0.6J_{\parallel}$ but the position of the maximum is at $T_{\text{max}} \approx 0.2J_{\parallel} \dots 0.3J_{\parallel}$. Using the parameter set obtained from the susceptibility fit, the specific heat data cannot be reproduced with the same quality. But for the above given values the HTSE representation showed the best tendency to be the relevant one for $\text{SrCu}_2(\text{BO}_3)_2$. Concerning the specific heat, further investigations relying on other methods have to be done to improve the consistency between theory and experiment.

The second part of this thesis presents results for a one-dimensional spin system coupled to dispersionless phonons. The method to compute the results is different from the previous approaches. A direct expansion in the inverse temperature fails due to a divergence which results from the infinite phononic Hilbert space. A formal expansion about the limit $J = 0$ is performed using the cluster expansion technique. It is the first approach of a cluster expansion at finite temperatures for the spin-phonon problem. For each order of expansion both connected and disconnected clusters and their weights have to be determined. The calculational details are emphasized to highlight the complexity of the necessary evaluations. In the explicit calculations no cutoff in the phonon subspace is required. The full

phonon dynamics is taken into account. The susceptibility can be expanded up to order 10(12) and the free energy up to order 11(13) in J . The orders given in brackets denote results obtained by J. Oitmaa using floating point arithmetics instead of a representation as fractions of integers. To improve the representation of the results Dlog-Padé extrapolations are used. For each temperature a separate extrapolation in J has to be done. The results are not stabilized in the low temperature regime since no well-known information as for the pure spin-models is available so far. The comparison of the high temperature series expansion results to a numerical method, namely quantum Monte-Carlo, shows a very good consistency between the two approaches. Detailed information in the low temperature limit and in the limit $J \rightarrow \infty$ for fixed temperature would be required to improve the representations of the susceptibility for temperatures below $T \lesssim 0.15J$.

Outlook

Higher orders in the series expansions will always constitute a further refinement of the results. Especially the results of the two dimensional Shastry-Sutherland model could be improved significantly by higher orders, leading to improved estimates of the model parameters describing $\text{SrCu}_2(\text{BO}_3)_2$. However, temperatures below $T \approx 0.15J$, where J denotes the overall energy scale, are always difficult to describe reliably by means of HTSE extrapolations. In particular, the discrepancy between theory and experimental data in the specific heat needs further investigation. The inclusion of a spin-phonon coupling to the model can serve as a first approach since the spin-phonon coupling is expected to be important [129, 138, 141].

The results of the spin-phonon model can be improved by additional knowledge on the low temperature properties of the system and by information on the limit $J \rightarrow \infty$ for a given temperature. With this information at hand the extrapolations of the HTSE results can be stabilized in the low temperature regime as is the case for the pure spin-models. But such information is also of general interest. So far, these limits are poorly understood. Further investigations relying on other methods have to be done.

Another aspect concerns higher-dimensional systems, like the three-dimensional generalization of the Shastry-Sutherland model, ladders with more than two legs, or the frustrated square lattice to mention just a few. With the methods for high temperature series expansions and the extrapolation techniques developed and applied in this thesis, reliable results for the thermodynamical quantities of interest can be obtained in a straightforward fashion. The results can then serve for a better understanding of the thermodynamical properties of these systems.

The methods used in this thesis are not restricted to $S = \frac{1}{2}$. A natural extension of the presented models is to consider systems with higher values of the spin. For instance, a comparison to known $S = 1$ chain-systems like NENP and NINO [168–170] would be possible. The results can then serve for a detailed and reliable analysis of the thermodynamical quantities of these systems. The methods applied here remain the same leading only to slight changes in the calculations. However, for increasing spin S the increasing dimension of the Hilbert space poses a problem concerning the possible orders one is able to achieve.

A. Coefficients

A.1. Dimerized, Frustrated Chain

Table A.1.: Series coefficients $a_{n,k,l}$ of the high temperature expansion of the magnetic susceptibility $\chi = \frac{1}{T} \sum_{n,k,l} a_{n,k,l} \delta^k \alpha^l (\beta J)^n$ for the dimerized, frustrated chain. Only nonzero coefficients are presented.

(n,k,l)	$a_{n,k,l}$	(n,k,l)	$a_{n,k,l}$	(n,k,l)	$a_{n,k,l}$	(n,k,l)	$a_{n,k,l}$	(n,k,l)	$a_{n,k,l}$
(0,0,0)	$\frac{1}{4}$	(6,0,1)	$\frac{9}{1280}$	(7,4,3)	$\frac{-583}{245760}$	(9,0,4)	$\frac{317}{229376}$	(10,0,6)	$\frac{599639}{594542592}$
(1,0,0)	$\frac{-1}{8}$	(6,0,2)	$\frac{221}{61440}$	(7,6,0)	$\frac{-307}{92160}$	(9,0,5)	$\frac{-969}{655360}$	(10,0,7)	$\frac{791221}{1486356480}$
(1,0,1)	$\frac{-1}{8}$	(6,0,3)	$\frac{-163}{92160}$	(7,6,1)	$\frac{-3167}{1474560}$	(9,0,6)	$\frac{93463}{61931520}$	(10,0,8)	$\frac{-367481}{1486356480}$
(2,0,1)	$\frac{1}{8}$	(6,0,4)	$\frac{7}{15360}$	(8,0,0)	$\frac{1269}{4587520}$	(9,0,7)	$\frac{-67097}{82575360}$	(10,0,9)	$\frac{22433}{148635648}$
(2,2,0)	$\frac{-1}{16}$	(6,0,5)	$\frac{23}{7680}$	(8,0,1)	$\frac{-23629}{20643840}$	(9,0,8)	$\frac{-361}{1720320}$	(10,0,10)	$\frac{-339691}{5945425920}$
(3,0,0)	$\frac{1}{96}$	(6,0,6)	$\frac{-133}{122880}$	(8,0,2)	$\frac{-58651}{13762560}$	(9,0,9)	$\frac{3737}{74317824}$	(10,2,0)	$\frac{-215221}{5945425920}$
(3,0,1)	$\frac{1}{128}$	(6,2,0)	$\frac{-83}{40960}$	(8,0,3)	$\frac{28751}{5160960}$	(9,2,0)	$\frac{979}{3440640}$	(10,2,1)	$\frac{-322247}{247726080}$
(3,0,2)	$\frac{-1}{32}$	(6,2,1)	$\frac{1}{1536}$	(8,0,4)	$\frac{-59}{20160}$	(9,2,1)	$\frac{-3899}{1474560}$	(10,2,2)	$\frac{515117}{123863040}$
(3,0,3)	$\frac{1}{96}$	(6,2,2)	$\frac{49}{30720}$	(8,0,5)	$\frac{-877}{1290240}$	(9,2,2)	$\frac{79}{458752}$	(10,2,3)	$\frac{-1295087}{743178240}$
(3,2,1)	$\frac{3}{128}$	(6,2,3)	$\frac{97}{30720}$	(8,0,6)	$\frac{5389}{20643840}$	(9,2,3)	$\frac{-29209}{9175040}$	(10,2,4)	$\frac{3402433}{1486356480}$
(4,0,0)	$\frac{5}{1536}$	(6,2,4)	$\frac{-13}{2560}$	(8,0,7)	$\frac{-1271}{1720320}$	(9,2,4)	$\frac{4099}{2949120}$	(10,2,5)	$\frac{52919}{106168320}$
(4,0,1)	$\frac{-23}{768}$	(6,4,0)	$\frac{-21}{40960}$	(8,0,8)	$\frac{1269}{4587520}$	(9,2,5)	$\frac{-1387}{430080}$	(10,2,6)	$\frac{-379969}{212336640}$
(4,0,2)	$\frac{1}{512}$	(6,4,1)	$\frac{3}{2560}$	(8,2,0)	$\frac{89}{229376}$	(9,2,6)	$\frac{-13529}{20643840}$	(10,2,7)	$\frac{14941}{99090432}$
(4,0,3)	$\frac{-1}{96}$	(6,4,2)	$\frac{-117}{20480}$	(8,2,1)	$\frac{36983}{20643840}$	(9,2,7)	$\frac{5233}{9175040}$	(10,2,8)	$\frac{-31027}{99090432}$
(4,0,4)	$\frac{5}{1536}$	(6,6,0)	$\frac{-1129}{368640}$	(8,2,2)	$\frac{-4293}{655360}$	(9,4,0)	$\frac{481}{1376256}$	(10,4,0)	$\frac{195049}{2972712960}$
(4,2,0)	$\frac{7}{768}$	(7,0,0)	$\frac{1}{16128}$	(8,2,3)	$\frac{479}{1290240}$	(9,4,1)	$\frac{-2423}{1835008}$	(10,4,1)	$\frac{-15173}{7741440}$
(4,2,1)	$\frac{-3}{256}$	(7,0,1)	$\frac{5863}{1474560}$	(8,2,4)	$\frac{5119}{2580480}$	(9,4,2)	$\frac{699}{458752}$	(10,4,2)	$\frac{2661047}{2972712960}$
(4,2,2)	$\frac{7}{512}$	(7,0,2)	$\frac{-805}{73728}$	(8,2,5)	$\frac{-61}{64512}$	(9,4,3)	$\frac{-74989}{27525120}$	(10,4,3)	$\frac{-1311053}{743178240}$
(4,4,0)	$\frac{7}{512}$	(7,0,3)	$\frac{3923}{737280}$	(8,2,6)	$\frac{6095}{4128768}$	(9,4,4)	$\frac{12337}{20643840}$	(10,4,4)	$\frac{-128473}{41287680}$
(5,0,0)	$\frac{-7}{5120}$	(7,0,4)	$\frac{-381}{81920}$	(8,4,0)	$\frac{1507}{20643840}$	(9,4,5)	$\frac{69103}{41287680}$	(10,4,5)	$\frac{153863}{495452160}$
(5,0,1)	$\frac{-49}{6144}$	(7,0,5)	$\frac{943}{368640}$	(8,4,1)	$\frac{76009}{20643840}$	(9,6,0)	$\frac{263}{1474560}$	(10,4,6)	$\frac{-816989}{2972712960}$
(5,0,2)	$\frac{37}{1536}$	(7,0,6)	$\frac{67}{368640}$	(8,4,2)	$\frac{1061}{393216}$	(9,6,1)	$\frac{-12323}{6881280}$	(10,6,0)	$\frac{145961}{990904320}$
(5,0,3)	$\frac{-1}{128}$	(7,0,7)	$\frac{1}{16128}$	(8,4,3)	$\frac{-3947}{5160960}$	(9,6,2)	$\frac{22877}{20643840}$	(10,6,1)	$\frac{-14683}{9175040}$
(5,0,4)	$\frac{1}{512}$	(7,2,0)	$\frac{-59}{92160}$	(8,4,4)	$\frac{29}{15360}$	(9,6,3)	$\frac{138421}{82575360}$	(10,6,2)	$\frac{-33937}{27525120}$
(5,0,5)	$\frac{-7}{5120}$	(7,2,1)	$\frac{4289}{491520}$	(8,6,0)	$\frac{-10831}{10321920}$	(9,8,0)	$\frac{15607}{13762560}$	(10,6,3)	$\frac{943507}{743178240}$
(5,2,0)	$\frac{1}{1536}$	(7,2,2)	$\frac{-131}{36864}$	(8,6,1)	$\frac{-1927}{983040}$	(9,8,1)	$\frac{158933}{165150720}$	(10,6,4)	$\frac{102007}{495452160}$

continued on next page . . .

. . . continued from previous page

(n,k,l)	$a_{n,k,l}$	(n,k,l)	$a_{n,k,l}$	(n,k,l)	$a_{n,k,l}$	(n,k,l)	$a_{n,k,l}$	(n,k,l)	$a_{n,k,l}$
(5,2,1)	$\frac{-67}{3072}$	(7,2,3)	$\frac{1009}{122880}$	(8,6,2)	$\frac{33017}{41287680}$	(10,0,0)	$\frac{-339691}{5945425920}$	(10,8,0)	$\frac{1374211}{1981808640}$
(5,2,2)	$\frac{1}{512}$	(7,2,4)	$\frac{113}{147456}$	(8,8,0)	$\frac{9623}{13762560}$	(10,0,1)	$\frac{-22843}{1486356480}$	(10,8,1)	$\frac{97039}{70778880}$
(5,2,3)	$\frac{-1}{384}$	(7,2,5)	$\frac{-199}{368640}$	(9,0,0)	$\frac{3737}{74317824}$	(10,0,2)	$\frac{15205963}{5945425920}$	(10,8,2)	$\frac{1754671}{5945425920}$
(5,4,0)	$\frac{23}{3072}$	(7,4,0)	$\frac{-11}{9216}$	(9,0,1)	$\frac{-34337}{23592960}$	(10,0,3)	$\frac{-311903}{82575360}$	(10,10,0)	$\frac{-4776949}{29727129600}$
(5,4,1)	$\frac{7}{6144}$	(7,4,1)	$\frac{571}{98304}$	(9,0,2)	$\frac{14125}{4128768}$	(10,0,4)	$\frac{9659}{3932160}$		
(6,0,0)	$\frac{-133}{122880}$	(7,4,2)	$\frac{-857}{368640}$	(9,0,3)	$\frac{-1249}{35389440}$	(10,0,5)	$\frac{-1177787}{825753600}$		

Table A.2.: Series coefficients $a_{n,k,l}$ of the high temperature expansion of the magnetic specific heat $C = \sum_{n,k,l} a_{n,k,l} \delta^k \alpha^l (\beta J_{\perp})^n$ for the dimerized, frustrated chain. Only nonzero coefficients are presented.

(n,k,l)	$a_{n,k,l}$	(n,k,l)	$a_{n,k,l}$	(n,k,l)	$a_{n,k,l}$	(n,k,l)	$a_{n,k,l}$	(n,k,l)	$a_{n,k,l}$
(2,0,0)	$\frac{3}{16}$	(6,0,6)	$\frac{21}{4096}$	(8,0,1)	$\frac{-4793}{61440}$	(9,0,7)	$\frac{-2229}{573440}$	(10,0,8)	$\frac{38993}{1572864}$
(2,0,2)	$\frac{3}{16}$	(6,2,0)	$\frac{-177}{4096}$	(8,0,2)	$\frac{2323}{24576}$	(9,0,9)	$\frac{-4303}{688128}$	(10,0,10)	$\frac{-334433}{110100480}$
(2,2,0)	$\frac{3}{16}$	(6,2,1)	$\frac{15}{128}$	(8,0,3)	$\frac{-59}{960}$	(9,2,0)	$\frac{-1401}{286720}$	(10,2,0)	$\frac{-240061}{22020096}$
(3,0,0)	$\frac{3}{32}$	(6,2,2)	$\frac{303}{2048}$	(8,0,4)	$\frac{35}{2048}$	(9,2,1)	$\frac{-7821}{143360}$	(10,2,1)	$\frac{6463}{172032}$
(3,0,1)	$\frac{-9}{32}$	(6,2,3)	$\frac{-45}{512}$	(8,0,5)	$\frac{-407}{61440}$	(9,2,2)	$\frac{-6261}{286720}$	(10,2,2)	$\frac{6235}{393216}$
(3,0,3)	$\frac{3}{32}$	(6,2,4)	$\frac{-69}{1024}$	(8,0,6)	$\frac{-2449}{40960}$	(9,2,3)	$\frac{1359}{35840}$	(10,2,3)	$\frac{38011}{393216}$
(3,2,0)	$\frac{9}{32}$	(6,4,0)	$\frac{-333}{4096}$	(8,0,8)	$\frac{1417}{327680}$	(9,2,4)	$\frac{-111}{896}$	(10,2,4)	$\frac{116115}{1835008}$
(3,2,1)	$\frac{9}{32}$	(6,4,1)	$\frac{-123}{512}$	(8,2,0)	$\frac{2199}{81920}$	(9,2,5)	$\frac{-26673}{286720}$	(10,2,5)	$\frac{-14075}{688128}$
(4,0,0)	$\frac{-15}{256}$	(6,4,2)	$\frac{-579}{4096}$	(8,2,1)	$\frac{-1999}{20480}$	(9,2,6)	$\frac{-27}{143360}$	(10,2,6)	$\frac{3069}{57344}$
(4,0,1)	$\frac{-3}{32}$	(6,6,0)	$\frac{73}{4096}$	(8,2,2)	$\frac{-1347}{40960}$	(9,2,7)	$\frac{-11103}{573440}$	(10,2,7)	$\frac{-53813}{2752512}$
(4,0,2)	$\frac{-3}{32}$	(7,0,0)	$\frac{917}{40960}$	(8,2,3)	$\frac{-41}{1280}$	(9,4,0)	$\frac{3177}{573440}$	(10,2,8)	$\frac{-324557}{11010048}$
(4,0,4)	$\frac{-15}{256}$	(7,0,1)	$\frac{-2611}{40960}$	(8,2,4)	$\frac{-259}{2048}$	(9,4,1)	$\frac{-5913}{286720}$	(10,4,0)	$\frac{-133325}{11010048}$
(4,2,0)	$\frac{3}{128}$	(7,0,2)	$\frac{-119}{4096}$	(8,2,5)	$\frac{2951}{61440}$	(9,4,2)	$\frac{-7923}{57344}$	(10,4,1)	$\frac{-981}{458752}$
(4,2,1)	$\frac{3}{32}$	(7,0,3)	$\frac{-413}{4096}$	(8,2,6)	$\frac{6943}{122880}$	(9,4,3)	$\frac{-4311}{71680}$	(10,4,2)	$\frac{-276889}{5505024}$
(4,4,0)	$\frac{-15}{256}$	(7,0,4)	$\frac{651}{20480}$	(8,4,0)	$\frac{5803}{163840}$	(9,4,4)	$\frac{21597}{286720}$	(10,4,3)	$\frac{-297061}{2752512}$
(5,0,0)	$\frac{-15}{256}$	(7,0,5)	$\frac{-245}{8192}$	(8,4,1)	$\frac{59}{4096}$	(9,4,5)	$\frac{537}{81920}$	(10,4,4)	$\frac{5375}{688128}$
(5,0,1)	$\frac{25}{128}$	(7,0,7)	$\frac{917}{40960}$	(8,4,2)	$\frac{-1369}{40960}$	(9,6,0)	$\frac{3531}{286720}$	(10,4,5)	$\frac{-83087}{1376256}$

continued on next page. . .

. . . continued from previous page

(n,k,l)	$a_{n,k,l}$	(n,k,l)	$a_{n,k,l}$	(n,k,l)	$a_{n,k,l}$	(n,k,l)	$a_{n,k,l}$	(n,k,l)	$a_{n,k,l}$
(5,0,2)	$\frac{-5}{128}$	(7,2,0)	$\frac{1393}{40960}$	(8,4,3)	$\frac{571}{3840}$	(9,6,1)	$\frac{14211}{143360}$	(10,4,6)	$\frac{-9087}{131072}$
(5,0,3)	$\frac{15}{128}$	(7,2,1)	$\frac{1281}{40960}$	(8,4,4)	$\frac{1287}{10240}$	(9,6,2)	$\frac{40137}{286720}$	(10,6,0)	$\frac{-33811}{3670016}$
(5,0,5)	$\frac{-15}{256}$	(7,2,2)	$\frac{1491}{10240}$	(8,6,0)	$\frac{11221}{245760}$	(9,6,3)	$\frac{1131}{35840}$	(10,6,1)	$\frac{621}{114688}$
(5,2,0)	$\frac{-15}{128}$	(7,2,3)	$\frac{651}{10240}$	(8,6,1)	$\frac{1981}{12288}$	(9,8,0)	$\frac{-18369}{1146880}$	(10,6,2)	$\frac{51407}{917504}$
(5,2,2)	$\frac{-15}{128}$	(7,2,4)	$\frac{637}{20480}$	(8,6,2)	$\frac{4679}{40960}$	(9,8,1)	$\frac{-16347}{573440}$	(10,6,3)	$\frac{-35787}{917504}$
(5,2,3)	$\frac{-25}{128}$	(7,2,5)	$\frac{3297}{40960}$	(8,8,0)	$\frac{-4997}{983040}$	(10,0,0)	$\frac{-334433}{110100480}$	(10,6,4)	$\frac{-125561}{1835008}$
(5,4,0)	$\frac{-35}{256}$	(7,4,0)	$\frac{623}{40960}$	(9,0,0)	$\frac{-4303}{688128}$	(10,0,1)	$\frac{92629}{2752512}$	(10,8,0)	$\frac{-431449}{22020096}$
(5,4,1)	$\frac{-25}{128}$	(7,4,1)	$\frac{-2009}{40960}$	(9,0,1)	$\frac{2613}{573440}$	(10,0,2)	$\frac{-420475}{11010048}$	(10,8,1)	$\frac{-205055}{2752512}$
(6,0,0)	$\frac{21}{4096}$	(7,4,2)	$\frac{-819}{20480}$	(9,0,2)	$\frac{3855}{57344}$	(10,0,3)	$\frac{59305}{2752512}$	(10,8,2)	$\frac{-214825}{3670016}$
(6,0,1)	$\frac{63}{512}$	(7,4,3)	$\frac{1379}{20480}$	(9,0,3)	$\frac{1}{10240}$	(10,0,4)	$\frac{-138811}{2752512}$	(10,10,0)	$\frac{49649}{36700160}$
(6,0,2)	$\frac{-363}{4096}$	(7,6,0)	$\frac{399}{8192}$	(9,0,4)	$\frac{-261}{286720}$	(10,0,5)	$\frac{51701}{1376256}$		
(6,0,3)	$\frac{17}{512}$	(7,6,1)	$\frac{3339}{40960}$	(9,0,5)	$\frac{5901}{81920}$	(10,0,6)	$\frac{27641}{2752512}$		
(6,0,4)	$\frac{105}{1024}$	(8,0,0)	$\frac{1417}{327680}$	(9,0,6)	$\frac{-2411}{143360}$	(10,0,7)	$\frac{-1817}{917504}$		

A.2. Dimerized Chain

The coefficients for orders below β^{11} are listed in Tabs. A.1, and A.2.

Table A.3.: Series coefficients $a_{n,k}$ of the high temperature expansion of the magnetic susceptibility $\chi = \frac{1}{T} \sum_{n,k} a_{n,k} \delta^k (\beta J)^n$ for the dimerized chain. Only nonzero coefficients are presented from order β^{11} up to order β^{18} .

(n,k,l)	$a_{n,k,l}$	(n,k,l)	$a_{n,k,l}$	(n,k,l)	$a_{n,k,l}$	(n,k,l)	$a_{n,k,l}$
(11,0)	$\frac{-1428209}{54499737600}$	(13,6)	$\frac{16757}{19818086400}$	(15,8)	$\frac{1134039913}{173130802790400}$	(17,6)	$\frac{-804378832603}{228532659683328000}$
(11,2)	$\frac{-2683}{29030400}$	(13,8)	$\frac{-56220473}{3923981107200}$	(15,10)	$\frac{86433646963}{11426632984166400}$	(17,8)	$\frac{-1051886885537}{342798989524992000}$
(11,4)	$\frac{-674059}{7431782400}$	(13,10)	$\frac{-9467111}{71345111040}$	(15,12)	$\frac{125245014907}{1713994947624960}$	(17,10)	$\frac{-535584743809}{228532659683328000}$
(11,6)	$\frac{-56827}{1238630400}$	(13,12)	$\frac{2172449}{21799895040}$	(15,14)	$\frac{-104930723893}{3808877661388800}$	(17,12)	$\frac{344293742347}{228532659683328000}$
(11,8)	$\frac{98731}{707788800}$	(14,0)	$\frac{-358847}{3957275492352}$	(16,0)	$\frac{-258645079463}{498616712036352000}$	(17,14)	$\frac{-22234161820843}{68597979049984000}$
(11,10)	$\frac{-9539}{27525120}$	(14,2)	$\frac{361148659}{35876398694400}$	(16,2)	$\frac{-15175092143}{3767021862912000}$	(17,16)	$\frac{52097662147}{7031774144102400}$
(12,0)	$\frac{18710029}{2242274918400}$	(14,4)	$\frac{9492225643}{466393183027200}$	(16,4)	$\frac{-8706451935593}{1371195958099968000}$	(18,0)	$\frac{1116582102301823}{447558360723829552000}$
(12,2)	$\frac{-35760853}{2615987404800}$	(14,6)	$\frac{5394474767}{296795661926400}$	(16,6)	$\frac{-381013820701}{85699747381248000}$	(18,2)	$\frac{33268250832001}{27124749134777548800}$
(12,4)	$\frac{-59519537}{1046394961920}$	(14,8)	$\frac{7897101007}{652950456238080}$	(16,8)	$\frac{-6536122273267}{2742391916199936000}$	(18,4)	$\frac{301983779893}{208944145996185600}$
(12,6)	$\frac{-18989863}{35672555200}$	(14,10)	$\frac{-10743048697}{652950456238080}$	(16,10)	$\frac{176252096491}{342798989524992000}$	(18,6)	$\frac{30860378761391}{74593060120638259200}$
(12,8)	$\frac{-212653873}{5231974809600}$	(14,12)	$\frac{378600476623}{3264752281190400}$	(16,12)	$\frac{32635888627387}{1371195958099968000}$	(18,8)	$\frac{-182357607317269}{745930601206382592000}$
(12,10)	$\frac{-161307977}{523197480960}$	(14,14)	$\frac{-656281799}{76947023462400}$	(16,14)	$\frac{-150602416817}{3808877661388800}$	(18,10)	$\frac{-114706799537333}{248643533735460864000}$
(12,12)	$\frac{193615997}{5231974809600}$	(15,0)	$\frac{-65174099663}{28566582460416000}$	(16,16)	$\frac{10785364513867}{5484783832399872000}$	(18,12)	$\frac{-90442750894411}{74593060120638259200}$
(13,0)	$\frac{7045849}{809710387200}$	(15,2)	$\frac{-49949749}{11719623573504}$	(17,0)	$\frac{1228065600079}{2590036809744384000}$	(18,14)	$\frac{-169097404668739}{106561514485805465600}$
(13,2)	$\frac{2790083}{118908518400}$	(15,4)	$\frac{373889611}{357082280755200}$	(17,2)	$\frac{146506668199}{685597979049984000}$	(18,16)	$\frac{6285092004168191}{49728706747921728000}$
(13,4)	$\frac{9861031}{653996851200}$	(15,6)	$\frac{196672854197}{34279898952499200}$	(17,4)	$\frac{-134460640739}{62327089004544000}$	(18,18)	$\frac{-468309667465837}{1032826986285760512000}$

Table A.4.: Series coefficients $a_{n,k}$ of the high temperature expansion of the magnetic specific heat $C = \sum_{n,k} a_{n,k} \delta^k (\beta J)^n$ for the dimerized chain. Only nonzero coefficients are presented from order β^{11} up to order β^{18} .

(n,k)	$a_{n,k}$	(n,k)	$a_{n,k}$	(n,k)	$a_{n,k}$	(n,k)	$a_{n,k}$
(11,0)	$\frac{37543}{31457280}$	(13,6)	$\frac{63260587}{19818086400}$	(15,8)	$\frac{-3750596387}{5580773130240}$	(17,6)	$\frac{65018005163}{453437816832000}$
(11,2)	$\frac{-2943281}{1981808640}$	(13,8)	$\frac{168008737}{58133053440}$	(15,10)	$\frac{-28368692533}{51821464780800}$	(17,8)	$\frac{747694294049}{114266329841664000}$
(11,4)	$\frac{-1231703}{198180864}$	(13,10)	$\frac{2484478763}{435997900800}$	(15,12)	$\frac{-110329916941}{43530030415872}$	(17,10)	$\frac{-170193679963}{5713316492083200}$
(11,6)	$\frac{-2446939}{330301440}$	(13,12)	$\frac{-140182523}{96888422400}$	(15,14)	$\frac{5917497137}{14510010138624}$	(17,12)	$\frac{-221041384979}{1269625887129600}$

continued on next page. . .

. . . continued from previous page

(n,k)	$a_{n,k}$	(n,k)	$a_{n,k}$	(n,k)	$a_{n,k}$	(n,k)	$a_{n,k}$
(11,8)	$\frac{-4199591}{396361728}$	(14,0)	$\frac{-369233453}{930128855040}$	(16,0)	$\frac{851758334701}{8706006083174400}$	(17,14)	$\frac{28645978566427}{28566582460416000}$
(11,10)	$\frac{9792739}{1981808640}$	(14,2)	$\frac{-967322681}{1195879956480}$	(16,2)	$\frac{48804050567}{692523211161600}$	(17,16)	$\frac{-25549233744557}{228532659683328000}$
(12,0)	$\frac{3987607}{3170893824}$	(14,4)	$\frac{29175427}{1993133260800}$	(16,4)	$\frac{-448010792927}{1171962357350400}$	(18,0)	$\frac{-80067486241427}{4875363406577664000}$
(12,2)	$\frac{47342317}{13212057600}$	(14,6)	$\frac{5006543507}{5979399782400}$	(16,6)	$\frac{-577431395917}{846417258086400}$	(18,2)	$\frac{5145779287709}{108341409035059200}$
(12,4)	$\frac{70948027}{26424115200}$	(14,8)	$\frac{2068244921}{1993133260800}$	(16,8)	$\frac{-199750102373}{307788093849600}$	(18,4)	$\frac{8816140320217}{36934571261952000}$
(12,6)	$\frac{16985329}{19818086400}$	(14,10)	$\frac{1193462617}{664377753600}$	(16,10)	$\frac{-141175079351}{217650152079360}$	(18,6)	$\frac{129505647760939}{406280283881472000}$
(12,8)	$\frac{-238381}{1056964608}$	(14,12)	$\frac{-1410199439}{543581798400}$	(16,12)	$\frac{-6744074943121}{5078503548518400}$	(18,8)	$\frac{211128422793049}{812560567762944000}$
(12,10)	$\frac{2809583}{377487360}$	(14,14)	$\frac{3603293663}{41855798476800}$	(16,14)	$\frac{718080430229}{846417258086400}$	(18,10)	$\frac{19613319318773}{90284507529216000}$
(12,12)	$\frac{-40555}{117440512}$	(15,0)	$\frac{-31504270817}{362750253465600}$	(16,16)	$\frac{-1288308081349}{60942042582220800}$	(18,12)	$\frac{88360795513999}{406280283881472000}$
(13,0)	$\frac{-1925339}{41523609600}$	(15,2)	$\frac{-7632645211}{10364292956160}$	(17,0)	$\frac{184265505341}{3627502534656000}$	(18,14)	$\frac{5854118848751}{8291434364928000}$
(13,2)	$\frac{60223033}{39636172800}$	(15,4)	$\frac{-89314894561}{72550050693120}$	(17,2)	$\frac{501069785641}{1904438830694400}$	(18,16)	$\frac{-85986647608741}{325024227105177600}$
(13,4)	$\frac{2856603451}{871995801600}$	(15,6)	$\frac{-210219285347}{217650152079360}$	(17,4)	$\frac{1750455145427}{5193924083712000}$	(18,18)	$\frac{6827887220393}{1329644565430272000}$

A.3. Ladder with Cyclic Exchange

A.3.1. Pure 4-Spin Operator

Table A.5.: Series coefficients $a_{n,k,l}$ of the high temperature expansion of the magnetic susceptibility $\chi = \frac{1}{T} \sum_{n,k,l} a_{n,k,l} \chi_{\text{cyc}}^k \chi_{\text{cyc}}^l (\beta J_{\perp})^n$ for the ladder with cyclic exchange using the pure 4-spin operator as defined in eq. 1.55. Only nonzero coefficients are presented up to order β^{10} .

(n,k,l)	$a_{n,k,l}$	(n,k,l)	$a_{n,k,l}$	(n,k,l)	$a_{n,k,l}$	(n,k,l)	$a_{n,k,l}$
(0,0,0)	$\frac{1}{4}$	(6,3,1)	$\frac{383}{81920}$	(8,3,2)	$\frac{-6539}{5898240}$	(9,8,0)	$\frac{-361}{3440640}$
(1,0,0)	$\frac{-1}{16}$	(6,3,2)	$\frac{1919}{245760}$	(8,3,3)	$\frac{943027}{165150720}$	(9,8,1)	$\frac{-105959}{110100480}$
(1,1,0)	$\frac{-1}{8}$	(6,3,3)	$\frac{-5459}{491520}$	(8,3,4)	$\frac{-615847}{55050240}$	(9,9,0)	$\frac{3737}{74317824}$
(2,0,0)	$\frac{-1}{64}$	(6,4,0)	$\frac{-71}{61440}$	(8,3,5)	$\frac{26613359}{1321205760}$	(10,0,0)	$\frac{37873}{59454259200}$
(2,0,1)	$\frac{3}{64}$	(6,4,1)	$\frac{-79}{122880}$	(8,4,0)	$\frac{271}{4587520}$	(10,0,1)	$\frac{-222073}{3963617280}$
(2,0,2)	$\frac{-7}{128}$	(6,4,2)	$\frac{-239}{163840}$	(8,4,1)	$\frac{95821}{41287680}$	(10,0,2)	$\frac{-5201201}{792723456}$
(2,1,0)	$\frac{1}{16}$	(6,5,0)	$\frac{23}{15360}$	(8,4,2)	$\frac{-1312273}{165150720}$	(10,0,3)	$\frac{120721}{22020096}$
(2,1,1)	$\frac{3}{64}$	(6,5,1)	$\frac{231}{81920}$	(8,4,3)	$\frac{273829}{13762560}$	(10,0,4)	$\frac{-10476939}{1174405120}$
(3,0,0)	$\frac{1}{768}$	(6,6,0)	$\frac{-133}{122880}$	(8,4,4)	$\frac{-2644417}{132120576}$	(10,0,5)	$\frac{-594935779}{158544691200}$
(3,0,1)	$\frac{9}{256}$	(7,0,0)	$\frac{-823}{20643840}$	(8,5,0)	$\frac{-233}{1146880}$	(10,0,6)	$\frac{1350882611}{47563407360}$
(3,0,2)	$\frac{-23}{512}$	(7,0,1)	$\frac{147}{327680}$	(8,5,1)	$\frac{-56353}{82575360}$	(10,0,7)	$\frac{-544422823}{13589544960}$
(3,0,3)	$\frac{17}{512}$	(7,0,2)	$\frac{2513}{327680}$	(8,5,2)	$\frac{-37993}{8257536}$	(10,0,8)	$\frac{5622454921}{217432719360}$
(3,1,0)	$\frac{1}{128}$	(7,0,3)	$\frac{-9263}{393216}$	(8,5,3)	$\frac{5436317}{330301440}$	(10,0,9)	$\frac{-534001343}{56371445760}$
(3,1,1)	$\frac{-1}{64}$	(7,0,4)	$\frac{87053}{2621440}$	(8,6,0)	$\frac{4483}{10321920}$	(10,0,10)	$\frac{18833526053}{15220290355200}$
(3,2,0)	$\frac{-1}{64}$	(7,0,5)	$\frac{-49197}{2621440}$	(8,6,1)	$\frac{397}{2293760}$	(10,1,0)	$\frac{-20353}{2972712960}$
(3,2,1)	$\frac{3}{256}$	(7,0,6)	$\frac{193321}{47185920}$	(8,6,2)	$\frac{-147835}{33030144}$	(10,1,1)	$\frac{459167}{3963617280}$
(3,3,0)	$\frac{1}{96}$	(7,0,7)	$\frac{6199}{9437184}$	(8,7,0)	$\frac{-1271}{3440640}$	(10,1,2)	$\frac{856039}{990904320}$
(4,0,0)	$\frac{5}{3072}$	(7,1,0)	$\frac{377}{1474560}$	(8,7,1)	$\frac{3583}{5505024}$	(10,1,3)	$\frac{-19634801}{11890851840}$
(4,0,1)	$\frac{1}{512}$	(7,1,1)	$\frac{3}{10240}$	(8,8,0)	$\frac{1269}{4587520}$	(10,1,4)	$\frac{-7766669}{23781703680}$
(4,0,2)	$\frac{-55}{2048}$	(7,1,2)	$\frac{-4361}{983040}$	(9,0,0)	$\frac{11593}{2972712960}$	(10,1,5)	$\frac{-226360787}{95126814720}$
(4,0,3)	$\frac{89}{2048}$	(7,1,3)	$\frac{-8719}{2949120}$	(9,0,1)	$\frac{73}{917504}$	(10,1,6)	$\frac{462768779}{47563407360}$
(4,0,4)	$\frac{-75}{8192}$	(7,1,4)	$\frac{197191}{11796480}$	(9,0,2)	$\frac{-731629}{330301440}$	(10,1,7)	$\frac{-1130618981}{95126814720}$
(4,1,0)	$\frac{-1}{192}$	(7,1,5)	$\frac{-112939}{5898240}$	(9,0,3)	$\frac{112003}{47185920}$	(10,1,8)	$\frac{140947399}{19025362944}$
(4,1,1)	$\frac{-1}{64}$	(7,1,6)	$\frac{5287}{23592960}$	(9,0,4)	$\frac{1876243}{176160768}$	(10,1,9)	$\frac{-1566470397867495911}{622577612487697367040}$

continued on next page . . .

. . . continued from previous page

(n,k,l)	$a_{n,k,l}$	(n,k,l)	$a_{n,k,l}$	(n,k,l)	$a_{n,k,l}$	(n,k,l)	$a_{n,k,l}$
(4,1,2)	$\frac{1}{1024}$	(7,2,0)	$\frac{-43}{81920}$	(9,0,5)	$\frac{-1745333}{47185920}$	(10,2,0)	$\frac{3229}{123863040}$
(4,1,3)	$\frac{-73}{12288}$	(7,2,1)	$\frac{439}{327680}$	(9,0,6)	$\frac{728717183}{15854469120}$	(10,2,1)	$\frac{-309377}{990904320}$
(4,2,0)	$\frac{1}{256}$	(7,2,2)	$\frac{2509}{491520}$	(9,0,7)	$\frac{-22416883}{754974720}$	(10,2,2)	$\frac{-119887}{110100480}$
(4,2,2)	$\frac{139}{6144}$	(7,2,3)	$\frac{-20213}{1966080}$	(9,0,8)	$\frac{418303271}{42278584320}$	(10,2,3)	$\frac{37796869}{3963617280}$
(4,3,0)	$\frac{-1}{192}$	(7,2,4)	$\frac{10111}{393216}$	(9,0,9)	$\frac{-170984203}{126835752960}$	(10,2,4)	$\frac{-31116917}{1132462080}$
(4,3,1)	$\frac{-17}{1024}$	(7,2,5)	$\frac{21983}{23592960}$	(9,1,0)	$\frac{-4031}{165150720}$	(10,2,5)	$\frac{115216775}{3170893824}$
(4,4,0)	$\frac{5}{1536}$	(7,3,0)	$\frac{229}{368640}$	(9,1,1)	$\frac{-7219}{20643840}$	(10,2,6)	$\frac{-235085639}{7046430720}$
(5,0,0)	$\frac{13}{61440}$	(7,3,1)	$\frac{-11}{40960}$	(9,1,2)	$\frac{10247}{5505024}$	(10,2,7)	$\frac{168368671}{13589544960}$
(5,0,1)	$\frac{-15}{2048}$	(7,3,2)	$\frac{-607}{491520}$	(9,1,3)	$\frac{-31211}{41287680}$	(10,2,8)	$\frac{491092319363551663}{408566558195051397120}$
(5,0,2)	$\frac{17}{24576}$	(7,3,3)	$\frac{-235}{36864}$	(9,1,4)	$\frac{4725871}{1321205760}$	(10,3,0)	$\frac{-97}{2064384}$
(5,0,3)	$\frac{103}{8192}$	(7,3,4)	$\frac{-27391}{2949120}$	(9,1,5)	$\frac{-4300931}{330301440}$	(10,3,1)	$\frac{133949}{396361728}$
(5,0,4)	$\frac{-1997}{98304}$	(7,4,0)	$\frac{-179}{368640}$	(9,1,6)	$\frac{48046393}{2642411520}$	(10,3,2)	$\frac{-243883}{5945425920}$
(5,0,5)	$\frac{443}{98304}$	(7,4,1)	$\frac{17309}{2949120}$	(9,1,7)	$\frac{-1687363}{377487360}$	(10,3,3)	$\frac{24821399}{5945425920}$
(5,1,0)	$\frac{-11}{6144}$	(7,4,2)	$\frac{-14867}{5898240}$	(9,1,8)	$\frac{60880307}{21139292160}$	(10,3,4)	$\frac{-47475935}{2378170368}$
(5,1,1)	$\frac{13}{3072}$	(7,4,3)	$\frac{187}{9216}$	(9,2,0)	$\frac{251}{5160960}$	(10,3,5)	$\frac{5812786927}{190253629440}$
(5,1,2)	$\frac{23}{4096}$	(7,5,0)	$\frac{31}{61440}$	(9,2,1)	$\frac{43283}{82575360}$	(10,3,6)	$\frac{-1731259583}{63417876480}$
(5,1,3)	$\frac{-139}{12288}$	(7,5,1)	$\frac{-13}{15360}$	(9,2,2)	$\frac{-1983647}{330301440}$	(10,3,7)	$\frac{-49043139202699931}{12767704943595356160}$
(5,1,4)	$\frac{599}{49152}$	(7,5,2)	$\frac{-1559}{196608}$	(9,2,3)	$\frac{9195673}{660602880}$	(10,4,0)	$\frac{42727}{1486356480}$
(5,2,0)	$\frac{5}{1536}$	(7,6,0)	$\frac{67}{737280}$	(9,2,4)	$\frac{-371659}{15728640}$	(10,4,1)	$\frac{-2927431}{2972712960}$
(5,2,1)	$\frac{-3}{256}$	(7,6,1)	$\frac{5341}{983040}$	(9,2,5)	$\frac{18895367}{1321205760}$	(10,4,2)	$\frac{32280961}{11890851840}$
(5,2,2)	$\frac{395}{24576}$	(7,7,0)	$\frac{1}{16128}$	(9,2,6)	$\frac{-4260689}{301989888}$	(10,4,3)	$\frac{-66641}{82575360}$
(5,2,3)	$\frac{-1721}{49152}$	(8,0,0)	$\frac{25}{16515072}$	(9,2,7)	$\frac{2168765}{1409286144}$	(10,4,4)	$\frac{-216205225}{19025362944}$
(5,3,0)	$\frac{-1}{384}$	(8,0,1)	$\frac{3781}{6881280}$	(9,3,0)	$\frac{-4129}{61931520}$	(10,4,5)	$\frac{1515430003}{95126814720}$
(5,3,1)	$\frac{7}{6144}$	(8,0,2)	$\frac{-27373}{41287680}$	(9,3,1)	$\frac{-41327}{82575360}$	(10,4,6)	$\frac{47754059428979}{8866461766385664}$
(5,3,2)	$\frac{11}{768}$	(8,0,3)	$\frac{-305401}{27525120}$	(9,3,2)	$\frac{12269}{20643840}$	(10,5,0)	$\frac{-143369}{7431782400}$
(5,4,0)	$\frac{1}{1024}$	(8,0,4)	$\frac{22639489}{660602880}$	(9,3,3)	$\frac{3970003}{495452160}$	(10,5,1)	$\frac{42183}{73400320}$
(5,4,1)	$\frac{-47}{4096}$	(8,0,5)	$\frac{-14079311}{330301440}$	(9,3,4)	$\frac{-3863767}{220200960}$	(10,5,2)	$\frac{-62421}{165150720}$
(5,5,0)	$\frac{-7}{5120}$	(8,0,6)	$\frac{38583691}{1321205760}$	(9,3,5)	$\frac{90132691}{2642411520}$	(10,5,3)	$\frac{-11691713}{11890851840}$
(6,0,0)	$\frac{-77}{737280}$	(8,0,7)	$\frac{-3140731}{440401920}$	(9,3,6)	$\frac{-17539733}{2642411520}$	(10,5,4)	$\frac{-23339681}{3397386240}$
(6,0,1)	$\frac{-223}{81920}$	(8,0,8)	$\frac{1263251}{1174405120}$	(9,4,0)	$\frac{1739}{16515072}$	(10,5,5)	$\frac{-999565836841199}{62342309294899200}$

continued on next page . . .

. . . continued from previous page

(n,k,l)	$a_{n,k,l}$	(n,k,l)	$a_{n,k,l}$	(n,k,l)	$a_{n,k,l}$	(n,k,l)	$a_{n,k,l}$
(6,0,2)	$\frac{3457}{245760}$	(8,1,0)	$\frac{191}{10321920}$	(9,4,1)	$\frac{-80509}{82575360}$	(10,6,0)	$\frac{-25103}{396361728}$
(6,0,3)	$\frac{-4181}{245760}$	(8,1,1)	$\frac{-15727}{13762560}$	(9,4,2)	$\frac{-342589}{82575360}$	(10,6,1)	$\frac{-188311}{220200960}$
(6,0,4)	$\frac{957}{655360}$	(8,1,2)	$\frac{-2759}{5505024}$	(9,4,3)	$\frac{5300497}{660602880}$	(10,6,2)	$\frac{665629}{165150720}$
(6,0,5)	$\frac{2827}{1966080}$	(8,1,3)	$\frac{42103}{165150720}$	(9,4,4)	$\frac{-78941959}{2642411520}$	(10,6,3)	$\frac{-2809157}{594542592}$
(6,0,6)	$\frac{-8279}{2359296}$	(8,1,4)	$\frac{874613}{82575360}$	(9,4,5)	$\frac{48105823}{5284823040}$	(10,6,4)	$\frac{5022615765967}{389639433093120}$
(6,1,0)	$\frac{17}{61440}$	(8,1,5)	$\frac{-1295099}{66060288}$	(9,5,0)	$\frac{-15637}{82575360}$	(10,7,0)	$\frac{18131}{212336640}$
(6,1,1)	$\frac{457}{81920}$	(8,1,6)	$\frac{6903373}{660602880}$	(9,5,1)	$\frac{101117}{165150720}$	(10,7,1)	$\frac{-4287079}{11890851840}$
(6,1,2)	$\frac{-47}{40960}$	(8,1,7)	$\frac{62327}{587202560}$	(9,5,2)	$\frac{-411179}{330301440}$	(10,7,2)	$\frac{12944777}{11890851840}$
(6,1,3)	$\frac{-2153}{245760}$	(8,2,0)	$\frac{-463}{4128768}$	(9,5,3)	$\frac{311}{24576}$	(10,7,3)	$\frac{-123633817411}{12176232284160}$
(6,1,4)	$\frac{8899}{491520}$	(8,2,1)	$\frac{2081}{917504}$	(9,5,4)	$\frac{-997141}{188743680}$	(10,8,0)	$\frac{-416443}{2972712960}$
(6,1,5)	$\frac{-17561}{1966080}$	(8,2,2)	$\frac{-21659}{3932160}$	(9,6,0)	$\frac{13219}{123863040}$	(10,8,1)	$\frac{275143}{2972712960}$
(6,2,0)	$\frac{-1}{30720}$	(8,2,3)	$\frac{70209}{9175040}$	(9,6,1)	$\frac{-861709}{330301440}$	(10,8,2)	$\frac{390790361}{126835752960}$
(6,2,1)	$\frac{-749}{122880}$	(8,2,4)	$\frac{170095}{33030144}$	(9,6,2)	$\frac{-1008967}{660602880}$	(10,9,0)	$\frac{22433}{297271296}$
(6,2,2)	$\frac{1147}{81920}$	(8,2,5)	$\frac{47983}{23592960}$	(9,6,3)	$\frac{-5001313}{1321205760}$	(10,9,1)	$\frac{-599785}{792723456}$
(6,2,3)	$\frac{-2209}{61440}$	(8,2,6)	$\frac{-1647739}{528482304}$	(9,7,0)	$\frac{-125}{2064384}$	(10,10,0)	$\frac{-339691}{5945425920}$
(6,2,4)	$\frac{6311}{491520}$	(8,3,0)	$\frac{167}{1032192}$	(9,7,1)	$\frac{86179}{165150720}$		
(6,3,0)	$\frac{1}{5760}$	(8,3,1)	$\frac{-74653}{41287680}$	(9,7,2)	$\frac{4315}{3145728}$		

Table A.6.: Series coefficients $a_{n,k,l}$ of the high temperature expansion of the specific heat $C = \sum_{n,k,l} a_{n,k,l} x^k x_{\text{cyc}}^l (\beta J_{\perp})^n$ for the ladder with cyclic exchange using the pure 4-spin operator as defined in eq. 1.55. Only nonzero coefficients are presented up to order β^{10} .

(n,k,l)	$a_{n,k,l}$	(n,k,l)	$a_{n,k,l}$	(n,k,l)	$a_{n,k,l}$	(n,k,l)	$a_{n,k,l}$
(2,0,0)	$\frac{3}{32}$	(6,5,1)	$\frac{225}{1024}$	(8,4,1)	$\frac{-595}{12288}$	(10,0,0)	$\frac{-11593}{220200960}$
(2,0,2)	$\frac{21}{128}$	(6,6,0)	$\frac{21}{4096}$	(8,4,2)	$\frac{28739}{491520}$	(10,0,1)	$\frac{-1095}{917504}$
(2,2,0)	$\frac{3}{16}$	(7,0,0)	$\frac{77}{81920}$	(8,4,3)	$\frac{163693}{491520}$	(10,0,2)	$\frac{6592249}{176160768}$
(3,0,0)	$\frac{3}{64}$	(7,0,1)	$\frac{4683}{163840}$	(8,4,4)	$\frac{1167533}{3932160}$	(10,0,3)	$\frac{-947129}{22020096}$
(3,0,1)	$\frac{-27}{128}$	(7,0,2)	$\frac{-1813}{10240}$	(8,5,0)	$\frac{53}{10240}$	(10,0,4)	$\frac{-89241263}{352321536}$
(3,0,2)	$\frac{45}{128}$	(7,0,3)	$\frac{15631}{65536}$	(8,5,1)	$\frac{-1207}{12288}$	(10,0,5)	$\frac{4210853}{4194304}$
(3,0,3)	$\frac{-9}{128}$	(7,0,4)	$\frac{12187}{655360}$	(8,5,2)	$\frac{4373}{81920}$	(10,0,6)	$\frac{-2138777213}{1409286144}$

continued on next page. . .

. . . continued from previous page

(n,k,l)	$a_{n,k,l}$	(n,k,l)	$a_{n,k,l}$	(n,k,l)	$a_{n,k,l}$	(n,k,l)	$a_{n,k,l}$
(3,1,2)	$\frac{45}{128}$	(7,0,5)	$\frac{-236439}{1310720}$	(8,5,3)	$\frac{-124507}{327680}$	(10,0,7)	$\frac{150822989}{117440512}$
(3,2,1)	$\frac{-27}{128}$	(7,0,6)	$\frac{62545}{262144}$	(8,6,0)	$\frac{-101}{122880}$	(10,0,8)	$\frac{-1164141973}{1879048192}$
(3,3,0)	$\frac{3}{32}$	(7,0,7)	$\frac{-29183}{655360}$	(8,6,1)	$\frac{-37}{12288}$	(10,0,9)	$\frac{53167375}{352321536}$
(4,0,0)	$\frac{-3}{512}$	(7,1,1)	$\frac{133}{5120}$	(8,6,2)	$\frac{46649}{327680}$	(10,0,10)	$\frac{-609596261}{37580963840}$
(4,0,1)	$\frac{-27}{128}$	(7,1,2)	$\frac{-6937}{163840}$	(8,7,1)	$\frac{-1897}{16384}$	(10,1,1)	$\frac{-1969}{786432}$
(4,0,2)	$\frac{195}{512}$	(7,1,3)	$\frac{11347}{81920}$	(8,8,0)	$\frac{1417}{327680}$	(10,1,2)	$\frac{160927}{11010048}$
(4,0,3)	$\frac{-15}{32}$	(7,1,4)	$\frac{27867}{327680}$	(9,0,0)	$\frac{-25}{1376256}$	(10,1,3)	$\frac{2072929}{22020096}$
(4,0,4)	$\frac{687}{8192}$	(7,1,5)	$\frac{16919}{81920}$	(9,0,1)	$\frac{-34029}{4587520}$	(10,1,4)	$\frac{-8829221}{14680064}$
(4,1,1)	$\frac{-3}{32}$	(7,1,6)	$\frac{18165}{131072}$	(9,0,2)	$\frac{22989}{2293760}$	(10,1,5)	$\frac{78431033}{58720256}$
(4,1,2)	$\frac{51}{128}$	(7,2,0)	$\frac{49}{20480}$	(9,0,3)	$\frac{134079}{655360}$	(10,1,6)	$\frac{-1329005}{786432}$
(4,1,3)	$\frac{-105}{512}$	(7,2,1)	$\frac{5369}{163840}$	(9,0,4)	$\frac{-2671551}{3670016}$	(10,1,7)	$\frac{93173795}{117440512}$
(4,2,0)	$\frac{-3}{128}$	(7,2,2)	$\frac{-21637}{81920}$	(9,0,5)	$\frac{40437777}{36700160}$	(10,1,8)	$\frac{-10757935}{25195824}$
(4,2,1)	$\frac{-3}{32}$	(7,2,3)	$\frac{16023}{32768}$	(9,0,6)	$\frac{-34368001}{36700160}$	(10,1,9)	$\frac{227886305}{5637144576}$
(4,2,2)	$\frac{15}{256}$	(7,2,4)	$\frac{-55909}{81920}$	(9,0,7)	$\frac{25496703}{73400320}$	(10,2,0)	$\frac{-6463}{22020096}$
(4,3,1)	$\frac{-27}{128}$	(7,2,5)	$\frac{297773}{1310720}$	(9,0,8)	$\frac{-4511205}{58720256}$	(10,2,1)	$\frac{-4453}{1376256}$
(4,4,0)	$\frac{-15}{256}$	(7,3,0)	$\frac{77}{40960}$	(9,0,9)	$\frac{-605197}{146800640}$	(10,2,2)	$\frac{47621}{524288}$
(5,0,0)	$\frac{-5}{512}$	(7,3,1)	$\frac{2373}{20480}$	(9,1,1)	$\frac{-873}{286720}$	(10,2,3)	$\frac{-478015}{1835008}$
(5,0,1)	$\frac{-15}{1024}$	(7,3,2)	$\frac{-25319}{81920}$	(9,1,2)	$\frac{-249861}{4587520}$	(10,2,4)	$\frac{1166805}{7340032}$
(5,0,2)	$\frac{285}{1024}$	(7,3,3)	$\frac{81879}{81920}$	(9,1,3)	$\frac{676539}{2293760}$	(10,2,5)	$\frac{5444555}{29360128}$
(5,0,3)	$\frac{-1215}{2048}$	(7,3,4)	$\frac{-111097}{655360}$	(9,1,4)	$\frac{-8441883}{9175040}$	(10,2,6)	$\frac{-151700371}{352321536}$
(5,0,4)	$\frac{1325}{4096}$	(7,4,0)	$\frac{161}{20480}$	(9,1,5)	$\frac{4870461}{4587520}$	(10,2,7)	$\frac{-66831817}{352321536}$
(5,0,5)	$\frac{-265}{2048}$	(7,4,1)	$\frac{-119}{5120}$	(9,1,6)	$\frac{-28715067}{36700160}$	(10,2,8)	$\frac{-522790885}{2818572288}$
(5,1,1)	$\frac{-5}{64}$	(7,4,2)	$\frac{-25557}{163840}$	(9,1,7)	$\frac{488319}{9175040}$	(10,3,0)	$\frac{-1235}{5505024}$
(5,1,2)	$\frac{225}{1024}$	(7,4,3)	$\frac{228781}{655360}$	(9,1,8)	$\frac{-803055}{14680064}$	(10,3,1)	$\frac{-149273}{11010048}$
(5,1,3)	$\frac{-155}{256}$	(7,5,0)	$\frac{259}{20480}$	(9,2,0)	$\frac{423}{1146880}$	(10,3,2)	$\frac{836749}{5505024}$
(5,1,4)	$\frac{-25}{256}$	(7,5,1)	$\frac{861}{10240}$	(9,2,1)	$\frac{-53757}{2293760}$	(10,3,3)	$\frac{-5490767}{14680064}$
(5,2,0)	$\frac{-5}{256}$	(7,5,2)	$\frac{-371}{20480}$	(9,2,2)	$\frac{55569}{573440}$	(10,3,4)	$\frac{25421351}{44040192}$
(5,2,1)	$\frac{15}{128}$	(7,6,1)	$\frac{4179}{163840}$	(9,2,3)	$\frac{22707}{1835008}$	(10,3,5)	$\frac{-2248381}{3670016}$
(5,2,2)	$\frac{-15}{256}$	(7,7,0)	$\frac{917}{40960}$	(9,2,4)	$\frac{-3872079}{9175040}$	(10,3,6)	$\frac{50003147}{88080384}$
(5,2,3)	$\frac{265}{4096}$	(8,0,0)	$\frac{823}{1966080}$	(9,2,5)	$\frac{7991037}{9175040}$	(10,3,7)	$\frac{-37153187}{1409286144}$

continued on next page . . .

. . . continued from previous page

(n,k,l)	$a_{n,k,l}$	(n,k,l)	$a_{n,k,l}$	(n,k,l)	$a_{n,k,l}$	(n,k,l)	$a_{n,k,l}$
(5,3,0)	$-\frac{5}{256}$	(8,0,1)	$-\frac{441}{81920}$	(9,2,6)	$-\frac{1638201}{18350080}$	(10,4,0)	$-\frac{16435}{22020096}$
(5,3,1)	$-\frac{5}{64}$	(8,0,2)	$-\frac{10627}{98304}$	(9,2,7)	$-\frac{4324581}{293601280}$	(10,4,1)	$\frac{12845}{1572864}$
(5,3,2)	$-\frac{305}{1024}$	(8,0,3)	$\frac{999}{2560}$	(9,3,0)	$\frac{169}{1146880}$	(10,4,2)	$\frac{808649}{12582912}$
(5,4,1)	$\frac{105}{1024}$	(8,0,4)	$-\frac{5997587}{7864320}$	(9,3,1)	$-\frac{19689}{573440}$	(10,4,3)	$-\frac{1546407}{3670016}$
(5,5,0)	$-\frac{15}{256}$	(8,0,5)	$\frac{826373}{1966080}$	(9,3,2)	$\frac{70137}{4587520}$	(10,4,4)	$\frac{8881069}{14680064}$
(6,0,0)	$-\frac{13}{8192}$	(8,0,6)	$-\frac{197173}{2621440}$	(9,3,3)	$-\frac{13969}{573440}$	(10,4,5)	$-\frac{46675063}{29360128}$
(6,0,1)	$\frac{135}{2048}$	(8,0,7)	$-\frac{4395}{65536}$	(9,3,4)	$-\frac{3793533}{9175040}$	(10,4,6)	$\frac{256984747}{2818572288}$
(6,0,2)	$-\frac{63}{32768}$	(8,0,8)	$\frac{4452593}{167772160}$	(9,3,5)	$-\frac{250245}{917504}$	(10,5,0)	$-\frac{3721}{2752512}$
(6,0,3)	$-\frac{1731}{8192}$	(8,1,1)	$\frac{169}{20480}$	(9,3,6)	$\frac{1179963}{9175040}$	(10,5,1)	$-\frac{1757}{393216}$
(6,0,4)	$\frac{32067}{65536}$	(8,1,2)	$-\frac{9267}{81920}$	(9,4,0)	$-\frac{1773}{1146880}$	(10,5,2)	$\frac{2640349}{11010048}$
(6,0,5)	$-\frac{75}{256}$	(8,1,3)	$\frac{71147}{196608}$	(9,4,1)	$-\frac{89673}{4587520}$	(10,5,3)	$-\frac{24109823}{44040192}$
(6,0,6)	$\frac{22919}{262144}$	(8,1,4)	$-\frac{30043}{61440}$	(9,4,2)	$\frac{276753}{2293760}$	(10,5,4)	$\frac{90623959}{88080384}$
(6,1,1)	$\frac{3}{1024}$	(8,1,5)	$\frac{575971}{983040}$	(9,4,3)	$-\frac{12165}{65536}$	(10,5,5)	$-\frac{63131911}{176160768}$
(6,1,2)	$\frac{51}{512}$	(8,1,6)	$\frac{13819}{163840}$	(9,4,4)	$\frac{513573}{1310720}$	(10,6,0)	$-\frac{7937}{22020096}$
(6,1,3)	$-\frac{3141}{8192}$	(8,1,7)	$-\frac{13087}{1572864}$	(9,4,5)	$-\frac{24790869}{36700160}$	(10,6,1)	$-\frac{1883}{786432}$
(6,1,4)	$\frac{9}{512}$	(8,2,0)	$\frac{547}{245760}$	(9,5,0)	$-\frac{207}{229376}$	(10,6,2)	$\frac{2878133}{44040192}$
(6,1,5)	$-\frac{2925}{65536}$	(8,2,1)	$-\frac{233}{8192}$	(9,5,1)	$-\frac{25353}{286720}$	(10,6,3)	$-\frac{1247645}{2097152}$
(6,2,0)	$-\frac{21}{4096}$	(8,2,2)	$-\frac{5953}{81920}$	(9,5,2)	$\frac{39843}{163840}$	(10,6,4)	$\frac{18698327}{88080384}$
(6,2,1)	$\frac{279}{2048}$	(8,2,3)	$\frac{96757}{245760}$	(9,5,3)	$-\frac{220719}{327680}$	(10,7,0)	$-\frac{463}{172032}$
(6,2,2)	$-\frac{2103}{8192}$	(8,2,4)	$-\frac{281213}{393216}$	(9,5,4)	$\frac{1938039}{3670016}$	(10,7,1)	$\frac{255877}{5505024}$
(6,2,3)	$\frac{567}{2048}$	(8,2,5)	$\frac{156475}{196608}$	(9,6,0)	$-\frac{1219}{573440}$	(10,7,2)	$\frac{61567}{917504}$
(6,2,4)	$-\frac{5691}{16384}$	(8,2,6)	$\frac{304787}{2621440}$	(9,6,1)	$-\frac{25773}{1146880}$	(10,7,3)	$-\frac{500489}{44040192}$
(6,3,0)	$-\frac{7}{1024}$	(8,3,0)	$\frac{53}{30720}$	(9,6,2)	$\frac{12795}{114688}$	(10,8,0)	$-\frac{8601}{7340032}$
(6,3,1)	$\frac{141}{1024}$	(8,3,1)	$\frac{337}{245760}$	(9,6,3)	$-\frac{4816377}{9175040}$	(10,8,1)	$-\frac{79721}{5505024}$
(6,3,2)	$-\frac{657}{2048}$	(8,3,2)	$-\frac{14021}{61440}$	(9,7,0)	$-\frac{3333}{573440}$	(10,8,2)	$\frac{1439927}{176160768}$
(6,3,3)	$\frac{9285}{16384}$	(8,3,3)	$\frac{289231}{491520}$	(9,7,1)	$-\frac{13707}{286720}$	(10,9,1)	$\frac{135753}{3670016}$
(6,4,0)	$\frac{9}{1024}$	(8,3,4)	$-\frac{1813}{3072}$	(9,7,2)	$\frac{304827}{2293760}$	(10,10,0)	$-\frac{334433}{110100480}$
(6,4,1)	$\frac{57}{1024}$	(8,3,5)	$-\frac{174227}{1966080}$	(9,8,1)	$-\frac{49941}{917504}$		
(6,4,2)	$-\frac{8523}{32768}$	(8,4,0)	$\frac{167}{163840}$	(9,9,0)	$-\frac{4303}{688128}$		

A.3.2. Permutation Operator

Table A.7.: Series coefficients $a_{n,k,l}$ of the high temperature expansion of the magnetic susceptibility $\chi = \frac{1}{T} \sum_{n,k,l} a_{n,k,l} \chi_{\text{cyc}}^k (\beta J_{\perp})^n$ for the ladder with cyclic exchange using the permutation operator as defined in Eq. 1.56. Only nonzero coefficients are presented up to order β^8 .

(n,k,l)	$a_{n,k,l}$	(n,k,l)	$a_{n,k,l}$	(n,k,l)	$a_{n,k,l}$	(n,k,l)	$a_{n,k,l}$	(n,k,l)	$a_{n,k,l}$
(0,0,0)	$\frac{1}{4}$	(4,4,0)	$\frac{5}{1536}$	(6,1,4)	$\frac{-319}{491520}$	(7,2,1)	$\frac{-5843}{983040}$	(8,1,4)	$\frac{19321}{11796480}$
(1,0,0)	$\frac{-1}{16}$	(5,0,0)	$\frac{13}{61440}$	(6,1,5)	$\frac{3853}{393216}$	(7,2,2)	$\frac{-2021}{92160}$	(8,1,5)	$\frac{9968183}{330301440}$
(1,0,1)	$\frac{-3}{16}$	(5,0,1)	$\frac{-33}{4096}$	(6,2,0)	$\frac{-1}{30720}$	(7,2,3)	$\frac{-28109}{983040}$	(8,1,6)	$\frac{2007809}{165150720}$
(1,1,0)	$\frac{-1}{8}$	(5,0,2)	$\frac{-679}{24576}$	(6,2,1)	$\frac{-151}{24576}$	(7,2,4)	$\frac{-5537}{327680}$	(8,1,7)	$\frac{-13836643}{1761607680}$
(2,0,0)	$\frac{-1}{64}$	(5,0,3)	$\frac{5}{4096}$	(6,2,2)	$\frac{-907}{30720}$	(7,2,5)	$\frac{-42217}{23592960}$	(8,2,0)	$\frac{-463}{4128768}$
(2,0,1)	$\frac{5}{64}$	(5,0,4)	$\frac{1387}{98304}$	(6,2,3)	$\frac{-2579}{49152}$	(7,3,0)	$\frac{229}{368640}$	(8,2,1)	$\frac{1327}{1720320}$
(2,0,2)	$\frac{11}{128}$	(5,0,5)	$\frac{-2413}{491520}$	(6,2,4)	$\frac{-12007}{491520}$	(7,3,1)	$\frac{743}{147456}$	(8,2,2)	$\frac{1039981}{82575360}$
(2,1,0)	$\frac{1}{16}$	(5,1,0)	$\frac{-11}{6144}$	(6,3,0)	$\frac{1}{5760}$	(7,3,2)	$\frac{1807}{163840}$	(8,2,3)	$\frac{4750559}{82575360}$
(2,1,1)	$\frac{7}{64}$	(5,1,1)	$\frac{1}{1536}$	(6,3,1)	$\frac{649}{245760}$	(7,3,3)	$\frac{12421}{737280}$	(8,2,4)	$\frac{1712181}{18350080}$
(3,0,0)	$\frac{1}{768}$	(5,1,2)	$\frac{241}{4096}$	(6,3,2)	$\frac{-53}{81920}$	(7,3,4)	$\frac{126659}{5898240}$	(8,2,5)	$\frac{357549}{5242880}$
(3,0,1)	$\frac{3}{64}$	(5,1,3)	$\frac{517}{6144}$	(6,3,3)	$\frac{-179}{36864}$	(7,4,0)	$\frac{-179}{368640}$	(8,2,6)	$\frac{4872211}{293601280}$
(3,0,2)	$\frac{1}{512}$	(5,1,4)	$\frac{373}{16384}$	(6,4,0)	$\frac{-71}{61440}$	(7,4,1)	$\frac{-5989}{2949120}$	(8,3,0)	$\frac{167}{1032192}$
(3,0,3)	$\frac{3}{512}$	(5,2,0)	$\frac{5}{1536}$	(6,4,1)	$\frac{139}{40960}$	(7,4,2)	$\frac{-11197}{1966080}$	(8,3,1)	$\frac{-167}{4587520}$
(3,1,0)	$\frac{1}{128}$	(5,2,1)	$\frac{15}{1024}$	(6,4,2)	$\frac{533}{491520}$	(7,4,3)	$\frac{197}{2949120}$	(8,3,2)	$\frac{-5489}{10321920}$
(3,1,1)	$\frac{-7}{128}$	(5,2,2)	$\frac{887}{24576}$	(6,5,0)	$\frac{23}{15360}$	(7,5,0)	$\frac{31}{61440}$	(8,3,3)	$\frac{22921}{82575360}$
(3,1,2)	$\frac{-11}{256}$	(5,2,3)	$\frac{677}{49152}$	(6,5,1)	$\frac{-293}{245760}$	(7,5,1)	$\frac{1757}{737280}$	(8,3,4)	$\frac{37293}{9175040}$
(3,2,0)	$\frac{-1}{64}$	(5,3,0)	$\frac{-1}{384}$	(6,6,0)	$\frac{-133}{122880}$	(7,5,2)	$\frac{551}{184320}$	(8,3,5)	$\frac{1182217}{440401920}$
(3,2,1)	$\frac{-5}{256}$	(5,3,1)	$\frac{-7}{2048}$	(7,0,0)	$\frac{-823}{20643840}$	(7,6,0)	$\frac{67}{737280}$	(8,4,0)	$\frac{271}{4587520}$
(3,3,0)	$\frac{1}{96}$	(5,3,2)	$\frac{-25}{2048}$	(7,0,1)	$\frac{209}{491520}$	(7,6,1)	$\frac{-833}{589824}$	(8,4,1)	$\frac{-2869}{41287680}$
(4,0,0)	$\frac{5}{3072}$	(5,4,0)	$\frac{1}{1024}$	(7,0,2)	$\frac{3901}{327680}$	(7,7,0)	$\frac{1}{16128}$	(8,4,2)	$\frac{-384413}{165150720}$
(4,0,1)	$\frac{5}{1536}$	(5,4,1)	$\frac{29}{12288}$	(7,0,3)	$\frac{7277}{491520}$	(8,0,0)	$\frac{25}{16515072}$	(8,4,3)	$\frac{-399181}{82575360}$
(4,0,2)	$\frac{-105}{2048}$	(5,5,0)	$\frac{-7}{5120}$	(7,0,4)	$\frac{-301039}{23592960}$	(8,0,1)	$\frac{2395}{4128768}$	(8,4,4)	$\frac{-116389}{31457280}$
(4,0,3)	$\frac{-277}{6144}$	(6,0,0)	$\frac{-77}{737280}$	(7,0,5)	$\frac{-21031}{983040}$	(8,0,2)	$\frac{160679}{82575360}$	(8,5,0)	$\frac{-233}{1146880}$
(4,0,4)	$\frac{-379}{24576}$	(6,0,1)	$\frac{-151}{49152}$	(7,0,6)	$\frac{-300671}{47185920}$	(8,0,3)	$\frac{-1346833}{82575360}$	(8,5,1)	$\frac{-7389}{9175040}$
(4,1,0)	$\frac{-1}{192}$	(6,0,2)	$\frac{259}{30720}$	(7,0,7)	$\frac{512147}{110100480}$	(8,0,4)	$\frac{-2998131}{73400320}$	(8,5,2)	$\frac{949}{1966080}$

continued on next page. . .

. . . continued from previous page

(n,k,l)	$a_{n,k,l}$	(n,k,l)	$a_{n,k,l}$	(n,k,l)	$a_{n,k,l}$	(n,k,l)	$a_{n,k,l}$	(n,k,l)	$a_{n,k,l}$
(4,1,1)	$\frac{-25}{512}$	(6,0,3)	$\frac{3983}{92160}$	(7,1,0)	$\frac{377}{1474560}$	(8,0,5)	$\frac{-1139443}{36700160}$	(8,5,3)	$\frac{20609}{5242880}$
(4,1,2)	$\frac{-3}{64}$	(6,0,4)	$\frac{77567}{1966080}$	(7,1,1)	$\frac{481}{163840}$	(8,0,6)	$\frac{-3012551}{264241152}$	(8,6,0)	$\frac{4483}{10321920}$
(4,1,3)	$\frac{-341}{12288}$	(6,0,5)	$\frac{5425}{393216}$	(7,1,2)	$\frac{-6949}{491520}$	(8,0,7)	$\frac{-3367013}{1321205760}$	(8,6,1)	$\frac{-16937}{20643840}$
(4,2,0)	$\frac{1}{256}$	(6,0,6)	$\frac{32867}{11796480}$	(7,1,3)	$\frac{-36737}{491520}$	(8,0,8)	$\frac{-2069707}{10569646080}$	(8,6,2)	$\frac{-27599}{55050240}$
(4,2,1)	$\frac{3}{512}$	(6,1,0)	$\frac{17}{61440}$	(7,1,4)	$\frac{-1146997}{11796480}$	(8,1,0)	$\frac{191}{10321920}$	(8,7,0)	$\frac{-1271}{3440640}$
(4,2,2)	$\frac{31}{2048}$	(6,1,1)	$\frac{993}{81920}$	(7,1,5)	$\frac{-627061}{11796480}$	(8,1,1)	$\frac{-3547}{2293760}$	(8,7,1)	$\frac{2489}{16515072}$
(4,3,0)	$\frac{-1}{192}$	(6,1,2)	$\frac{5231}{122880}$	(7,1,6)	$\frac{-40261}{7864320}$	(8,1,2)	$\frac{-13243}{688128}$	(8,8,0)	$\frac{1269}{4587520}$
(4,3,1)	$\frac{5}{3072}$	(6,1,3)	$\frac{29}{1024}$	(7,2,0)	$\frac{-43}{81920}$	(8,1,3)	$\frac{-5753921}{165150720}$		

Table A.8.: Series coefficients $a_{n,k,l}$ of the high temperature expansion of the magnetic specific heat $C = \sum_{n,k,l} a_{n,k,l} x_{\text{cyc}}^k x_{\text{cyc}}^l (\beta J_{\perp})^n$ for the ladder with cyclic exchange using the permutation operator as defined in Eq. 1.56. Only nonzero coefficients are presented up to order β^8 .

(n,k,l)	$a_{n,k,l}$	(n,k,l)	$a_{n,k,l}$	(n,k,l)	$a_{n,k,l}$	(n,k,l)	$a_{n,k,l}$	(n,k,l)	$a_{n,k,l}$
(2,0,0)	$\frac{3}{32}$	(5,0,4)	$\frac{305}{4096}$	(6,2,3)	$\frac{-729}{4096}$	(7,2,5)	$\frac{77413}{1310720}$	(8,1,7)	$\frac{-166983}{262144}$
(2,0,1)	$\frac{3}{16}$	(5,0,5)	$\frac{-765}{8192}$	(6,2,4)	$\frac{687}{16384}$	(7,3,0)	$\frac{77}{40960}$	(8,2,0)	$\frac{547}{245760}$
(2,0,2)	$\frac{45}{128}$	(5,1,1)	$\frac{5}{32}$	(6,3,0)	$\frac{-7}{1024}$	(7,3,1)	$\frac{-161}{5120}$	(8,2,1)	$\frac{-45}{8192}$
(2,1,1)	$\frac{3}{16}$	(5,1,2)	$\frac{255}{512}$	(6,3,1)	$\frac{-9}{1024}$	(7,3,2)	$\frac{-14483}{81920}$	(8,2,2)	$\frac{8477}{491520}$
(2,2,0)	$\frac{3}{16}$	(5,1,3)	$\frac{355}{512}$	(6,3,2)	$\frac{483}{2048}$	(7,3,3)	$\frac{-2079}{10240}$	(8,2,3)	$\frac{20071}{81920}$
(3,0,0)	$\frac{3}{64}$	(5,1,4)	$\frac{2305}{4096}$	(6,3,3)	$\frac{3727}{8192}$	(7,3,4)	$\frac{-3717}{32768}$	(8,2,4)	$\frac{111709}{1966080}$
(3,0,1)	$\frac{-9}{128}$	(5,2,0)	$\frac{-5}{256}$	(6,4,0)	$\frac{9}{1024}$	(7,4,0)	$\frac{161}{20480}$	(8,2,5)	$\frac{133049}{245760}$
(3,0,2)	$\frac{-9}{128}$	(5,2,1)	$\frac{-15}{512}$	(6,4,1)	$\frac{105}{1024}$	(7,4,1)	$\frac{581}{20480}$	(8,2,6)	$\frac{11111}{131072}$
(3,0,3)	$\frac{9}{256}$	(5,2,2)	$\frac{-35}{256}$	(6,4,2)	$\frac{2733}{32768}$	(7,4,2)	$\frac{28329}{163840}$	(8,3,0)	$\frac{53}{30720}$
(3,1,1)	$\frac{-9}{32}$	(5,2,3)	$\frac{-835}{4096}$	(6,5,1)	$\frac{-237}{4096}$	(7,4,3)	$\frac{32109}{131072}$	(8,3,1)	$\frac{-593}{40960}$
(3,1,2)	$\frac{-45}{128}$	(5,3,0)	$\frac{-5}{256}$	(6,6,0)	$\frac{21}{4096}$	(7,5,0)	$\frac{259}{20480}$	(8,3,2)	$\frac{-3251}{40960}$
(3,2,1)	$\frac{27}{128}$	(5,3,1)	$\frac{15}{128}$	(7,0,0)	$\frac{77}{81920}$	(7,5,1)	$\frac{-245}{8192}$	(8,3,3)	$\frac{-129599}{491520}$
(3,3,0)	$\frac{3}{32}$	(5,3,2)	$\frac{5}{64}$	(7,0,1)	$\frac{5761}{163840}$	(7,5,2)	$\frac{-21}{1024}$	(8,3,4)	$\frac{-27117}{32768}$
(4,0,0)	$\frac{-3}{512}$	(5,4,1)	$\frac{-185}{1024}$	(7,0,2)	$\frac{161}{16384}$	(7,6,1)	$\frac{2289}{32768}$	(8,3,5)	$\frac{-298457}{327680}$
(4,0,1)	$\frac{-15}{64}$	(5,5,0)	$\frac{-15}{256}$	(7,0,3)	$\frac{-26691}{81920}$	(7,7,0)	$\frac{917}{40960}$	(8,4,0)	$\frac{167}{163840}$

continued on next page. . .

. . . continued from previous page

(n,k,l)	$a_{n,k,l}$	(n,k,l)	$a_{n,k,l}$	(n,k,l)	$a_{n,k,l}$	(n,k,l)	$a_{n,k,l}$	(n,k,l)	$a_{n,k,l}$
(4,0,2)	$\frac{-165}{512}$	(6,0,0)	$\frac{-13}{8192}$	(7,0,4)	$\frac{-72597}{131072}$	(8,0,0)	$\frac{823}{1966080}$	(8,4,1)	$\frac{-6659}{122880}$
(4,0,3)	$\frac{-75}{256}$	(6,0,1)	$\frac{231}{4096}$	(7,0,5)	$\frac{-481453}{1310720}$	(8,0,1)	$\frac{-25}{12288}$	(8,4,2)	$\frac{-4419}{163840}$
(4,0,4)	$\frac{-2745}{8192}$	(6,0,2)	$\frac{10617}{32768}$	(7,0,6)	$\frac{3717}{262144}$	(8,0,2)	$\frac{-4569}{32768}$	(8,4,3)	$\frac{24827}{491520}$
(4,1,1)	$\frac{3}{128}$	(6,0,3)	$\frac{215}{512}$	(7,0,7)	$\frac{336539}{2621440}$	(8,0,3)	$\frac{-97027}{245760}$	(8,4,4)	$\frac{-234977}{3932160}$
(4,1,2)	$\frac{-3}{64}$	(6,0,4)	$\frac{20439}{65536}$	(7,1,1)	$\frac{-1421}{40960}$	(8,0,4)	$\frac{-976461}{2621440}$	(8,5,0)	$\frac{53}{10240}$
(4,1,3)	$\frac{-87}{256}$	(6,0,5)	$\frac{8955}{32768}$	(7,1,2)	$\frac{-60221}{163840}$	(8,0,5)	$\frac{-228293}{983040}$	(8,5,1)	$\frac{119}{6144}$
(4,2,0)	$\frac{-3}{128}$	(6,0,6)	$\frac{69605}{262144}$	(7,1,3)	$\frac{-35077}{40960}$	(8,0,6)	$\frac{-1773971}{7864320}$	(8,5,2)	$\frac{-8221}{61440}$
(4,2,1)	$\frac{-3}{32}$	(6,1,1)	$\frac{153}{4096}$	(7,1,4)	$\frac{-160069}{163840}$	(8,0,7)	$\frac{-322627}{1310720}$	(8,5,3)	$\frac{-44923}{196608}$
(4,2,2)	$\frac{-27}{128}$	(6,1,2)	$\frac{-219}{2048}$	(7,1,5)	$\frac{-54117}{65536}$	(8,0,8)	$\frac{-6491669}{33554432}$	(8,6,0)	$\frac{-101}{122880}$
(4,3,1)	$\frac{-3}{64}$	(6,1,3)	$\frac{-3075}{8192}$	(7,1,6)	$\frac{-708743}{1310720}$	(8,1,1)	$\frac{-4667}{245760}$	(8,6,1)	$\frac{-2449}{40960}$
(4,4,0)	$\frac{-15}{256}$	(6,1,4)	$\frac{219}{4096}$	(7,2,0)	$\frac{49}{20480}$	(8,1,2)	$\frac{-267}{10240}$	(8,6,2)	$\frac{-593}{196608}$
(5,0,0)	$\frac{-5}{512}$	(6,1,5)	$\frac{16551}{32768}$	(7,2,1)	$\frac{8099}{163840}$	(8,1,3)	$\frac{94703}{245760}$	(8,7,1)	$\frac{1717}{30720}$
(5,0,1)	$\frac{-65}{1024}$	(6,2,0)	$\frac{-21}{4096}$	(7,2,2)	$\frac{10171}{81920}$	(8,1,4)	$\frac{79939}{81920}$	(8,8,0)	$\frac{1417}{327680}$
(5,0,2)	$\frac{165}{1024}$	(6,2,1)	$\frac{147}{2048}$	(7,2,3)	$\frac{6461}{20480}$	(8,1,5)	$\frac{1511111}{1966080}$		
(5,0,3)	$\frac{645}{2048}$	(6,2,2)	$\frac{-327}{8192}$	(7,2,4)	$\frac{28987}{81920}$	(8,1,6)	$\frac{-251057}{983040}$		

A.4. Shastry-Sutherland Model

Table A.9.: Series coefficients $a_{n,k}$ of the high temperature expansion of the magnetic susceptibility $\chi = \frac{1}{T} \sum_{n,k} a_{n,k} x^k (\beta J_1)^n$ for the Shastry-Sutherland model. Only nonzero coefficients are presented up to order β^7 .

(n,k)	$a_{n,k}$	(n,k)	$a_{n,k}$	(n,k)	$a_{n,k}$	(n,k)	$a_{n,k}$	(n,k)	$a_{n,k}$
(0,0)	$\frac{1}{4}$	(3,0)	$\frac{1}{768}$	(4,2)	$\frac{17}{1536}$	(5,3)	$\frac{-17}{1024}$	(6,3)	$\frac{43}{11520}$
(1,0)	$\frac{-1}{16}$	(3,1)	$\frac{1}{64}$	(4,3)	$\frac{19}{768}$	(5,4)	$\frac{-17}{1536}$	(6,4)	$\frac{19}{10240}$
(1,1)	$\frac{-1}{4}$	(3,2)	$\frac{-11}{128}$	(4,4)	$\frac{13}{768}$	(5,5)	$\frac{-71}{7680}$	(6,5)	$\frac{191}{15360}$
(2,0)	$\frac{-1}{64}$	(3,3)	$\frac{-1}{24}$	(5,0)	$\frac{13}{61440}$	(6,0)	$\frac{-77}{737280}$	(6,6)	$\frac{367}{184320}$
(2,1)	$\frac{1}{8}$	(4,0)	$\frac{5}{3072}$	(5,1)	$\frac{-11}{3072}$	(6,1)	$\frac{17}{30720}$		
(2,2)	$\frac{1}{8}$	(4,1)	$\frac{-1}{96}$	(5,2)	$\frac{29}{3072}$	(6,2)	$\frac{-77}{61440}$		

Table A.10.: Series coefficients $a_{n,k}$ of the high temperature expansion of the magnetic specific heat $C = \sum_{n,k} a_{n,k} x^k (\beta J_1)^n$ for the Shastry-Sutherland model. Only nonzero coefficients are presented up to order β^8 .

(n,k)	$a_{n,k}$	(n,k)	$a_{n,k}$	(n,k)	$a_{n,k}$	(n,k)	$a_{n,k}$	(n,k)	$a_{n,k}$
(2,0)	$\frac{3}{32}$	(4,3)	$\frac{-3}{32}$	(6,0)	$\frac{-13}{8192}$	(7,2)	$\frac{693}{40960}$	(8,2)	$\frac{-1349}{122880}$
(2,2)	$\frac{3}{8}$	(4,4)	$\frac{-21}{128}$	(6,2)	$\frac{153}{2048}$	(7,3)	$\frac{7}{320}$	(8,3)	$\frac{263}{61440}$
(3,0)	$\frac{3}{64}$	(5,0)	$\frac{-5}{512}$	(6,3)	$\frac{7}{1024}$	(7,4)	$\frac{-2961}{20480}$	(8,4)	$\frac{-26281}{245760}$
(3,2)	$\frac{-9}{32}$	(5,2)	$\frac{5}{256}$	(6,4)	$\frac{171}{1024}$	(7,5)	$\frac{245}{2048}$	(8,5)	$\frac{-851}{10240}$
(3,3)	$\frac{3}{16}$	(5,3)	$\frac{-5}{64}$	(6,5)	$\frac{111}{512}$	(7,6)	$\frac{-973}{5120}$	(8,6)	$\frac{-499}{12288}$
(4,0)	$\frac{-3}{512}$	(5,4)	$\frac{5}{16}$	(6,6)	$\frac{65}{2048}$	(7,7)	$\frac{2597}{20480}$	(8,7)	$\frac{-3731}{15360}$
(4,2)	$\frac{-15}{64}$	(5,5)	$\frac{-25}{128}$	(7,0)	$\frac{77}{81920}$	(8,0)	$\frac{823}{1966080}$	(8,8)	$\frac{9593}{491520}$

A.5. Spin-Phonon System

Table A.11.: Series coefficients $a_{n,k,l,m}$ of the cluster expansion of the magnetic susceptibility $\chi = \frac{1}{T} \sum_{n,k,l,m} a_{n,k,l,m} (z_0 \omega^2)^k (\beta \omega)^l e^{m\beta \omega} (-\frac{J}{\omega})^n$ for the spin-phonon system as defined in Eq. 2.1 with $z_0 = 1/(1 - \exp(-\beta \omega))$. Only nonzero coefficients are presented up to order J^{10} .

(n,k,l,m)	$a_{n,k,l,m}$	(n,k,l,m)	$a_{n,k,l,m}$	(n,k,l,m)	$a_{n,k,l,m}$	(n,k,l,m)	$a_{n,k,l,m}$
(0,0,0,0)	$\frac{1}{4}$	(7,3,3,0)	$\frac{27}{2048}$	(9,2,2,0)	$-\frac{130557}{32768}$	(10,2,6,-1)	$-\frac{3961}{98304}$
(1,0,1,0)	$\frac{1}{8}$	(7,3,3,-1)	$\frac{25}{2048}$	(9,2,2,-2)	$\frac{130557}{32768}$	(10,2,6,-2)	$-\frac{20237}{786432}$
(2,1,1,0)	$-\frac{1}{16}$	(7,3,3,-2)	$\frac{25}{2048}$	(9,2,3,0)	$\frac{6749}{32768}$	(10,2,7,0)	$\frac{46367}{7864320}$
(2,1,1,-1)	$\frac{1}{16}$	(7,3,3,-3)	$\frac{27}{2048}$	(9,2,3,-1)	$\frac{7}{512}$	(10,2,7,-2)	$-\frac{46367}{7864320}$
(3,0,3,0)	$-\frac{1}{96}$	(7,3,4,0)	$-\frac{5}{3072}$	(9,2,3,-2)	$\frac{6749}{32768}$	(10,2,8,0)	$\frac{1269}{655360}$
(4,0,4,0)	$\frac{5}{1536}$	(7,3,4,-1)	$-\frac{25}{1536}$	(9,2,4,0)	$\frac{27403}{98304}$	(10,2,8,-1)	$-\frac{14563}{9175040}$
(4,1,1,0)	$-\frac{1}{8}$	(7,3,4,-2)	$\frac{25}{1536}$	(9,2,4,-2)	$-\frac{27403}{98304}$	(10,2,8,-2)	$\frac{1269}{655360}$
(4,1,1,-1)	$\frac{1}{8}$	(7,3,4,-3)	$\frac{5}{3072}$	(9,2,5,0)	$-\frac{19}{768}$	(10,3,1,0)	$-\frac{177314759}{7962624}$
(4,1,2,0)	$\frac{1}{16}$	(8,0,8,0)	$\frac{1269}{4587520}$	(9,2,5,-1)	$-\frac{89}{6144}$	(10,3,1,-1)	$\frac{7971}{32768}$
(4,1,2,-1)	$\frac{1}{16}$	(8,1,1,0)	$-\frac{71}{32}$	(9,2,5,-2)	$-\frac{19}{768}$	(10,3,1,-2)	$-\frac{7971}{32768}$
(4,1,3,0)	$\frac{1}{64}$	(8,1,1,-1)	$\frac{71}{32}$	(9,2,6,0)	$-\frac{677}{32768}$	(10,3,1,-3)	$\frac{177314759}{7962624}$
(4,1,3,-1)	$-\frac{1}{64}$	(8,1,2,0)	$\frac{71}{64}$	(9,2,6,-2)	$\frac{677}{32768}$	(10,3,2,0)	$\frac{109688839}{10616832}$
(4,2,1,0)	$\frac{3}{128}$	(8,1,2,-1)	$\frac{71}{64}$	(9,2,7,0)	$-\frac{1}{3072}$	(10,3,2,-1)	$\frac{3008017}{131072}$
(4,2,1,-2)	$-\frac{3}{128}$	(8,1,3,0)	$-\frac{53}{2048}$	(9,2,7,-1)	$\frac{767}{368640}$	(10,3,2,-2)	$\frac{3008017}{131072}$
(4,2,2,-1)	$-\frac{3}{64}$	(8,1,3,-1)	$\frac{53}{2048}$	(9,2,7,-2)	$-\frac{1}{3072}$	(10,3,2,-3)	$\frac{109688839}{10616832}$
(5,0,5,0)	$\frac{7}{5120}$	(8,1,4,0)	$-\frac{977}{12288}$	(9,3,1,0)	$-\frac{196151}{32768}$	(10,3,3,0)	$-\frac{823405}{1769472}$
(5,1,2,0)	$-\frac{3}{128}$	(8,1,4,-1)	$-\frac{977}{12288}$	(9,3,1,-1)	$\frac{196151}{32768}$	(10,3,3,-1)	$-\frac{5701}{16384}$
(5,1,2,-1)	$\frac{3}{128}$	(8,1,5,0)	$\frac{23}{8192}$	(9,3,1,-2)	$\frac{196151}{32768}$	(10,3,3,-2)	$\frac{5701}{16384}$
(5,1,3,0)	$\frac{3}{256}$	(8,1,5,-1)	$-\frac{23}{8192}$	(9,3,1,-3)	$-\frac{196151}{32768}$	(10,3,3,-3)	$\frac{823405}{1769472}$
(5,1,3,-1)	$-\frac{3}{256}$	(8,1,6,0)	$\frac{277}{40960}$	(9,3,2,0)	$\frac{551351}{221184}$	(10,3,4,0)	$-\frac{478393}{884736}$
(5,1,4,0)	$-\frac{5}{768}$	(8,1,6,-1)	$\frac{277}{40960}$	(9,3,2,-1)	$\frac{76851}{16384}$	(10,3,4,-1)	$-\frac{109720}{196608}$
(5,1,4,-1)	$\frac{5}{768}$	(8,1,7,0)	$\frac{1}{4608}$	(9,3,2,-2)	$-\frac{76851}{16384}$	(10,3,4,-2)	$-\frac{109720}{196608}$
(5,2,1,0)	$\frac{1}{8}$	(8,1,7,-1)	$-\frac{1}{4608}$	(9,3,2,-3)	$-\frac{551351}{221184}$	(10,3,4,-3)	$-\frac{478393}{884736}$
(5,2,1,-1)	$-\frac{1}{4}$	(8,2,1,0)	$\frac{44777}{16384}$	(9,3,3,0)	$\frac{9257}{294912}$	(10,3,5,0)	$\frac{4669}{98304}$
(5,2,1,-2)	$\frac{1}{8}$	(8,2,1,-2)	$-\frac{44777}{16384}$	(9,3,3,-1)	$-\frac{4251}{32768}$	(10,3,5,-1)	$\frac{847}{98304}$

continued on next page...

. . . continued from previous page

(n,k,l,m)	$a_{n,k,l,m}$	(n,k,l,m)	$a_{n,k,l,m}$	(n,k,l,m)	$a_{n,k,l,m}$	(n,k,l,m)	$a_{n,k,l,m}$
(5,2,2,0)	$\frac{-7}{128}$	(8,2,2,0)	$\frac{-17561}{16384}$	(9,3,3,-2)	$\frac{-4251}{32768}$	(10,3,5,-2)	$\frac{-847}{98304}$
(5,2,2,-2)	$\frac{7}{128}$	(8,2,2,-1)	$\frac{-1701}{512}$	(9,3,3,-3)	$\frac{9257}{294912}$	(10,3,5,-3)	$\frac{-4669}{98304}$
(5,2,3,0)	$\frac{-1}{128}$	(8,2,2,-2)	$\frac{-17561}{16384}$	(9,3,4,0)	$\frac{-553}{4096}$	(10,3,6,0)	$\frac{1723}{65536}$
(5,2,3,-2)	$\frac{-1}{128}$	(8,2,3,0)	$\frac{-431}{8192}$	(9,3,4,-1)	$\frac{-8579}{49152}$	(10,3,6,-1)	$\frac{3749}{245760}$
(6,0,6,0)	$\frac{-133}{122880}$	(8,2,3,-2)	$\frac{431}{8192}$	(9,3,4,-2)	$\frac{8579}{49152}$	(10,3,6,-2)	$\frac{3749}{245760}$
(6,1,1,0)	$\frac{-15}{32}$	(8,2,4,0)	$\frac{1137}{16384}$	(9,3,4,-3)	$\frac{553}{4096}$	(10,3,6,-3)	$\frac{1723}{65536}$
(6,1,1,-1)	$\frac{15}{32}$	(8,2,4,-1)	$\frac{391}{3072}$	(9,3,5,0)	$\frac{-21}{16384}$	(10,3,7,0)	$\frac{5}{18432}$
(6,1,2,0)	$\frac{15}{64}$	(8,2,4,-2)	$\frac{1137}{16384}$	(9,3,5,-1)	$\frac{943}{49152}$	(10,3,7,-1)	$\frac{-647}{147456}$
(6,1,2,-1)	$\frac{15}{64}$	(8,2,5,0)	$\frac{-7}{98304}$	(9,3,5,-2)	$\frac{943}{49152}$	(10,3,7,-2)	$\frac{647}{147456}$
(6,1,3,0)	$\frac{1}{256}$	(8,2,5,-2)	$\frac{7}{98304}$	(9,3,5,-3)	$\frac{-21}{16384}$	(10,3,7,-3)	$\frac{-5}{18432}$
(6,1,3,-1)	$\frac{-1}{256}$	(8,2,6,0)	$\frac{-133}{32768}$	(9,3,6,0)	$\frac{133}{49152}$	(10,4,1,0)	$\frac{3089585}{589824}$
(6,1,4,0)	$\frac{-11}{512}$	(8,2,6,-1)	$\frac{7}{40960}$	(9,3,6,-1)	$\frac{637}{81920}$	(10,4,1,-1)	$\frac{3563821}{294912}$
(6,1,4,-1)	$\frac{-11}{512}$	(8,2,6,-2)	$\frac{-133}{32768}$	(9,3,6,-2)	$\frac{-637}{81920}$	(10,4,1,-3)	$\frac{-3563821}{294912}$
(6,1,5,0)	$\frac{-7}{2048}$	(8,3,1,0)	$\frac{-14603}{9216}$	(9,3,6,-3)	$\frac{-133}{49152}$	(10,4,1,-4)	$\frac{-3089585}{589824}$
(6,1,5,-1)	$\frac{7}{2048}$	(8,3,1,-1)	$\frac{-179}{1024}$	(9,4,1,0)	$\frac{245639}{221184}$	(10,4,2,0)	$\frac{-9006329}{3538944}$
(6,2,1,0)	$\frac{319}{1024}$	(8,3,1,-2)	$\frac{179}{1024}$	(9,4,1,-1)	$\frac{1673}{1728}$	(10,4,2,-1)	$\frac{-12003655}{884736}$
(6,2,1,-2)	$\frac{-319}{1024}$	(8,3,1,-3)	$\frac{14603}{9216}$	(9,4,1,-2)	$\frac{-17029}{4096}$	(10,4,2,-2)	$\frac{-1241849}{65536}$
(6,2,2,0)	$\frac{-83}{1024}$	(8,3,2,0)	$\frac{14987}{24576}$	(9,4,1,-3)	$\frac{1673}{1728}$	(10,4,2,-3)	$\frac{-12003655}{884736}$
(6,2,2,-1)	$\frac{-59}{128}$	(8,3,2,-1)	$\frac{15191}{8192}$	(9,4,1,-4)	$\frac{245639}{221184}$	(10,4,2,-4)	$\frac{-9006329}{3538944}$
(6,2,2,-2)	$\frac{-83}{1024}$	(8,3,2,-2)	$\frac{15191}{8192}$	(9,4,2,0)	$\frac{-27377}{73728}$	(10,4,3,0)	$\frac{-6739}{786432}$
(6,2,3,0)	$\frac{-45}{2048}$	(8,3,2,-3)	$\frac{14987}{24576}$	(9,4,2,-1)	$\frac{-23161}{12288}$	(10,4,3,-1)	$\frac{24349}{73728}$
(6,2,3,-2)	$\frac{45}{2048}$	(8,3,3,0)	$\frac{211}{12288}$	(9,4,2,-3)	$\frac{23161}{12288}$	(10,4,3,-3)	$\frac{-24349}{73728}$
(6,2,4,0)	$\frac{5}{1024}$	(8,3,3,-1)	$\frac{185}{2048}$	(9,4,2,-4)	$\frac{27377}{73728}$	(10,4,3,-4)	$\frac{6739}{786432}$
(6,2,4,-1)	$\frac{35}{3072}$	(8,3,3,-2)	$\frac{-185}{2048}$	(9,4,3,0)	$\frac{-347}{24576}$	(10,4,4,0)	$\frac{40547}{393216}$
(6,2,4,-2)	$\frac{5}{1024}$	(8,3,3,-3)	$\frac{-211}{12288}$	(9,4,3,-1)	$\frac{-309}{4096}$	(10,4,4,-1)	$\frac{30529}{98304}$
(6,3,1,0)	$\frac{-11}{192}$	(8,3,4,0)	$\frac{-261}{8192}$	(9,4,3,-2)	$\frac{97}{4096}$	(10,4,4,-2)	$\frac{10807}{32768}$
(6,3,1,-1)	$\frac{-9}{64}$	(8,3,4,-1)	$\frac{-1523}{24576}$	(9,4,3,-3)	$\frac{-309}{4096}$	(10,4,4,-3)	$\frac{30529}{98304}$
(6,3,1,-2)	$\frac{9}{64}$	(8,3,4,-2)	$\frac{-1523}{24576}$	(9,4,3,-4)	$\frac{-347}{24576}$	(10,4,4,-4)	$\frac{40547}{393216}$
(6,3,1,-3)	$\frac{11}{192}$	(8,3,4,-3)	$\frac{-261}{8192}$	(9,4,4,0)	$\frac{173}{16384}$	(10,4,5,0)	$\frac{259}{196608}$
(6,3,2,0)	$\frac{3}{256}$	(8,3,5,0)	$\frac{-7}{4096}$	(9,4,4,-1)	$\frac{315}{4096}$	(10,4,5,-1)	$\frac{-521}{16384}$

continued on next page . . .

. . . continued from previous page

(n,k,l,m)	$a_{n,k,l,m}$	(n,k,l,m)	$a_{n,k,l,m}$	(n,k,l,m)	$a_{n,k,l,m}$	(n,k,l,m)	$a_{n,k,l,m}$
(6,3,2,-1)	$\frac{37}{256}$	(8,3,5,-1)	$\frac{3}{1024}$	(9,4,4,-3)	$\frac{-315}{4096}$	(10,4,5,-3)	$\frac{521}{16384}$
(6,3,2,-2)	$\frac{37}{256}$	(8,3,5,-2)	$\frac{-3}{1024}$	(9,4,4,-4)	$\frac{-173}{16384}$	(10,4,5,-4)	$\frac{-259}{196608}$
(6,3,2,-3)	$\frac{3}{256}$	(8,3,5,-3)	$\frac{7}{4096}$	(9,4,5,0)	$\frac{7}{16384}$	(10,4,6,0)	$\frac{-133}{131072}$
(6,3,3,0)	$\frac{1}{768}$	(8,4,1,0)	$\frac{2983}{24576}$	(9,4,5,-1)	$\frac{-13}{12288}$	(10,4,6,-1)	$\frac{-3383}{491520}$
(6,3,3,-1)	$\frac{1}{256}$	(8,4,1,-1)	$\frac{10427}{12288}$	(9,4,5,-2)	$\frac{-143}{24576}$	(10,4,6,-2)	$\frac{835}{65536}$
(6,3,3,-2)	$\frac{-1}{256}$	(8,4,1,-3)	$\frac{-10427}{12288}$	(9,4,5,-3)	$\frac{-13}{12288}$	(10,4,6,-3)	$\frac{-3383}{491520}$
(6,3,3,-3)	$\frac{-1}{768}$	(8,4,1,-4)	$\frac{-2983}{24576}$	(9,4,5,-4)	$\frac{7}{16384}$	(10,4,6,-4)	$\frac{-133}{131072}$
(7,0,7,0)	$\frac{-1}{16128}$	(8,4,2,0)	$\frac{-317}{12288}$	(10,0,10,0)	$\frac{-339691}{5945425920}$	(10,5,1,0)	$\frac{-115123}{368640}$
(7,1,2,0)	$\frac{-9}{256}$	(8,4,2,-1)	$\frac{-5995}{12288}$	(10,1,1,0)	$\frac{-12441}{1024}$	(10,5,1,-1)	$\frac{-459733}{110592}$
(7,1,2,-1)	$\frac{9}{256}$	(8,4,2,-2)	$\frac{-1183}{1024}$	(10,1,1,-1)	$\frac{12441}{1024}$	(10,5,1,-2)	$\frac{-588599}{73728}$
(7,1,3,0)	$\frac{9}{512}$	(8,4,2,-3)	$\frac{-5995}{12288}$	(10,1,2,0)	$\frac{12441}{2048}$	(10,5,1,-3)	$\frac{588599}{73728}$
(7,1,3,-1)	$\frac{9}{512}$	(8,4,2,-4)	$\frac{-317}{12288}$	(10,1,2,-1)	$\frac{12441}{2048}$	(10,5,1,-4)	$\frac{459733}{110592}$
(7,1,4,0)	$\frac{-25}{6144}$	(8,4,3,0)	$\frac{-21}{8192}$	(10,1,3,0)	$\frac{-1795}{8192}$	(10,5,1,-5)	$\frac{115123}{368640}$
(7,1,4,-1)	$\frac{25}{6144}$	(8,4,3,-1)	$\frac{-5}{4096}$	(10,1,3,-1)	$\frac{1795}{8192}$	(10,5,2,0)	$\frac{23251}{294912}$
(7,1,5,0)	$\frac{7}{12288}$	(8,4,3,-3)	$\frac{5}{4096}$	(10,1,4,0)	$\frac{-6499}{16384}$	(10,5,2,-1)	$\frac{573631}{294912}$
(7,1,5,-1)	$\frac{7}{12288}$	(8,4,3,-4)	$\frac{21}{8192}$	(10,1,4,-1)	$\frac{-6499}{16384}$	(10,5,2,-2)	$\frac{1324747}{147456}$
(7,1,6,0)	$\frac{133}{40960}$	(8,4,4,0)	$\frac{5}{24576}$	(10,1,5,0)	$\frac{59}{1536}$	(10,5,2,-3)	$\frac{1324747}{147456}$
(7,1,6,-1)	$\frac{-133}{40960}$	(8,4,4,-1)	$\frac{1}{384}$	(10,1,5,-1)	$\frac{-59}{1536}$	(10,5,2,-4)	$\frac{573631}{294912}$
(7,2,1,0)	$\frac{65}{64}$	(8,4,4,-2)	$\frac{-103}{12288}$	(10,1,6,0)	$\frac{7393}{327680}$	(10,5,2,-5)	$\frac{23251}{294912}$
(7,2,1,-1)	$\frac{-65}{32}$	(8,4,4,-3)	$\frac{1}{384}$	(10,1,6,-1)	$\frac{7393}{327680}$	(10,5,3,0)	$\frac{169}{49152}$
(7,2,1,-2)	$\frac{65}{64}$	(8,4,4,-4)	$\frac{5}{24576}$	(10,1,7,0)	$\frac{-1829}{983040}$	(10,5,3,-1)	$\frac{-233}{3072}$
(7,2,2,0)	$\frac{-1009}{2048}$	(9,0,9,0)	$\frac{-3737}{74317824}$	(10,1,7,-1)	$\frac{1829}{983040}$	(10,5,3,-2)	$\frac{-7427}{16384}$
(7,2,2,-2)	$\frac{1009}{2048}$	(9,1,2,0)	$\frac{7}{2048}$	(10,1,8,0)	$\frac{-69313}{41287680}$	(10,5,3,-3)	$\frac{7427}{16384}$
(7,2,3,0)	$\frac{-15}{2048}$	(9,1,2,-1)	$\frac{-7}{2048}$	(10,1,8,-1)	$\frac{-69313}{41287680}$	(10,5,3,-4)	$\frac{233}{3072}$
(7,2,3,-1)	$\frac{-1}{64}$	(9,1,3,0)	$\frac{-7}{4096}$	(10,1,9,0)	$\frac{3737}{16515072}$	(10,5,3,-5)	$\frac{-169}{49152}$
(7,2,3,-2)	$\frac{-15}{2048}$	(9,1,3,-1)	$\frac{-7}{4096}$	(10,1,9,-1)	$\frac{-3737}{16515072}$	(10,5,4,0)	$\frac{-43}{32768}$
(7,2,4,0)	$\frac{175}{4096}$	(9,1,4,0)	$\frac{-211}{8192}$	(10,2,1,0)	$\frac{5828605}{262144}$	(10,5,4,-1)	$\frac{-877}{98304}$
(7,2,4,-2)	$\frac{-175}{4096}$	(9,1,4,-1)	$\frac{211}{8192}$	(10,2,1,-2)	$\frac{-5828605}{262144}$	(10,5,4,-2)	$\frac{1677}{16384}$
(7,2,5,0)	$\frac{7}{2048}$	(9,1,5,0)	$\frac{5}{384}$	(10,2,2,0)	$\frac{-2672701}{262144}$	(10,5,4,-3)	$\frac{1677}{16384}$
(7,2,5,-1)	$\frac{-11}{2048}$	(9,1,5,-1)	$\frac{5}{384}$	(10,2,2,-1)	$\frac{-49311}{2048}$	(10,5,4,-4)	$\frac{-877}{98304}$

continued on next page . . .

. . . continued from previous page

(n,k,l,m)	$a_{n,k,l,m}$	(n,k,l,m)	$a_{n,k,l,m}$	(n,k,l,m)	$a_{n,k,l,m}$	(n,k,l,m)	$a_{n,k,l,m}$
(7,2,5,-2)	$\frac{7}{2048}$	(9,1,6,0)	$\frac{7}{5120}$	(10,2,2,-2)	$\frac{-2672701}{262144}$	(10,5,4,-5)	$\frac{-43}{32768}$
(7,3,1,0)	$\frac{-21}{64}$	(9,1,6,-1)	$\frac{-7}{5120}$	(10,2,3,0)	$\frac{41897}{131072}$	(10,5,5,0)	$\frac{-7}{163840}$
(7,3,1,-1)	$\frac{21}{64}$	(9,1,7,0)	$\frac{-1741}{983040}$	(10,2,3,-2)	$\frac{-41897}{131072}$	(10,5,5,-1)	$\frac{25}{98304}$
(7,3,1,-2)	$\frac{21}{64}$	(9,1,7,-1)	$\frac{-1741}{983040}$	(10,2,4,0)	$\frac{486503}{786432}$	(10,5,5,-2)	$\frac{49}{16384}$
(7,3,1,-3)	$\frac{-21}{64}$	(9,1,8,0)	$\frac{-1269}{1146880}$	(10,2,4,-1)	$\frac{697}{768}$	(10,5,5,-3)	$\frac{-49}{16384}$
(7,3,2,0)	$\frac{307}{3072}$	(9,1,8,-1)	$\frac{1269}{1146880}$	(10,2,4,-2)	$\frac{486503}{786432}$	(10,5,5,-4)	$\frac{-25}{98304}$
(7,3,2,-1)	$\frac{313}{1024}$	(9,2,1,0)	$\frac{1931}{256}$	(10,2,5,0)	$\frac{-60695}{786432}$	(10,5,5,-5)	$\frac{7}{163840}$
(7,3,2,-2)	$\frac{-313}{1024}$	(9,2,1,-1)	$\frac{-1931}{128}$	(10,2,5,-2)	$\frac{60695}{786432}$		
(7,3,2,-3)	$\frac{-307}{3072}$	(9,2,1,-2)	$\frac{1931}{256}$	(10,2,6,0)	$\frac{-20237}{786432}$		

Table A.12.: Series coefficients $a_{n,k,l,m}$ of the cluster expansion of the free energy $-\beta f = a_{0,0,0,0} \ln z_0 + \sum_{n>0,k,l,m} a_{n,k,l,m} (z_0 \omega^2)^k (\beta \omega)^l e^{m\beta \omega} \left(-\frac{J}{\omega}\right)^n$ for the spin-phonon system as defined in Eq. 2.1 with $z_0 = 1/(1 - \exp(-\beta \omega))$. Only nonzero coefficients are presented up to order J^{11} .

(n,k,l,m)	$a_{n,k,l,m}$	(n,k,l,m)	$a_{n,k,l,m}$	(n,k,l,m)	$a_{n,k,l,m}$	(n,k,l,m)	$a_{n,k,l,m}$
(0,0,0,0)	$\frac{1}{1}$	(8,2,4,-2)	$\frac{-1}{8192}$	(10,1,3,-1)	$\frac{-1143}{1024}$	(11,1,7,-1)	$\frac{4607}{655360}$
(2,0,2,0)	$\frac{3}{32}$	(8,2,5,0)	$\frac{65}{2048}$	(10,1,4,0)	$\frac{-33}{1024}$	(11,1,8,0)	$\frac{-5151}{4587520}$
(2,1,1,0)	$\frac{3}{16}$	(8,2,5,-2)	$\frac{-65}{2048}$	(10,1,4,-1)	$\frac{-33}{1024}$	(11,1,8,-1)	$\frac{5151}{4587520}$
(2,1,1,-1)	$\frac{-3}{16}$	(8,2,6,0)	$\frac{21}{32768}$	(10,1,5,0)	$\frac{-245}{8192}$	(11,1,9,0)	$\frac{-23257}{55050240}$
(3,0,3,0)	$\frac{-1}{64}$	(8,2,6,-1)	$\frac{-189}{81920}$	(10,1,5,-1)	$\frac{245}{8192}$	(11,1,9,-1)	$\frac{-23257}{55050240}$
(3,1,2,0)	$\frac{-3}{32}$	(8,2,6,-2)	$\frac{21}{32768}$	(10,1,6,0)	$\frac{727}{81920}$	(11,1,10,0)	$\frac{334433}{1981808640}$
(3,1,2,-1)	$\frac{3}{32}$	(8,3,1,0)	$\frac{9505}{4608}$	(10,1,6,-1)	$\frac{727}{81920}$	(11,1,10,-1)	$\frac{-334433}{1981808640}$
(4,0,4,0)	$\frac{-5}{1024}$	(8,3,1,-1)	$\frac{225}{512}$	(10,1,7,0)	$\frac{169}{196608}$	(11,2,1,0)	$\frac{-58983}{1024}$
(4,1,1,0)	$\frac{3}{16}$	(8,3,1,-2)	$\frac{-225}{512}$	(10,1,7,-1)	$\frac{-169}{196608}$	(11,2,1,-1)	$\frac{58983}{512}$
(4,1,1,-1)	$\frac{-3}{16}$	(8,3,1,-3)	$\frac{-9505}{4608}$	(10,1,8,0)	$\frac{-13837}{13762560}$	(11,2,1,-2)	$\frac{-58983}{1024}$
(4,1,2,0)	$\frac{-3}{32}$	(8,3,2,0)	$\frac{-3835}{3072}$	(10,1,8,-1)	$\frac{-13837}{13762560}$	(11,2,2,0)	$\frac{12284013}{262144}$
(4,1,2,-1)	$\frac{-3}{32}$	(8,3,2,-1)	$\frac{-2115}{1024}$	(10,1,9,0)	$\frac{-4303}{11010048}$	(11,2,2,-2)	$\frac{-12284013}{262144}$
(4,1,3,0)	$\frac{3}{128}$	(8,3,2,-2)	$\frac{-2115}{1024}$	(10,1,9,-1)	$\frac{4303}{11010048}$	(11,2,3,0)	$\frac{-3552045}{262144}$
(4,1,3,-1)	$\frac{-3}{128}$	(8,3,2,-3)	$\frac{-3835}{3072}$	(10,2,1,0)	$\frac{-387789}{16384}$	(11,2,3,-1)	$\frac{-18471}{2048}$

continued on next page . . .

. . . continued from previous page

(n,k,l,m)	$a_{n,k,l,m}$	(n,k,l,m)	$a_{n,k,l,m}$	(n,k,l,m)	$a_{n,k,l,m}$	(n,k,l,m)	$a_{n,k,l,m}$
(4,2,1,0)	$\frac{-3}{64}$	(8,3,3,0)	$\frac{933}{4096}$	(10,2,1,-2)	$\frac{387789}{16384}$	(11,2,3,-2)	$\frac{-3552045}{262144}$
(4,2,1,-2)	$\frac{3}{64}$	(8,3,3,-1)	$\frac{1101}{4096}$	(10,2,2,0)	$\frac{281805}{16384}$	(11,2,4,0)	$\frac{27731}{32768}$
(4,2,2,0)	$\frac{3}{128}$	(8,3,3,-2)	$\frac{-1101}{4096}$	(10,2,2,-1)	$\frac{207}{16}$	(11,2,4,-2)	$\frac{-27731}{32768}$
(4,2,2,-1)	$\frac{3}{64}$	(8,3,3,-3)	$\frac{-933}{4096}$	(10,2,2,-2)	$\frac{281805}{16384}$	(11,2,5,0)	$\frac{103103}{262144}$
(4,2,2,-2)	$\frac{3}{128}$	(8,3,4,0)	$\frac{27}{2048}$	(10,2,3,0)	$\frac{-317289}{65536}$	(11,2,5,-1)	$\frac{4111}{16384}$
(5,0,5,0)	$\frac{3}{1024}$	(8,3,4,-1)	$\frac{1}{256}$	(10,2,3,-2)	$\frac{317289}{65536}$	(11,2,5,-2)	$\frac{103103}{262144}$
(5,1,2,0)	$\frac{-3}{32}$	(8,3,4,-2)	$\frac{1}{256}$	(10,2,4,0)	$\frac{16973}{65536}$	(11,2,6,0)	$\frac{-34679}{524288}$
(5,1,2,-1)	$\frac{3}{32}$	(8,3,4,-3)	$\frac{27}{2048}$	(10,2,4,-1)	$\frac{-149}{1024}$	(11,2,6,-2)	$\frac{34679}{524288}$
(5,1,3,0)	$\frac{3}{64}$	(8,3,5,0)	$\frac{-15}{4096}$	(10,2,4,-2)	$\frac{16973}{65536}$	(11,2,7,0)	$\frac{-30469}{2621440}$
(5,1,3,-1)	$\frac{3}{64}$	(8,3,5,-1)	$\frac{-45}{4096}$	(10,2,5,0)	$\frac{23339}{131072}$	(11,2,7,-1)	$\frac{-11497}{983040}$
(5,1,4,0)	$\frac{5}{512}$	(8,3,5,-2)	$\frac{45}{4096}$	(10,2,5,-2)	$\frac{-23339}{131072}$	(11,2,7,-2)	$\frac{-30469}{2621440}$
(5,1,4,-1)	$\frac{-5}{512}$	(8,3,5,-3)	$\frac{15}{4096}$	(10,2,6,0)	$\frac{-2705}{131072}$	(11,2,8,0)	$\frac{3155}{786432}$
(5,2,1,0)	$\frac{-3}{16}$	(8,4,1,0)	$\frac{-751}{4096}$	(10,2,6,-1)	$\frac{23}{20480}$	(11,2,8,-2)	$\frac{-3155}{786432}$
(5,2,1,-1)	$\frac{3}{8}$	(8,4,1,-1)	$\frac{-2969}{2048}$	(10,2,6,-2)	$\frac{-2705}{131072}$	(11,2,9,0)	$\frac{4303}{5505024}$
(5,2,1,-2)	$\frac{-3}{16}$	(8,4,1,-3)	$\frac{2969}{2048}$	(10,2,7,0)	$\frac{-12527}{1310720}$	(11,2,9,-1)	$\frac{-4927}{5505024}$
(5,2,2,0)	$\frac{15}{128}$	(8,4,1,-4)	$\frac{751}{4096}$	(10,2,7,-2)	$\frac{12527}{1310720}$	(11,2,9,-2)	$\frac{4303}{5505024}$
(5,2,2,-2)	$\frac{-15}{128}$	(8,4,2,0)	$\frac{599}{8192}$	(10,2,8,0)	$\frac{1417}{2621440}$	(11,3,1,0)	$\frac{5220813}{65536}$
(5,2,3,0)	$\frac{-3}{256}$	(8,4,2,-1)	$\frac{1801}{2048}$	(10,2,8,-1)	$\frac{367}{9175040}$	(11,3,1,-1)	$\frac{-5220813}{65536}$
(5,2,3,-1)	$\frac{-3}{128}$	(8,4,2,-2)	$\frac{7077}{4096}$	(10,2,8,-2)	$\frac{1417}{2621440}$	(11,3,1,-2)	$\frac{-5220813}{65536}$
(5,2,3,-2)	$\frac{-3}{256}$	(8,4,2,-3)	$\frac{1801}{2048}$	(10,3,1,0)	$\frac{32950553}{1327104}$	(11,3,1,-3)	$\frac{5220813}{65536}$
(6,0,6,0)	$\frac{7}{40960}$	(8,4,2,-4)	$\frac{599}{8192}$	(10,3,1,-1)	$\frac{13257}{16384}$	(11,3,2,0)	$\frac{-50936345}{884736}$
(6,1,1,0)	$\frac{9}{16}$	(8,4,3,0)	$\frac{-27}{4096}$	(10,3,1,-2)	$\frac{-13257}{16384}$	(11,3,2,-1)	$\frac{-714759}{16384}$
(6,1,1,-1)	$\frac{-9}{16}$	(8,4,3,-1)	$\frac{-99}{1024}$	(10,3,1,-3)	$\frac{-32950553}{1327104}$	(11,3,2,-2)	$\frac{714759}{16384}$
(6,1,2,0)	$\frac{-9}{32}$	(8,4,3,-3)	$\frac{99}{1024}$	(10,3,2,0)	$\frac{-7549927}{442368}$	(11,3,2,-3)	$\frac{50936345}{884736}$
(6,1,2,-1)	$\frac{-9}{32}$	(8,4,3,-4)	$\frac{27}{4096}$	(10,3,2,-1)	$\frac{-337197}{16384}$	(11,3,3,0)	$\frac{8906471}{589824}$
(6,1,3,0)	$\frac{9}{256}$	(8,4,4,0)	$\frac{-5}{16384}$	(10,3,2,-2)	$\frac{-337197}{16384}$	(11,3,3,-1)	$\frac{878661}{65536}$
(6,1,3,-1)	$\frac{-9}{256}$	(8,4,4,-1)	$\frac{9}{4096}$	(10,3,2,-3)	$\frac{-7549927}{442368}$	(11,3,3,-2)	$\frac{878661}{65536}$
(6,1,4,0)	$\frac{3}{512}$	(8,4,4,-2)	$\frac{133}{8192}$	(10,3,3,0)	$\frac{303145}{73728}$	(11,3,3,-3)	$\frac{8906471}{589824}$
(6,1,4,-1)	$\frac{3}{512}$	(8,4,4,-3)	$\frac{9}{4096}$	(10,3,3,-1)	$\frac{29757}{8192}$	(11,3,4,0)	$\frac{-1236169}{1769472}$
(6,1,5,0)	$\frac{-15}{2048}$	(8,4,4,-4)	$\frac{-5}{16384}$	(10,3,3,-2)	$\frac{-29757}{8192}$	(11,3,4,-1)	$\frac{-40605}{65536}$

continued on next page . . .

. . . continued from previous page

(n,k,l,m)	$a_{n,k,l,m}$	(n,k,l,m)	$a_{n,k,l,m}$	(n,k,l,m)	$a_{n,k,l,m}$	(n,k,l,m)	$a_{n,k,l,m}$
(6,1,5,-1)	$\frac{15}{2048}$	(9,0,9,0)	$\frac{4303}{49545216}$	(10,3,3,-3)	$\frac{-303145}{73728}$	(11,3,4,-2)	$\frac{40605}{65536}$
(6,2,1,0)	$\frac{-57}{128}$	(9,1,2,0)	$\frac{-399}{256}$	(10,3,4,0)	$\frac{-10853}{147456}$	(11,3,4,-3)	$\frac{1236169}{1769472}$
(6,2,1,-2)	$\frac{57}{128}$	(9,1,2,-1)	$\frac{399}{256}$	(10,3,4,-1)	$\frac{-1969}{16384}$	(11,3,5,0)	$\frac{-1012117}{2359296}$
(6,2,2,0)	$\frac{39}{128}$	(9,1,3,0)	$\frac{399}{512}$	(10,3,4,-2)	$\frac{-1969}{16384}$	(11,3,5,-1)	$\frac{-47243}{262144}$
(6,2,2,-1)	$\frac{9}{32}$	(9,1,3,-1)	$\frac{399}{512}$	(10,3,4,-3)	$\frac{-10853}{147456}$	(11,3,5,-2)	$\frac{-47243}{262144}$
(6,2,2,-2)	$\frac{39}{128}$	(9,1,4,0)	$\frac{-111}{2048}$	(10,3,5,0)	$\frac{-11957}{98304}$	(11,3,5,-3)	$\frac{-1012117}{2359296}$
(6,2,3,0)	$\frac{-75}{1024}$	(9,1,4,-1)	$\frac{111}{2048}$	(10,3,5,-1)	$\frac{-2647}{32768}$	(11,3,6,0)	$\frac{44051}{983040}$
(6,2,3,-2)	$\frac{75}{1024}$	(9,1,5,0)	$\frac{-155}{4096}$	(10,3,5,-2)	$\frac{2647}{32768}$	(11,3,6,-1)	$\frac{385}{131072}$
(6,2,4,0)	$\frac{-15}{2048}$	(9,1,5,-1)	$\frac{-155}{4096}$	(10,3,5,-3)	$\frac{11957}{98304}$	(11,3,6,-2)	$\frac{-385}{131072}$
(6,2,4,-1)	$\frac{5}{1024}$	(9,1,6,0)	$\frac{33}{10240}$	(10,3,6,0)	$\frac{315}{65536}$	(11,3,6,-3)	$\frac{-44051}{983040}$
(6,2,4,-2)	$\frac{-15}{2048}$	(9,1,6,-1)	$\frac{-33}{10240}$	(10,3,6,-1)	$\frac{3157}{327680}$	(11,3,7,0)	$\frac{19521}{1310720}$
(6,3,1,0)	$\frac{3}{32}$	(9,1,7,0)	$\frac{43}{16384}$	(10,3,6,-2)	$\frac{3157}{327680}$	(11,3,7,-1)	$\frac{4409}{1310720}$
(6,3,1,-1)	$\frac{9}{32}$	(9,1,7,-1)	$\frac{43}{16384}$	(10,3,6,-3)	$\frac{315}{65536}$	(11,3,7,-2)	$\frac{4409}{1310720}$
(6,3,1,-2)	$\frac{-9}{32}$	(9,1,8,0)	$\frac{-1417}{4587520}$	(10,3,7,0)	$\frac{917}{393216}$	(11,3,7,-3)	$\frac{19521}{1310720}$
(6,3,1,-3)	$\frac{-3}{32}$	(9,1,8,-1)	$\frac{1417}{4587520}$	(10,3,7,-1)	$\frac{255}{131072}$	(11,3,8,0)	$\frac{-1417}{2621440}$
(6,3,2,0)	$\frac{-9}{256}$	(9,2,1,0)	$\frac{-525}{64}$	(10,3,7,-2)	$\frac{-255}{131072}$	(11,3,8,-1)	$\frac{-31959}{18350080}$
(6,3,2,-1)	$\frac{-63}{256}$	(9,2,1,-1)	$\frac{525}{32}$	(10,3,7,-3)	$\frac{-917}{393216}$	(11,3,8,-2)	$\frac{31959}{18350080}$
(6,3,2,-2)	$\frac{-63}{256}$	(9,2,1,-2)	$\frac{-525}{64}$	(10,4,1,0)	$\frac{-9794909}{1179648}$	(11,3,8,-3)	$\frac{1417}{2621440}$
(6,3,2,-3)	$\frac{-9}{256}$	(9,2,2,0)	$\frac{25713}{4096}$	(10,4,1,-1)	$\frac{-2373487}{147456}$	(11,4,1,0)	$\frac{-33671093}{884736}$
(6,3,3,0)	$\frac{1}{512}$	(9,2,2,-2)	$\frac{-25713}{4096}$	(10,4,1,-3)	$\frac{2373487}{147456}$	(11,4,1,-1)	$\frac{-29255}{1728}$
(6,3,3,-1)	$\frac{9}{512}$	(9,2,3,0)	$\frac{-6561}{4096}$	(10,4,1,-4)	$\frac{9794909}{1179648}$	(11,4,1,-2)	$\frac{1801839}{16384}$
(6,3,3,-2)	$\frac{-9}{512}$	(9,2,3,-1)	$\frac{-147}{128}$	(10,4,2,0)	$\frac{119471}{24576}$	(11,4,1,-3)	$\frac{-29255}{1728}$
(6,3,3,-3)	$\frac{-1}{512}$	(9,2,3,-2)	$\frac{-6561}{4096}$	(10,4,2,-1)	$\frac{287735}{16384}$	(11,4,1,-4)	$\frac{-33671093}{884736}$
(7,0,7,0)	$\frac{-131}{245760}$	(9,2,4,0)	$\frac{331}{16384}$	(10,4,2,-2)	$\frac{673677}{32768}$	(11,4,2,0)	$\frac{76593479}{3145728}$
(7,1,2,0)	$\frac{-81}{256}$	(9,2,4,-2)	$\frac{-331}{16384}$	(10,4,2,-3)	$\frac{287735}{16384}$	(11,4,2,-1)	$\frac{35171555}{589824}$
(7,1,2,-1)	$\frac{81}{256}$	(9,2,5,0)	$\frac{933}{16384}$	(10,4,2,-4)	$\frac{119471}{24576}$	(11,4,2,-3)	$\frac{-35171555}{589824}$
(7,1,3,0)	$\frac{81}{512}$	(9,2,5,-1)	$\frac{79}{2048}$	(10,4,3,0)	$\frac{-119287}{131072}$	(11,4,2,-4)	$\frac{-76593479}{3145728}$
(7,1,3,-1)	$\frac{81}{512}$	(9,2,5,-2)	$\frac{933}{16384}$	(10,4,3,-1)	$\frac{-25047}{8192}$	(11,4,3,0)	$\frac{-8323519}{1572864}$
(7,1,4,0)	$\frac{-1}{512}$	(9,2,6,0)	$\frac{-693}{163840}$	(10,4,3,-3)	$\frac{25047}{8192}$	(11,4,3,-1)	$\frac{-2737121}{196608}$
(7,1,4,-1)	$\frac{1}{512}$	(9,2,6,-2)	$\frac{693}{163840}$	(10,4,3,-4)	$\frac{119287}{131072}$	(11,4,3,-2)	$\frac{-297987}{32768}$

continued on next page . . .

. . . continued from previous page

(n,k,l,m)	$a_{n,k,l,m}$	(n,k,l,m)	$a_{n,k,l,m}$	(n,k,l,m)	$a_{n,k,l,m}$	(n,k,l,m)	$a_{n,k,l,m}$
(7,1,5,0)	$\frac{-25}{2048}$	(9,2,7,0)	$\frac{-917}{327680}$	(10,4,4,0)	$\frac{-15}{1024}$	(11,4,3,-3)	$\frac{-2737121}{196608}$
(7,1,5,-1)	$\frac{-25}{2048}$	(9,2,7,-1)	$\frac{331}{163840}$	(10,4,4,-1)	$\frac{945}{16384}$	(11,4,3,-4)	$\frac{-8323519}{1572864}$
(7,1,6,0)	$\frac{-21}{40960}$	(9,2,7,-2)	$\frac{-917}{327680}$	(10,4,4,-2)	$\frac{5557}{32768}$	(11,4,4,0)	$\frac{88441}{1179648}$
(7,1,6,-1)	$\frac{21}{40960}$	(9,3,1,0)	$\frac{58071}{8192}$	(10,4,4,-3)	$\frac{945}{16384}$	(11,4,4,-1)	$\frac{405839}{589824}$
(7,2,1,0)	$\frac{-159}{128}$	(9,3,1,-1)	$\frac{-58071}{8192}$	(10,4,4,-4)	$\frac{-15}{1024}$	(11,4,4,-3)	$\frac{-405839}{589824}$
(7,2,1,-1)	$\frac{159}{64}$	(9,3,1,-2)	$\frac{-58071}{8192}$	(10,4,5,0)	$\frac{35}{2048}$	(11,4,4,-4)	$\frac{-88441}{1179648}$
(7,2,1,-2)	$\frac{-159}{128}$	(9,3,1,-3)	$\frac{58071}{8192}$	(10,4,5,-1)	$\frac{1113}{16384}$	(11,4,5,0)	$\frac{46939}{393216}$
(7,2,2,0)	$\frac{1815}{2048}$	(9,3,2,0)	$\frac{-911}{192}$	(10,4,5,-3)	$\frac{-1113}{16384}$	(11,4,5,-1)	$\frac{20395}{98304}$
(7,2,2,-2)	$\frac{-1815}{2048}$	(9,3,2,-1)	$\frac{-17961}{4096}$	(10,4,5,-4)	$\frac{-35}{2048}$	(11,4,5,-2)	$\frac{111}{1024}$
(7,2,3,0)	$\frac{-363}{2048}$	(9,3,2,-2)	$\frac{17961}{4096}$	(10,4,6,0)	$\frac{21}{131072}$	(11,4,5,-3)	$\frac{20395}{98304}$
(7,2,3,-1)	$\frac{-45}{256}$	(9,3,2,-3)	$\frac{911}{192}$	(10,4,6,-1)	$\frac{-437}{163840}$	(11,4,5,-4)	$\frac{46939}{393216}$
(7,2,3,-2)	$\frac{-363}{2048}$	(9,3,3,0)	$\frac{533}{512}$	(10,4,6,-2)	$\frac{-253}{327680}$	(11,4,6,0)	$\frac{-189}{65536}$
(7,2,4,0)	$\frac{-15}{1024}$	(9,3,3,-1)	$\frac{4833}{4096}$	(10,4,6,-3)	$\frac{-437}{163840}$	(11,4,6,-1)	$\frac{-4307}{163840}$
(7,2,4,-2)	$\frac{15}{1024}$	(9,3,3,-2)	$\frac{4833}{4096}$	(10,4,6,-4)	$\frac{21}{131072}$	(11,4,6,-3)	$\frac{4307}{163840}$
(7,2,5,0)	$\frac{15}{2048}$	(9,3,3,-3)	$\frac{533}{512}$	(10,5,1,0)	$\frac{214561}{491520}$	(11,4,6,-4)	$\frac{189}{65536}$
(7,2,5,-2)	$\frac{15}{2048}$	(9,3,4,0)	$\frac{17}{1536}$	(10,5,1,-1)	$\frac{1903025}{294912}$	(11,4,7,0)	$\frac{-917}{786432}$
(7,3,1,0)	$\frac{483}{1024}$	(9,3,4,-1)	$\frac{53}{2048}$	(10,5,1,-2)	$\frac{609895}{49152}$	(11,4,7,-1)	$\frac{-593}{163840}$
(7,3,1,-1)	$\frac{-483}{1024}$	(9,3,4,-2)	$\frac{-53}{2048}$	(10,5,1,-3)	$\frac{-609895}{49152}$	(11,4,7,-2)	$\frac{5711}{655360}$
(7,3,1,-2)	$\frac{-483}{1024}$	(9,3,4,-3)	$\frac{-17}{1536}$	(10,5,1,-4)	$\frac{-1903025}{294912}$	(11,4,7,-3)	$\frac{-593}{163840}$
(7,3,1,-3)	$\frac{483}{1024}$	(9,3,5,0)	$\frac{-135}{4096}$	(10,5,1,-5)	$\frac{-214561}{491520}$	(11,4,7,-4)	$\frac{-917}{786432}$
(7,3,2,0)	$\frac{-139}{512}$	(9,3,5,-1)	$\frac{-65}{2048}$	(10,5,2,0)	$\frac{-2931}{16384}$	(11,5,1,0)	$\frac{16908323}{3538944}$
(7,3,2,-1)	$\frac{-15}{32}$	(9,3,5,-2)	$\frac{-65}{2048}$	(10,5,2,-1)	$\frac{-10631}{3072}$	(11,5,1,-1)	$\frac{2966871}{131072}$
(7,3,2,-2)	$\frac{15}{32}$	(9,3,5,-3)	$\frac{-135}{4096}$	(10,5,2,-2)	$\frac{-218485}{16384}$	(11,5,1,-2)	$\frac{-6063365}{221184}$
(7,3,2,-3)	$\frac{139}{512}$	(9,3,6,0)	$\frac{-7}{16384}$	(10,5,2,-3)	$\frac{-218485}{16384}$	(11,5,1,-3)	$\frac{-6063365}{221184}$
(7,3,3,0)	$\frac{39}{1024}$	(9,3,6,-1)	$\frac{273}{81920}$	(10,5,2,-4)	$\frac{-10631}{3072}$	(11,5,1,-4)	$\frac{2966871}{131072}$
(7,3,3,-1)	$\frac{135}{1024}$	(9,3,6,-2)	$\frac{-273}{81920}$	(10,5,2,-5)	$\frac{-2931}{16384}$	(11,5,1,-5)	$\frac{16908323}{3538944}$
(7,3,3,-2)	$\frac{135}{1024}$	(9,3,6,-3)	$\frac{7}{16384}$	(10,5,3,0)	$\frac{315}{16384}$	(11,5,2,0)	$\frac{-3612739}{1474560}$
(7,3,3,-3)	$\frac{39}{1024}$	(9,4,1,0)	$\frac{-24435}{16384}$	(10,5,3,-1)	$\frac{483}{1024}$	(11,5,2,-1)	$\frac{-675911}{32768}$
(7,3,4,0)	$\frac{5}{2048}$	(9,4,1,-1)	$\frac{-183}{128}$	(10,5,3,-2)	$\frac{18645}{16384}$	(11,5,2,-2)	$\frac{-743737}{32768}$
(7,3,4,-1)	$\frac{5}{2048}$	(9,4,1,-2)	$\frac{47859}{8192}$	(10,5,3,-3)	$\frac{-18645}{16384}$	(11,5,2,-3)	$\frac{743737}{32768}$

continued on next page . . .

. . . continued from previous page

(n,k,l,m)	$a_{n,k,l,m}$	(n,k,l,m)	$a_{n,k,l,m}$	(n,k,l,m)	$a_{n,k,l,m}$	(n,k,l,m)	$a_{n,k,l,m}$
$(7,3,4,-2)$	$\frac{-5}{2048}$	$(9,4,1,-3)$	$\frac{-183}{128}$	$(10,5,3,-4)$	$\frac{-483}{1024}$	$(11,5,2,-4)$	$\frac{675911}{32768}$
$(7,3,4,-3)$	$\frac{-5}{2048}$	$(9,4,1,-4)$	$\frac{-24435}{16384}$	$(10,5,3,-5)$	$\frac{-315}{16384}$	$(11,5,2,-5)$	$\frac{3612739}{1474560}$
$(8,0,8,0)$	$\frac{1417}{18350080}$	$(9,4,2,0)$	$\frac{4831}{6144}$	$(10,5,4,0)$	$\frac{3}{4096}$	$(11,5,3,0)$	$\frac{49539}{131072}$
$(8,1,1,0)$	$\frac{309}{128}$	$(9,4,2,-1)$	$\frac{81163}{24576}$	$(10,5,4,-1)$	$\frac{-197}{8192}$	$(11,5,3,-1)$	$\frac{508821}{131072}$
$(8,1,1,-1)$	$\frac{-309}{128}$	$(9,4,2,-3)$	$\frac{-81163}{24576}$	$(10,5,4,-2)$	$\frac{-1697}{8192}$	$(11,5,3,-2)$	$\frac{353189}{49152}$
$(8,1,2,0)$	$\frac{-309}{256}$	$(9,4,2,-4)$	$\frac{-4831}{6144}$	$(10,5,4,-3)$	$\frac{-1697}{8192}$	$(11,5,3,-3)$	$\frac{353189}{49152}$
$(8,1,2,-1)$	$\frac{-309}{256}$	$(9,4,3,0)$	$\frac{-921}{8192}$	$(10,5,4,-4)$	$\frac{-197}{8192}$	$(11,5,3,-4)$	$\frac{508821}{131072}$
$(8,1,3,0)$	$\frac{195}{1024}$	$(9,4,3,-1)$	$\frac{-5113}{8192}$	$(10,5,4,-5)$	$\frac{3}{4096}$	$(11,5,3,-5)$	$\frac{49539}{131072}$
$(8,1,3,-1)$	$\frac{-195}{1024}$	$(9,4,3,-2)$	$\frac{-903}{1024}$	$(10,5,5,0)$	$\frac{-3}{32768}$	$(11,5,4,0)$	$\frac{115}{16384}$
$(8,1,4,0)$	$\frac{11}{2048}$	$(9,4,3,-3)$	$\frac{-5113}{8192}$	$(10,5,5,-1)$	$\frac{-15}{32768}$	$(11,5,4,-1)$	$\frac{-4531}{24576}$
$(8,1,4,-1)$	$\frac{11}{2048}$	$(9,4,3,-4)$	$\frac{-921}{8192}$	$(10,5,5,-2)$	$\frac{25}{8192}$	$(11,5,4,-2)$	$\frac{-58613}{98304}$
$(8,1,5,0)$	$\frac{-15}{2048}$	$(9,4,4,0)$	$\frac{-21}{4096}$	$(10,5,5,-3)$	$\frac{-25}{8192}$	$(11,5,4,-3)$	$\frac{58613}{98304}$
$(8,1,5,-1)$	$\frac{15}{2048}$	$(9,4,4,-1)$	$\frac{7}{2048}$	$(10,5,5,-4)$	$\frac{15}{32768}$	$(11,5,4,-4)$	$\frac{4531}{24576}$
$(8,1,6,0)$	$\frac{63}{40960}$	$(9,4,4,-3)$	$\frac{-7}{2048}$	$(10,5,5,-5)$	$\frac{3}{32768}$	$(11,5,4,-5)$	$\frac{-115}{16384}$
$(8,1,6,-1)$	$\frac{63}{40960}$	$(9,4,4,-4)$	$\frac{21}{4096}$	$(11,0,11,0)$	$\frac{-3413}{314572800}$	$(11,5,5,0)$	$\frac{-145}{32768}$
$(8,1,7,0)$	$\frac{917}{491520}$	$(9,4,5,0)$	$\frac{15}{16384}$	$(11,1,2,0)$	$\frac{-18825}{2048}$	$(11,5,5,-1)$	$\frac{-913}{32768}$
$(8,1,7,-1)$	$\frac{-917}{491520}$	$(9,4,5,-1)$	$\frac{45}{8192}$	$(11,1,2,-1)$	$\frac{18825}{2048}$	$(11,5,5,-2)$	$\frac{1953}{16384}$
$(8,2,1,0)$	$\frac{-13053}{4096}$	$(9,4,5,-2)$	$\frac{-125}{8192}$	$(11,1,3,0)$	$\frac{18825}{4096}$	$(11,5,5,-3)$	$\frac{1953}{16384}$
$(8,2,1,-2)$	$\frac{13053}{4096}$	$(9,4,5,-3)$	$\frac{45}{8192}$	$(11,1,3,-1)$	$\frac{18825}{4096}$	$(11,5,5,-4)$	$\frac{-913}{32768}$
$(8,2,2,0)$	$\frac{9285}{4096}$	$(9,4,5,-4)$	$\frac{15}{16384}$	$(11,1,4,0)$	$\frac{-843}{2048}$	$(11,5,5,-5)$	$\frac{-145}{32768}$
$(8,2,2,-1)$	$\frac{471}{256}$	$(10,0,10,0)$	$\frac{-334433}{9909043200}$	$(11,1,4,-1)$	$\frac{843}{2048}$	$(11,5,6,0)$	$\frac{-21}{655360}$
$(8,2,2,-2)$	$\frac{9285}{4096}$	$(10,1,1,0)$	$\frac{3231}{256}$	$(11,1,5,0)$	$\frac{-2003}{16384}$	$(11,5,6,-1)$	$\frac{761}{655360}$
$(8,2,3,0)$	$\frac{-4869}{8192}$	$(10,1,1,-1)$	$\frac{-3231}{256}$	$(11,1,5,-1)$	$\frac{-2003}{16384}$	$(11,5,6,-2)$	$\frac{807}{327680}$
$(8,2,3,-2)$	$\frac{4869}{8192}$	$(10,1,2,0)$	$\frac{-3231}{512}$	$(11,1,6,0)$	$\frac{9253}{327680}$	$(11,5,6,-3)$	$\frac{-807}{327680}$
$(8,2,4,0)$	$\frac{-1}{8192}$	$(10,1,2,-1)$	$\frac{-3231}{512}$	$(11,1,6,-1)$	$\frac{-9253}{327680}$	$(11,5,6,-4)$	$\frac{-761}{655360}$
$(8,2,4,-1)$	$\frac{-1}{64}$	$(10,1,3,0)$	$\frac{1143}{1024}$	$(11,1,7,0)$	$\frac{4607}{655360}$	$(11,5,6,-5)$	$\frac{21}{655360}$

B. Perturbation Theory for Spin-Phonon System

This Appendix refers to the ideas introduced for the extrapolations of the results of the isolated spin models, see the first part of this thesis. There, the extrapolations of the results for the susceptibility could be biased in the low temperature regime by the incorporation of the known value of the gap, even if it was zero. The spin-phonon problem is different from the isolated spin models. As mentioned in Chapter 2 the extrapolations are not performed in the inverse temperature, but in the magnetic exchange coupling J . Thus, one is interested in the behavior of the susceptibility as a function of J for fixed temperature in the limit $J \rightarrow \infty$.

Fixing the temperature T and the phonon frequency ω , the limit $J \rightarrow \infty$ corresponds to the adiabatic limit. In that limit it was shown that even a marginal spin-phonon interaction leads to a dimerization of the spin system [143, 145]. An essential feature for the phase transition to occur is that the phonon mode responsible for the dimerization is softening already above the transition temperature and its energy vanishes at the transition itself.

Here, a mean-field ansatz is used in the limit $J \rightarrow \infty$. Such an ansatz is well justified in the adiabatic limit. Fixing the temperature T and the phonon frequency ω the limit $J \rightarrow \infty$ corresponds to $J \gg T$, $J \gg \omega$, and $\beta\omega = \text{const}$. A first approach to get information on the behavior of the system in the limit $J \rightarrow \infty$ is to regard the spin system to be at zero temperature perturbed by the finite temperature fluctuations of the phonons.

An analysis of the ground state energy in the adiabatic limit yields that it is energetically most favorable for the spin system to be fully dimerized. The gain in magnetic energy due to the dimerization δ (notation as in Chapter 1.4, see Eq. 1.25) is proportional to $J\delta^{4/3}$ which overcompensates the loss in elastic energy proportional to $\omega\delta^2$ [145]. This leads to a full dimerization of the spin system in the limit $J \rightarrow \infty$ where the phonons are completely softened. The strength of the magnetic exchange coupling alternates between 0 and $2J$ on every second bond.

To perform a systematic perturbation expansion for the ground state energy and for the energy of the first excited state of the spin-phonon problem (see Chapter 2) the starting point is a fully dimerized spin system with a thermodynamically averaged number of phonons on each bond. In this limit the ground state energy per site of the spin sector is simply $e_0^{\text{spin}} = -\frac{3}{8}J$ and the singlet-triplet gap Δ_{01} to the first excited state is given by $\Delta_{01} = 2J$. Switching on the perturbation, i.e. the thermal fluctuations of the phonons, the gap will be influenced significantly.

The adiabatic limit is justified not only by $\omega \ll J$ but also by $\omega \ll \Delta_{01}$ assuming the

obvious proportionality $\Delta_{01} \propto J$. In Ref. [171] it was shown that $\omega \ll \Delta_{01}$ is also a necessary condition for the adiabatic limit to hold.

The following analysis is similar to the one performed in Ref. [155] except that the phononic subsystem is regarded to be at finite temperatures. The results presented here are thermodynamically averaged in the phononic subspace. Two quantities will be expanded in a second order perturbation theory: the ground state energy and the energy of the first excited state leading to the dispersion $\omega(k)$ and thus to the singlet-triplet gap with $\Delta_{01} = \Delta_{01}(\omega, g, T)$. In order to perform the perturbation expansion the Hamilton operator 2.1 is split in its diagonal part H_0 and in the perturbation V with the expansion parameter λ , where $\lambda = 1$ is the limit of interest. In analogy to the shifted harmonic oscillator which is exactly solvable the phonon operators on the dimer bonds (strong bonds) are shifted independently from the phonons between the dimer bonds (weak bonds) through

$$\text{strong bonds: } b_i^{(\dagger)} = \tilde{b}_i^{(\dagger)} - x_D \quad (\text{B.1a})$$

$$\text{weak bonds: } b_j^{(\dagger)} = \tilde{b}_j^{(\dagger)} - x_I . \quad (\text{B.1b})$$

In the canonical ensemble the free energy is minimized. Thus, the results are optimized finding the shifts of the phonon operators which yield the minimum value of the free energy. Once the optimal shifts are obtained, the gap can be evaluated.

The Hamilton operator 2.1 is divided into H_0 diagonal in the singlet-triplet representation of the magnetic dimer system and its perturbation V with

$$\begin{aligned} H &= H_0 + \lambda V \text{ with} \\ H_0 &= \sum_{\text{dimers } i} J(1 - 2gx_D) \mathbf{S}_i \mathbf{S}_{i+1} + \omega \sum_{\text{dimers } i} \tilde{b}_i^\dagger \tilde{b}_i \\ &\quad + \omega \sum_{\text{inter dimers } j} \tilde{b}_j^\dagger \tilde{b}_j + f(\omega; x_D, x_I) \end{aligned} \quad (\text{B.2a})$$

$$\begin{aligned} V &= \sum_{\text{inter dimers } j} \left\{ J \left(1 - 2gx_I + g \left(\tilde{b}_j^\dagger + \tilde{b}_j \right) \right) \mathbf{S}_j \mathbf{S}_{j+1} - \omega x_I \left(\tilde{b}_j^\dagger + \tilde{b}_j \right) \right\} \\ &\quad + \sum_{\text{dimers } i} \left\{ gJ \left(\tilde{b}_i^\dagger + \tilde{b}_i \right) \mathbf{S}_i \mathbf{S}_{i+1} - \omega x_D \left(\tilde{b}_i^\dagger + \tilde{b}_i \right) \right\} . \end{aligned} \quad (\text{B.2b})$$

The function $f(\omega; x_D, x_I)$ results from the shift of the phonons and yields a constant contribution which does not affect the value of the gap.

Starting from a product state of singlets on every dimer with a macroscopic number of thermodynamically distributed phonons on each bond the ground state energy is expanded about the limit of isolated dimers. Each dimer is in a singlet state. Using standard second order perturbation theory where the phononic subspace is thermodynamically averaged

yields the ground state energy per site

$$\begin{aligned}
\langle e_0 \rangle_{\text{therm.}} &= -\frac{3}{8}J(1-2gx_D) + \frac{\omega}{e^{\beta\omega}-1} + \frac{\omega}{2}(x_D^2 + x_I^2) \\
&+ \lambda^2 \left\{ \frac{3}{32}J \left(-\frac{1}{2} \frac{(1-2gx_I)^2}{1-2gx_D} + g^2 J \frac{\left(-4 \frac{J(1-2gx_D)}{e^{\beta\omega}-1} - 2J(1-2gx_D) + \omega \right)}{(4J^2(1-2gx_D)^2 - \omega^2)} \right) \right. \\
&\left. - \frac{\omega}{2}x_I^2 - \frac{\left(\frac{3}{4}Jg + \omega x_D \right)^2}{2\omega} \right\} + \mathcal{O}(\lambda^3), \tag{B.3}
\end{aligned}$$

where the angular brackets denote the thermodynamically averaging of the phononic subspace. Fixing T , ω , and g , and assuming $x_D < \frac{1}{2g}$ the ground state energy will always diverge to $-\infty$ for $J \rightarrow \infty$ which is plausible since J sets the overall energy scale and the fixed values for the other parameters can thus be neglected in this limit. Additionally, the second order contribution to the ground state energy is always negative, amplifying this effect.

To calculate the dispersion and the gap, the energy of the first excited state subtracted by the ground state energy has to be evaluated. Therefore, a second order perturbation theory is performed also for the first excited state. The first excited state is given by a product state of singlets on every dimer except for one dimer where a triplet is injected. The unperturbed base state is thus given by a superposition of all states where on the l th dimer a triplet is excited, denoted as $|l\rangle$. The Fourier transformed state yields the unperturbed base state for a nondegenerate perturbation theory with

$$|k\rangle = \sqrt{\frac{2}{N}} \sum_{\text{dimers}} e^{-ikl} |l\rangle, \tag{B.4}$$

characterized by its momentum k . The value of the gap Δ_{01} is obtained as the minimum of the dispersion.

Applying the second order perturbation theory yields the dispersion relation $\omega(k)$ up to second order in λ where the phonons have been thermodynamically averaged

$$\begin{aligned}
\langle \omega(k) \rangle_{\text{therm.}} &= J(1-2gx_D) - \frac{1}{2}\lambda J(1-2gx_I) \cos(k) \\
&+ \lambda^2 \left\{ -\frac{J(1-2gx_I)^2 \left(\frac{1}{16} + \frac{1}{16}\cos(2k) + \frac{1}{4}\cos(k) \right)}{1-2gx_D} \right. \\
&- \frac{3}{8}J^2g^2 \frac{\left(-4 \frac{J(1-2gx_D)}{e^{\beta\omega}-1} - 2J(1-2gx_D) + \omega \right)}{(4J^2(1-2gx_D)^2 - \omega^2)} \\
&+ \frac{1}{4}J^2g^2 \frac{\left(-\frac{J(1-2gx_D)}{e^{\beta\omega}-1} - J(1-2gx_D) + \omega \right)}{(J^2(1-2gx_D)^2 - \omega^2)} \\
&\left. + 2\omega x_I - 2 \frac{\left(\frac{1}{4}Jg + \omega x_I \right)^2}{\omega} + \frac{\left(\frac{3}{4}Jg + \omega x_D \right)^2}{\omega} - \frac{\left(\frac{1}{4}Jg - \omega x_D \right)^2}{\omega} \right\} + \mathcal{O}(\lambda^3). \tag{B.5}
\end{aligned}$$

Suppose the optimal phonon-shifts x_D and x_I are determined by minimizing the free energy. The value of the gap does not only depend linearly on the magnetic exchange coupling J but also quadratically. This can be seen from the three last addends in Eq. B.5. Independent of the obtained phonon-shifts, the value of Δ_{01}/J will always diverge in the limit $J \rightarrow \infty$. Thus, the approach performed here does probably not contain the most relevant processes describing the dynamics of the spin-phonon system in the limit $J \rightarrow \infty$. Further investigations need to be done to get a deeper understanding of that limit.

Bibliography

- [1] I. S. Osborne. Electronic cooperation. *Science*, 288(21):461, April 2000.
- [2] L. Hulthén. *Ark. Mat., Astron. Fys.*, 26A:1, 1938.
- [3] A. Klümper. Thermodynamics of the anisotropic spin-1/2 Heisenberg chain and related quantum chains. *Z. Phys. B*, 91:507, 1993.
- [4] M. P. Gelfand and R. R. P. Singh. High order convergent expansions for quantum many particle systems. *Adv. Phys.*, 49(1):93–140, 2000.
- [5] G. S. Rushbrooke, G. A. Baker, Jr., and P. J. Wood. Heisenberg model. In C. Domb and J. Lebowitz, editors, *Phase Transition and Critical Phenomena*, volume 3, chapter 5, pages 245–356. Academic Press, New York, 1974.
- [6] R. Navarro. Application of high- and low-temperature series expansions to two-dimensional magnetic systems. In L. J. de Jongh, editor, *Magnetic properties of layered transition metal compounds*, volume 9, chapter 6, pages 105–190. Kluwer Academic Publishers, Dordrecht, Netherlands, 1990.
- [7] K. Fabricius, A. Klümper, U. Löw, B. Büchner, T. Lorenz, G. Dhalenne, and A. Revcolevschi. Re-examination of the microscopic couplings of the quasi-one-dimensional antiferromagnet CuGeO_3 . *Phys. Rev. B*, 57:1102, 1998.
- [8] H. G. Evertz. The loop algorithm. *Adv. Phys.*, 52:1, 2003.
- [9] R. J. Bursill, T. Xiang, and G. A. Gehring. The density matrix renormalization group for a quantum spin chain at non-zero temperature. *J. Phys.: Condens. Matter*, 66:2221, 1997.
- [10] X. Q. Wang and T. Xiang. Transfer-matrix density-matrix renormalization-group theory for thermodynamics of one-dimensional quantum systems. *Phys. Rev. B*, 56:5061, 1998.
- [11] D. C. Johnston, M. Troyer, S. Miyahara, D. Lidsky, K. Ueda, M. Azuma, Z. Hiroi, M. Takano, M. Isobe, Y. Ueda, M.A. Korotin, V. I. Anisimov, A. V. Mahajan, and L. L. Miller. Magnetic susceptibilities of spin-1/2 antiferromagnetic Heisenberg ladders and applications to ladder oxide compounds. *cond-mat/0001147*, 2000.

- [12] D. C. Johnston, R. K. Kremer, M. Troyer, X. Wang, A. Klümper, S. L. Budko, A. F. Panchula, and P. C. Canfield. Thermodynamics of spin $S = 1/2$ antiferromagnetic uniform and alternating-exchange Heisenberg chains. *Phys. Rev. B*, 61(14):9558, April 2000.
- [13] S. Liang, B. Douçot, and P. W. Anderson. Some new variational resonating-valence-bond- type wave functions for spin- $\frac{1}{2}$ antiferromagnetic Heisenberg model on a square lattice. *Phys. Rev. Lett.*, 61:365, 1988.
- [14] G. S. Uhrig. *Niedrigdimensionale Spinsysteme und Spin-Phonon-Kopplung*. Habilitation thesis, Universität zu Köln, 1999.
- [15] K. P. Schmidt and G. S. Uhrig. Excitations in one-dimensional $S = 1/2$ quantum antiferromagnets. *Phys. Rev. Lett.*, 90:227204, June 2003.
- [16] M. Uehara, T. Nagata, J. Akimitsu, H. Takahashi, N. Mori, and K. Kinoshita. Superconductivity in the ladder material $\text{Sr}_{0.4}\text{Ca}_{13.6}\text{Cu}_{24}\text{O}_{41.84}$. *J. Phys. Soc. Jpn.*, 65(9):2764, September 1996.
- [17] N. D. Mermin and H. Wagner. Absence of ferromagnetism or antiferromagnetism in one- or two-dimensional isotropic Heisenberg models. *Phys. Rev. Lett.*, 17:1133, 1966.
- [18] P. C. Hohenberg. Existence of long-range order in one and two dimensions. *Phys. Rev.*, 158:383, 1967.
- [19] T. Nagata, M. Uehara, J. Goto, J. Akimitsu, N. Motoyama, H. Eisaki, S. Uchida, H. Takahashi, T. Nakanishi, and N. Mōri. Pressure-induced dimensional crossover and superconductivity in the hole-doped two-leg ladder compound $\text{Sr}_{14-x}\text{Ca}_x\text{Cu}_{24}\text{O}_{41}$. *Phys. Rev. Lett.*, 81(5):1090, August 1998.
- [20] A. Bühler. Hochtemperaturentwicklung für Spinketten und effektive Spinmodelle für Spin-Peierls-Systeme. *Diploma Thesis*, June 1999. Universität zu Köln.
- [21] A. Bühler, N. Elstner, and G. S. Uhrig. High temperature expansion for frustrated and unfrustrated $S=1/2$ spin chains. *Eur. Phys. J. B*, 16:475, 2000.
- [22] C. J. Hamer H.-X. He and J. Oitmaa. High-temperature series expansion for the (2+1)-dimensional Ising-model. *J. Phys. A: Math. Gen.*, 23(10):1775, May 1990.
- [23] M. P. Gelfand, R. R. P. Singh, and D. A. Huse. Perturbation expansions for quantum many-body systems. *J. Stat. Phys.*, 59:1093, 1990.
- [24] M. Troyer, H. Tsunetsugu, and D. Würtz. Thermodynamics and spin gap of the Heisenberg ladder calculated by the look-ahead Lanczos algorithm. *Phys. Rev. B*, 50:13515, 1994. There is a misprint in Eqs. (38) and (39), T/Δ must be replaced by Δ/T .

- [25] I. N. Bronstein, K. A. Semendjadew, and G. Musiol. *Taschenbuch der Mathematik*. Verlag Harri Deutsch, Thun und Frankfurt am Main, 1993.
- [26] A. Guttman. Asymptotic analysis of power-series expansions. In C. Domb and J. Lebowitz, editors, *Phase Transition and Critical Phenomena*, volume 13, chapter 1, pages 1–234. Academic Press, New York, 1989.
- [27] A. Furusaki, M. Sigrist, E. Westerberg, P. A. Lee, K. B. Tanaka, and N. Nagaosa. Random-exchange quantum Heisenberg chains. *Phys. Rev. B*, 52(22):15930, December 1995.
- [28] B. Bernu and G. Misguich. Specific heat and high-temperature series of lattice models: Interpolation scheme and examples on quantum spin systems in one and two dimensions. *Phys. Rev. B*, 63:134409, 2001.
- [29] A. W. Garrett, S. E. Nagler, D. A. Tennant, B. C. Sales, and T. Barnes. Magnetic excitations in the $S = 1/2$ alternating chain compound $(VO)_2P_2O_7$. *Phys. Rev. Lett.*, 79:745, 1997.
- [30] A. V. Prokofiev, F. Büllfeld, W. Assmus, H. Schwenk, D. Wichert, U. Löw, and B. Lüthi. Magnetic properties of the low dimensional spin system $(VO)_2P_2O_7$: ESR and susceptibility. *Eur. Phys. J. B*, 5:313, 1998.
- [31] G. S. Uhrig and B. Normand. Magnetic properties of $(VO)_2P_2O_7$ from frustrated interchain coupling. *Phys. Rev. B*, 58:R14705, 1998.
- [32] G. Chaboussant, P. A. Crowell, L. P. Lévy, O. Piovesana, A. Madouri, and D. Mailly. Experimental phase diagram of $Cu_2(C_5H_{12}N_2)_2Cl_4$: A quasi-one-dimensional anti-ferromagnetic spin- $\frac{1}{2}$ Heisenberg ladder. *Phys. Rev. B*, 55:3046, 1997.
- [33] G. Chaboussant, M.-H. Julien, Y. Fagot-Revurat, L. P. Lévy, C. Berthier, M. Horvatić, and O. Piovesana. Identification of nuclear relaxation processes in a gapped quantum magnet: H NMR in the $S = 1/2$ Heisenberg ladder $Cu_2(C_5H_{12}N_2)_2Cl_4$. *Phys. Rev. Lett.*, 79(5):925, August 1997.
- [34] P. R. Hammar, D. H. Reich, C. Broholm, and F. Trouw. Spin gap in a quasi-one-dimensional $S=1/2$ antiferromagnet: $Cu_2(1,4\text{-diazacycloheptane})_2Cl_4$. *Phys. Rev. B*, 57(13):7846, 1998.
- [35] N. Elstner and R. R. P. Singh. Field dependent thermodynamics and quantum critical phenomena in the dimerized spin system $Cu_2(C_5H_{12}N_2)_2Cl_4$. *Phys. Rev. B*, 58:11484, 1998.
- [36] C. Knetter and G. S. Uhrig. Triplet dispersion in $CuGeO_3$: Perturbative analysis. *Phys. Rev. B*, 63(1):094401, March 2001.
- [37] M. Azuma, Z. Hiroi, M. Takano, K. Ishida, and Y. Kitaoka. Observation of a spin gap in $SrCu_2O_3$ comprising spin- $1/2$ quasi-1D two-leg ladders. *Phys. Rev. Lett.*, 73(25):3463, December 1994.

- [38] D. C. Johnston, J. W. Johnston, D. P. Goshorn, and A. J. Jacobson. Magnetic susceptibility of $(VO)_2P_2O_7$: A one-dimensional spin-1/2 Heisenberg antiferromagnet with a ladder spin configuration and a singlet ground state. *Phys. Rev. B*, 35(1):219, January 1987.
- [39] R. S. Eccleston, T. Barnes, J. Brody, and J. W. Johnson. Inelastic neutron scattering from the spin ladder compound $(VO)_2P_2O_7$. *Phys. Rev. Lett.*, 73(19):2626, November 1994.
- [40] T. Barnes and J. Riera. Susceptibility and excitation spectrum of $(VO)_2P_2O_7$ in ladder and dimer-chain models. *Phys. Rev. B*, 50:6817, 1994.
- [41] M. Grove, P. Lemmens, G. Güntherodt, B. C. Sales, F. Büllersfeld, and W. Assmus. Magnetoelastic coupling and spin excitations in the spin-gap system $(VO)_2P_2O_7$: A Raman scattering study. *Phys. Rev. B*, 61(9):6126–6132, 2000.
- [42] A. Bühler, U. Löw, and G. S. Uhrig. Thermodynamic properties of the dimerized and frustrated $S=1/2$ chain. *Phys. Rev. B*, 64:024428, 2001.
- [43] J. Oitmaa, R. R. P. Singh, and Z. Weihong. Quantum spin ladders at $T=0$ and at high temperatures studied by series expansions. *Phys. Rev. B*, 54(2):1009, 1996.
- [44] R. Chitra, S. Pati, H. R. Krishnamurthy, D. Sen, and S. Ramasesha. Density-matrix renormalization group studies of the spin- $\frac{1}{2}$ Heisenberg system with dimerization and frustration. *Phys. Rev. B*, 52:6581, 1995.
- [45] G. S. Uhrig and H. J. Schulz. Magnetic excitations spectrum of dimerized antiferromagnetic chains. *Phys. Rev. B*, 54:R9624, 1996.
- [46] G. S. Uhrig and H. J. Schulz. Erratum: “Magnetic excitations spectrum of dimerized antiferromagnetic chains”. *Phys. Rev. B*, 58:2900, 1998.
- [47] S. R. White and I. Affleck. Dimerization and incommensurate spiral spin correlations in the zigzag chain: Analogies to the Kondo lattice. *Phys. Rev. B*, 54(14):9862, 1996.
- [48] S. Brehmer, H. J. Mikeska, and U. Neugebauer. The phase diagram and hidden order for generalized spin ladders. *J. Phys.: Condens. Matter*, 8:7161, 1996.
- [49] H. Yokoyama and Y. Saiga. Spin dynamics of the one-dimensional J-J' model and spin-Peierls transition in $CuGeO_3$. *J. Phys. Soc. Jpn.*, 66:3617, 1997.
- [50] S. Brehmer, A. K. Kolezhuk, H. J. Mikeska, and U. Neugebauer. Elementary excitations in the gapped phase of a frustrated $S=1/2$ spin ladder: From spinons to the Haldane triplet. *J. Phys.: Condens. Matter*, 10:1103, 1998.
- [51] C. Knetter and G. S. Uhrig. Perturbation theory by flow equations: dimerized and frustrated $S=1/2$ chain. *Eur. Phys. J. B*, 13(2):209–225, 2000.

- [52] S. Eggert. Numerical evidence for multiplicative logarithmic corrections from marginal operators. *Phys. Rev. B*, 54:R9612, 1996.
- [53] C. K. Majumdar and D. K. Gosh. On next-nearest-neighbor interaction in linear chain. i. *J. Math. Phys.*, 10:1388, 1969.
- [54] C. K. Majumdar. Antiferromagnetic model with known ground state. *J. Phys. C*, 3:911, 1969.
- [55] I. Affleck. Universal term in the free energy at a critical point and the conformal anomaly. *Phys. Rev. Lett.*, 56(7):746, February 1986.
- [56] A. Klümper, R. Raupach, and F. Schönfeld. Finite temperature DMRG investigation of the spin-Peierls transition in CuGeO_3 . *Phys. Rev. B*, 59:3612, 1999.
- [57] C. Knetter. private communication.
- [58] K. P. Schmidt. private communication.
- [59] U. Löw. Habilitation thesis, Dortmund, 2000.
- [60] G. S. Uhrig and B. Normand. Magnetic properties of $(\text{VO})_2\text{P}_2\text{O}_7$: Two-plane structure and spin-phonon interaction. *Phys. Rev. B*, 63:134418, 2001.
- [61] R. W. Kühne and U. Löw. Thermodynamical properties of a spin-1/2-Heisenberg chain coupled to phonons. *Phys. Rev. B*, 60(17):12125, November 1999.
- [62] R. E. Rapp, E. P. de Souza, H. Godfrin, and R. Calvo. The exchange interactions and magnetic behavior of $\text{Cu}(\text{L-Alanina})(2)$ - specific-heat measurements. *J. Phys.: Condens. Matter*, 7(49):9595, December 1995.
- [63] H. Kuroe, J. Sasaki, T. Sekine, N. Koide, Y. Sasago, K. Uchinokura, and M. Hase. Spin fluctuations in CuGeO_3 probed by light scattering. *Phys. Rev. B*, 55:409, 1997.
- [64] Ute Löw. private communication.
- [65] M. Takahashi. Half-filled Hubbard model at low temperatures. *J. Phys. C*, 10:1289, 1977.
- [66] A. H. MacDonald, S. M. Girvin, and D. Yoshioka. t/U expansion for the Hubbard model. *Phys. Rev. B*, 37(16):9753, June 1988.
- [67] A. Reischl and E. Müller-Hartmann. Derivation of effective spin models from a three band model for CuO_2 -planes. *Eur. Phys. J. B*, 28:173, 2002.
- [68] E. Dagotto and T. M. Rice. Surprises on the way from one- to two-dimensional quantum magnets: The ladder materials. *Science*, 271:618, 1996.

- [69] S. Brehmer, H.-J. Mikeska, M. Müller, N. Nagaosa, and S. Uchida. Effects of biquadratic exchange on the spectrum of elementary excitations in spin ladders. *Phys. Rev. B*, 60(1):329, 1999.
- [70] T. Senthil and M. P. A. Fisher. Fractionalization in the cuprates: Detecting the topological order. *Phys. Rev. Lett.*, 86(2):292, January 2001.
- [71] L. Balents, M. P. A. Fisher, and S. M. Girvin. Fractionalization in an easy-axis Kagome antiferromagnet. *Phys. Rev. B*, 65:224412, 2002.
- [72] G. Misguich, B. Bernu, C. Lhuillier, and C. Waldtmann. Spin liquid in the multiple-spin exchange model on the triangular lattice: ^3He on graphite. *Phys. Rev. Lett.*, 81(5):1098, August 1998.
- [73] K. Voelker and S. Chakravarty. Multiparticle ring exchange in the Wigner glass and its possible relevance to strongly interacting two-dimensional electron systems in the presence of disorder. *Phys. Rev. B*, 64(15):235125, December 2001.
- [74] H. J. Schmidt and Y. Kuramoto. Four-spin interaction as an effective interaction in high- T_c copper oxides. *Physica C*, 167:263–266, 1990.
- [75] Y. Honda, Y. Kuramoto, and T. Watanabe. Effects of cyclic four-spin exchange in the magnetic properties of the CuO_2 plane. *Phys. Rev. B*, 47(17):11329, 1993.
- [76] W. LiMing, G. Misguich, P. Sindzingre, and C. Lhuillier. From Néel long-range order to spin liquids in the multiple-spin exchange model. *Phys. Rev. B*, 62(10):6372, September 2000.
- [77] Y. Mizuno, T. Tohyama, and S. Maekawa. Magnetic interaction in insulating cuprates. *J. Low Temp. Phys.*, 117:389–393, 1999.
- [78] M. Matsuda, K. Katsumata, R. S. Eccleston, S. Brehmer, and H.-J. Mikeska. Magnetic excitations and exchange interactions in the $S=1/2$ two-leg ladders compound in $\text{La}_6\text{Ca}_8\text{Cu}_{24}\text{O}_{41}$. *Phys. Rev. B*, 62(13):8903, 2000.
- [79] M. Windt, M. Grüninger, T. Nunner, C. Knetter, K. Schmidt, G. S. Uhrig, T. Kopp, A. Freimuth, U. Ammerahl, B. Büchner, and A. Revcolevschi. Observation of two-magnon bound states in the two-leg ladders of $(\text{Ca},\text{La})_{14}\text{Cu}_{24}\text{O}_{41}$. *Phys. Rev. Lett.*, 87:127002, 2001.
- [80] K. P. Schmidt, C. Knetter, and G. S. Uhrig. Raman response in antiferromagnetic two-leg $S=1/2$ Heisenberg ladders. *Europhys. Lett.*, 56:877, 2001.
- [81] T. S. Nunner, P. Brune, T. Kopp, M. Windt, and M. Grüninger. Cyclic spin exchange in cuprate spin ladders. *Phys. Rev. B*, 66:180404, 2002.
- [82] J. Lorenzana, J. Eroles, and S. Sorella. Does the Heisenberg model describe the multimagnon spin dynamics in antiferromagnetic CuO layers? *Phys. Rev. Lett.*, 83(24):5122, 1999.

- [83] R. Coldea, S. M. Hayden, G. Aeppli, T. G. Perring, C. D. Frost, T. E. Mason, S.-W. Cheong, and Z. Fisk. Spin waves and electronic interactions in La_2CuO_4 . *Phys. Rev. Lett.*, 86:5377, 2001.
- [84] A. A. Katanin and A. P. Kampf. Spin excitations in La_2CuO_4 : Consistent description by inclusion of ring-exchange. *Phys. Rev. B*, 66:100403, September 2002.
- [85] A. Göbbling, U. Kuhlmann, C. Thomsen, A. Löffert, C. Gross, and W. Assmus. Magnetic excitations in SrCu_2O_3 : A Raman scattering study. *Phys. Rev. B*, 67:052403, February 2003.
- [86] R. S. Eccleston, M. Uehara, J. Akimitsu, H. Eisaki, N. Motoyama, and S. Uchida. Spin dynamics of the spin-ladder dimer-chain material $\text{Sr}_{14}\text{Cu}_{24}\text{O}_{41}$. *Phys. Rev. Lett.*, 81(8):1702, August 1998.
- [87] T. F. A. Müller, V. Anisimov, T. M. Rice, I. Dasgupta, and T. Saha-Dasgupta. Electronic structure of ladder cuprates. *Phys. Rev. B*, 57(20):R12655, May 1998.
- [88] M. Matsuda, K. Katsumata, R. S. Eccleston, S. Brehmer, and H.-J. Mikeska. Magnetic excitations from $S=1/2$ two-leg ladders in $\text{La}_6\text{Ca}_8\text{Cu}_{24}\text{O}_{41}$. *J. Appl. Phys.*, 87(9):6271, 2000.
- [89] K. Hijii and K. Nomura. Universality class of an $S=1/2$ quantum spin ladder system with the four spin exchange. *Phys. Rev. B*, 65(1):104413, March 2001.
- [90] E. Müller-Hartmann and A. Reischl. Derivation of effective spin models from a three band model for CuO_2 -planes. *Eur. Phys. J. B*, 28:173, 2002.
- [91] T. Granlund. *GNU Multiple Precision Library*. Swox AB, <http://swox.com/gmp>.
- [92] K. P. Schmidt, H. Monien, and G. S. Uhrig. Rung-singlet phase of the $S=1/2$ two-leg spin-ladder with four-spin cyclic exchange. *Phys. Rev. B*, 2003.
- [93] J. C. Bonner and M. E. Fisher. Linear magnetic chains with anisotropic coupling. *Phys. Rev.*, 135(3A):A640, August 1964.
- [94] Z. Weihong, R. R. P. Singh, and J. Oitmaa. Field dependence of the magnetization for the spin-ladder material $\text{Cu}_2(\text{C}_5\text{H}_{12}\text{N}_2)_2\text{Cl}_4$. *Phys. Rev. B*, 55(13):8052, April 1997.
- [95] B. Frischmuth, B. Ammon, and M. Troyer. Susceptibility and low temperature thermodynamics of spin-1/2 Heisenberg ladders. *Phys. Rev. B*, 54(6):R3714, 1996.
- [96] A. A. Nersisyan and A. M. Tsvelik. One-dimensional spin-liquid without magnon excitations. *Phys. Rev. Lett.*, 78:3939, 1997.
- [97] M. Müller, T. Vekua, and H.-J. Mikeska. Perturbation theories for the $S=1/2$ spin ladder with four-spin ring exchange. *Phys. Rev. B*, 66:134423, 2002.

- [98] A. Läuchli, G. Schmid, and M. Troyer. Phase diagram of the spin ladder with cyclic four spin exchange. *cond-mat/0206153*, 2002.
- [99] K. P. Schmidt, C. Knetter, M. Grüniger, and G. S. Uhrig. Charge order induced sharp Raman peak in $\text{Sr}_{14}\text{Cu}_{24}\text{O}_{41}$. *cond-mat/0210092*, 2002.
- [100] Z. Hiroi, M. Azuma, M. Takano, and Y. Bando. A new homologues series $\text{Sr}_{n-1}\text{Cu}_{n+1}\text{O}_{2n}$ found in the SrO-CuO system treated under high-pressure. *J. Solid State Chem.*, 95(1):230, November 1991.
- [101] T. M. Rice, S. Gopalan, and M. Sigrist. Superconductivity, spin gaps and Luttinger liquids in a class of cuprates. *Europhys. Lett.*, 23(6):445, August 1993.
- [102] C. de Graaf, I. de P. R. Moreira, and F. Illas. Ab initio study of the magnetic interactions in the spin-ladder compound SrCu_2O_3 . *Phys. Rev. B*, 60(5):3457, August 1999.
- [103] K. Ishida, Y. Kitaoka, K. Asayama, M. Azuma, Z. Hiroi, and M. Takano. Spin gap behavior in ladder-type of quasi-one-dimensional spin ($S=1/2$) system SrCu_2O_3 . *J. Phys. Soc. Jpn.*, 63(9):3222, September 1994.
- [104] K. Kojima, A. Keren, G. M. Luke, B. Nachumi, W. D. Wu, Y. J. Uemura, M. Azuma, and M. Takano. Magnetic behavior of the 2-leg and 3-leg spin ladder cuprates $\text{Sr}_{n-1}\text{Cu}_{n+1}\text{O}_{2n}$. *Phys. Rev. Lett.*, 74:2812, 1995.
- [105] H. Schwenk and D. König, M. Sieling, S. Schmidt, W. Palme, B. Lüthi, S. Zvyagin, R. S. Eccleston, M. Azuma, and M. Takano. Magnetic resonance in spin ladder systems $(\text{VO})_2\text{P}_2\text{O}_7$, SrCu_2O_3 and $\text{Sr}_2\text{Cu}_3\text{O}_5$. *Physica B*, 237:115, 1997.
- [106] M. Azuma, M. Takano, and R. S. Eccleston. Disappearance of the spin gap in Zn-doped 2-leg ladder compound $\text{Sr}(\text{Cu}_{1-x}\text{Zn}_x)_2\text{O}_3$. *J. Phys. Soc. Jpn.*, 67(3):740, March 1998.
- [107] A. W. Sandvik and E. Dagotto. Spin dynamics of SrCu_2O_3 and the Heisenberg ladder. *Phys. Rev. B*, 53:R2934, February 1996.
- [108] S. Gopalan, T. M. Rice, and M. Sigrist. Spin ladders with spin gaps: A description of a class of cuprates. *Phys. Rev. B*, 49(13):8901, April 1994.
- [109] M. Miyahara, M. Troyer, and D. C. Johnston and K. Ueda. Quantum Monte Carlo simulation for the trellis lattice Heisenberg model for SrCu_2O_3 and CaV_2O_5 . *J. Phys. Soc. Jpn.*, 67(11):3918, November 1998.
- [110] D. C. Johnston. Antiferromagnetic exchange in two-leg spin-1/2 ladders. *Phys. Rev. B*, 54(18):13009, November 1996.
- [111] B. Wolf. private communication.

- [112] B. S. Shastry and B. Sutherland. Exact ground state of a quantum mechanical antiferromagnet. *Physica B*, 108:1069–1070, 1981.
- [113] R. W. Smith and D. A. Keszler. Synthesis, structure and properties of the orthoborate $\text{SrCu}_2(\text{BO}_3)_2$. *J. Solid State Chem.*, 93:430–435, 1991.
- [114] U. Löw and E. Müller-Hartmann. Exact bound states on the critical frustration in the Shastry-Sutherland model. *J. Low Temp. Phys.*, 126(3-4):1135, February 2002.
- [115] M. Albrecht and F. Mila. First-order transition between magnetic order and valence bond order in a 2D frustrated Heisenberg model. *Europhys. Lett.*, 34(2):145, April 1996.
- [116] D. Carpentier and L. Balents. Field theory for generalized Shastry-Sutherland models. *Phys. Rev. B*, 65:024427, December 2002.
- [117] C. H. Chung, J. B. Marston, and S. Sachdev. Quantum phases of the Shastry-Sutherland antiferromagnet: Application to $\text{SrCu}_2(\text{BO}_3)_2$. *Phys. Rev. B*, 64:134407, September 2001.
- [118] S. Miyahara and K. Ueda. Exact dimer ground state of the two dimensional Heisenberg spin system $\text{SrCu}_2(\text{BO}_3)_2$. *Phys. Rev. Lett.*, 82(18):3701, 1999.
- [119] Z. Weihong, C. J. Hamer, and J. Oitmaa. Series expansions for a Heisenberg antiferromagnetic model for $\text{SrCu}_2(\text{BO}_3)_2$. *Phys. Rev. B*, 60(9):6608, 1999.
- [120] C. Knetter, A. Bühler, E. Müller-Hartmann, and G. S. Uhrig. Dispersion and symmetry of bound states in the Shastry-Sutherland model. *Phys. Rev. Lett.*, 85:3958, 2000.
- [121] Z. Weihong, J. Oitmaa, and C. J. Hamer. The phase diagram of the Shastry-Sutherland antiferromagnet. *Phys. Rev. B*, 65(1):014408, January 2002.
- [122] A. Läuchli, S. Wessel, and M. Sigrist. Phase diagram of the quadrumerized Shastry-Sutherland model. *Phys. Rev. B*, 66(1):014401, July 2002.
- [123] T. Munehisa and Y. Munehisa. Numerical study of excited states in the Shastry-Sutherland model. *J. Phys. Soc. Jpn.*, 72(1):160, January 2003.
- [124] C. Knetter. *Perturbative Continuous Unitary Transformations: Spectral Properties of Low Dimensional Spin Systems*. PhD thesis, Universität zu Köln, 2003.
- [125] A. Koga and N. Kawakami. Quantum phase transitions in the Shastry-Sutherland model for $\text{SrCu}_2(\text{BO}_3)_2$. *Phys. Rev. Lett.*, 84(19):4461–4464, May 2000.
- [126] K. Ueda and S. Miyahara. A class of Heisenberg models with orthogonal dimer ground states. *J. Phys.: Condens. Matter*, 11:L175, May 1999.

- [127] N. Surendran and R. Shankar. Generalised Shastry-Sutherland models in three and higher dimensions. *Phys. Rev. B*, 66(2):024415, July 2002.
- [128] K. Sparta, G. J. Redhammer, P. Roussel, G. Heger, G. Roth, P. Lemmens, A. Ionescu, M. Grove, G. Güntherodt, F. Hüning, H. Lueken, H. Kageyama, K. Onizuka, and Y. Ueda. Structural phase transition in the 2D spin dimer compound $\text{SrCu}_2(\text{BO}_3)_2$. *Eur. Phys. J. B*, 19(4):507, February 2001.
- [129] S. Miyahara and K. Ueda. Thermodynamic properties of three-dimensional orthogonal dimer model for $\text{SrCu}_2(\text{BO}_3)_2$. *J. Phys. Soc. Jpn.*, 72:72, May 2000.
- [130] H. Kageyama, M. Nishi, N. Aso, K. Onizuka, T. Yoshizawa, K. Nukui, K. Kodama, K. Kakurai, and Y. Ueda. Direct evidence for the localized single-triplet excitations and the dispersive multi-triplets excitations in $\text{SrCu}_2(\text{BO}_3)_2$. *Phys. Rev. Lett.*, 84(25):5876, June 2000.
- [131] H. Kageyama, K. Yoshimura, R. Stern, N. V. Mushnikov, K. Onizuka, M. Kato, K. Kosuge, C. P. Slichter, and T. Goto and Y. Ueda. Exact dimer ground state and quantized magnetization plateaus in the two-dimensional spin system $\text{SrCu}_2(\text{BO}_3)_2$. *Phys. Rev. Lett.*, 82(15):3168–3171, April 1999.
- [132] H. Nojiri, H. Kageyama, K. Onizuka, Y. Ueda, and M. Motokawa. Direct observation of the multiple spin gap excitations in two-dimensional dimer systems $\text{SrCu}_2(\text{BO}_3)_2$. *J. Phys. Soc. Jpn.*, 68(9):2906–2909, September 1999.
- [133] T. Room, U. Nagel, E. Lippmaa, H. Kageyama, K. Onizuka, and Y. Ueda. Far-infrared study of the two-dimensional dimer spin system $\text{SrCu}_2(\text{BO}_3)_2$. *Phys. Rev. B*, 61(21):14342–14345, June 2000.
- [134] K. Kodama, J. Yamazaki, M. Takigawa, H. Kageyama, K. Onizuka, and Y. Ueda. Cu nuclear spin-spin coupling in the dimer singlet state in $\text{SrCu}_2(\text{BO}_3)_2$. *J. Phys.: Condens. Matter*, 14(17):L319, May 2002.
- [135] P. Lemmens, M. Grove, M. Fischer, G. Güntherodt, V. N. Kotov, H. Kageyama, K. Onizuka, and Y. Ueda. Collective singlet excitations and evolution of Raman spectral weights in the 2D spin dimer compound $\text{SrCu}_2(\text{BO}_3)_2$. *Phys. Rev. Lett.*, 85(12):2605, September 2000.
- [136] H. Nojiri, T. Asano, Y. Ajiro, H. Kageyama, Y. Ueda, and M. Motokawa. High-field ESR on quantum spin systems. *Physica B*, 294-295:14, 2001.
- [137] C. Knetter, E. Müller-Hartmann, and G. S. Uhrig. Symmetries and triplet dispersion in a modified Shastry-Sutherland model for $\text{SrCu}_2(\text{BO}_3)_2$. *J. Phys.: Condens. Matter*, 12(42):9069, October 2000.
- [138] S. Miyahara and K. Ueda. Theory of the orthogonal dimer Heisenberg spin model for $\text{SrCu}_2(\text{BO}_3)_2$. *J. Phys.: Condens. Matter*, 15(9):R327, March 2003.

- [139] H. Kageyama, K. Onizuka, T. Yamauchi, Y. Ueda, s. Hane, H. Mitamura, T. Goto, K. Yoshimura, and K. Kosuge. Anomalous magnetizations in single crystalline $\text{SrCu}_2(\text{BO}_3)_2$. *J. Phys. Soc. Jpn.*, 68(6):1821–1823, June 1999.
- [140] H. Kageyama, K. Onizuka, Y. Ueda, M. Nohara, H. Suzuki, and H. Takagi. Low-temperature specific heat study of $\text{SrCu}_2(\text{BO}_3)_2$ with an exactly solvable ground state. *J. of Exp. and Theor. Phys.*, 90(1):129, 2000.
- [141] S. Zherlitsyn, S. Schmidt, B. Wolf, H. Schwenk, B. Lüthi, H. Kageyama, K. Onizuka, Y. Ueda, and K. Ueda. Soundwave anomalies in $\text{SrCu}_2(\text{BO}_3)_2$. *Phys. Rev. B*, 62(10):R6097, September 2000.
- [142] T. Holstein. Studies of polaron motion Part I. The molecular-crystal model. *Ann. Physik*, 8:325, 1959.
- [143] E. Pytte. Peierls instability in Heisenberg chains. *Phys. Rev. B*, 10:4637, 1974.
- [144] J. W. Bray, L. V. Interrante, I. C. Jacobs, and J. C. Bonner. The Spin-Peierls Transition. In J. S. Miller, editor, *Extended Linear Chain Compounds*, volume 3, page 353, New York, 1983. Plenum Press.
- [145] M. C. Cross and D. S. Fisher. A new theory of the spin-Peierls transition with special relevance to the experiments on TTCuBDT . *Phys. Rev. B*, 19(1):402, January 1979.
- [146] M. Hase, I. Terasaki, and K. Uchinokura. Observation of the spin-Peierls transition in linear Cu^{2+} (spin- $\frac{1}{2}$) chains in an inorganic compound CuGeO_3 . *Phys. Rev. Lett.*, 70:3651, 1993.
- [147] W. Geertsma and D. Khomskii. Influence of side groups on 90° superexchange: A modification of the Goodenough-Kanamori-Anderson rules. *Phys. Rev. B*, 54:3011, 1996.
- [148] D. Khomskii, W. Geertsma, and M. Mostovoy. Elementary excitations, exchange interaction and spin-peierls transition in CuGeO_3 . *Czech. Journ. of Physics*, 46:3239, 1996.
- [149] R. Werner, C. Gros, and M. Braden. The microscopic spin-phonon coupling constants in CuGeO_3 . *Phys. Rev. B*, 59:14356, 1999.
- [150] R. J. Bursill, R. H. McKenzie, and C. J. Hamer. Phase diagram of a Heisenberg spin-Peierls model with quantum phonons. *Phys. Rev. Lett.*, 83(2):408–411, 1999.
- [151] G. S. Uhrig. Nonadiabatic approach to spin-Peierls transitions via flow equations. *Phys. Rev. B*, 57:R14004, 1998.
- [152] C. Raas, A. Bühler, and G. S. Uhrig. Effective spin models for spin-phonon chains by flow equations. *Eur. Phys. J. B*, 21:369, 2001.

- [153] C. Raas, U. Löw, G. S. Uhrig, and R. W. Kühne. Spin-phonon chains with bond coupling. *Phys. Rev. B*, 65:144438, 2002.
- [154] A. Weiße, G. Wellein, and H. Fehske. Quantum lattice fluctuations in a frustrated Heisenberg spin-Peierls chain. *Phys. Rev. B*, 60(9):6566–6573, 1999.
- [155] S. Trebst, N. Elstner, and H. Monien. Renormalization of the spin-Peierls transition due to phonon dynamics. *Europhys. Lett.*, 56(2):268, October 2001.
- [156] P. Sun, D. Schmeltzer, and A. R. Bishop. Analytic approach to the one-dimensional spin-Peierls system in the entire frequency range. *Phys. Rev. B*, 62(17):11308, November 2000.
- [157] A. W. Sandvik, R. R. P. Singh, and D.K. Campbell. Quantum Monte Carlo in the interaction representation: Application to a spin-Peierls model. *Phys. Rev. B*, 56(22):14510–14528, 1997.
- [158] A. W. Sandvik and D. K. Campbell. Spin-Peierls transition in the Heisenberg chain with finite frequency phonons. *Phys. Rev. Lett.*, 83(1):195, July 1999.
- [159] C. H. Aits. Quanten-Monte-Carlo Untersuchungen effektiver Spinmodelle mit Spin-Phonon-Kopplung. *Diploma Thesis*, 2002. Universität zu Köln.
- [160] C. H. Aits and U. Löw. Thermodynamic properties of the two-dimensional $S=1/2$ Heisenberg antiferromagnet coupled to bond phonons. *cond-mat/0306745*, 2003.
- [161] C. Domb and M. S. Green, editors. *Phase transitions and critical phenomena*, volume 3. Academic Press, New York, 1974.
- [162] J. Oitmaa. private communication.
- [163] S. Eggert, I. Affleck, and M. Takahashi. Susceptibility of the spin $1/2$ Heisenberg antiferromagnetic chain. *Phys. Rev. Lett.*, 73:332, 1994.
- [164] A. Klümper. The spin- $1/2$ Heisenberg chain: Thermodynamics, quantum criticality and spin-Peierls exponents. *Eur. Phys. J. B*, 5:677, 1998.
- [165] G. Castilla, S. Chakravarty, and V. J. Emery. Quantum magnetism of CuGeO_3 . *Phys. Rev. Lett.*, 75:1823, 1995.
- [166] J. Riera and A. Dobry. Magnetic susceptibility in the spin-Peierls system CuGeO_3 . *Phys. Rev. B*, 51:16098, 1995.
- [167] F. J. Wegner. Flow equations for hamiltonians. *Ann. Physik*, 3:77, 1994.
- [168] A. Meyer, A. Gleizes, J.J. Girerd, M. Verdaguer, and O. Kahn. Crystal-structures, magnetic-anisotropy properties, and orbital interactions in catena-(mu-nitritio)-bis(ethylenediamine)nickel(ii) perchlorate and triiodide. *Inorg. Chem.*, 21(5):1729, 1982.

- [169] J. P. Renard, M. Verdaguer, L. P. Regnault, W. A. C. Erkelens, J. Rossatmignod, J. Ribas, W. G. Stirling, and C. Vettier. Quantum energy-gap in 2 quasi-one-dimensional $S = 1$ Heisenberg antiferromagnets. *J. Appl. Phys.*, 63(8):3538, April 1988.
- [170] T. Yosida and M. Fukui. Crystal-structure of $\text{Ni}(\text{C}_3\text{H}_{10}\text{N}_2)_2\text{NO}_2\text{ClO}_4$. *J. Phys. Soc. Jpn.*, 61(7):2304, July 1992.
- [171] L. G. Caron and S. Moukouri. Density matrix renormalization group applied to the ground state of the XY spin-Peierls system. *Phys. Rev. Lett.*, 76:4050, 1996.

Abstract

In this thesis the thermodynamical properties of spin- and spin-phonon-systems are investigated. In the first part of the thesis pure spin-1/2 models are addressed: the dimerized, frustrated chain, the ladder with cyclic exchange, and the two-dimensional Shastry-Sutherland model. The second part presents results for a spin-1/2 system coupled to lattice vibrations, i.e. phonons.

By means of high temperature series expansions quantities like the magnetic susceptibility and the specific heat are calculated. These quantities are in most cases easily accessible experimentally. The obtained truncated series have the full dependence of the model parameters. Thus, fitting procedures become a fast and easy task. The coefficients of the truncated series are given as fractions of integers such that no accuracy is lost. The results are exact up to the given order. To improve the representations of the results extrapolation techniques are applied, namely Padé and Dlog-Padé extrapolations. The extrapolations are stabilized in the low temperature region using well-known information on the $T = 0$ and on the low temperature behavior. The extrapolated series expansion results are gauged carefully by investigating their convergence and by comparing them to numerical data obtained from other methods like exact complete diagonalization, quantum Monte-Carlo, and transfer matrix-renormalization group.

For the dimerized, frustrated spin system the difficulty is discussed to extract more than two coupling constants from the temperature dependence of the magnetic susceptibility. The ladder system is extended by the inclusion of a four-spin (cyclic) exchange. The impact of this new type of interaction is investigated. Comparison to experimental data of the ladder system SrCu_2O_3 shows, that the ladder model with a significant but small amount of cyclic exchange can serve as a description of the experimental data just as well as a pure ladder model. The inclusion of cyclic exchange leads to more realistic values for the coupling constants than the values obtained from fitting the ladder model without this type of exchange. The two-dimensional Shastry-Sutherland model has a realization in the compound $\text{SrCu}_2(\text{BO}_3)_2$ allowing a detailed comparison between theory and experiment. The three-dimensionality of the substance is explicitly taken into account in the calculations using a mean-field like ansatz for the inter-layer coupling. The extrapolations of the high temperature series data can reproduce the experimental susceptibility data down to very low temperatures.

The explicit calculations for the spin-1/2 system coupled to dispersionless phonons are performed using the cluster expansion technique. No cut-off in the phonon subspace is necessary such that the full phonon dynamics are taken into account. The influence of the additional coupling to the phononic degrees of freedom is addressed concerning the magnetic susceptibility and the specific heat.

Deutsche Zusammenfassung

Die vorliegende Arbeit beschäftigt sich mit den thermodynamischen Eigenschaften von Spin- und Spin-Phonon-Systemen. Im ersten Teil der Arbeit werden reine Spin-1/2 Modelle untersucht: Die dimerisierte, frustrierte Kette, die Leiter mit Ringaustausch und das zweidimensionale Shastry-Sutherland Modell. Der zweite Teil der Arbeit beschäftigt sich mit einem Spin-1/2 System, das an Gitterschwingungen angekoppelt ist, den Phononen. Mittels Hochtemperaturentwicklungen werden Größen wie die magnetische Suszeptibilität und die spezifische Wärme berechnet. Diese Größen sind experimentell meist sehr gut zugänglich. Die endlichen Reihen weisen die volle Abhängigkeit der Modellparameter auf. Die Anpassung an experimentelle Daten kann dadurch schnell und einfach durchgeführt werden. Die Koeffizienten der endlichen Reihen liegen als rationale Zahlen vor, sodass keine Rundungsfehler auftreten. Die Ergebnisse sind exakt bis zur berechneten Ordnung. Zur Verbesserung der Darstellung der Ergebnisse werden Extrapolationstechniken angewandt. Dabei handelt es sich um Padé und Dlog-Padé Extrapolationen. Die Extrapolationen lassen sich im Tieftemperaturbereich durch die Verwendung von bekannten $T = 0$ und bekannten Tieftemperatureigenschaften stabilisieren. Die extrapolierten Reihenentwicklungen werden sorgfältig in ihre Genauigkeit beurteilt, indem sie auf ihre Konvergenz untersucht werden, und indem sie mit Ergebnissen numerischer Methoden wie exakter kompletter Diagonalisierung, Quanten Monte-Carlo und Transfer-Matrixrenormalisierungsgruppe verglichen werden.

Für das dimerisierte, frustrierte Kettenmodell wird die Schwierigkeit diskutiert, in wieweit es möglich ist mehr als zwei Kopplungskonstanten aus der Temperaturabhängigkeit der magnetischen Suszeptibilität zu gewinnen. Das Leitersystem wird durch einen zusätzlich vier-Spin (zyklischen) Austausch erweitert. Der Einfluss dieser neuartigen Kopplung wird untersucht. Der Vergleich mit experimentellen Daten des Leitersystem SrCu_2O_3 zeigt, dass das Leitermodell mit einer signifikantem aber immer noch kleinen zyklischen Austauschkopplung die experimentellen Daten genauso gut wie ein reines Leitersystem beschreiben kann. Der zusätzliche zyklische Austausch führt zu realistischeren Kopplungskonstanten als dies der Fall für das Modell ohne zyklischen Austausch ist. Das zweidimensionale Shastry-Sutherland-Modell ist in der Substanz $\text{SrCu}_2(\text{BO}_3)_2$ realisiert. Dies ermöglicht einen detaillierten Vergleich zwischen theoretischen und experimentellen Ergebnissen. Der Dreidimensionalität der Substanz wird durch einen Molekularfeld ähnlichen Zugang für die Zwischenebenenkopplung genüge getan. Die Extrapolationen der Reihenentwicklung können die experimentellen Daten bis zu sehr kleinen Temperaturen wiedergeben.

Die expliziten Berechnungen für das Spin-1/2 System gekoppelt an dispersionslose Phononen werden mittels einer Clusterentwicklung durchgeführt. Der Unterraum der Phononen muss nicht künstlich abgeschnitten werden, sodass die volle Dynamik der Phononen behandelt werden kann. Der Einfluss der zusätzlichen Kopplung des Spinsystems an phononische Freiheitsgrade wird anhand der magnetischen Suszeptibilität und spezifischen Wärme untersucht.

Danksagung

Ein ganz besonderes Dankeschön geht an Herrn Priv.-Doz. Dr. G. S. Uhrig. Seine Diskussions- und Hilfsbereitschaft trugen wesentlich zum Gelingen dieser Arbeit bei. Insbesondere seine Aufmerksamkeit und Unterstützung in den letzten Jahren lernte ich sehr zu schätzen. Eine solch nette Zusammenarbeit wünsche ich mir auch für die Zukunft.

Ein weiteres Dankeschön geht an Herrn Prof. E. Müller-Hartmann, der immer für eine gute Atmosphäre in seiner Arbeitsgruppe sorgte und mein Interesse für die Physik ständig auffrischte.

Einen lieben Dank an Frau Priv.-Doz. Dr. U. Löw, ihren Blick für das Detail schätze ich sehr.

Den Herren Prof. J. Oitmaa und Prof. C. Hamer sei an dieser Stelle für ihre freundliche Aufnahme in ihre Arbeitsgruppe an der University of New South Wales, Australien, gedankt. Die Zusammenarbeit mit Jaan Oitmaa lieferten mir wichtige Bestandteile des Spin-Phonon Kapitels, das ohne ihn nicht in der vorliegenden Form zustande gekommen wäre.

Die sowohl entspannte als auch produktive Stimmung in Raum 110 mit Christian Knetter, Alexander Reischl, Kai Schmidt und Friedhelm Schönfeld schufen eine sehr nette Arbeitatmosphäre. Desweiteren danke ich Christian Knetter für die gemeinsam verbrachte Zeit, in der wir zunächst zusammen Übungen gelöst und später gemeinsam gestellt haben. Die Zimmernachbarn Ansgar Kirchner, Christian Dziurzik und Andreas Kemper hatten immer ein offenes Ohr für meine Fragen, dafür ein Dankeschön.

Danken möchte ich auch Andreas Sindermann, so manches Computerprogramm wäre ohne sein Hilfe sicherlich nicht so schnell zustande gekommen.

Für die Bereitstellung von Daten und/oder Abbildungen, die in dieser Arbeit verwendet wurden danke ich C. Aits, M. Azuma, H. Kageyama, A. Klümper, C. Knetter, P. Lemmens, T. Lorenz, U. Löw, J. Oitmaa, C. Raas, R. Raupach, K. Schmidt und F. Schönfeld.

Für das sehr aufmerksame Korrekturlesen der vorliegenden Arbeit bin ich Carsten Aits, Ute Löw, Jean Lunny, Alexander Reischl und Götz Uhrig sehr dankbar.

Der Fussballmannschaft des Instituts verdanke ich so manchen Muskelkater aber auch eine sehr nette Zeit zum Abschalten von der Arbeit.

Für ihre Geduld während der ganzen Zeit der Entstehung dieser Arbeit und vielmehr noch für ihre geliebte Ungeduld in der Endphase dieser Arbeit danke ich ganz besonders Joana[♥].

Meine Tochter Louise Mai[♥] gab mir die schlafraubende Motivation für die letzten Monate dieser Arbeit. Euch beiden gilt mehr als nur ein Dankeschön.

Erklärung

Ich versichere, dass ich die von mir vorgelegte Dissertation selbständig angefertigt, die benutzten Quellen und Hilfsmittel vollständig angegeben und die Stellen der Arbeit – einschliesslich Tabellen, Karten, und Abbildungen –, die anderen Werken im Wortlaut oder dem Sinn nach entnommen sind, in jedem Einzelfall als Entlehnung kenntlich gemacht habe; dass diese Dissertation noch keiner anderen Fakultät oder Universität zur Prüfung vorgelegen hat; dass sie – abgesehen von unten angegebenen Teilpublikationen – noch nicht veröffentlicht worden ist sowie, dass ich eine solche Veröffentlichung vor Abschluss des Promotionsverfahrens nicht vornehmen werde. Die Bestimmungen dieser Promotionsordnung sind mir bekannt. Die von mir vorgelegte Dissertation ist von Herrn Privat-Dozent Dr. Götz S. Uhrig betreut worden.

Köln, den 9. Dezember 2003

Alexander Bühler

Teilpublikationen

- A. Bühler, G. S. Uhrig und N. Elstner. High Temperature Expansion for Frustrated and Unfrustrated $S = 1/2$ Spin Chains. *Eur. Phys. J. B*, 16:475, 2000.
- C. Knetter, A. Bühler, E. Müller-Hartmann und G. S. Uhrig. Dispersion and Symmetry of Bound States in the Shastry-Sutherland Model. *Phys. Rev. Lett.*, 85:3958, 2000.
- C. Knetter, A. Bühler, E. Müller-Hartmann und G. S. Uhrig. $\text{SrCu}_2(\text{BO}_3)_2$ - A Two Dimensional Spin Liquid. *Can. J. Phys.*, 79(11-12):1565, 2001
- A. Bühler, U. Löw und G. S. Uhrig. Thermodynamic properties of the dimerized and frustrated $S=1/2$ chain. *Phys. Rev. B*, 64:024428, 2001.
- A. Bühler, U. Löw, K. P. Schmidt und G. S. Uhrig. Thermodynamic properties of spin ladders with cyclic exchange. *Phys. Rev. B*, 67:134428, 2003.

Lebenslauf

Persönliche Daten:

Name	Alexander Bühler
Geburtstag	11.07.1971
Geburtsort	Karlsruhe
Familienstand	ledig, ein Kind
Staatsangehörigkeit	deutsch

Schulbildung:

1978-1982	Grundschule Kuppenheim
1982-1991	Richard-Wagner-Gymnasium Baden-Baden
Juni 1991	Abschluss: Allgemeine Hochschulreife

Zivildienst/Auslandsaufenthalt:

Sept. 1991 - Dez. 1992	Zivildienst im Jugendhilfezentrum Michaelshoven, Coenaculum Köln
Jan. - Mai 1993	Reise nach Kolumbien

Studium:

WS 1993/1994	Immatrikulation an der Universität zu Köln, Studiengang: Physik, Diplom
WS 1995/1996	Aufnahme Zweitstudiengang: Lehramt Sek. 2 Mathematik/Physik
April 1996	Vordiplom Physik, Zwischenprüfung Mathematik/Physik
Sept. 1996	Schulpraktikum an der Kurt-Schwitters-Gesamtschule, Berlin
Juni 1998	Beginn der Diplomarbeit bei Prof. Müller-Hartmann am Institut für Theoretische Physik, Universität zu Köln
Juni 1999	Abschluss: Diplom Physik
seit Juli 1999	Promotion in theoretischer Physik bei Priv.-Doz. Götz S. Uhrig
Feb. 2001 - Okt. 2001	Forschungsaufenthalt an der University of New South Wales, Sydney, Australien, gefördert durch ein Doktoranden-Stipendium des DAAD.

Arbeitsverhältnisse:

am Institut für Theoretische Physik, Universität zu Köln	
April 1998 - Juni 1999	Studentische Hilfskraft
Juli 1999 - Okt. 1999	Wissenschaftliche Hilfskraft
seit Nov. 1999	Wissenschaftlicher Mitarbeiter